Behaviour and application of colloids stabilised by hydrophobically modified starch: Impact of amylose content

Mingduo Mu

Submitted in accordance with the requirements for the degree of
Doctor of Philosophy

The University of Leeds
School of Food Science and Nutrition

June, 2021

The candidate confirms that the work submitted is her own, except where work which has formed part of jointly-authored publications has been included. The contribution of the candidate and the other authors to this work has been explicitly indicated below. The candidate confirms that appropriate credit has been given within the thesis where reference has been made to the work of others. Details of the jointly-authored publications and the contributions of the candidate and the other authors are outlined on the next pages.

Details of the jointly-authored publications and the author contribution are included below:

Chapter 2

Mu, M., Holmes, M. and Ettelaie, R., 2021 Relating structure to functionality: a literature review on OSA-modified starch. To be submitted to *Current Opinion in Food Science*.

Chapter 3

Mu, M., Farshchi, A., Holmes, M., Chen, J. and Ettelaie, R., 2019. Effect of storage temperature and relative humidity on long-term colloidal stability of reconstitutable emulsions stabilised by hydrophobically modified starch. *Food Hydrocolloids*, *95*, pp.62-75.

Chapter 4

Mu, M., Karthik, P., Chen, J., Holmes, M. and Ettelaie, R., 2021. Effect of amylose and amylopectin content on the colloidal behaviour of emulsions stabilised by OSA-Modified starch. *Food Hydrocolloids*, *111*, p106363.

Chapter 5

Mu, M., Holmes, M. and Ettelaie, R., 2021. Effect of polymer architecture on the adsorption behaviour of amphiphilic copolymers: A theoretical study. To be submitted to *Macromolecules*.

Details of author contribution

Mingduo Mu: Experimental designs, conduction of the experiments and theoretical work, data collection and interpretation, drafting and editing of the manuscripts, as well as the replies to the reviewers' comments.

Amin Farshchi: Conduction of rheological measurements on hydrophobically modified starch solutions.

Karthik Pothiyappan: Feedback on *in vivo* and *in vitro* oral digestion experiments, collection of microscopic images for the *in vitro* experiment.

Jianshe Chen: Supervision and feedback for *in vivo* and *in vitro* oral digestion experiments, which were conducted at the Lab of Food Oral Processing, Zhejiang Gongshang University, Hangzhou, China.

Rammile Ettelaie and Melvin Holmes: Supervision, feedback, proofreading and editing of the manuscripts and the reply to reviewers' comments.

List of accepted abstracts

Poster presentations

Mu, M., Ettelaie, R., & Holmes, M. Evaluation of Reconstituted Freeze-Dried Emulsions Stabilized by Modified Starch. *Food Colloids 2018 Conference* – University of Leeds, Leeds, UK, April 8-11, 2018.

Mu, M., Ettelaie, R., & Holmes, M. Effect of storage conditions on reconstitutable freeze-dried oil-in-water emulsion stabilised by hydrophobically modified starch. *The 5th Annual Food Science and Nutrition PhD Conference* – University of Leeds, Leeds, UK, November 30, 2018.

Mu, M., Ettelaie, R., & Holmes, M. Effect of storage temperature and relative humidity on reconstitutable freeze-dried oil-in-water emulsion stabilised by hydrophobically modified starch. *Industry Day: Nutrition, Health and Wellness* – Weetwood Hall Estate, Leeds, UK, January 18, 2019.

Mu, M., Farshchi, A., Holmes, M., Chen, J., & Ettelaie, R. The long-term stability of reconstitutable emulsions stabilised by hydrophobically modified starch under the effect of powder storage conditions. *4th UK Hydrocolloids Symposium* – University of Leeds, Leeds, UK, September 12, 2019.

Oral presentations

Mu, M., Farshchi, A., Holmes, M., Chen, J., & Ettelaie, R. Effect of storage temperature and relative humidity on reconstitutable freeze-dried oil-in-water emulsion stabilised by hydrophobically modified starch. *Physics in Food Manufacturing Conference* – Campden BRI, Chipping Campden, Gloucestershire, UK, January 9-10, 2019.

Mu, M., Karthik, P., Chen, J., Holmes, M., & Ettelaie, R. Effect of Amylose to Amylopectin Ratio on Oral Behaviour of OSA-Modified Starch Stabilised Emulsion. *The 6th Annual Food Science and Nutrition PhD Conference* – University of Leeds, Leeds, UK, November 21, 2019.

Mu, M., Karthik, P., Chen, J., Holmes, M., & Ettelaie, R. Effect of Amylose to Amylopectin Ratio on Oral Behaviour of OSA-Modified Starch Stabilised Emulsion. *Physics in Food Manufacturing Conference* – Weetwood Hall Estate, Leeds, UK, January 15-17, 2020.

Mu, M., Karthik, P., Chen, J., Holmes, M., & Ettelaie, R. Effect of Amylose to Amylopectin Ratio on Oral Behaviour of OSA-Modified Starch Stabilised Emulsion. *Food Colloids 2020 Conference* – Lund University, Lund, Sweden, April 19-22, 2020. [Conference postponed to 2022]

Acknowledgements

First of all, I would like to express my wholehearted gratitude to my main supervisor, Dr. Rammile Ettelaie for his expert guidance, endless support, and generous encouragement through every project I have undertaken during these four years. Such a PhD project with both experimental exploration and theoretical computation would not have been possible without his supervision. I am also grateful to my second supervisor, Dr. Melvin Holmes, who always comes in with insightful comments and offers the kindest reassurance. It has been a great pleasure to have both of them in this journey.

My gratitude extends to Prof. Jianshe Chen and his research team from the Food Oral Processing Laboratory, Zhejiang Gongshang University, China, for their hospitality and professional support during my 3-month visit to his lab. I was deeply impressed by their inclusive environment and rigorous scholarly research.

I would like to acknowledge Prof. Francisco M. Goycoolea and Dr. Yadira Gonzalez for their kind assistance in obtaining the molecular weight of a commercial modified starch, and Prof. Michael Rappolt for his great help in determining the physical state of frozen oil from X-Ray Diffraction patterns.

I also sincerely appreciate all the support I received from the technical team, Miles Ratcliff, Ian hardy, Neil Rigby, Dr. Joanne Brown, Amie Lister and Dr. Nataricha Phisarnchananan, and from all friends and colleagues at the School of Food Science and Nutrition.

I would also like to thank my friends who are living their colourful life outside the UK, especially Mengdi Xing, for being herself and bringing me laughter and strength. Lastly, my appreciation goes out to my parents who are as caring, encouraging, supportive and amusing as they have always been. I really look forward to seeing you.

Abstract

Normally hydrophilic starch is modified with octenyl succinic anhydride (OSA) to provide it with emulsifying and colloid stabilising properties. As a biopolymer emulsifier, OS-starch stabilised emulsions have higher resistance to changes in environmental conditions such as pH and electrolyte, when compared to protein-based emulsifiers. This is thought to be mainly due to the provision of stronger steric stabilisation. There has been much interest in seeking the most fundamental factors leading to further improvement of OS-starch functionality, as well as its novel applications. As an example of the latter, a truly reconstitutable O/W emulsion that can be stored and transported as dried powder, and upon simple rehydration can be restored to its original droplet size, was studied here. The storage temperature of emulsion powder was found to greatly affect the rehydrated droplet size, with a powder storage temperature below the supercooling point of the oil phase being successful in fabrication of such truly reconstitutable emulsion. The achieved oil droplets were of 2 μm post rehydration. In the effort to fundamentally understand and enhance the functionality of OS-starch, a systematic investigation into the relationship between the amylose content (AC) of OS-starch and its colloidal stabilising behaviour was conducted. Changes in pH and electrolyte concentration revealed that the OS-starch with lower AC exerted stronger steric stabilisation, but the interfacial layers it formed were more rapidly degraded by α-amylase. The results were further examined in light of a theoretical study concerning the impact of polymer architecture on their ability to stabilise colloids/emulsions. Linear, star-like, and dendritic amphiphilic polymers were compared for their surface affinity using Self-Consistent Field (SCF) calculations. A method for extrapolating Henry's constant from SCF calculated adsorption isotherms was established. Just as linear diblock polymers have higher affinity for adsorption than their triblock or multi-block counterparts, the same seemed to apply for the more complex architectures. Those chains, having all hydrophobic residues concentrated in a single block, provided higher surface affinity than those with hydrophobic groups distributed in several smaller blocks. Understanding the behavioural difference of OS-starch of varying AC not only provides opportunity for further improving its functionality, but also opens possibility for customising tailored release profiles. This can be achieved by suitable mixing of multiple OS-starch emulsions, stabilised by OS- starch of disparate amylose contents.

Table of Contents

List of Tables

List of Figures

Chapter 1
General introduction

1.1 Colloids and emulsions

Colloid is a mixture of two immiscible components, where one (*i.e.* the dispersed phase) is distributed within another (*i.e.* the continuous phase) with domains in a scale ranging from 1 nm to 1 μm. Depending on the physical state of the components, colloids can be classified into various categories as listed in Table 1.1 (Hunter, 2001). In relation to foods, colloidal systems have great prevalence. Designing food colloids with desired features has always been a challenge faced by food scientists. The two types of colloids of most interest in food science are foams and emulsions. Whipped cream and beer foam are but two examples of such food foams. Emulsions in food mainly include oil-in-water (O/W) emulsion, such as salad dressings, and water in oil (W/O) type, such as butter. Food colloids can also be more complicated than just a two-phase system, as for example with ice cream, which contains emulsified fat globules, ice crystals, solid foams and an unfrozen serum phase (Gelin et al., 1994; Goff, 1997).

Table 1.1 Classification of colloids based on the physical states of its components.

Continuous phase \ Dispersed phase	Solid	Liquid	Gas
Solid	Solid dispersion	Solid emulsion	Solid foam
Liquid	Sol	Emulsion	Foam
Gas	Aerosol	Aerosol	/

1.2 Stability of colloidal systems

Food scientists have always been seeking to control the stability of colloids. Colloids are sometimes expected to stay stable throughout the shelf life of a product, whilst at other occasions they are expected to partially lose their stability under certain conditions, as in releasing flavour once orally ingested. Therefore, understanding factors influencing the stability of a

colloidal system, or those leading to its destabilisation are of crucial interest to food scientists.

1.2.1 Colloidal stability and destabilisation

By dispersing the dispersed phase in the continuous phase, a large unfavourable interfacial area is created. Associated with this there is an excess amount of free energy (Dickinson, 1992). In the process of making a colloid, surface active emulsifiers, *i.e.* surfactants and biopolymers, are required to lower the surface tension and maintain such large surface area, at least for a desired period of time. Therefore, all colloidal systems are by nature thermodynamically unstable and colloidal stability usually refers to the kinetic stability of systems (i.e. a long lived metastable state) made possible by the existence of a sufficiently large energy barrier between the colloidal and the phase separated states (Figure 1.1).
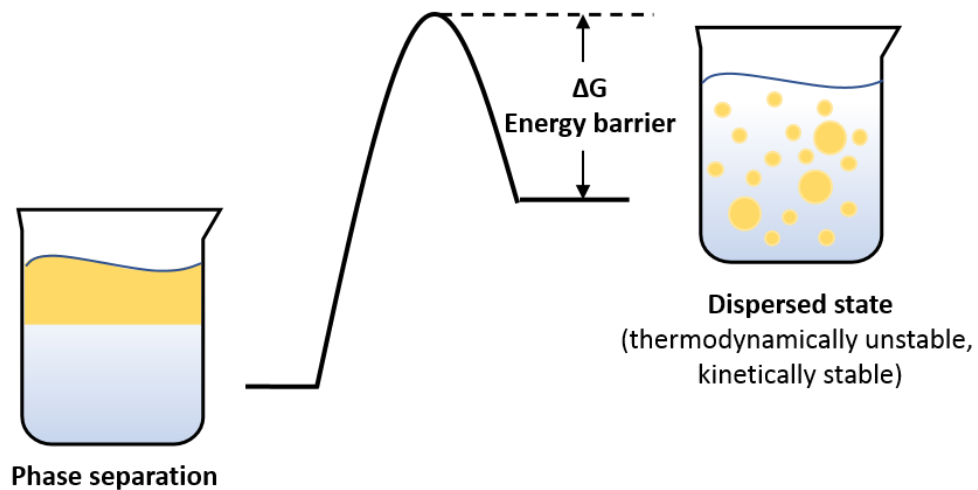
Figure 1.1 A schematic illustration of the thermodynamically stable separated phase and the kinetically stable dispersed states. A sufficiently large energy barrier between the two effectively renders the latter a long-lived metastable state.

A colloidal system is considered kinetically stable if no detectable aggregation of droplets occurs during a certain desirable amount of time (Dickinson, 1992). There are mainly three types of colloidal instabilities. One is settling or rise of droplets under the effect of gravitational force. In liquid emulsions, where this effect is referred to as creaming, over time the phase with lower density (*i.e.* oil) rises to the top and the other with higher density (*i.e.* water) settles to the bottom. The rate of creaming depends on the density difference of the two phases, as well as the size of droplets. The

second type of instability is flocculation, which refers to the aggregation of droplets by weak attractive forces. These attractive forces can have different possible origins. Van der Waals forces can cause droplets to aggregate when the repulsive forces present are not enough to counteract them. In addition, in liquid emulsions, bridging flocculation happens when two regions of one emulsifying molecule simultaneously adsorbs to two droplet surfaces. Furthermore, depletion flocculation can occur under the effect of osmotic pressure gradient created by an excess amount of dissolved polymer in the continuous phase, but its exclusion from the small gaps between the closely spaced particles. Coalescence is the third type and often the most severe form of instability. Coalescence is an irreversible process of droplets merging together, forming increasingly bigger droplets. Apart from the above modes, some colloids may also become destabilised by means of Ostwald ripening. This process refers to the situation where the larger droplets grow at the expense of smaller ones, due to transport of dispersed phase through the dispersion medium. The main factor affecting the severity of Ostwald ripening is the solubility of dispersed phase in the continuous phase (Dickinson, 1992). Therefore, its effect in most food emulsions is relatively negligible, as triglycerides are almost insoluble in water, unless emulsions are kept for periods of many months.

Van der Waals forces between two molecules might be small, but the collective attraction between two colloidal particles, each made of many molecules, become large enough to be responsible for coming together of droplets (Dickinson, 1992). They are in fact the principle attractive forces between colloidal droplets, always present and if not counteracted leading to instability. For equally sized droplets, the Van der Waals forces can be calculated as follows (Everett, 1988):

$$V_{Van\ der\ Waals} = -\frac{A_H R}{12r}$$

Where R is the radius of droplets, and r is the closest distance between them. A_H is so-called the Hamaker constant, which can be calculated as following:

$$A_H = \pi^2 \rho_i \rho_j A_{i,j}$$

where ρ_i and ρ_j are the density of materials i and j, and $A_{i,j}$ is a constant depending on the polarizability of the two materials (Dickinson and Stainsby, 1982). In order to have a stable colloid, some repulsive forces are necessary so as to balance out these ever present van der Waals attractive interactions.

1.2.2 Mechanisms of stabilisation

There are mainly two types of stabilisation mechanisms for colloidal systems: electrostatic and steric (Figure 1.2).
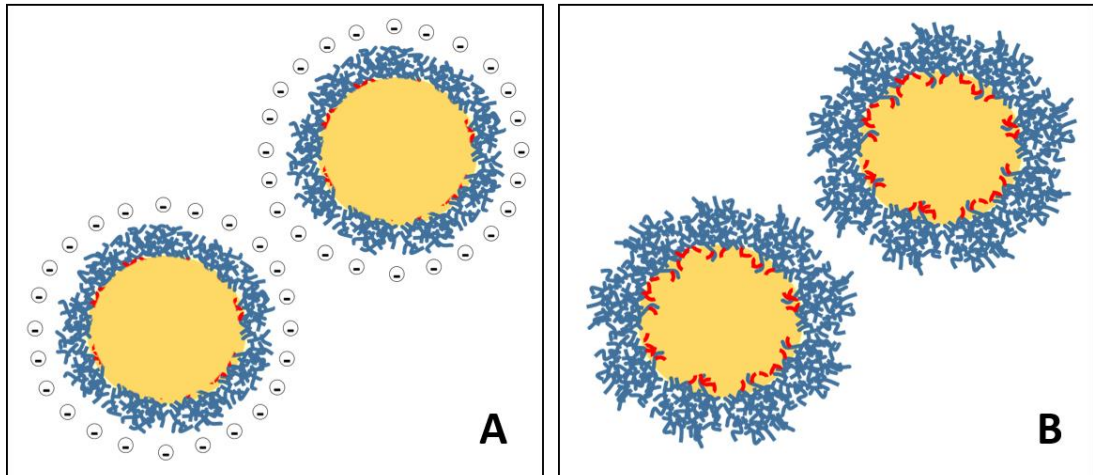
Figure 1.2 A schematic illustration of (A) electrostatic stabilisation and (B) steric stabilisation. Red entities intruding into the oil phase are hydrophobic regions of the emulsifier.

Electrostatic stabilisation exhibits among charged droplets. When a colloidal droplet with a charged surface is surrounded with solvent containing ions, an electrical double layer is induced. In a region close to the charged interface the distribution of ions is non-uniform resulting in variation of the electrical potential as one moves away from the interface (Dickinson, 1992). Charges from the adsorbed material on the surface forms the so-called inner Stern layer, which is usually densely packed. The outer part of the interfacial region is called the "diffuse layer", referring to the fact that here the ions are not bounded to the interface and the value of the electric potential drops exponentially with distance away from the surface. It is loosely packed with an excess of counter-ions and depletion of co-ions attracted or repelled to the surface by the virtue of electrical Coulombic forces. A schematic drawing of an electric double layer is provided in Figure 1.3. The extend of the double layer is indicated by the Debye length (κ^{-1}), where

$$\kappa = \sqrt{\frac{z_i{}^2 e^2 \sum n_{0i}}{\varepsilon_r \varepsilon_0 kT}}$$

Here n_{0i} is the concentration of type i ionic species in the bulk solution, z_i is its valency, e is the elementary charge (1.602 x 10^{-19} C), ε_0 is the dielectric

constant of a vacuum, and ε_r is the relative dielectric constant of the solution (Dickinson, 1992; McClements, 2015).
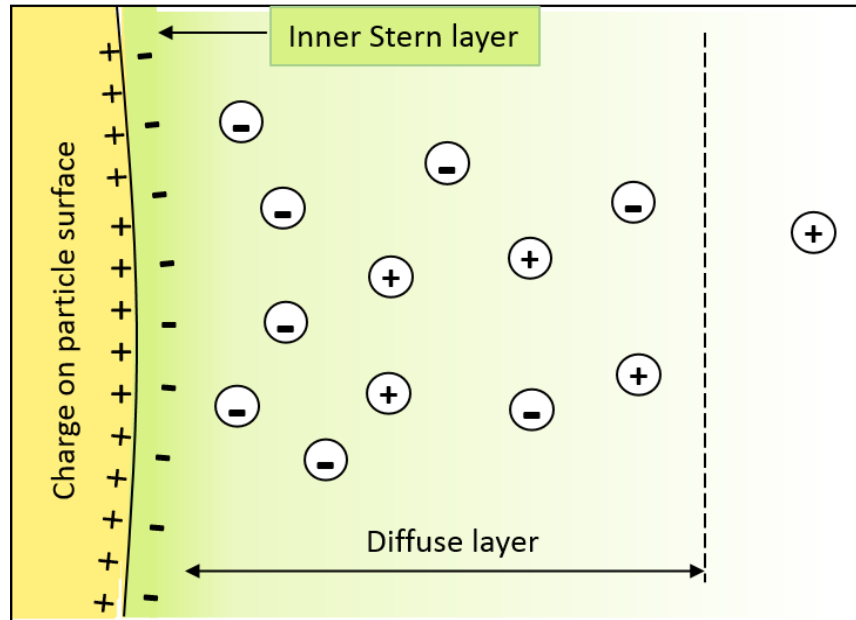
Figure 1.3 A schematic illustration of an electric double layer.

In a colloidal system, the charge of the droplets is screened by the presence of the excess counter charge in the surrounding double layer. As such, at distances large compared to Debye length, two droplets essentially see each other as electrically neutral entities. However, when two identically charged droplets approach each other closely, so as to cause the overlap of their electrical double layers, the picture alters. Now the droplets feel the charge of their neighbouring droplet and this generates a "double layer repulsion" between the two droplets, thus protecting them from flocculation and eventual coalescence (Everett, 1988). The thicker the double layer is, the longer ranged will the forces be, as the layers overlap at larger separation distances. This is more beneficial for ensuring colloidal stability and leads to larger energy barriers for droplets to overcome, when they approach each other. The thickness of an electrical double layer is primarily determined by the Debye length, and the strength of a double layer repulsion is related to surface charge density and also the salt concentration in the bulk (McClements, 2015). Therefore, a large surface charge is preferred for a stronger electrostatic repulsion, and high salt conditions would mitigate the effect of electrostatic repulsion by making such repulsion short ranged.

The second type of stabilisation is polymeric or steric stabilisation. It is induced by amphiphilic macromolecules that strongly adsorb onto the droplet surface. Consider an oil-in-water emulsion system as an example. The hydrophobic region of a macromolecule will prefer to be in the oil phase, whereas the hydrophilic region protrudes into the continuous aqueous phase. As two droplets covered by such macromolecules approach each other, the extended hydrophilic segments start to overlap, resulting in an increased local concentration of polymer in the gap between the droplets. This causes a local osmotic pressure gradient between the gap and outside which causes the continuous phase to flow into the overlapping region, thus preventing the droplets from approaching any further (Dickinson, 1992).

For such repulsive steric interaction to take place effectively, the chains need to have segments that strongly adsorb onto the surface, such macromolecules also need to have sections that extend significantly into the continuous phase. For this reason, the continuous phase needs to be a good solvent for the extended part of macromolecules, so that polymer-solvent interaction is favoured over any polymer-polymer interaction. The presence of such macromolecules on the surface of droplets leads to a large energy barrier at suitable separation distances between the droplets (Dickinson, 1992; McClements, 2015). Additionally, it is important that the surface of droplets needs to be fully covered by the adsorbed macromolecule. Partial coverage might result in a type of colloidal instability called bridging flocculation. This involves one polymer anchoring onto two neighbouring droplets, hence forming a "bridge" between them. Such behaviour only takes place with polymers that have several different hydrophobic sections on their backbone. Unfortunately, most proteins qualify as such. On the other hand, after achieving full coverage, excess amount of polymers left in the bulk solution would result in another type of aggregation. This results from the depletion of the macromolecules from the small gaps between the particles. The difference between the concentration of polymers in and outside the gap leads to an attractive inter-particle force, due to the created osmotic pressure gradient. This type of aggregation is commonly known as depletion flocculation (Asakura and Oosawa, 1954; Jenkins and Snowden, 1996).

For systems that mainly rely on electrostatic stabilisation, the overall potential energy can be described by the classic DLVO theory established by Derjaguin, Landau, Verwey, and Overbeek in the 1940s (Deraguin and Landau, 1941; Verwey, 1947). This theory assumes that the repulsive

electrostatic forces and the attractive Van der Waals forces are independent of each other and can be added at each separation distance for two droplets. A characteristic energy profile for DLVO theory is illustrated in Figure 1.4A. When the electrostatic repulsion is sufficiently large, an energy barrier develops in the droplet-droplet interaction potential. If this is sufficiently large (say 20 k_BT), it can prevent close approach of most droplets during their collisions. Rarely two droplets approach with enough kinetic energy to overcome this barrier. Thus, the rate of collisions leading to successful sticking of droplets to each other is vastly reduced, and the system can be considered colloidally stable. Note that a second energy minimum also occurs in the interaction potential. Droplets trapped in these minima can turn the colloid into a soft solid-gel-like system. However, if the electrostatic forces are weakened by high ionic strength in the medium, the energy barrier would be lowered and hence easier to overcome, resulting in a larger number of successful collisions and agglomeration of droplets (Dickinson, 1992; Adair et al., 2001).
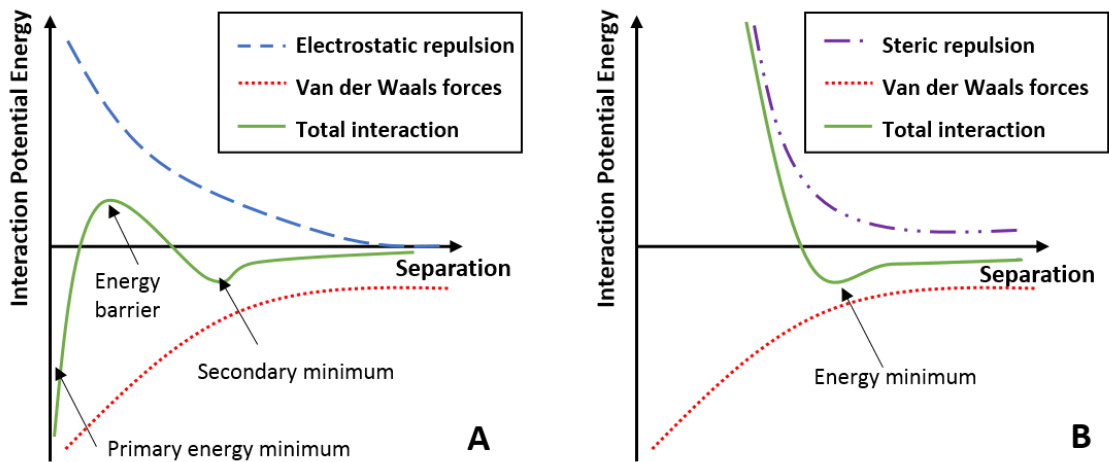
Figure 1.4 Schematic illustrations of interactions between two droplets with (A) identical electric charge as in DLVO theory and (B) identical adsorbed layer of macromolecules.

The total pair potential, potentials derived from van der Waals attractions, and either electrostatic repulsion or steric repulsion are plotted as a function of separation distance between droplets.

Similar total interaction potential profile can also be plotted for the combination of steric repulsion and attractive Van der Waals forces (Figure 1.4B). At a separation distance where the adsorbed layers start to overlap, repulsion energy increases steeply, completely overwhelming the attractive van der Waals interactions. At the distance right before the overlap, where

repulsion is still negligible but the van der Waal forces are starting to be significant, there is an energy minimum. The depth of this minimum is largely determined by the strength of VW interactions at the distance of overlap. Therefore, for it to remain small the macromolecules have to have formed a rather thick layer. The thickness of the interfacial layer formed by adsorbed macromolecule is the crucial factor for the colloidal behaviour of droplets. Unlike electrostatic repulsion, steric forces are not overly sensitive to environmental factors such as ionic strength and pH (Dickinson, 1992).

1.3 Emulsifiers and stabilisers

To produce emulsions, an emulsifier needs to adsorb quickly to the interface and to sufficiently lower the interfacial tension over the time scale of homogenization (Dickinson, 2018). To obtain a stable O/W emulsion with a reasonable shelf-life, a stabiliser needs to be present to provide enough repulsion against agglomeration or decrease the rate of droplets encountering during a desirable period of time (McClements, 2015). These are often contrasting requirements since large macromolecules, best suited to forming thick interfacial layers, also tend to have slow adsorption dynamics. However some proteins, such as sodium caseinate, seem to be able to fulfil both roles quite well, through a combination of their moderate size and provision of a sufficient combined electrostatic and steric repulsion.

1.3.1 Surfactants, biopolymers and particles

Selection of emulsifiers and stabilisers is vital for designing a colloid system with desirable stability. There are three general types of food emulsifiers: low molecular-weight surfactants, high molecular-weight biomolecules, and fine insoluble particles.

In terms of adsorption speed, it is known that the larger an emulsifier is, the slower it travels in the dispersion medium, and therefore the slower it adsorbs onto the newly created interface. Surfactants are the quickest to adsorb, allowing a rapid decrease in interfacial tension (Dickinson, 1992). However, they also detach and re-adsorb constantly and rapidly, and are not suited for providing long-term stabilisation. In comparison, despite being slower in finding their way to the interface, biopolymers do not tend to spontaneously desorb, and fine particles, which form Pickering emulsions, have even higher detachment energy once lodged on the interface. Therefore, biopolymers and particles are more advantageous at long-term stabilisation of emulsions (Dickinson, 1992). While Pickering stabilization is

most stable against coalescence, it is restricted by the size of particles. Pickering emulsion droplets usually have sizes at least an order of magnitude larger than those of the particles stabilising such droplets (Dickinson, 2012).

1.3.1.1 Biopolymers as food emulsifier

Most surface active biopolymer stabilisers currently in use are protein based (Dickinson, 2013; Wijaya et al., 2017). However, the use of proteins as emulsifiers suffers from many shortcomings, not least poor control over stability of emulsions under varying processing conditions. In the past few decades, food researchers continue to explore the possibility of utilising polysaccharides for emulsification and stabilisation, as they are an economical, versatile, and accessible resource.

Amongst the few natural polysaccharides possessing any kind of appreciable interfacial activity, Gum Arabic is probably the best-known example. As the proteinaceous component of the gum is rather low, only as much as 1-2% of the gum ends up adsorbing onto the surface of the emulsion droplets (Randall et al., 1988). This necessitates the use of a disproportionately large amount of gum Arabic (compare to other emulsifiers) in a formulation to achieve the desirable effect. One possible way of overcoming this problem has been to produce protein-polysaccharide conjugates through Millard reactions between the two biopolymers (Garti, 1999; Dickinson, 2009). Despite their various advantages, conjugates have limited use due to the difficulties in the commercialisation, arising from the relatively high cost of the dry heating manufacturing process. Another approach was to completely move away from proteins, and to improve the surface activity of polysaccharides. This is usually attempted by attaching small hydrophobic groups to the hydrocarbon backbone, making polysaccharides amphiphilic (Nilsson, Lars and Bergenståhl, 2006; Nilsson, Lars and Bergenståhl, 2007). A prominent example of such modified polysaccharides is hydrophobically modified starch, with long and bulky hydrophilic starch backbones having great potential for steric stabilisation.

1.4 OS-starch as food emulsifier

Octenyl succinic anhydride (OSA) is a proven modifying agent of starch for the purpose of emulsification, and it has legally been approved by

both the US Food and Drug Administration (FDA) and the European Food Safety Authority (EFSA). The amount of OSA is legally limited to 3 wt% of the starch (US DSA). This formulation was first discovered and patented in the United States in 1953 (Caldwell and Wurzburg, 1953). With its impressive emulsifying and stabilising properties, OSA modified starch has started to provide a viable industrial alternative to Gum Arabic (Sweedman et al., 2013).

1.4.1 Structure of OSA-modified starch

Starch, as the energy storage unit for most green plants, is a low cost abundant plant-based natural material. In plant seeds, tubers or roots, starch exists in the form of semi-crystalline granules with sizes ranging from 1 to 100 µm (Wurzburg, 1986). The two types of molecules consisting starch granules, amylose and amylopectin, are both polymers of α-D-glucose. Amylose has a mostly linear structure with α-1,4 linear linkage, while amylopectin is highly branched with α-1,4 linear linkage on the backbone and α-1,6 linear linkage at branch points (Figure 1.5). Both the size and molecular weight of amylopectin are far larger than those of amylose (Sweedman et al., 2013). Amylose has molecular weight in the order of 10^5 to 10^6 Daltons, whereas the molecular weight of amylopectin can range from 10^6 to 10^8 Daltons (Potter and Hassid, 1948; Sweedman et al., 2013).
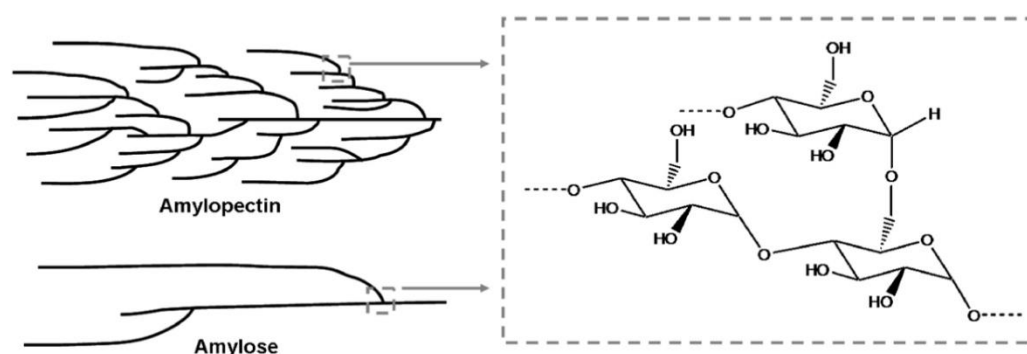
Figure 1.5 A schematic illustration of structural and chemical composition of amylose and amylopectin (Sweedman et al., 2013, p.906).

Evidence suggests that starch granules have a layered structure with a hollow central cavity, and as shown in Figure 1.6, there are pores on the surface that are connected to the central cavity through channels (Huber and BeMiller, 2000; Liu et al., 2018). In starch granules, the shorter branches (DP 10-15) of amylopectin would form helices and constitute the crystalline

region, while the longer branches and amylose mostly sit in the amorphous region.
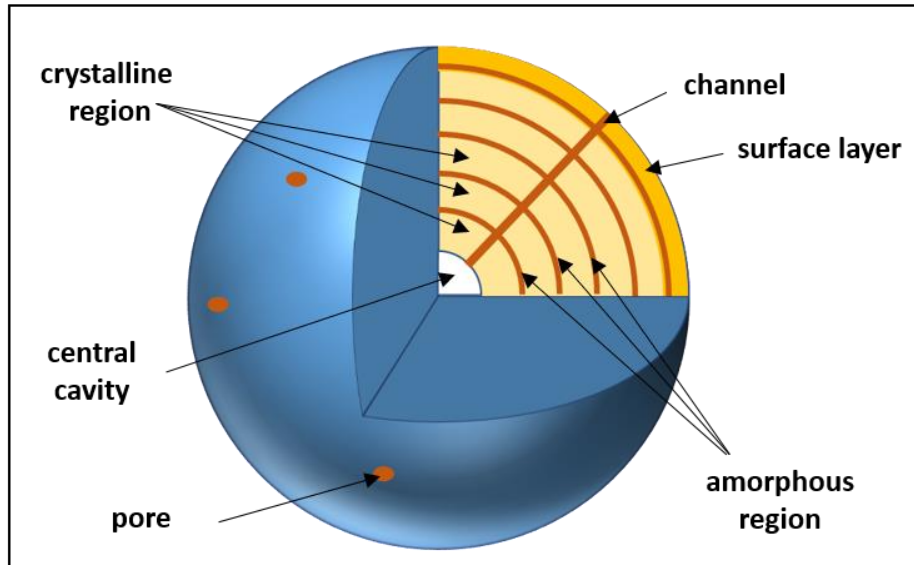
Figure 1.6 A schematic illustration of the structure of a starch granule (Adapted from Liu et al. (2018), p. 216).

The aim of OSA modification is to introduce hydrophobic groups to the native hydrophilic starch molecules, making them surface active. OSA is an acid anhydride that contains a hydrophobic octenyl group, which is an eight-carbon hydrocarbon chain. The modification process is an esterification reaction that involves partial substitution of the hydroxy groups from starch with the octenyl succinic groups, as illustrated in Figure 1.7. The resulted OSA-modified starch (or OS-starch) has a small negative charge, due to the hydrated succinic acid group.
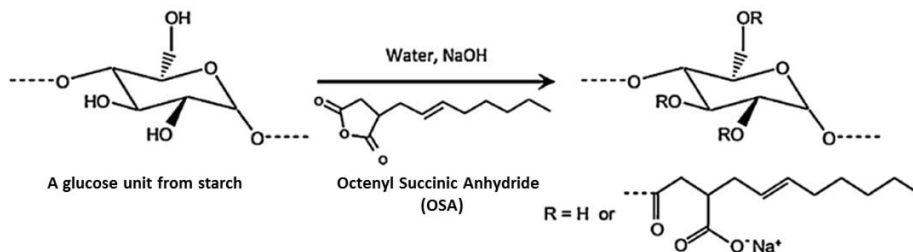
Figure 1.7 A schematic illustration of OSA modified starch structure (Adapted from Sweedman et al. (2013), p907).

The maximal level of OSA allowed by the US FDA for starch modification is 3 wt% with respect to starch. The degree of substitution (DS)

is the primary indicator of the resulting of the chemical reaction. Provided that the 3% OSA reacts fully, the degree of substitution can be estimated to be approximately 0.0231, which indicates that there are on average 0.0231 OS groups attached per glucose unit:

$$DS = \frac{n_{OSA}}{n_{glucose}} = \frac{3\% \times Mass_{starch}/MW_{OSA}}{\left(\frac{Mass_{starch}}{MW_{starch}}\right) \times \left(\frac{MW_{starch}}{MW_{glucose}}\right)}$$

$$= \frac{0.03/MW_{OSA}}{1/MW_{glucose}} = \frac{0.03 \times MW_{glucose}}{MW_{OSA}}$$

Where MW_{OSA} is the molecular weight of OSA (210.27 g/mol), and $MW_{glucose}$ is the molecular weight of an anhydrous glucose unit (162 g/mol). However, the experimentally obtained values are often lower than this theoretical value, due to incomplete reaction.

1.4.2 Advantages and applications

Even though the modification process is usually conducted on granular starch whose diameter is in microns, OSA-modified starch can also be used as an emulsifier that adsorbs at a molecular level. Once heated up above a critical temperature, starch granules start to gelatinize because the hydrogen bonds holding the granular structure are weakened. Modified amylose and amylopectin molecules get hydrated and become solubilised (Wurzburg, 1986). Through gelatinisation, a Pickering type emulsifier (modified starch granule) is transformed into biopolymers (modified amylose and amylopectin) that are capable of producing emulsions of much smaller droplet size. It has been widely reported that gelatinised OS-starch can stabilise emulsions with sub-micron droplet diameter (Chanamai and McClements, 2001; Tesch et al., 2002; Sweedman et al., 2014), while a few example of coarser Pickering emulsions fabricated using OS-starch are studies by Yusoff and Murray (2011), Song et al. (2015), Marefati et al. (2017).

Despite being slightly negatively charged, OS-starch is mostly reliant on steric repulsion for providing colloidal stability. It has been shown that an adsorbed layer of OSA modified starch can provide strong enough steric stabilization, so that the colloid system is more resistant to changes in environmental conditions, such as pH, ionic strength, and temperature (Chanamai and McClements, 2002; Tesch et al., 2002; Lin et al., 2018). Therefore, as compared to protein-based emulsifiers, OS-starch has better compatibility with a wider range of food matrices and can be applied to more complex food formulations under broader range of environmental conditions.

In fact, other than its traditional application in the beverage industry, researchers have also examined the possibility of incorporating OS-starch into fields such as encapsulation of flavours or fish oils, drug delivery systems, and moreover in personal care industries (Nair and Yamarik, 2002; Cheuk et al., 2015; Samakradhamrongthai et al., 2016; Garcia-Tejeda et al., 2018; Marto et al., 2018).

1.4.3 Research gap

Even though OS-starch has already been a successful product in the industry and has been carefully examined by researchers, there are still unresolved issues regarding its functionality and applications, owing to the high complexity in starch structure.

In recent years, an increasing number of researchers have been focusing on the granular or molecular structure of starch and its relation to the emulsifying and stabilising properties of OS-starch. Studies have been conducted to compare OS-starch from various botanical origin and cultivar, trying to relate their structural characteristics to functionalities (Nilsson, L. and Bergenstahl, 2007; Song et al., 2014). Examples of structural characteristics that has caught attention include crystallinity of granules, molecular weight, chain length, degree of branching, amylose content, and the distribution of OS groups (Song et al., 2013; Simsek et al., 2015; Wang et al., 2016; Whitney et al., 2016; Cruz-Benítez et al., 2019; Lopez-Silva et al., 2019). Among these, amylose content has the potential to be one of the most influential factors and is selected as the studied subject of a major part of this Thesis. The recent advances in relating various OS-starch structural characteristics (including amylose content) to their emulsification and stabilising properties will be reviewed more thoroughly in Chapter 2.

Even though both experimental and theoretical attempts have been made to investigate the colloidal stability of emulsions stabilised by gelatinised OS-starch of various types, there are still questions remaining to be answered regarding the role of amylose content. For example, the reasons that modified amylose and amylopectin behave differently at the interface, the possible dissimilarity of interfacial layers constituted by OS-starch of various amylose contents, the possible different colloidal behaviour of emulsions stabilised by OS-starch of various amylose contents, as well as the possible novel or enhanced applications of OS-starch because of its certain level of amylose content.

1.5 Main characterization techniques

In this study, both theoretical and experimental methods have been employed to characterise the difference between amylose and amylopectin, as well as the emulsions stabilised by OS-starch.

1.5.1 Theoretical predictions

Theoretical methods are extremely valuable especially when approaching situations that are difficult to realise in the real world. When trying to understand how polymers with different structures adsorb onto the surface, some more revealing but practically harder to realise conditions or parameters (*e.g.* theta solvent for starch) can easily be modelled theoretically.

1.5.1.1 Thermal and statistical physics

Thermal and statistical physics is the foundation of many theoretical methods including self-consistent field (SCF) theory deployed in this work. It provides a way for scientists to study the internal motion of many-body systems.

With the help from statistics, the macroscopic behaviour of a closed thermal system consisting of a great number of molecules can be investigated by accounting for the characteristics of the individual molecules. Each molecule in the system can take a large number of configurations, and the possible ways that these configurations can occur for a given state of the system is referred to as the number of "microstates". Based on the macroscopic quantities measured, such as pressure or volume, the number of such microstates can be considered as a measure of the entropy of that "macrostate", as defined below.

Macromolecules are constantly performing Brownian motion and changing from one microstate to another. Assuming that the possibility of visiting each microstate is the same (ergodic theorem), then the macrostate with overwhelmingly more microstates (highest entropy) will be the one that eventually manifest itself, when equilibrium is achieved (Schroeder, 1999). From such a statistical point of view, the crucial concept of entropy (S) mentioned above has been more precisely defined as proportional to the logarithm of the number of microstates in the system:

$$S = k_B \cdot ln\Omega$$

where k_B is Boltzmann constant and Ω is the number of microstates that all correspond to a certain macrostate. That is to say, an isolated system

always ends up in equilibrium with the macrostate that has the maximum entropy, irrelevant of its initial conditions. This is the assertion of the second law of thermodynamics.

Compared to closed systems, a more realistic consideration would be an open system, which interacts with a reservoir or the rest of the surrounding. In this case, the second law of thermodynamics still applies, but now to the combined system and environment. In this case the probability (P) of finding a system in a particular microstate with energy E_i is given by the Boltzmann factor for the system, and is:

$$P_i = \frac{1}{Z} \cdot exp\left(-\frac{E_i}{k_B T}\right)$$

where T is the temperature of the system, and Z is the partition function (sum of all Boltzmann factors for all energy states). This is a crucial equation in linking thermodynamics and statistical physics (Finn, 1993). Similarly, considering all microstates associated with a macrostate (j) of energy E_j, the probability of the system being in such a macrostate is then:

$$P_{E_j} \propto \Omega_j exp\left(-\frac{E_j}{k_B T}\right) = exp\left(-\frac{F_j}{k_B T}\right)$$

Now free energy $F_j = E_j - TS_j$ is introduced to the relationship, and the macrostate with the highest probability is the one with the lowest free energy. According to these probabilities and their relationship to entropy and free energy, prediction of the equilibrium state of systems is made possible.

1.5.1.2 Self-consistent field (SCF) theory

Self-consistent field (SCF) calculations has a long history of application to polymeric systems, but was modified by Scheutjens and Fleer in a scheme now associated with their names. This allowed such calculations to be applied to complex polymers such as copolymers or polymers with complicated structures (Scheutjens and Fleer, 1979; Scheutjens and Fleer, 1980). There has also been many successful applications of this improved scheme to biopolymers, for example α_{s1}-caseins, β-casein, and also modified starch chains (Atkinson et al., 1995; Akinshina et al., 2008; Ettelaie et al., 2014a; Ettelaie et al., 2016).

The Scheutjens-Fleer scheme of SCF calculations considers two parallel flat surfaces facing each other, with a solution of polymers in the gap between them. The space in between the surfaces is divided into L layers parallel to the surfaces, and each layer is further divided into a 3D lattice (in this project a cubic lattice). All cubic sites have the same dimensions with

side length a_0, which is taken as the nominal monomer size of approximately 0.3 nm (typical size of a peptide bond, though other values can be used). All sites in the lattice need to be occupied by one of the following species present in the lattice: solvent, ions, or monomers making up the polymer chains. Solvent and ions are treated as monomeric entities here, and the same as monomers, they each occupy 1 cubic space. As the amount of these components is the same as the number of unit space they take up, in this system the concentration by number density is equivalent to the concentration by volume, i.e. volume fraction. A density profile, or a volume fraction profile is generated in the direction perpendicular to the planar surfaces (Ettelaie et al., 2008; Ettelaie et al., 2014b). A 2D schematic illustration of such a lattice system is included in Figure 1.8.
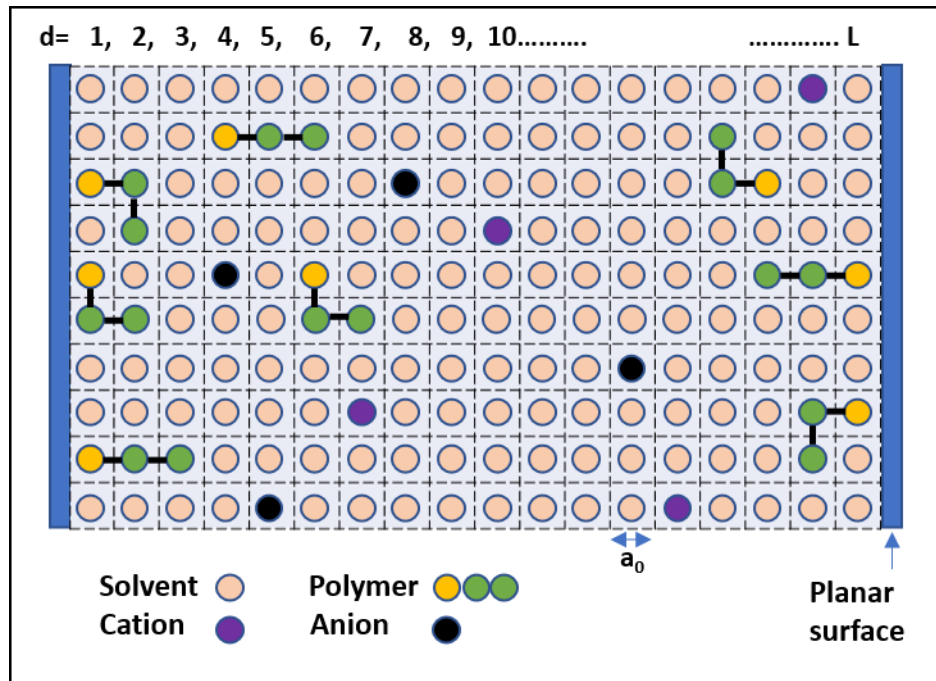
Figure 1.8 A schematic illustration of the 2D lattice model between two planar surfaces, as employed by SCF theory.

A monomer experiences many-body interactions with its neighbouring components. In the present model four of the neighbours are in the same layer as the monomer, and one each from the two adjacent layers in front and behind. The possible interactions that might arise include Van der Waals forces, electrostatic interactions, and possible volume exclusion effect. The averaged interaction generates an "effective field" around the monomer, which in terms of energy results in the potential of mean force derived from free energy. Such mean force from interacting fields decides in which layer a

certain type of monomer may prefer to sit, and determines the density profiles of all species. In turn, each density profile is associated with a free energy, establishing the probability for the occurrence of such a profile. As with all mean-field theories, SCF assumes that the density profile with the highest probability dominates and the occurrence of all others are negligible (Ettelaie et al., 2014b). In other words, any density fluctuations around this most probable density profile are ignored. Under this assumption, the free energy and potential of mean force can be calculated from this dominating density profile, if it can be determined. In dense surface layers the fluctuations in the density of adsorbed polymers in the interfacial region are small and therefore SCF provides an excellent tool to investigate the behaviour of such adsorbed polymeric films.

SCF calculations are intended to determine the most probable state for all components of the system, in other words to minimize the free energy. In order to assess free energy, the density profile is necessary. However, the density profile itself is determined by the energy potential of the net interaction. SCF theory approaches this "circular" problem with an iterative process, where it first takes a random trial set of interaction fields, and calculates the concentration profile resulted from the influence of these chosen fields. Then, based on the calculated concentration profiles just obtained, the potential of the interacting fields is calculated. The fields are used to generate new profiles and the process is repeated until the calculations converge. That is to say that the potential of mean force and the concentration profile no longer change with further iterations and "self-consistently" lead to one another. Often the process is stopped once a certain level of accuracy is achieved. With convergence, the equilibrium density profile is now obtained.

Once the components and their Flory-Huggins interaction parameters are specified, the volume fraction profile can be calculated for a range of separation distances using an in-house previously developed SCF program in Leeds University. The colloidal interaction potential as a function of surface-to-surface separation distance can also be obtained, by separately adding other more direct inter-particle interactions (e.g. Van der Waals forces) to the free energy changes calculated from SCF. For this project, the amount of polymers adsorbed at a series of manually defined bulk volume fractions is studied. The results are used to obtain Henry's adsorption constant k_H, for different chain architectures, with a view of assessing differences in adsorption behaviour of OSA modified amylose and

amylopectin at hydrophobic-hydrophilic interfaces. The study is extended to more complex structures, too (Chapter 3).

1.5.2 Experimental methods

Experimental analysis is paramount in food colloid research, especially when sourcing a new ingredient or developing a new application for the industry. In this project, various techniques are used to characterise the OS-starch produced in-house, as well as fresh or condition-treated emulsions stabilised by such OS-starch.

1.5.2.1 Amylose content

Amylose content of starch varies depending on the botanical source and cultivar. There are many techniques for determination of amylose content, including iodine colorimetry, concanavalin A precipitation, and size exclusion chromatograph (Juliano et al., 1981; Morrison and Laignelet, 1983; Yun and Matheson, 1990; Zhu et al., 2008). Among those, iodine colorimetry is by far the most frequently used method.

The linear amylose forms a deep blue complex when reacting with iodine solution. The colour intensity can be measured with a spectrophotometer (wavelength 590-720 nm), and then translated to amylose content. This provides the basis for quantitative determination of amylose content. Amylose can bind with polyiodide ions to form single left-handed V-type helices, which contains six anhydrous glucose units per turn (Morrison and Laignelet, 1983). Long chains of amylopectin also have the possibility to bind with iodine, forming a purple complex with wavelength of 530 nm. Therefore, in the methodology adopted by this project (Hoover and Ratnayake, 2001), in the effort to minimise the interference from amylopectin, a standard curve is first established with amylose and amylopectin mixtures that have amylose content of 0% to 100%. The measuring wavelength is set to 600 nm for the same purpose.

1.5.2.2 Modification of starch with OSA

Modification of starch with OSA is usually conducted on granular starch. The most widely described method involves suspending starch granules in a mild alkaline aqueous medium. Under this condition, the formation of alkoxide and hydrogen bonding between starch molecules is limited. Thus, swelling of starch granules is favoured, and the contact area of OSA molecules and starch granules are maximized (Sweedman et al., 2013). OSA is a lightly yellow, oily liquid at room temperature. It is added dropwise to the starch slurry, to enhance the reaction efficacy. In order to

keep the reaction forward, pH of the medium needs to be maintained at above 8.0 by a pH stat. After the addition of OSA is completed, usually more reaction time (from 6 h to 24 h) is allowed to enhance reaction efficiency (Bhosale and Singhal, 2006).

1.5.2.3 Degree of substitution (DS)

Degree of substitution refers to the average number of hydroxyl groups substituted per glucose unit (see Figure 1.7 for the substitution reaction and structure of modified starch). It is an important indicator for modification efficiency, and has been found to be correlated to the emulsifying capacity and ζ-potential of OS-starch (Miao et al., 2014). There has been a variety of methods for determining DS, with an analytical titration method and an instrumental method nuclear magnetic resonance (NMR) spectroscopy being the most commonly used ones.

There are two types of titration methods. To perform an alkaline titration, OS-starch is mixed with HCl to hydrolyse, and the acid product is titrated by NaOH (Mattisson and Legendre, 1952; Song et al., 2006). There is also a back titration method that saponifies the OS-starch with NaOH, and then determines the amount of excess alkali by back titration (Bhosale and Singhal, 2006). It is necessary for both titration methods to titrate a native starch sample as blank, and a relatively large sample size (3 x 5g) is required for accuracy.
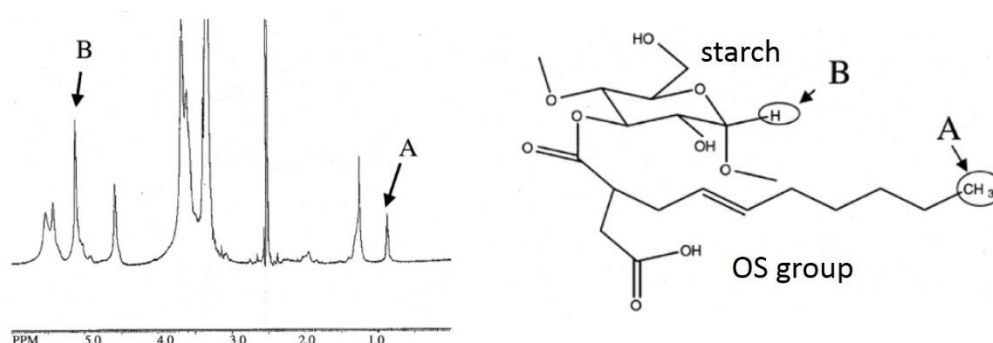
Figure 1.9 ^{1}H NMR spectrum and an illustrated structure of OS-starch (Adapted from Shih and Daigle, (2003), p.65).

^{1}H-NMR can also be used to quantify modification of OS-starch (Wang et al., 2013; Zhao et al., 2018). As OS-starch is highly polydispersed, DMSO-d6/LiBr is preferred as a better solvent than D_2O (Schmitz et al., 2009). The intensity of OS groups and starch protons can be measured and

their ratio is used to calculate the DS (Shih and Daigle, 2003).An example spectrum of OS-starch is shown in Figure 1.9. The ^{1}H-NMR method only requires a minute amount of sample (several milligrams), and no unmodified starch is needed as blank.

1.5.2.4 Static light scattering

The sizing of emulsion droplets plays an important role in assessing the quality and stability of a colloidal system. In this project, emulsion droplet size is measured via static light scattering (SLS), also known as laser diffraction, which has a measuring size range between 100 nm to 1 mm. SLS is an optical technique that measures the angular variation in the intensity of light that is scattered as a laser beam passes through a dispersed sample. When measuring, a laser is used to illuminate the sample in the cuvette, and detectors at a wide range of angles measure the scattering intensity. Large particles scatter light more strongly at small angles and small particles scatter light at larger angles. The intensity distribution is then plotted as a function of scattering angle (θ), or the so-called scattering curve. This data is analysed to create a size distribution curve, by using the Mie theory of light scattering.

Mean diameter of a particle can be expressed in many ways depending on the basis of the required distribution. The most commonly used ones are the volume mean diameter $d_{4,3}$ and the surface mean diameter $d_{3,2}$ (Horiba Scientific, 2012). They are calculated using the equations below:

$$d_{4,3} = \left(\sum n_i d_i^4 / \sum n_i d_i^3 \right)$$

$$d_{3,2} = \left(\sum n_i d_i^3 / \sum n_i d_i^2 \right)$$

Where n_i denotes the number of droplets with a diameter d_i. The $d_{4,3}$ mean diameter is more sensitive to the presence of large particles, whereas $d_{3,2}$ is a better measure of the surface area presented by the particle-solution interface, more sensitive to small particles in the system (McClements, 2015).

1.5.2.5 ζ-potential

ζ-potential is a key parameter of emulsions that indicates the strength of electrostatic repulsion between droplets (Everett, 1988). When charged droplets are dispersed in a solvent, an electric double layer is developed and an electrical potential is generated close to the surface of droplets. This ζ-

potential, also called the electrokinetic potential, is the electric potential of the interfacial double layer with reference to a position slightly inside the continuous phase away from the droplet surface. The plane at which ζ-potential is measured is also known as the shear-plane. When an electric field is applied, the droplet and all the liquid (co- and counter-) closer than this plane move in one direction. The dispersion medium further away moves in the opposite direction. For most purposes the ζ-potential is sufficiently close to the surface electric potential on the droplets. Ionic strength and the pH of the solvent are the most important factors that affect the surface potential and hence also ζ-potential.

Experimentally, ζ-potential is measured using electrophoresis.

1.5.2.6 Shear viscosity

Rheology is the study of flow and deformation behaviour of materials. For colloids, such behaviour is crucially dependent on the colloidal state of the particles. As such, rheological behaviour can also provide information on the structure and morphology of the system. In this project, the shear viscosity of OS-starch solutions and emulsions stabilised by OS-starch was measured, in the effort to understand the aggregation state of the droplets and interactions in those systems.

Fluids can be generally classified into categories based on their flow behaviour under shear. If the viscosity of a fluid does not vary with shear rate, it is known as a Newtonian fluid (such as water and honey). However, most fluids encountered in foods are non-Newtonian, meaning that their viscosity is dependent on either shear rate (shear-thinning or shear-thickening) or the history of deformation (thixotropic, and very rarely rheopectic, fluids). The behaviour of Newtonian, shear-thinning and shear-thickening fluid can be summarised by the power law model below:

$$\eta = k\dot{\gamma}^{n-1}$$

where η is viscosity, $\dot{\gamma}$ is shear rate, k is the consistency index and n is the flow behaviour index. An n value lower than 1 indicates shear-thinning type behaviour, whilst an n value higher than 1 indicates shear-thickening. When $n = 1$, the fluid is Newtonian (Dickinson, 1992; McClements, 2015).

In foods, shear-thinning is the most common type of flow behaviour encountered. In response to shear, in polymer solutions the chains deform and re-align themselves in the direction of shear, resulting in decreasing entanglement between them and hence a decrease of viscosity with increasing shear rate. In emulsions, shear-thinning behaviour arises

because of the breakup of open (sometimes called fractal) droplet aggregates. Its existence in such emulsion systems is considered as an indication of the presence of flocculation between droplets. In systems where flocs are formed due to depletion flocculation the shear thinning is particularly pronounced and occurs almost immediately, even at low shear rates, as weakly associated flocs start to breakdown under shear.

1.6 Research aims and objectives

This project aims to advance the research about OS-starch as a biopolymer emulsifier on multiple fronts. While continuously seeking the possibility for novel application of OS-starch, the project intends to systematically investigate the effect of amylose content of OS-starch on its efficacy as biopolymer emulsifiers. This work hopes to provide guidance on the selection of suitable starch for OSA modification, where the resulted OS-starch is to be employed in various food emulsions applications, including but not limited to the beverage industry. It also hopes to open up the possibility for novel applications of OS-starch, based on the discovered interfacial features, such as controlled release and fabrication of reconstitutable emulsions.

Firstly, the project pursues the fabrication of truly reconstitutable emulsions with OS-starch, proposing a new application of the emulsifier. These are dried emulsions that redisperse upon hydration with a minimal level of effort (certainly with no need for any re-homogenisation), and in an ideal case, the hydration leads to emulsions of the same size as those prior to drying, with a significant level of subsequent colloidal stability expected. The great advantage in storage and transportation of such dried, truly reconstitutable emulsions is apparent.

Apart from this new possibility for utilisation of OS-starch, the project aims to advance the understanding of the linkage between OS-starch structure and their functionalities as an emulsifier, with a focus on the effect of amylose content. On the experimental side, this work intends to systematically examine the strength of steric stabilisation provided by OS-starch of various amylose content, as provision of stronger steric interactions is a characteristic advantage of OS-starch over protein based emulsifiers. The project also seeks to provide insights into how amylose content of OS-starch might affect their application in the beverage industry, by means of *in vitro* and *in vivo* oral digestion experiments.

Lastly, in the effort to understand the origin of such differences induced by various amylose content, the problem is simplified, and a theoretical approach is taken to tackle it. The computational modelling section of the project is expected to investigate the general and fundamental differences in adsorption behaviours of amphiphilic linear and various branched polymers, of which modified amylose and amylopectin can be considered as examples. Such calculations are intended to unveil not only the variations between linear and branched structures, but also those between branched polymers of varying architecture.

1.7 An outline of Thesis

This Thesis consists of 5 further chapters. The following one includes a focused and detailed literature review of recent progress on understanding the relationship between structural characteristics of OS-starch and its efficacy on emulsification and stabilisation, positioning this project in the context of other research in the field and justifying the selection of amylose content as the independent variable for further study. The experimental part of the Thesis starts with a study investigating reconstitutable O/W emulsion stabilised with low amylose content OS-starch in the effort to explore a possible novel application, followed by the systematic examination of the colloidal behaviour of emulsions stabilised by OS-starch of various amylose contents when subjected to multiple environmental treatments. Finally, to understand why amylose content has its effect on the emulsifying and stabilising properties of OS-starch, a theoretical investigation, on a more general level, of the fundamental relation between polymer architecture of the amphiphilic chains and their adsorption behaviour is included.

In **Chapter 2**, a thorough and up-to-date literature review on the relations between OS-starch structure and its emulsifying and stabilising properties is presented. The recently examined structural characteristics of OS-starch are highlighted, and current knowledge gaps are identified.

In **Chapter 3**, the study investigated the possibility of producing reconstitutable emulsions with low amylose content OS-starch. It focused on the storage conditions of dried emulsion powder, and pin-pointed the key influencers for the long-term colloidal stability of the subsequently reconstituted emulsions, produced from such powders.

In **Chapter 4**, the effect of amylose content on the colloidal behaviours of emulsions stabilised by OS-starch was examined

experimentally. The impact of environmental stress on colloidal stability investigated here included pH and electrolyte strength variations. A preliminary oral digestion study was also included to show in principle the potential for tailoring complex flavour release profiles, using a combination of emulsion droplets stabilised by OS-starch of different amylose contents.

In **Chapter 5**, the different adsorption behaviours of amphiphilic polymers with various architecture were examined through SCF calculations. This work investigated the linear region of the Langmuir adsorption isotherm, and therefore obtained Henry's constant (k_H), calculated for each structure as an indication of their surface affinity. While the models are simpler and more general than the specific case involving OSA modified amylose and amylopectin, such theoretical study provides important insights into reasons as to why different modified starch may exhibit different interfacial behaviours.

In the final chapter, **Chapter 6**, a general discussion is provided and the main conclusions from this project are summarised.

References

Adair, J.H., Suvaci, E. and Sindel, J. 2001. Surface and Colloid Chemistry. In: Buschow, K.H.J., et al. eds. *Encyclopedia of Materials: Science and Technology.* Oxford: Elsevier, pp.1-10.

Akinshina, A., Ettelaie, R., Dickinson, E. and Smyth, G. 2008. Interactions between adsorbed layers of αS1-casein with covalently bound side chains: a self-consistent field study. *Biomacromolecules.* **9**(11), pp.3188-3200.

Asakura, S. and Oosawa, F. 1954. On interaction between two bodies immersed in a solution of macromolecules. *The Journal of chemical physics.* **22**(7), pp.1255-1256.

Atkinson, P.J., Dickinson, E., Horne, D.S. and Richardson, R.M. 1995. Neutron reflectivity of adsorbed β-casein and β-lactoglobulin at the air/water interface. *Journal of the Chemical Society, Faraday Transactions.* **91**(17), pp.2847-2854.

Bhosale, R. and Singhal, R. 2006. Process optimization for the synthesis of octenyl succinyl derivative of waxy corn and amaranth starches. *Carbohydrate Polymers.* **66**(4), pp.521-527.

Caldwell, C.G. and Wurzburg, O.B. 1953. *Polysaccharide derivatives of substituted dicarboxylic acids.* U.S. Patent 2,661,349. Dec. 1, 1953.

Chanamai, R. and McClements, D.J. 2001. Depletion Flocculation of Beverage Emulsions by Gum Arabic and Modified Starch. *Journal of Food Science.* **66**(3), pp.457-463.

Chanamai, R. and McClements, D.J. 2002. Comparison of Gum Arabic, Modified Starch, and Whey Protein Isolate as Emulsifiers: Influence of

pH, CaCl2 and Temperature. *Journal of Food Science.* **67**, pp.120-125.

Cheuk, S.Y., Shih, F.F., Champagne, E.T., Daigle, K.W., Patindol, J.A., Mattison, C.P. and Boue, S.M. 2015. Nano-encapsulation of coenzyme Q10 using octenyl succinic anhydride modified starch. *Food Chem.* **174**, pp.585-590.

Cruz-Benítez, M.M., Gómez-Aldapa, C.A., Castro-Rosas, J., Hernández-Hernández, E., Gómez-Hernández, E. and Fonseca-Florido, H.A. 2019. Effect of amylose content and chemical modification of cassava starch on the microencapsulation of Lactobacillus pentosus. *Lwt.* **105**, pp.110-117.

Deraguin, B. and Landau, L. 1941. Theory of the stability of strongly charged lyophobic sols and of the adhesion of strongly charged particles in solution of electrolytes. *Acta Physicochim: USSR.* **14**, pp.633-662.

Dickinson, E. 1992. *An Introduction to Food Colloid.* Oxford University Press.

Dickinson, E. 2009. Hydrocolloids as emulsifiers and emulsion stabilizers. *Food hydrocolloids.* **23**(6), pp.1473-1482.

Dickinson, E. 2012. Use of nanoparticles and microparticles in the formation and stabilization of food emulsions. *Trends in Food Science & Technology.* **24**(1), pp.4-12.

Dickinson, E. 2013. Stabilising emulsion-based colloidal structures with mixed food ingredients. *J Sci Food Agric.* **93**(4), pp.710-721.

Dickinson, E. 2018. Hydrocolloids acting as emulsifying agents – How do they do it? *Food Hydrocolloids.* **78**, pp.2-14.

Dickinson, E. and Stainsby, G. 1982. *Colloids in food.* Applied Science Publishers.

Ettelaie, R., Akinshina, A. and Dickinson, E. 2008. Mixed protein-polysaccharide interfacial layers: a self consistent field calculation study. *Faraday Discuss.* **139**, pp.161-178; discussion 213-128, 419-120.

Ettelaie, R., Holmes, M., Chen, J. and Farshchi, A. 2016. Steric stabilising properties of hydrophobically modified starch: Amylose vs. amylopectin. *Food Hydrocolloids.* **58**, pp.364-377.

Ettelaie, R., Khandelwal, N. and Wilkinson, R. 2014a. Interactions between casein layers adsorbed on hydrophobic surfaces from self consistent field theory: κ-casein versus para-κ-casein. *Food Hydrocolloids.* **34**, pp.236-246.

Ettelaie, R., Zengin, A. and Lee, H. 2014b. Fragmented proteins as food emulsion stabilizers: A theoretical study. *Biopolymers.* **101**(9), pp.945-958.

Everett, D.H. 1988. Why are colloidal dispersions stable? 1. Basic principles. In: Everett, D.H. ed. *Basic principles of colloid science.* London: Royal Society of Chemistry.

Finn, C.B.P. 1993. *Thermal Physics, Second Edition.* Second edition. ed. Boca Raton, FL: CRC Press.

Garcia-Tejeda, Y.V., Salinas-Moreno, Y., Barrera-Figueroa, V. and Martinez-Bustos, F. 2018. Preparation and characterization of octenyl succinylated normal and waxy starches of maize as encapsulating agents for anthocyanins by spray-drying. *J Food Sci Technol.* **55**(6), pp.2279-2287.

Garti, N. 1999. Hydrocolloids as emulsifying agents for oil-in-water emulsions. *Journal of Dispersion Science and Technology.* **20**(1-2), pp.327-355.

Gelin, J.L., Poyen, L., Courthaudon, J.L., Le Meste, M. and Lorient, D. 1994. Structural changes in oil-in-water emulsions during the manufacture of ice cream. *Food Hydrocolloids.* **8**(3), pp.299-308.

Goff, H.D. 1997. Colloidal aspects of ice cream—A review. *International Dairy Journal.* **7**(6), pp.363-373.

Hoover, R. and Ratnayake, W.S. 2001. Determination of Total Amylose Content of Starch. *Current Protocols in Food Analytical Chemistry.* pp.E2.3.1-E2.3.5

Horiba Scientific. 2012. *A guidbook to particle size analysis.* Irvin, USA: Horiba Instruments Inc.

Huber, K.C. and BeMiller, J.N. 2000. Channels of maize and sorghum starch granules. *Carbohydr Polym.* **41**, pp.269-276.

Hunter, R.J. 2001. *Foundations of colloid science.* Oxford university press.

Jenkins, P. and Snowden, M. 1996. Depletion flocculation in colloidal dispersions. *Advances in colloid and interface science.* **68**, pp.57-96.

Juliano, B., Perez, C., Blakeney, A., Castillo, T., Kongseree, N., Laignelet, B., Lapis, E., Murty, V., Paule, C. and Webb, B. 1981. International cooperative testing on the amylose content of milled rice. *Starch? St rke.* **33**(5), pp.157-162.

Lin, Q., Liang, R., Zhong, F., Ye, A. and Singh, H. 2018. Physical properties and biological fate of OSA-modified-starch-stabilized emulsions containing β-carotene: Effect of calcium and pH. *Food Hydrocolloids.* **77**, pp.549-556.

Liu, W., Li, Y., Goff, H.D., Nsor-Atindana, J. and Zhong, F. 2018. Distribution of octenylsuccinic groups in modified waxy maize starch: An analysis at granular level. *Food Hydrocolloids.* **84**, pp.210-218.

Lopez-Silva, M., Bello-Perez, L.A., Agama-Acevedo, E. and Alvarez-Ramirez, J. 2019. Effect of amylose content in morphological, functional and emulsification properties of OSA modified corn starch. *Food Hydrocolloids.* **97**.

Marefati, A., Wiege, B., Haase, N.U., Matos, M. and Rayner, M. 2017. Pickering emulsifiers based on hydrophobically modified small granular starches - Part I: Manufacturing and physico-chemical characterization. *Carbohydr Polym.* **175**, pp.473-483.

Marto, J., Pinto, P., Fitas, M., Gonçalves, L., Almeida, A. and Ribeiro, H. 2018. Safety assessment of starch-based personal care products: Nanocapsules and pickering emulsions. *Toxicology and applied pharmacology.* **342**, pp.14-21.

Mattisson, M. and Legendre, K. 1952. Determination of carboxyl content of oxidized starches. *Analytical Chemistry.* **24**(12), pp.1942-1944.

McClements, D.J. 2015. *Food emulsions: principles, practices, and techniques.* CRC press.

Miao, M., Li, R., Jiang, B., Cui, S.W., Zhang, T. and Jin, Z. 2014. Structure and physicochemical properties of octenyl succinic esters of sugary maize soluble starch and waxy maize starch. *Food Chem.* **151**, pp.154-160.

Morrison, W.R. and Laignelet, B. 1983. An improved colorimetric procedure for determining apparent and total amylose in cereal and other starches. *Journal of cereal Science.* **1**(1), pp.9-20.

Nair, B. and Yamarik, T.A. 2002. Final report on the safety assessment of aluminum starch octenylsuccinate. *International journal of toxicology.* **21**, pp.1-7.

Nilsson, L. and Bergenstahl, B. 2007. Emulsification and Adsorption Properties of Hydrophobically Modified Potato and Barley Starch. *J Agric Food Chem.* **55**, pp.1469-1474.

Nilsson, L. and Bergenståhl, B. 2006. Adsorption of hydrophobically modified starch at oil/water interfaces during emulsification. *Langmuir.* **22**(21), pp.8770-8776.

Nilsson, L. and Bergenståhl, B. 2007. Emulsification and adsorption properties of hydrophobically modified potato and barley starch. *Journal of agricultural and food chemistry.* **55**(4), pp.1469-1474.

Potter, A.L. and Hassid, W.Z. 1948. Starch. II. Molecular Weights of Amyloses and Amylopectins from Starches of Various Plant Origins. *Journal of the American Chemical Society.* **70**(11), pp.3774-3777.

Randall, R., Phillips, G. and Williams, P. 1988. The role of the proteinaceous component on the emulsifying properties of gum arabic. *Food hydrocolloids.* **2**(2), pp.131-140.

Samakradhamrongthai, R., Thakeow, P., Kopermsub, P. and Utama-Ang, N. 2016. Microencapsulation of white champaca (Michelia alba D.C.) extract using octenyl succinic anhydride (OSA) starch for controlled release aroma. *J Microencapsul.* **33**(8), pp.773-784.

Scheutjens, J. and Fleer, G. 1979. Statistical theory of the adsorption of interacting chain molecules. 1. Partition function, segment density distribution, and adsorption isotherms. *Journal of Physical Chemistry.* **83**(12), pp.1619-1635.

Scheutjens, J. and Fleer, G. 1980. Statistical theory of the adsorption of interacting chain molecules. 2. Train, loop, and tail size distribution. *The Journal of Physical Chemistry.* **84**(2), pp.178-190.

Schmitz, S., Dona, A.C., Castignolles, P., Gilbert, R.G. and Gaborieau, M. 2009. Assessment of the extent of starch dissolution in dimethyl sulfoxide by 1H NMR spectroscopy. *Macromol Biosci.* **9**(5), pp.506-514.

Schroeder, D.V. 1999. *An introduction to thermal physics.* American Association of Physics Teachers.

Shih, F.F. and Daigle, K.W. 2003. Gelatinization and pasting properties of rice starch modified with 2‐octen‐1‐ylsuccinic anhydride. *Food/Nahrung.* **47**(1), pp.64-67.

Simsek, S., Ovando-Martinez, M., Marefati, A., Sjoo, M. and Rayner, M. 2015. Chemical composition, digestibility and emulsification properties of octenyl succinic esters of various starches. *Food Res Int.* **75**, pp.41-49.

Song, X., Chen, Q.-h., Ruan, H., He, G.-q. and Xu, Q. 2006. Synthesis and paste properties of octenyl succinic anhydride modified early Indica rice starch. *Journal of Zhejiang University Science B.* **7**(10), pp.800-805.

Song, X., Pei, Y., Qiao, M., Ma, F., Ren, H. and Zhao, Q. 2015. Preparation and characterizations of Pickering emulsions stabilized by hydrophobic starch particles. *Food Hydrocolloids.* **45**, pp.256-263.

Song, X., Pei, Y., Zhu, W., Fu, D. and Ren, H. 2014. Particle-stabilizers modified from indica rice starches differing in amylose content. *Food Chem.* **153**, pp.74-80.

Song, X., Zhao, Q., Li, Z., Fu, D. and Dong, Z. 2013. Effects of amylose content on the paste properties and emulsification of octenyl succinic starch esters. *Starch - Stärke.* **65**(1-2), pp.112-122.

Sweedman, M.C., Hasjim, J., Schafer, C. and Gilbert, R.G. 2014. Structures of octenylsuccinylated starches: effects on emulsions containing beta-carotene. *Carbohydr Polym.* **112**, pp.85-93.

Sweedman, M.C., Tizzotti, M.J., Schaefer, C. and Gilbert, R.G. 2013. Structure and physicochemical properties of octenyl succinic anhydride modified starches: A review. *Carbohydrate Polymers.* **92**(1), pp.905-920.

Tesch, S., Gerhards, C. and Schubert, H. 2002. Stabilization of emulsions by OSA starches. *Journal of Food Engineering.* **54**, pp.167-174.

Verwey, E.J.W. 1947. Theory of the Stability of Lyophobic Colloids. *The Journal of Physical and Colloid Chemistry.* **51**(3), pp.631-636.

Wang, C., He, X., Fu, X., Huang, Q. and Zhang, B. 2016. Substituent distribution changes the pasting and emulsion properties of octenylsuccinate starch. *Carbohydr Polym.* **135**, pp.64-71.

Wang, C., He, X., Huang, Q., Fu, X., Luo, F. and Li, L. 2013. Distribution of octenylsuccinic substituents in modified A and B polymorph starch granules. *J Agric Food Chem.* **61**(51), pp.12492-12498.

Whitney, K., Reuhs, B.L., Ovando Martinez, M. and Simsek, S. 2016. Analysis of octenylsuccinate rice and tapioca starches: Distribution of octenylsuccinic anhydride groups in starch granules. *Food Chem.* **211**, pp.608-615.

Wijaya, W., Patel, A.R., Setiowati, A.D. and Van der Meeren, P. 2017. Functional colloids from proteins and polysaccharides for food applications. *Trends in Food Science & Technology.* **68**, pp.56-69.

Wurzburg, O.B. 1986. *Modified starches-properties and uses.* Boca Raton: CRC Press Inc.

Yun, S.H. and Matheson, N.K. 1990. Estimation of amylose content of starches after precipitation of amylopectin by concanavalin‐A. *Starch‐Stärke.* **42**(8), pp.302-305.

Yusoff, A. and Murray, B.S. 2011. Modified starch granules as particle-stabilizers of oil-in-water emulsions. *Food Hydrocolloids.* **25**(1), pp.42-55.

Zhao, S., Tian, G., Zhao, C., Lu, C., Bao, Y., Liu, X. and Zheng, J. 2018. Emulsifying stability properties of octenyl succinic anhydride (OSA) modified waxy starches with different molecular structures. *Food Hydrocolloids.* **85**, pp.248-256.

Zhu, T., Jackson, D.S., Wehling, R.L. and Geera, B. 2008. Comparison of amylose determination methods and the development of a dual wavelength iodine binding technique. *Cereal Chemistry.* **85**(1), pp.51-58.

Chapter 2
Relating structure to functionality: a literature review on OSA-modified starch

Abstract

OSA esterified starch gains amphiphilic properties and is an excellent biopolymer-based emulsifier. Researchers have always been interested in improving its functional properties as a food-grade emulsifier and investigating the fundamental influencers of its structure on its functionality. In recent years, increasing number of studies reported in literature have focused on elucidating the relation between OS-starch structure and its physiochemical properties. This review identifies four key structural features of OS-starch (namely, granule size, degree of branching, molecular weight, and amylose content), and reports on the most recent progress in relating these attributes to the emulsification properties of OSA modified starch. In general, small granule starch is expected to be favoured by OSA esterification due to its larger surface-area-to-volume ratio. Investigation on degree of branching and molecular weight often involves hydrolysis of a parent starch in order to obtain a gradient of the interested variable. Study on the effect of amylose is limited to naturally occurring starch types. Because of the sophisticated structure of starch, its structural characteristics are largely intertwined with each other. The greatest challenge in researching the relation between OS-starch structure and functionality remains selecting appropriate subjects of study, which have one structural feature in a proper gradient, whilst the others are maintained to be the same and uniform.

2.1 Introduction

As the main energy storage unit in plants, starch is regarded as a renewable, economical, and abundant resource. In food industry in particular, starch and starch derivatives have drawn increasing level of attention as potential functional ingredients. Octenyl succinic anhydride (OSA) has been extensively used to modify starch since it was first patented by Caldwell and Wurzburg (1953). After the esterification with OSA, starch of original hydrophilic nature becomes amphiphilic and gains emulsifying properties, resulting from the introduction of the small hydrophobic chains to its

structure. As legally permitted by the Food and Drug Administration of the US for emulsification in foods, OSA-modified starch has been proven to maintain high colloidal stability of emulsion droplets through provision of steric stabilisation. This is especially notable for systems at acidic pH and high electrolyte concentration, which makes OS-starch more suitable for many complex food formulations, when compared to protein-based food emulsifiers (Chanamai and McClements, 2002). The maximal amount of OSA allowed is currently 3 wt% in respect of the amount of starch (FDA, 2020).

For many years, researchers have been actively working on understanding the structure of OSA-modified starch, improving its functionality, and finding new applications. The esterification methods, improvements of those methods and structural characterisations of OSA-modified starch have been reviewed in great detail by Sweedman et al. (2013), and Altuna et al. (2018). The general purpose of modifying the esterification methods has been to increase OSA accessibility to the hydroxyl groups in starch molecules, so that a higher reaction efficiency can be reached (Altuna et al., 2018).

In this review, we would like to focus on the link between structural features of starch (namely granular size, degree of branching (DB), chain length distribution, and amylose content) and the emulsifying efficacy of their corresponding OSA-modified starch. This needs to be differentiated from the change in these features induced by the modification reaction, which has been reviewed in the paper by Altuna et al. (2018). Native starch undergoes structural changes during the esterification process. Inspection of such changes involves structural characterisation of both the native and the corresponding OSA-modified starch, followed by comparison of those values prior to and post OSA modification. On the other hand, in the scope of this review, usually multiple OSA-modified starches distinctive in one of the structural features are examined for their emulsification properties. Characterisation of such features can be conducted either before or after OSA modification, since the changes induced by the modification reaction are often considered relatively small as compared to the distinctions between samples, as revealed by the articles of Sweedman and co-workers (Sweedman et al., 2013; Sweedman et al., 2014a; Simsek et al., 2015).

This review identifies several key structural features that have been critically investigated with regards to their effect on the emulsifying performance of the resulted OS-starch.

2.2 Structural Characteristics of OS-starch

The structural characteristics of starch are largely dependent on its botanic origins (species and cultivars). In the current short review, both structural features on granular level (granule size) and those on molecular level (i.e. degree of branching, amylose content) are considered. Due to the requirement to consider features on molecular scale, most of the research work referenced here had conducted emulsification using gelatinised OS-starch, as opposed to OS-starch particles, unless indicated otherwise. The latter leads to emulsions that are of Pickering type and are not the main focus here.

2.2.1 Granule size

The esterification with OSA is most conventionally and most commonly conducted on starch granules in aqueous environment, and OSA attachment has been found to occur preferentially in the surface amorphous region of the granules (Shogren et al., 2000; Whitney et al., 2016; Liu et al., 2018). Thus, naturally granule sizes of starches have been examined for possible influence on reaction efficiency. Small granule starches are of particular interest due to their larger surface-area-to-volume ratio (Wang et al., 2016; Yao et al., 2020). Fine structures of amylopectin and granule crystallinity were found to correlate with granule size (Tang et al., 2001; Noda et al., 2005). Overall, starch of smaller granule sizes is expected to possess fine structural features, and be more beneficial for OSA modification.

As listed in Table 2.1, comparisons between naturally occurring starch of various granule sizes have been conducted on the emulsifying properties of their OSA-modified products. Yao et al. (2020) and Timgren et al. (2013) studied a group of fine starch granules (rice, maize, quinoa etc.) and compared them to starch of waxy maize origin with large granules. Yao et al (2020) focused on polymer-stabilised emulsion, and OSA modification induced greater changes in emulsification ability and emulsion stability for starches possessing small granules than those with larger ones. OS-starch comprising of small granules was associated with a higher emulsifying power, but found to have comparable emulsion stabilising capacity as that of larger granular starch. On the other hand, even as a Pickering emulsifier, starch with smaller granules were also found to be advantageous (Timgren et al., 2013).

Table 2.1 Relation between granule size and emulsification properties of OS-starch in recent literature.

Botanical source	Granule size	DS (3% modification)	Emulsification properties	Reference
amaranth and waxy maize	amaranth starch 1.71 µm, waxy maize 15.44 µm	waxy maize 0.0066 ± 0.0003, amaranth 0.0073 ± 0.0004	OS-starch of small granules had better emulsifying ability, but comparable stabilisation power than that of large granule starch	Yao et al. (2020)
rice, waxy rice, maize, waxy maize, high-amylose maize (Hylon VII), waxy barley, and quinoa	2 ~ 17 µm	/	OS-starch granules with smaller sizes produce more stable Pickering emulsion	Timgren et al. (2013)
potato	> 30 µm, 15–30 µm, and < 15 µm	0.0147 ~ 0.0219	/	Wang et al. (2016)

Caution is needed when selecting and comparing starch of various botanical sources, as they most often differ in more than one parameter. For example, the small granule starch samples in Yao et al. (2020), where granule size varies from 1.71 to 8.62 µm, had distinctive amylose content, ranging from 0.28% to 29.8%. Among the five smaller granule starches studied, amaranth starch had the most similar amylose content and largest disparity in granule size in comparison to the reference, i.e. waxy maize starch. Therefore, this pair of starch listed in Table 2.1, was considered suitable for the purpose of the comparative study of Yao et al. (2020). In order to obtain starch with a gradient of granule sizes, yet having similar microstructures and compositions, Wang et al. (2016) managed to separate a batch of potato starch into three categories based on the granule size. Emulsification properties was not assessed in this study, but based on the degree of substitution, starch with smaller granule size was more reactive with OSA, possibly due to their higher surface-area-to-volume ratio, as suggested by the authors.

2.2.2 Degree of branching (DB) and molecular weight (MW)

The microstructure of starch molecules is largely dependent on genetic variations. Hydrolysis has been widely employed in examining the fine structural parameters, such as the degree of branching (DB) and the

chain length. Thus, by using the same parent starch, starch with a gradient of DB can be created.

Table 2.2 Relation between degree and substitution (DB) and emulsification properties of OS-starch in recent literature

Botanical source	Hydrolysis method	DB	DS (3% modification)	Emulsification properties	Reference
waxy maize	Isoamylase, α-amylase, β-amylase, HCl	3.6% ~ 6.3%	0.007 ~ 0.036	OS-starch with higher DB tended to produce more stable emulsions, with smaller droplet size	Han et al. (2019)
waxy maize	β-amylase	4.36 ~ 13.04 %	0.0184 ~ 0.0349	OS-starch with higher DB can make more stable emulsions.	Xu et al. (2015)
waxy sorghum and waxy maize	acid hydrolysis prior to OSA modification, β-amylase or pullulanase after modification	1.81 ~ 7.45%	0.0121 ~ 0.0211	OS-starch with increased DB was not found advantageous.	Sweedman et al. (2014b)
waxy maize	Isoamylase, α-amylase, β-amylase, HCl	4.79 ~ 6.69%	0.019 ~ 0.027	molecular size is the dominant factor in emulsion droplet size, not substructures such as average chain length or DB. OS-starch with longer branch tended to form more stable	Zhang, H. et al. (2018)
rice	pullulanase	/	OSA 0.0138; DBOS 0.0195; OSDB 0.0110	Emulsion made with DBOS had smaller d_{32} droplet size than that with OSA, and emulsion made with OSDB was found with larger d_{43} than that with OSA.	Jain et al. (2019)

Most commonly, a highly branched parent starch is taken and hydrolysed by either acid or enzymes such as α-amylase, β-amylase, pullulanase, and isoamylase (Table 2.2). Among the hydrolysis method used, pullulanase and isoamylase achieve the debranching purpose by hydrolysing the α-1,6 bonds, resulting in a decrease in DB value and MW. Under the action of acid, α-amylase and β-amylase on the other hand, the branch chains are only shorten, resulting in increased DB and decreased MW.

The study by Han et al. (2019) revealed that a pre-treatment by β-amylase prior to debranching by isoamylase gave higher DB and DS than that by α-amylase and HCl. It was found that DB is positively correlated to emulsion stabilising ability, regardless hydrolysis method. The same correlation was found by Xu et al. (2015) with only β-amylase as the cleaving enzyme. However, Sweedman et al. (2014b) and Zhang, H. et al. (2018) concluded differently. In Sweedman et al. (2014b), prior to the OSA

esterification, both waxy sorghum and waxy maize were pre-treated by acid hydrolysis, which has been suggested as a way of controlling the size of resultant molecules (Tizzotti et al., 2013). After OSA modification, β-amylase or pullulanase was introduced to further hydrolyse the samples, but increased DB did not lead to better emulsification properties. Zhang, H. et al. (2018) carried out hydrolysis and debranching in the same order as Han et al. (2019). In this study, DB was not seen to be a major influencer on the emulsifying ability. Obtaining a gradient of DB by hydrolysing a parent starch induces changes to other structural characteristics, such as molecular weight and chain length distribution. Both Zhang, H. et al. (2018) and Sweedman et al. (2014b) suggested that examining one substructure such as DB alone could be misleading, as it could be less important than other structural features also altered in the process. The order of debranching and OSA esterification was examined by Jain et al. (2019). No specific DB values were given, but the order of treatment was found significant to the emulsifying properties of resultant OS-starch. The modification that was conducted first had the larger impact in such dual modification process.

Table 2.3 Relation between molecular weight (MW) and emulsification properties of OS-starch in recent literature

Botanical source	Hydrolysis method	Molecular weight	DS (3% modification)	Emulsification properties	Reference
waxy corn	HCl	peak of molecular weight distribution decreased from 10^8 to 10^5 g/mol	0.0152 ~ 0.0129	OS-starch with lower molecular weight tend to form more stable emulsions, even though with wider droplet size distributions	Hong et al. (2017)
waxy maize	β-amylase	2.0×10^5 Da; 1.282×10^5 Da; 8.95×10^4 Da; 2.21×10^4 Da; 1.41×10^4 Da	/	Medium molecular weight OSA-modified starch (8.95×10^4) was found with the highest naringin encapsulated content	Xiang et al. (2021)
waxy corn	α-amylase	1.257×10^6 ~ 1.577×10^8 Da	/	OS-starch of smaller molecular weight had better emulsification properties, but OS-starch of molecular weight that were too low are not able to form emulsions at all.	Li, Z. et al. (2014)

More branching, especially long branches, is expected to provide better steric stabilisation (Tesch et al., 2002). Such structure is bound to have higher molecular weight than those with less and shorter branches. The effect of molecular weight on emulsification is often studied by acid or

enzymatic hydrolysis as well. Acid, α-amylase, and β-amylase were all effective in creating a MW gradient ranging at least one order of magnitude (Table 2.3). Lower MW OS-starch formed emulsions with wider droplet size distribution, but higher stability (Hong et al., 2017). Li, Z. et al. (2014) also linked smaller MW to better emulsification properties, but also suggested that molecules that were hydrolysed to too small a size were not able to form emulsions at all. Extensive MW reduction lowers the chain size, and therefore might affect the degree of OSA substitution (Han et al., 2019), as well as reduce the potential to make thick interfacial layers and sufficient steric forces. The MW of hydrolysed starch in the above two studies both ranged from $10^6 \sim 10^8$ Da. In a study involving a smaller size range ($10^4 \sim 10^5$ Da), OS-starch of medium molecular weight had the highest efficiency for encapsulation applications (Xiang et al., 2021).

2.2.3 Amylose content (AC)

Amylose and amylopectin, the two types of molecules in starch, have naturally distinctive structures. Amylose is a mostly linear glucose polymer with α-1,4-linkage ($\sim 10^6$ Da), and amylopectin is a highly branched polymer with α-1,6-linkage at the branch points ($\sim 10^8$ Da) (Potter and Hassid, 1948; Sweedman et al., 2013). Such structural differences result in them having largely disparate gelatinisation, retrogradation and gelling properties, as well as susceptibility for digestion by enzymes (Wurzburg, 1986; Bean et al., 2019). Therefore, the properties of starch are quite likely linked with its amylose content (AC). Recently, high amylose starch has been associated with resistant starch and often examined as a potential calory-reducing ingredient (Li, X. et al., 2012; Bajaj et al., 2019; Jain et al., 2019).

When examining the distribution of OS groups within the starch granule, multiple studies found that the substitution mainly occurs in the amorphous region of the granules, with the surface being most strongly modified (Shogren et al., 2000; Whitney et al., 2016; Liu et al., 2018). Studies showed that apart from the surface layer, OSA was also capable of accessing the interior of starch granules through the pores on the surface and channels (Huber and BeMiller, 2000; Liu et al., 2018). This indicates that amylose molecules and the long branches of amylopectin, which constitute the amorphous region, are possibly the main receptors for OS groups in modified starch (Shogren et al., 2000; Wang et al., 2013; Whitney et al., 2016; Liu et al., 2018).

Many studies found that AC of OS-starch is negatively correlated to its emulsion stabilising ability (Table 2.4). Cheng et al. (2021) examined three starch from varying botanical sources. Even though DS did not change with varying AC, OS-starch with lower AC had more superior emulsion stabilising ability. Enhanced emulsion stability was also reported with lower AC in some

Table 2.4 Relation between amylose content (AC) and emulsification properties of OS-starch in recent literature

Botanical source	AC	DS (3% modification)	Assessment of emulsification properties	Emulsification properties	Reference
pea, normal corn, waxy corn	41.5%, 32.9%, 1.7%	0.0154 ± 0.0017, 0.0149 ± 0.0005, 0.0160 ± 0.0005	creaming index during storage, pH, and electrolyte variation	Emulsion stability order: OS-pea starch < gum Arabic ≤ OS-normal corn starch < OS-waxy corn starch.	Cheng et al. (2021)
waxy maize, normal corn	5.48%, 28.37%	0.0160, 0.0229	pH and electrolyte variation, *in vitro* and *in vivo* α-amylase digestion	low AC OS-starch formed emulsion with stronger steric stabilisation, but faster enzymatic degradation	Mu et al. (2021)
Japonica rice	33.3%, 18.8%	0.0177, 0.2250	creaming index during storage, in vitro digestion (α-amylase and amyloglucosidase)	OSA-starch with higher amylose contents had comparable emulsification properties as the normal corn starch	Zhang, W. et al. (2021)
waxy and non-waxy japonica rice	0%, 7–33%	0.0262, 0.0258	creaming index, oil adsorption capacity	OSA-modified waxy rice starch had lower creaming index than modified non-waxy rice starch.	No et al. (2019)
waxy, normal, and high-amylose maize	/	0.0103 ~ 0.0174	Color change of emulsion during storage, emulsion droplet size, and emulsion phase separation	OS-starch with low AC and high DB formed emulsion with the best stability.	Sweedman et al. (2014a)
indica rice	1.65% ~ 27.15%	0.0212 ~ 0.0252	emulsion droplet size distribution, phase separation during storage, florescence microscopy	No strong correlation was found between AC of OS-starch and the stability of emulsions that they stabilised.	Song et al. (2013)
indica rice	0% ~ 39.6%	0.024 to 0.030	/	/	He et al. (2006)
waxy, normal and Hylon VII corn starches	5.43%, 25.16%, 65.84%	0.0103, 0.0112, 0.0125	emulsion droplet size during storage, creaming stability	lower amylose content gives the best emulsion stability	Lopez-Silva et al. (2019)

studies involving starch from the same species, but different cultivar (Sweedman et al., 2014a; No et al., 2019). In the study by Song et al. (2013), stable emulsions with droplet sizes ranging from 1 to 2 μm were produced with gelatinised modified rice starch of various amylose contents. However, no connection was reported between AC of OS-starch and the stability of the emulsion.

Even though amylose might preferentially react with OSA, the stability of emulsion mainly depends on the repulsive interactions between droplets, and not necessarily the number of anchoring groups. For OS-starch, the characteristic stabilisation mechanism is mainly through provision of steric repulsive forces (Sweedman et al., 2013). As illustrated by Mu et al. (2021), OS-starch with lower AC provided stronger steric repulsion, but its interfacial layer was more prone to rapid digestion by α-amylase. With the same focus on steric repulsion, numerical Self-Consistent Field (SCF) calculations were conducted by Ettelaie et al. (2016) on modelled amylose and amylopectin molecules. Branched amylopectin was found to form a more compact interfacial film, while linear amylose had a more extended surface layer. The authors also reported that interfacial layer formed by amylose was more prone to bridging flocculation due to its extended nature, when coupled with the none specific, random distribution of hydrophobes along the chains. Despite extensive studies and respective findings on the relation of AC and emulsion stability so far, the exact mechanism for such behaviour of OS-starch interfacial layers still remains open to further exploration.

2.3 Conclusion

As many researchers point out, starch itself is a rather complex system. Many of the above discussed features intertwine and act together to influence the emulsification and stabilisation properties of the resultant OS-starch. In this short review, a few important structural features were highlighted, and recent progress on unveiling the relationship between these features and the emulsifying properties of OS-starch was carefully examined. The investigation of the impact of granule size has mostly involved comparing starch from different botanical origins, unfortunately also introducing other uncontrolled structural parameters. Similarly, examination of DB and MW parameters have heavily depended on acid or enzymatic

hydrolysis, while studies on the impact of AC have largely been restricted by the natural presence of starch of varying AC for the same botanical species. Isolating one structural feature and controlling other variables remains the largest challenge in deciphering the relation between specific structural traits of OS-starch and their functionality.

Reference

Altuna, L., Herrera, M.L. and Foresti, M.L. 2018. Synthesis and characterization of octenyl succinic anhydride modified starches for food applications. A review of recent literature. *Food Hydrocolloids.* **80**, pp.97-110.

Bajaj, R., Singh, N. and Kaur, A. 2019. Properties of octenyl succinic anhydride (OSA) modified starches and their application in low fat mayonnaise. *Int J Biol Macromol.* **131**, pp.147-157.

Bean, S., Zhu, L., Smith, B.M., Wilson, J.D., Ioerger, B.P. and Tilley, M. 2019. Starch and protein chemistry and functional properties. *Sorghum and Millets.* pp.131-170.

Caldwell, C.G. and Wurzburg, O.B. 1953. *Polysaccharide derivatives of substituted dicarboxylic acids.* U.S. Patent 2,661,349. Dec. 1, 1953.

Chanamai, R. and McClements, D.J. 2002. Comparison of Gum Arabic, Modified Starch, and Whey Protein Isolate as Emulsifiers: Influence of pH, CaCl2 and Temperature. *Journal of Food Science.* **67**, pp.120-125.

Cheng, F., Ai, Y. and Ghosh, S. 2021. Utilization of octenyl succinic anhydride-modified pea and corn starches for stabilizing oil-in-water emulsions. *Food Hydrocolloids.* **118**, p106773.

Ettelaie, R., Holmes, M., Chen, J. and Farshchi, A. 2016. Steric stabilising properties of hydrophobically modified starch: Amylose vs. amylopectin. *Food Hydrocolloids.* **58**, pp.364-377.

FDA. 2020. *Food‐starch modified.* [Online]. [Accessed 10th May, 2021]. Available from: https://www.accessdata.fda.gov/scripts/cdrh/cfdocs/cfcfr/CFRSearch.cfm?fr=172.892

Han, H., Zhang, H., Li, E., Li, C. and Wu, P. 2019. Structural and functional properties of OSA-starches made with wide-ranging hydrolysis approaches. *Food Hydrocolloids.* **90**, pp.132-145.

He, G., Song, X., Ruan, H. and Chen, F. 2006. Octenyl Succinic Anhydride Modified Early Indica Rice Starches Differing in Amylose Content. *Journal of Agricultural and Food Chemistry.* **54**, pp.2775-2779.

Hong, Y., Li, Z., Gu, Z., Wang, Y. and Pang, Y. 2017. Structure and emulsification properties of octenyl succinic anhydride starch using acid-hydrolyzed method. *Starch - Stärke.* **69**(1-2), p1600039.

Huber, K.C. and BeMiller, J.N. 2000. Channels of maize and sorghum starch granules. *Carbohydr Polym.* **41**, pp.269-276.

Jain, S., Winuprasith, T. and Suphantharika, M. 2019. Design and synthesis of modified and resistant starch-based oil-in-water emulsions. *Food Hydrocolloids.* **89**, pp.153-162.

Li, X., Zhang, P., Chen, L., Xie, F., Li, L. and Li, B. 2012. Structure and colon-targeted releasing property of resistant octenyl succinate starch. *Food Research International.* **47**(2), pp.246-252.

Li, Z., Hong, Y., Gu, Z., Tian, Y., Li, Z. and Cheng, L. 2014. Emulsification properties of enzymatically treated octenyl-succinic anhydride starch. *Starch - Stärke.* **66**(11-12), pp.1089-1095.

Liu, W., Li, Y., Goff, H.D., Nsor-Atindana, J. and Zhong, F. 2018. Distribution of octenylsuccinic groups in modified waxy maize starch: An analysis at granular level. *Food Hydrocolloids.* **84**, pp.210-218.

Lopez-Silva, M., Bello-Perez, L.A., Agama-Acevedo, E. and Alvarez-Ramirez, J. 2019. Effect of amylose content in morphological, functional and emulsification properties of OSA modified corn starch. *Food Hydrocolloids.* **97**.

Mu, M., Karthik, P., Chen, J., Holmes, M. and Ettelaie, R. 2021. Effect of amylose and amylopectin content on the colloidal behaviour of emulsions stabilised by OSA-Modified starch. *Food Hydrocolloids.* **111**, p106363.

No, J., Mun, S. and Shin, M. 2019. Properties and Digestibility of Octenyl Succinic Anhydride-Modified Japonica-Type Waxy and Non-Waxy Rice Starches. *Molecules.* **24**(4).

Noda, T., Takigawa, S., Matsuura-Endo, C., Kim, S.-J., Hashimoto, N., Yamauchi, H., Hanashiro, I. and Takeda, Y. 2005. Physicochemical properties and amylopectin structures of large, small, and extremely small potato starch granules. *Carbohydrate Polymers.* **60**(2), pp.245-251.

Potter, A.L. and Hassid, W.Z. 1948. Starch. II. Molecular Weights of Amyloses and Amylopectins from Starches of Various Plant Origins. *Journal of the American Chemical Society.* **70**(11), pp.3774-3777.

Shogren, R.L., Viswanathan, A., Felker, F. and Gross, R.A. 2000. Distribution of Octenyl Succinate Groups in Octenyl Succinic Anhydride Modified Waxy Maize Starch. *Starch/Stärke.* **52**, pp.196-204.

Simsek, S., Ovando-Martinez, M., Marefati, A., Sjoo, M. and Rayner, M. 2015. Chemical composition, digestibility and emulsification properties of octenyl succinic esters of various starches. *Food Res Int.* **75**, pp.41-49.

Song, X., Zhao, Q., Li, Z., Fu, D. and Dong, Z. 2013. Effects of amylose content on the paste properties and emulsification of octenyl succinic starch esters. *Starch - Stärke.* **65**(1-2), pp.112-122.

Sweedman, M.C., Hasjim, J., Schäfer, C. and Gilbert, R.G. 2014a. Structures of octenylsuccinylated starches: Effects on emulsions containing β-carotene. *Carbohydrate polymers.* **112**, pp.85-93.

Sweedman, M.C., Schafer, C. and Gilbert, R.G. 2014b. Aggregate and emulsion properties of enzymatically-modified octenylsuccinylated waxy starches. *Carbohydr Polym.* **111**, pp.918-927.

Sweedman, M.C., Tizzotti, M.J., Schaefer, C. and Gilbert, R.G. 2013. Structure and physicochemical properties of octenyl succinic anhydride modified starches: A review. *Carbohydrate Polymers.* **92**(1), pp.905-920.

Tang, H., Ando, H., Watanabe, K., Takeda, Y. and Mitsunaga, T. 2001. Physicochemical properties and structure of large, medium and small

granule starches in fractions of normal barley endosperm. *Carbohydrate Research.* **330**(2), pp.241-248.

Tesch, S., Gerhards, C. and Schubert, H. 2002. Stabilization of emulsions by OSA starches. *Journal of Food Engineering.* **54**, pp.167-174.

Timgren, A., Rayner, M., Dejmek, P., Marku, D. and Sjöö, M. 2013. Emulsion stabilizing capacity of intact starch granules modified by heat treatment or octenyl succinic anhydride. *Food Science & Nutrition.* **1**(2), pp.157-171.

Tizzotti, M.J., Sweedman, M.C., Schäfer, C. and Gilbert, R.G. 2013. The influence of macromolecular architecture on the critical aggregation concentration of large amphiphilic starch derivatives. *Food Hydrocolloids.* **31**(2), pp.365-374.

Wang, C., He, X., Huang, Q., Fu, X., Luo, F. and Li, L. 2013. Distribution of octenylsuccinic substituents in modified A and B polymorph starch granules. *J Agric Food Chem.* **61**(51), pp.12492-12498.

Wang, C., Tang, C., Fu, X., Huang, Q. and Zhang, B. 2016. Granular size of potato starch affects structural properties, octenylsuccinic anhydride modification and flowability. *Food Chemistry.* **212**, pp.453-459.

Whitney, K., Reuhs, B.L., Ovando Martinez, M. and Simsek, S. 2016. Analysis of octenylsuccinate rice and tapioca starches: Distribution of octenylsuccinic anhydride groups in starch granules. *Food Chem.* **211**, pp.608-615.

Wurzburg, O.B. 1986. *Modified starches-properties and uses.* Boca Raton: CRC Press Inc.

Xiang, L., Lu, S., Quek, S.Y., Liu, Z., Wang, L., Zheng, M., Tang, W. and Yang, Y. 2021. Exploring the effect of OSA-esterified waxy corn starch on naringin solubility and the interactions in their self-assembled aggregates. *Food Chemistry.* **342**, p128226.

Xu, Y., Huang, Q., Fu, X. and Jane, J.-l. 2015. Modification of starch octenylsuccinate by β-amylase hydrolysis in order to increase its emulsification properties. *Food Hydrocolloids.* **48**, pp.55-61.

Yao, T., Wen, Y., Xu, Z., Ma, M., Li, P., Brennan, C., Sui, Z. and Corke, H. 2020. Octenylsuccinylation differentially modifies the physicochemical properties and digestibility of small granule starches. *International Journal of Biological Macromolecules.* **144**, pp.705-714.

Zhang, H., Schäfer, C., Wu, P., Deng, B., Yang, G., Li, E., Gilbert, R.G. and Li, C. 2018. Mechanistic understanding of the relationships between molecular structure and emulsification properties of octenyl succinic anhydride (OSA) modified starches. *Food Hydrocolloids.* **74**, pp.168-175.

Zhang, W., Cheng, B., Li, J., Shu, Z., Wang, P. and Zeng, X. 2021. Structure and Properties of Octenyl Succinic Anhydride-Modified High-Amylose Japonica Rice Starches. *Polymers.* **13**(8).

Chapter 3
Effect of storage temperature and relative humidity on long-term colloidal stability of reconstitutable emulsions stabilised by hydrophobically modified starch
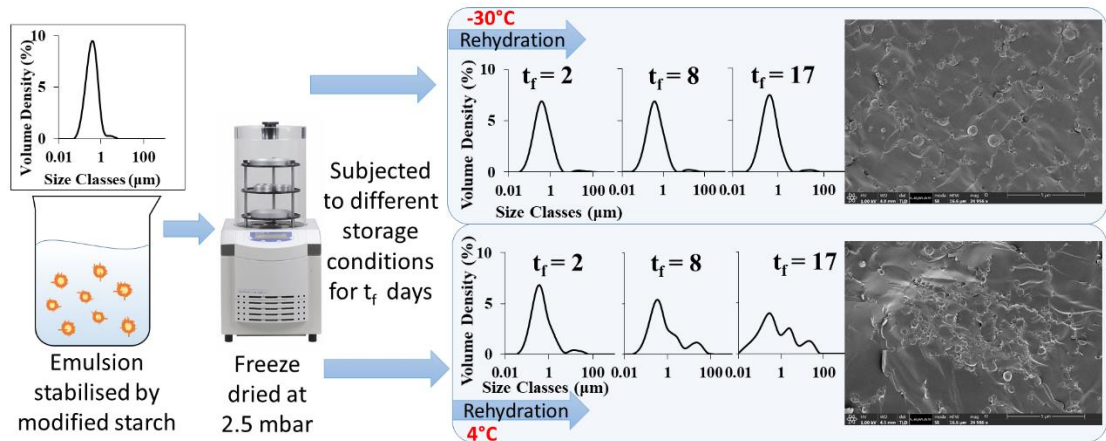
Abstract

Dried emulsions leading to formulations exhibiting a high level of colloidal stability post rehydration would have many potential industrial applications and are of significant interest to food scientists in that the dry formulations can be easily stored and more cheaply transported. The influence of powder storage time and conditions on the long-term colloidal stability of reconstituted oil-in-water emulsion has been examined here. Emulsion systems of 20% oil were prepared with 2.5% hydrophobically modified starch acting as the emulsifier. These were subjected to freeze drying followed by up to 3 weeks of powder storage under different conditions varying in relative humidity and temperature. Rehydration was performed at specific time intervals during storage for each set of powders. The change in droplet size and morphology of the reconstituted emulsion showed that powder storage temperature has a significant effect on the long-term colloidal stability of reconstituted emulsions. Powders stored under the lowest temperature condition produced the smallest droplet size and were the most colloidally stable emulsions once rehydrated, whereas those stored at higher temperatures showed inferior performance in this respect. Freeze-dried emulsion powder, stored at 30±1 °C for 3 weeks, once rehydrated gave liquid emulsions that were stable for at least 2 weeks. In contrast,

flocculation was observed upon reconstitution of dry powders that were stored at relatively high storage temperatures (4 ˚C and 20 ˚C), but neither creaming nor extensive coalescence were present, post rehydration. It is often assumed that little change to the colloidal state of the system occurs during storage, once the system has been fully dried. Our results indicate otherwise. Even in the dried form, emulsion droplets still undergo substantial changes in their surface properties, impacting the subsequent colloidal interactions and thus their colloidal stability during storage and particularly post reconstitution.

3.1   Introduction

Despite their high technological desirability in many different industries, formulating fully reconstitutable dry oil-in-water (O/W) emulsions continues to be a demanding and complex problem for colloid scientists. We specifically define a fully reconstitutable emulsion as one where, following the drying and after an extended period of storage in dried form, droplets of the same size as the original emulsion are retrieved by simple and gentle rehydration. Furthermore, the reconstituted emulsion thus formed without the need for further homogenisation, should exhibit a comparable level of long-term colloidal stability as it had prior to its drying. The difficulties of realising such formulations are probably nowhere more challenging than in food related systems. Food colloid scientists are rather limited in the variety of the stabilisers that they can include in food related dispersions. With an increasing demand on reducing, and the eventual phasing out of synthetic ingredients in foods, this choice is likely to become even narrower in the future. Central production of dry reconstitutable emulsions in one large facility may offer economies of scale efficiencies, as well as cost savings in such respect as the storage and transportation of raw materials to a single location. Of course, the extent of such savings will depend somewhat on the size and geographic distribution of local production sites.

The preparation of emulsions, followed by their drying, is also a common practice for making encapsulated (or microencapsulated) products. However, we wish to emphasise that the main aims of microencapsulation are quite different to those pursued here and often are focused on production of a dry powder that entraps an otherwise volatile food ingredient or flavour (Adachi et al., 2003; Madene et al., 2006; Tang and Li, 2013), or alternatively to protect a component from oxidative and other kind of damage during storage (Klinkesorn et al., 2005; Ghouchi-Eskandar et al., 2012;

Aberkane et al., 2014; Naik et al., 2014; Zhang et al., 2014). Other possible reasons for encapsulation are the provision of vehicles for obtaining a desirable controlled release profile (Ahmed and Aboul-Einien, 2007; Giardiello et al., 2012) and more recently, to achieve novel porous structures (Akartuna et al., 2008; Qian and Zhang, 2011) which for example can enhance the water dissolution behaviour of the resulting powder (Klinkesorn et al., 2006). In all of these applications, it is seldom the case that the rehydration of the dried systems is required to result, or indeed does lead to, the formation of colloidally stable emulsion droplets of the same size as those prior to drying (Christensen et al., 2001; Hogan et al., 2001; Millqvist-Fureby et al., 2001; Jena and Das, 2012; Holgado et al., 2013; Serfert et al., 2013; Tang and Li, 2013; Li et al., 2016; Domian et al., 2018).

An emulsion system undergoes major environmental changes during the drying operation (Garti and McClements, 2012), whether this is achieved through spray drying, freeze drying, heat drying or any other kind of drying process. Freeze drying has been considered the most suitable technique for drying food emulsions, where it is necessary to preserve most of the structures and properties of the matrix (Desai and Park, 2005; Ray et al., 2016). The porous structure of freeze-dried emulsion accounts for the relatively easy and quick rehydration process (Anwar and Kunz, 2011; Domian et al., 2018). However, the formation of ice crystals during the freeze part of the cycle can cause an increased concentration of droplets in the remaining unfrozen regions (Mun et al., 2008). The same also occurs for many salts and other ingredients originally dissolved in water as these are also excluded from the frozen ice (Thanasukarn et al., 2004). More tightly packed emulsions, in the presence of an increasing concentration of electrolyte are more prone to destabilisation, particularly if a part of the contribution to emulsion stability is through electrostatic means (Dickinson, 1992; Hunter, 2000). Similarly, the provision of steric repulsion by colloidal stabilisers relies heavily on the suitability of the dispersion medium being a satisfactory solvent, for at least some sections of the macromolecules (Dickinson, 1992; Russel et al., 1992) that are adsorbed at the surface of the droplets. It is known that the solubility of amino acids, including the hydrophilic residues, whether charged or polar, tends to decrease significantly as the temperature of water is lowered towards the freezing point (Dunn et al., 1933; Amend and Helgeson, 1997). Much of the same is also true for sugar moieties that make up the polysaccharide molecules. Thus, this decrease in repulsive colloidal forces, induced by the lowering of temperature, enhances the tendency of protein stabilised emulsion droplets

to aggregate. When combined with the possible formation of solid fat crystals in the dispersed phase, this makes the aggregated emulsion droplets, only separated from each other by thin protein layers, quite susceptible to the well-known phenomenon of partial coalescence (Walstra et al., 2006). Subsequently, full coalescence and breakup of the emulsion dispersion follows when the fat crystals begin to melt during the thawing part of the process. While each different drying process possesses its own particular difficulties, the above example typifies some of the challenges that are faced in formulating a reconstitutable dry emulsion.

Several relatively novel food-grade dispersants have been tried in preparation of emulsions for the purpose of microencapsulation in recent years. However, the suitability of these in formation of reconstitutable fine emulsions, possessing long-term colloidal stability has rarely been explored. One such technique is the layer by layer deposition method first introduced to food systems by McClements and co-workers (2005). This involves the adsorption of a layer of polysaccharide onto a primary emulsion, already stabilised by protein (Guzey and McClements, 2006; McClements, 2006). An alternative involves the covalent bonding of polysaccharide chains to proteins via Maillard reactions to produce amphiphilic conjugates. Yet one further method is to make the polysaccharides the actual emulsifying agents. This can be achieved by incorporation of an adequate number of hydrophobic side groups into the structure of the otherwise hydrophilic polysaccharide, thus turning it into an amphiphilic molecule (Nilsson, Lars and Bergenstahl, Bjorn, 2006; Nilsson and Bergenstahl, 2007; Yusoff and Murray, 2011). Each technique exhibits its own distinct advantages and disadvantages, as discussed in our recent review (Ettelaie et al., 2017).

Several authors have studied the stability of food emulsions stabilised by hydrophobically modified starch (HMS). Only octenyl succinic anhydride (OSA) is a permitted food-grade reagent for the modification of starch (Liu, Z. et al., 2008). Interestingly, in most of these studies the HMS remains in the form of granule particles. That is to say that the resulting emulsions are particle-stabilised, i.e. the so called "Pickering" emulsions. Yusoff and Murray (2011) produced starch particles by reacting non-swelling starch granules with OSA followed by freeze-milling process. They found that just like many Pickering type emulsions, the oil droplets stabilised by these starch particles showed excellent stability to coalescence, even after several months, but that the mean droplet size was relatively large, as big as 20 μm in some cases. Insensitivity to pH variations, increases in background

electrolyte and changes in temperature are other features associated with Pickering emulsions that have also been found to hold true for droplets stabilised by HMS granules (Murray et al., 2011; Marefati et al., 2013). Marefati et al. (2013) also considered the effects of freeze-thawing and freeze drying on the stability of such O/W dispersions. For cases where no thermal treatment had been applied to the emulsion before freeze drying, the mean droplet size in the freeze-dried-rehydrated system was seen to be similar to the original emulsion, although in both cases the droplets were quite large ~ 50 μm. Most food-grade particles suitable for making Pickering emulsions, even in the case of nano-sized primary particles, have been found to produce relatively coarse emulsions and bubbles, which are therefore more susceptible to creaming. In practice, it is relatively difficult to obtain an ideal dispersion of such individual particles due to their tendency to aggregate in the aqueous phase. This hinders the rapid diffusivity of the particles onto the interface (Ettelaie and Murray, 2014; Ettelaie and Murray, 2015) during high-pressure homogenization and high-intensity ultrasound (Murray et al., 2011; Dickinson, 2012). In contrast, the adsorption and formation of macromolecular HMS layers can produce significantly finer emulsions, ~ 1 μm, (Chanamai and McClements, 2001; Tesch et al., 2002). Recent theoretical work involving molecularly adsorbed HMS provided further evidence for the ability of such layers to provide strong long ranged steric repulsion between droplets (Ettelaie et al., 2016).

Freezing and drying of emulsions is nowadays quite a common practice, with the use of the technique for microencapsulating and protecting valuable active ingredients against oxidation well-studied in the literature. In contrast very few of such reported researches have reported on the long-term colloidal stability of reconstituted emulsions. Furthermore, in the few examples where such investigation has indeed been carried out, the reconstituted emulsions produced for long-term stability were obtained from dry powders immediately after their drying (Gallarate et al., 2009; O'Dwyer et al., 2013; Cheuk et al., 2015; Matsuura et al., 2015), involving no powder storage period between the end of drying and the start of rehydration processes. The assumption has been that once dried, any surviving droplets in the solid matrix undergo insignificant changes during the powder storage period, due to their immobilisation and the arrest of their Brownian motion. In this study, amongst other things, we wish to re-examine this assumption. Given the already reported potential of HMS for producing reconstitutable emulsions (Cheuk et al., 2015; Domian et al., 2018), we have chosen this as the emulsifying agent for our investigation here. An additional reason for our

choice was that, unlike protein + polysaccharide conjugates, for HMS, one only needs to consider the behaviour of a single type of biopolymer under the various encountered storage conditions. This makes an initial understanding of results somewhat easier to accomplish in such a preliminary study of the behaviour of colloids in a rehydrated system obtained post drying.

3.2 Materials and Methods

3.2.1 Materials

A commercial octenyl succinic anhydride (OSA) modified waxy maize starch was a gift from Ingredion UK Ltd. Typical molecular weight of OSA-modified starch is 10 – 30 MDa, with 3% modification (Nilsson, L. and Bergenstahl, B., 2006). The average molecular weight of this particular commercial product was determined to be ~10 MDa (PDI = 11.9) by asymmetrical flow field-flow fractionation (AF4), using the method described by Modig et al. (2006) with modification (see Appendix A, Figure A1 and Table A1). Such molecular weight indicates some likely degree of hydrolysis as one of the processing steps during the commercial production of this HMS. Tesco® Pure Sunflower Oil was purchased from a local supermarket. Sodium phosphate monobasic and sodium phosphate anhydrous were purchased from Acros Organics (USA). All other chemicals used were obtained from Sigma Chemical Co. (USA). Milli-Q water (Millipore Corp., USA) was used in all experiments.

3.2.2 Preparation of HMS solution

Phosphate buffer of 0.2 M at pH 5.5 was heated on a hotplate to 50 °C while stirred magnetically. HMS of different concentrations by weight was added slowly to the meniscus of the solution created by stirring. The solution was then left on the hotplate for 60 mins to ensure complete dissolution.

3.2.3 Preparation of O/W emulsion

Oil-in-water emulsions contained 20 wt% sunflower oil and 80 wt% HMS solution with various emulsifier concentrations, expressed as wt% of the total emulsion. Emulsions were prepared using a University of Leeds in-house made Jet homogenizer operating at a constant pressure of 250 bar (Burgaud et al., 1990). After emulsion preparation, 20 ml of each emulsion was transferred into a screw-cap glass sample tube.

3.2.4 Freeze drying, storage and reconstitution of emulsion

Emulsions used for freeze drying were made with 20 wt% sunflower oil and 2.5 wt% HMS at pH 5.5, using the method described. Exact 20 ± 0.1 g of each emulsion was weighed into six Petri dishes (internal diameter 92 mm), then stored in a freezer overnight at $-30 \pm 1°C$, which has an estimated freezing rate of 0.42 °C/min. The frozen samples were dried with a Christ Alpha 1-4 LD plus (Martin Christ Gefriertrocknungsanlagen GmbH, Germany) freeze dryer at a constant vacuum pressure of 2.5 mbar, which corresponds to a temperature of -10°C. The dried powder was stored at six different powder storage conditions varying in temperature and relative humidity:

1. 20 ± 1 °C, 75% RH (achieved by a desiccator with oversaturated NaCl solution), coded as HRH (high relative humidity)
2. 20 ± 1 °C, 2% RH (achieved by a desiccator with silica beads), coded as LRH (low relative humidity)
3. 20 ± 1 °C, sealed, coded as R (room temperature)
4. 4 ± 1 °C, sealed, coded as F (fridge temperature)
5. -18 ± 1 °C, sealed, coded as L (low temperature)
6. -30 ± 1 °C, sealed, coded as VL (very low temperature)

The amount of water lost during drying was determined by calculating the weight loss of sample. After certain periods (0, 1, 2, 5, 8, 11, 14, 17, 21 days) of powder storage in the above conditions, reconstitution was performed by adding back the weight loss with MilliQ water containing 0.02 wt% sodium azide. The tube containing reconstituted emulsion was then capped and placed on a Vortex Mixer for 15 mins. Droplet size measurements were taken 60 mins after the mixing. All reconstituted emulsions were stored under refrigeration temperature.

To clearly identify different samples and the conditions of their dry powder storage, the following naming system is adopted:

Non-freeze-dried emulsions are called fresh. All freeze-dried samples are coded by their storage conditions with the convention $Tt_f.t_s$ where T is the powder storage condition as coded above, t_f is defined as the powder storage time (in days) prior to reconstitution, and t_s is defined as the post reconstitution storage time. For example, R2.7 refers to a sample that was freeze-dried, sealed, and stored as powder under room temperature condition, i.e. 20 ± 1 °C and sealed (R) for 2 days. Once rehydrated, the resulting reconstituted emulsion was then kept for further 7 days before it was subjected to various measurements. Samples reconstituted immediately

after freeze-drying are designated as D0.t_s, (with t_s once again signifying the post reconstitution storage period).

3.2.5 Size measurement for starch in solution and oil droplets in emulsion

Hydrated size of starch in solution was determined using a dynamic light scattering instrument Zetasizer nano ZS (Malvern Panalytical, UK). Before the measurement, the samples were diluted to the appropriate concentration with 0.2 M phosphate buffer of pH 5.5 and then transferred to a disposable sizing cuvette. The refractive indices of water and starch were set at 1.330 and 1.520, respectively.

The droplet size of emulsions was measured using a laser light scattering instrument Mastersizer 3000 (Malvern Panalytical, UK). Before droplet size measurement, emulsions were shaken by hand to ensure homogeneity. Sample was added to the dispersion unit connected to the laser light scattering instrument until an obscuration between 1% and 4% was obtained. The mean droplet size was reported as the volume-weighted mean diameter, $d_{4,3} = (\sum n_i\, d_i^4 / \sum n_i\, d_i^3)$, where n_i denotes the number of droplets with a diameter d_i.

3.2.6 Rheological measurements

The apparent viscosity of both HMS solutions and emulsions was measured within 3h after their preparation using a Kinexus Ultra rheometer (Malvern Panalytical, UK) and a double gap concentric cylinder DG25 geometry (cup diameter 26.25 mm, bob internal diameter 24 mm, bob external diameter, 25 mm). The samples were gently mixed, poured into the temperature-controlled measurement cell, and allowed to equilibrate at 25 ˚C for 10 min prior to the measurement. Apparent viscosity of emulsions was measured at shear-rates in the range 0.2-200 s^{-1} using continuous shear, at 25 ˚C.

3.2.7 Water activity (a_w) and moisture determination

The value of a_w in the freeze-dried powders were determined using HygroLab C1 with HC2-AW accessary (Rotronic Instruments, UK). Care was exercised to ensure sufficient equilibration time before readings were taken. The moisture content of the powders (1 g) was determined gravimetrically by vacuum oven drying at 105 °C and 29 inHg for 24 h.

3.2.8 Scanning Electron Microscopy (SEM), and Cryo-SEM

Scanning Electron Microscopy on dried samples was performed by using Carl Zeiss EVO MA15 SEM (Carl Zeiss Microscopy, Jena). Cryo SEM images were obtained using an FEI Helios G4 CX (Fei, USA), and a Quorum PP3010 cryo-FIB/SEM preparation system (Quorum Technologies, UK) as the cryo system.

3.2.9 Differential Scanning Calorimetry (DSC)

A differential scanning calorimeter (Perkin Elmer DSC 8000, PerkinElmer, Norwalk, US) was used to record the DSC thermogram of the dried powders. Approximately 10 mg powder was placed in an aluminium pan and the pan was sealed hermetically. An empty pan was used as reference. The thermal analysis was performed using a three-cycle scan model, with temperature range from 25 °C to -45 °C, with heating and cooling rates of 10 °C/min under a stream of nitrogen with a flow rate of 20 mL/min.

3.2.10 Cold-Stage X-Ray Diffraction

Dried emulsion powder and bulk sunflower oil was observed for X-ray pattern using a Phillips PANalytical XPert pro MPD X-ray diffractometer (Malvern Panalytical Ltd., UK) with CuKα radiation (K-Alpha1 wavelength = 1.54 Å) generated from a copper source operating at a voltage of 40 kV and a current of 40 mA. The test samples were packed into an AP TTK-450 sample holder. The samples were scanned over the range of 4 – 40° 2θ (scan step size = 0.0334, scanning time per step = 135 s). Scans were performed at -70 °C, -18 °C, and 25 °C.

3.2.11 Statistical analysis

All measurements, unless stated otherwise, were repeated in triplicates. The mean value of the three readings was calculated and reported in each case. Pearson correlation and linear regressions with associated coefficient of determination R^2 were performed where applicable. All calculations were completed using Microsoft Excel 2013 and statistical significance was assigned at the level $p < 0.05$.

3.3 Results and discussions

3.3.1 Hydrophobically modified starch solution

Rheological behaviour of emulsions subjected to shear can often provide valuable information regarding the colloidal state of the droplets. In

order to be able to interpret such data correctly, it is necessary that any possible complications arising from the flow properties of the continuous phase itself are appropriately taken into account. In systems considered here, the continuous phase contains HMS. Depending on the level of the hydrophobic modification, as well as the value of pH and method for preparing the solution, HMS may remain in granular aggregated form. Alternatively, it can also be present as dissolved individual macromolecules in the solution and may or may not associate to form weak networks (Sweedman et al., 2013). As mentioned in the introduction, in both of these forms, HMS can stabilize emulsion droplets. In the latter case (Chanamai and McClements, 2002), the general stabilising mechanism will be similar to that for emulsions stabilised by other amphiphilic type macromolecules, whilst in the former the emulsions will be of particle stabilised "Pickering" type (Yusoff and Murray, 2011; Marefati et al., 2013). Measurements of low shear viscosity for dilute solutions can be used to determine the typical size of entities that are dispersed within the solution (Chanamai and McClements, 2001), and thus potentially allow us to distinguish between these alternative possible scenarios. In this section, we present and discuss the results of such rheological measurements for HMS solution in the absence of oil droplets.

At sufficiently low volume fractions of the dispersed phase/dissolved macromolecules, the viscosity of the solution, η (Pa·s), varies in a linear fashion with the concentration c (mol/L) of the molecules as shown in Eq. 3.1

$$\eta = \eta_0\left(1 + [\eta]c\right)$$

3.1

where η_0 is the viscosity of the pure solvent phase and $[\eta]$ the intrinsic viscosity of the macromolecules (or colloidal particles) added to the solution (Barnes, 2000). Indeed, Chanamai and McClements (2002) have already shown that the viscosity variation of well dissolved HMS solutions, at low concentrations, can reasonably be approximated by Eq. 3.1. Following their work, we also measured the viscosity variation of our HMS solution, as a function of biopolymer content in the low concentration limit. This was conducted for both the solution just prior to homogenisation and once it had passed through the homogeniser (without addition of any oil phase). In Figure 3.1, the data for both cases have been plotted as $[(\eta/\eta_0) - 1]$ vs. c. For both the homogenised and the non-homogenised solutions, a very reasonable fit to Eq. 3.1 was obtained. However, the value of intrinsic viscosity, $[\eta]$ was found to be somewhat higher at ~0.52 prior to homogenisation, as compared to 0.37 dl/g for that following homogenisation.

We suspect that this is due to small residual starch clusters that are not fully broken up and dissolved until the solution is subjected to the higher shears encountered in the homogeniser. More likely, it is also the result of some degradation of the HMS, known to take place in the homogenisation process (Modig et al., 2006).
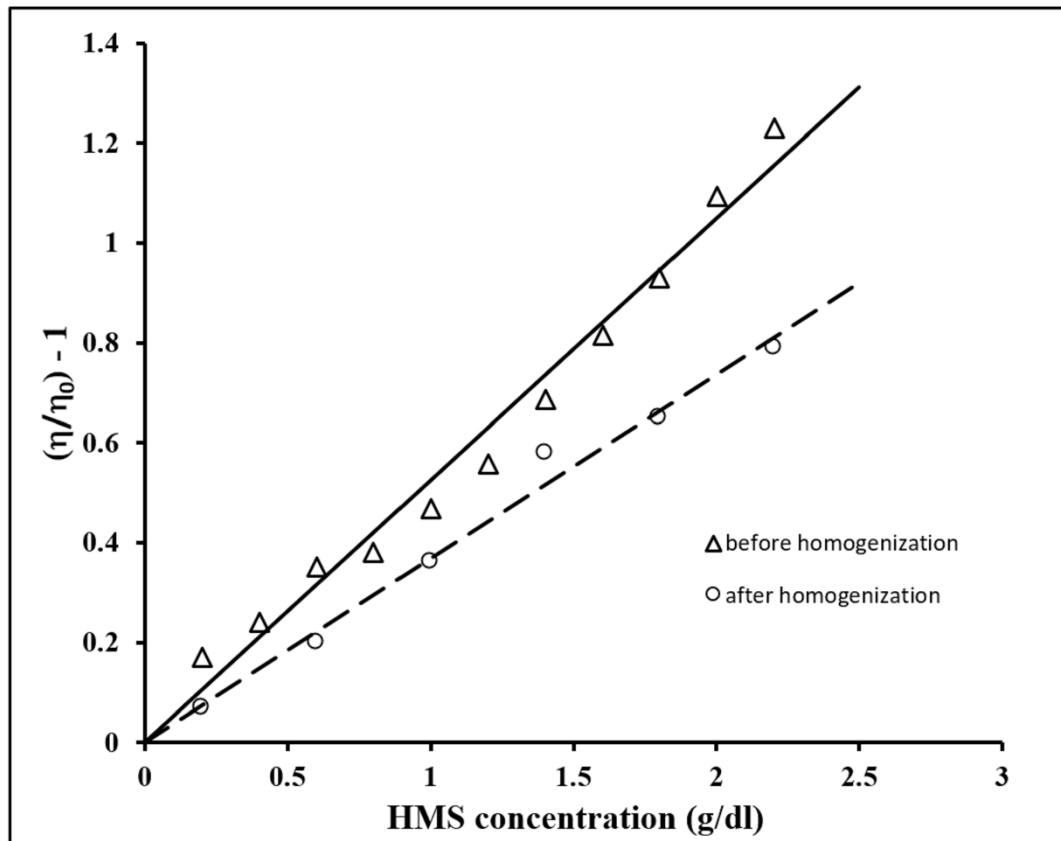
Figure 3.1 Intrinsic viscosity of modified starch solution before and after homogenization, where η **and** η_0 are the apparent viscosity of starch solution and pure solvent, respectively. The slopes of the best-fit lines in each case provides the corresponding intrinsic viscosities of the HMS solutions.

The value of intrinsic viscosity obtained from the slope of the graphs in Figure 3.1 can be used to obtain an estimate of the size of macromolecules (or their aggregates) present in the solution. In the low dilution limit, HMS molecules in the solution will not overlap with each other due to the strong excluded volume interactions between them. Therefore, the total effective volume fraction occupied by such molecules will be $\phi \sim 4\pi R_H^3 n/3$, where R_H is the hydrodynamic radius of the chains (approximately the same as their radius of gyration, R_g) and n the number

density of the HMS molecules as given by $10000cN_A/Mw$, if c is expressed in g/dl. Here, Mw denotes the average molecular weight of the HMS molecules and $N_A = 6.022 \times 10^{23}$ is the Avogadro's constant. For spherical dispersed entities, occupying a volume fraction ϕ, Equation 3.1 can also be expressed in term of ϕ, as given by Einstein equation:

$$\eta = \eta_0 \left(1 + 2.5\phi\right)$$

3.2

From a comparison of Equations 3.1 and 3.2, it follows that

$$R_H^3 = \frac{3M_w[\eta]}{10^5 \pi N_A}$$

3.3

Molecular weight for modified starch varies largely from one to several hundred MDa. Typical values following degradation due to shear are measured to be around 30 MDa (Nilsson, L. and Bergenstahl, B., 2006). Taking this value together with our measured $[\eta] = 0.37$ dl/g, we obtain $R_H = 56$ nm. The absolute size of the measured entities by itself is not an indication of their particulate nature or otherwise. However, the measured radius here agrees well with the value of the radius of gyration for a single HMS molecule, as reported by Nilsson, L. and Bergenstahl, B. (2006) measured using dynamic light scattering (DLS). The value is also in accord with our own data using AF4 (R ~ 50 nm), as well as our DLS results with d =112 nm (PDI < 0.1). This strongly indicates that our HMS was not in the form of granules, but much more likely that it had dissolved to form a starch solution. Subsequently, oil droplets that are emulsified in this solution cannot be classified as Pickering type, but are instead stabilised by adsorbed macromolecular layers of modified starch. There have been studies reporting on modified starch stabilised Pickering emulsions with droplet size of 391.5 nm (Liu, W. et al., 2018). However, this probably requires starch granules no larger than ~ 40 nm, which is as small as, if not smaller than the size of a single hydrated starch chain. Thus, even if such granules truly exist, they cannot contain more than very few HMS molecules.

3.3.2 Fresh liquid emulsion

In order to find the optimum HMS concentration for a 20% O/W system, emulsions with different HMS content were prepared. A very interesting relationship was observed when the normalised viscosity of emulsions was plotted against HMS concentration. The presence of a biopolymer such as starch in a solution can by itself cause a significant change in the solution viscosity. Therefore, here the normalised viscosity

(η/η_0) was plotted to compensate for the effect of increasing starch concentration, where η is the viscosity of emulsion, and η_0 is the viscosity of HMS solution at the same corresponding bulk concentration, but in the absence of oil droplets. It can be seen that the relative viscosity of the emulsion dropped to a minimum as the concentration of HMS increased to 2 wt%, and then started to rise again beyond a concentration of 4 wt% (Figure 3.2A).
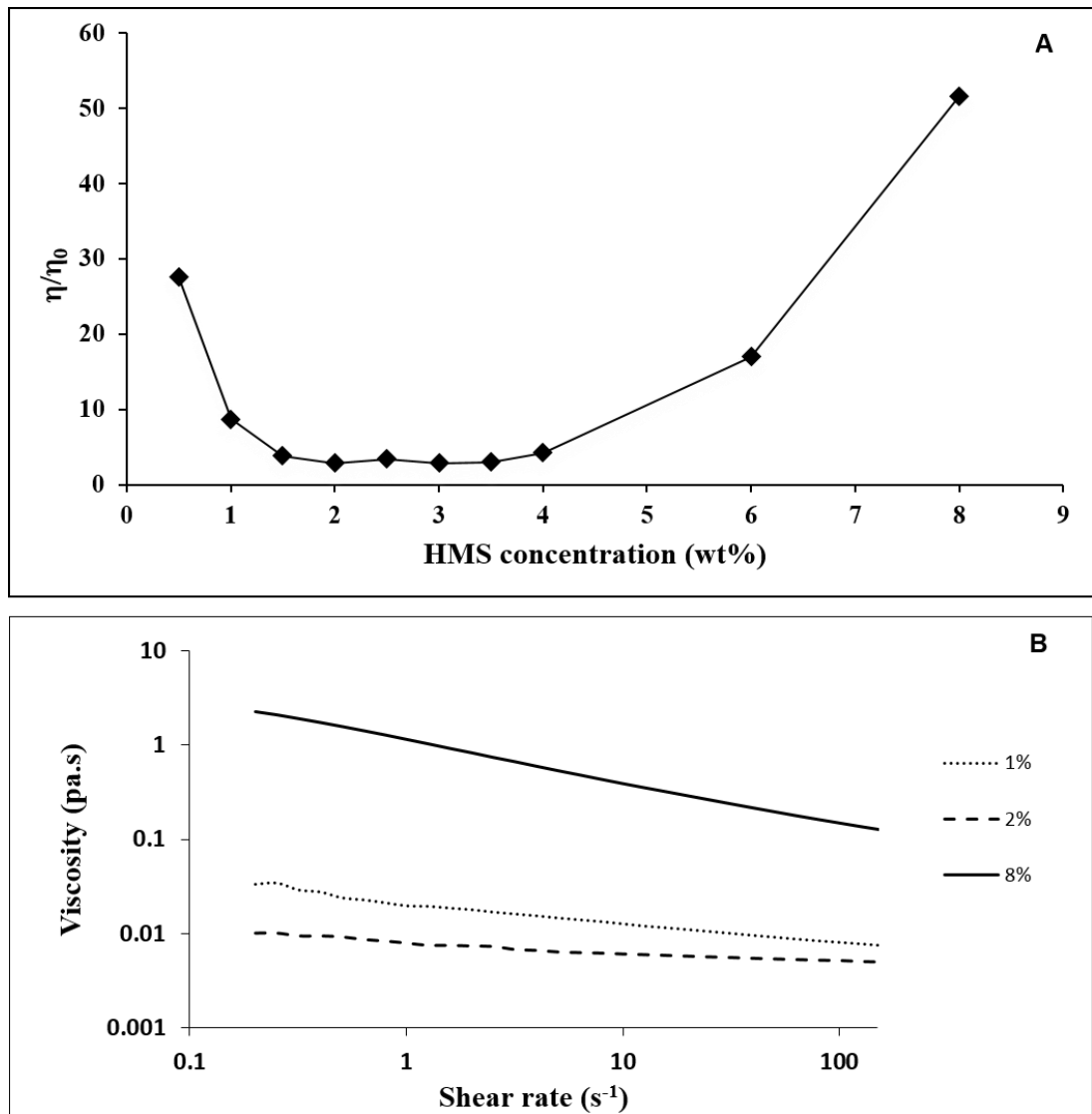
Figure 3.2 A) Normalised viscosity (at a shear rate of 2 s−1) of 20 wt% O/W HMS stabilised emulsions with different HMS concentrations (wt%).   B) Apparent viscosity of emulsions plotted as a function of shear rate. Curves for three different HMS concentrations (wt%), 1% (dotted), 2% (dashed) and 8% (solid line) are displayed.

Increase in viscosity is often associated with emulsion instability, especially flocculation, which often is considered as the very first step in the possible destabilization of emulsion (Dickinson, 2009). Bridging flocculation tends to occur at low emulsifier concentration, while depletion flocculation tends to occur at high emulsifier concentration (Dickinson, 1989) when significant excess biopolymer remains non-adsorbed in the bulk solution. Related to the results in Figure 3.2B, we also find a mild shear-thinning behaviour at HMS concentration of 1 wt%. This behaviour disappears and becomes completely Newtonian for emulsions at higher HMS concentrations from 2 wt% to 4 wt%. Yet, at still higher concentrations of HMS, the shear-thinning behaviour once again manifests itself (Figure 3.2B). These graphs in our opinion result from the classic bridging flocculation—stable emulsion—depletion flocculation trend as the concentration of HMS increases. It is particularly interesting to note that this situation is very similar to what occurs for other types of biomacromolecular emulsions, such as sodium caseinate emulsions (Berli et al., 2002). While the depletion flocculation part of this trend has been experimentally observed and presented for HMS in the research work of Chanamai and McClements (2001), the complete curve, showing both types of bridging and depletion flocculation occurring for the same HMS stabilised system over the varying range of HMS concentrations, has not been reported previously to the best of our knowledge. Such a common feature between the colloidally-induced behaviour in protein stabilised and HMS stabilised emulsions, is interesting and worthy of further investigation in future.

From the above results, 2.5 wt% HMS was determined to give excellent emulsion stability and therefore emulsions with this HMS concentration were used for subsequent freeze-drying studies. Emulsions stabilised with 2.5% HMS gave Sauter mean diameter $d_{3,2}$, ($d_{3,2} = (\sum n_i\, d_i^3 / \sum n_i\, d_i^2)$), of approximately 300 nm, and $d_{4,3}$ of 480 nm at pH 5.5. Fresh emulsion's stability was monitored over the course of four weeks. By appearance, there was no creaming visible to the naked eye after two months of storage at 4 °C. The values of both $d_{3,2}$ and $d_{4,3}$ remained stable over the whole storage period (Figure 3.3B) indicating very little or no flocculation in the emulsion system. Samples tested at different storage times all gave Newtonian type behaviour, as seen in Figure 3.3A, thus once again supporting the view that no aggregation of droplets occurred prior to drying. These results are largely in line with previously reported studies regarding the stability of properly prepared HMS stabilized emulsions.
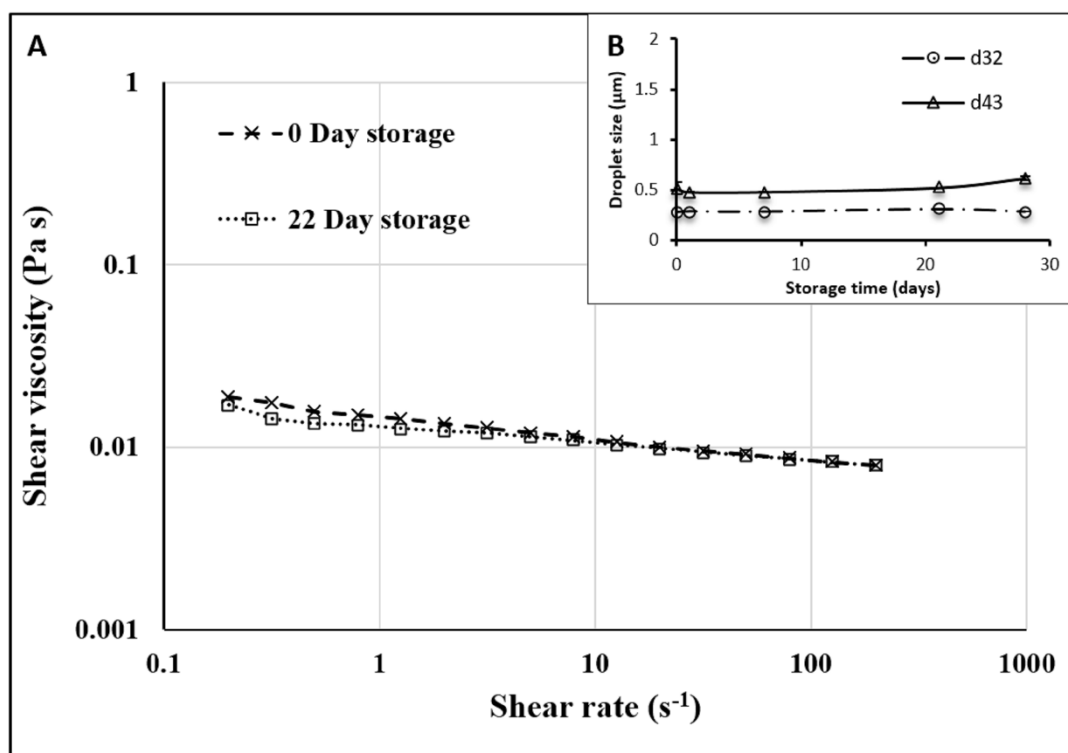
Figure 3.3 Apparent viscosity vs shear rate for non-freeze-dried emulsions, on the day they were made (dashed line) and after 22 days (dotted line). These emulsions contained 20 wt% oil and 2.5 wt% HMS. The inset shows the variation of the mean droplet size for non-freeze-dried emulsions over a period of 28 days.

3.3.3 Effect of freeze drying

Through the freeze-drying procedure, dried powders containing 80 wt% oil and 10 wt% HMS were prepared. The other 10% of the powder consisted of retained buffer salt and 3.02% ± 0.74% moisture, with water activity of 0.087 ± 0.035. The non-sticky, white-in-colour dried emulsion had a flaky texture and became powdery once broken gently. The droplet size distributions of both the fresh emulsion, as well as emulsions reconstituted straight after drying are shown in Figure 3.4. For the latter sample, the particle size was determined both immediately after reconstitution (D0.0) and 14 days post rehydration (D0.14). Comparing the fresh and D0.0 samples, the value of $d_{4,3}$ is seen to have changed four-fold from 0.50 μm to almost 2 μm. The distribution has also widened, and a second peak appeared at approximately 10 μm as a result of the drying process. Upon either ultrasonication or addition of SDS, the second peak was reduced, and the first peak increased in its height (data not shown). This indicates that the appearance of the second peak was mainly due to aggregation of droplets

either during drying or at the point of rehydration. However, once reconstituted, the average droplet size and its distribution did not change substantially over the next 14 days (Figure 3.4, D0.0 and D0.14). It is worth noting that even though sub-micron droplet size was lost after freeze-drying, the reconstituted 2 µm droplets are still reasonably fine and considerably smaller than HMS granule-based Pickering emulsions (Yusoff & Murray, 2011). Coupled with their excellent stability after rehydration, this should make them of useful practical interest in many potential applications.
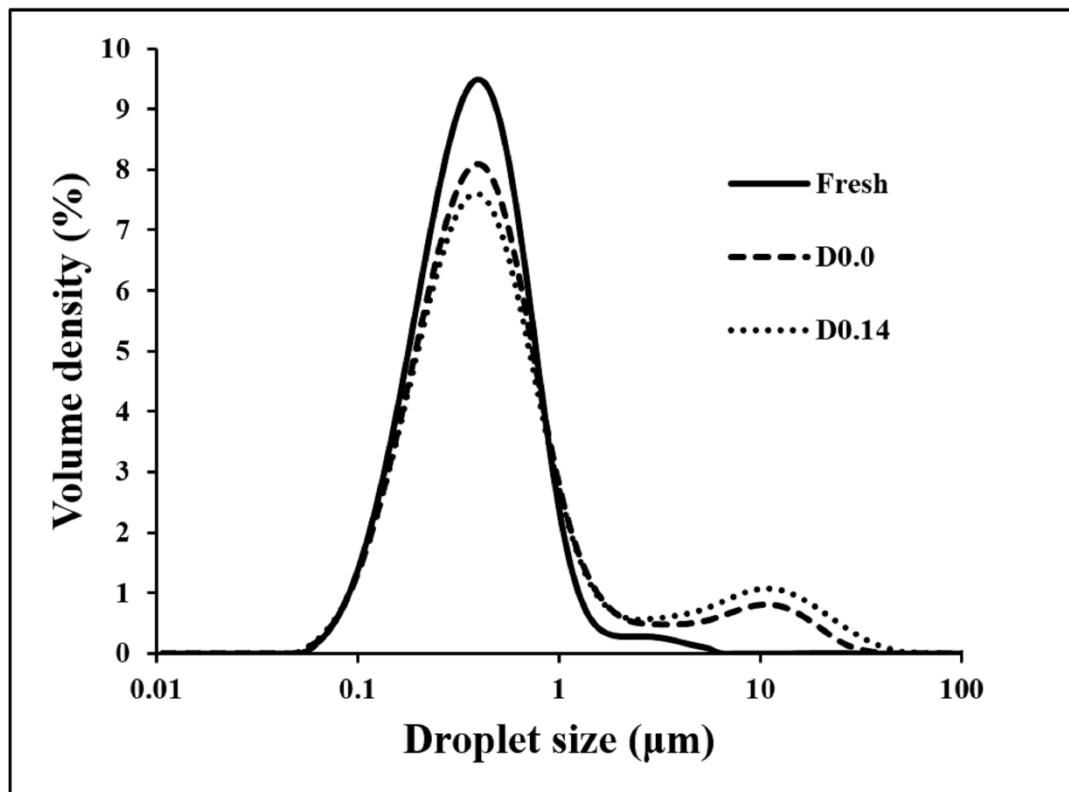
Figure 3.4 Droplet size distributions for non-freeze-dried emulsions (—), emulsions reconstituted immediately after freeze drying D0.0 (---), and the latter sample 14 days post rehydration D0.14 (.....).

During the freezing step, formation of ice crystals may have started to destabilise the emulsion droplets by limiting their spatial arrangements, by increasing the local electrolyte concentration in the none frozen regions, and possibly also by penetrating the adsorbed layer of emulsifier, as discussed extensively in previous studies (Mun et al., 2008; Marefati et al., 2013; Zhu et al., 2017). The freezing point of sunflower oil is -17 °C, but homogenized oil droplets in 300 nm size range are expected to have a very high degree of supercooling, (Cramp et al., 2004; Elwell et al., 2004). Despite this, the

freezing temperature of -30 °C was sufficiently low for fat crystallization to take place, as the crystallization temperature of freeze-dried emulsion powder was determined here to be -24 °C by DSC (See Appendix A, Figure A2). The lipid crystals penetrating the adsorbed interfacial layers would cause some desorption of the HMS. This in turn could cause further disruption to the provision of steric repulsion forces (Cramp et al., 2004; Marefati et al., 2013). When the drying phase of the freeze-dry cycle is initiated at a temperature of -10 °C, oil crystals would start to melt. As drying proceeds, there is an increasing reduction in the volume of the free aqueous phase. Despite this, the bulky hydrophilic parts of HMS, responsible for provision of strong steric forces, could still physically provide some protection against total coalescence (Donsì et al., 2011), though not necessarily against aggregation of droplets anymore. With a compromised adsorbed layer of HMS, and the combination of competing factors discussed above, some degree of aggregation and even partial coalescence may well be expected (Cramp et al., 2004). After all, the adsorption of HMS occurred at an oil-water interface during preparation of the original emulsion. In contrast, after drying, the interface is essentially one between the starch in the matrix and the oil phase. The adsorption behaviour of HMS molecules is not necessarily expected to be the same at these two rather different interfaces. The degree of aggregation (and possibly partial coalescence) proceeded further once rehydration happened and the droplets became more mobile again. We believe this is the main cause of the increase in droplet size and the wider size distribution seen for dried and then immediately rehydrated emulsions when they are compared to fresh ones (Figure 3.4).

Figure 3.5 shows the SEM images of the above freeze-dried emulsion, at several levels of magnification. The irregular flaky structure can be observed in Figure 3.5A, with internal porous structures evident on the breaking sites of the flakes. This is typical of freeze-dried materials (Laine et al., 2008; Sousdaleff et al., 2013). Reconstituted droplet size reduction upon ultrasonication or addition of SDS suggests aggregation, and this is supported by the fact that only a very small number of larger droplets can be observed in SEM micrographs. However, coalescence cannot be ruled out completely, as the arrows in Figure 3.5B indicate, there is possible evidence for partial coalescence of oil droplets. Despite these, as seen in Figure 3.5C, many oil droplets have survived the drying process, and retained their submicron droplet size. Considering that the dry powder consisted of 80 wt% oil and only 10 wt% HMS, the spherical entities observed are very likely oil

droplets, as there would not be enough HMS to form so many particulate entities, even in the extreme case where all HMS was to desorb from the surface of droplets.
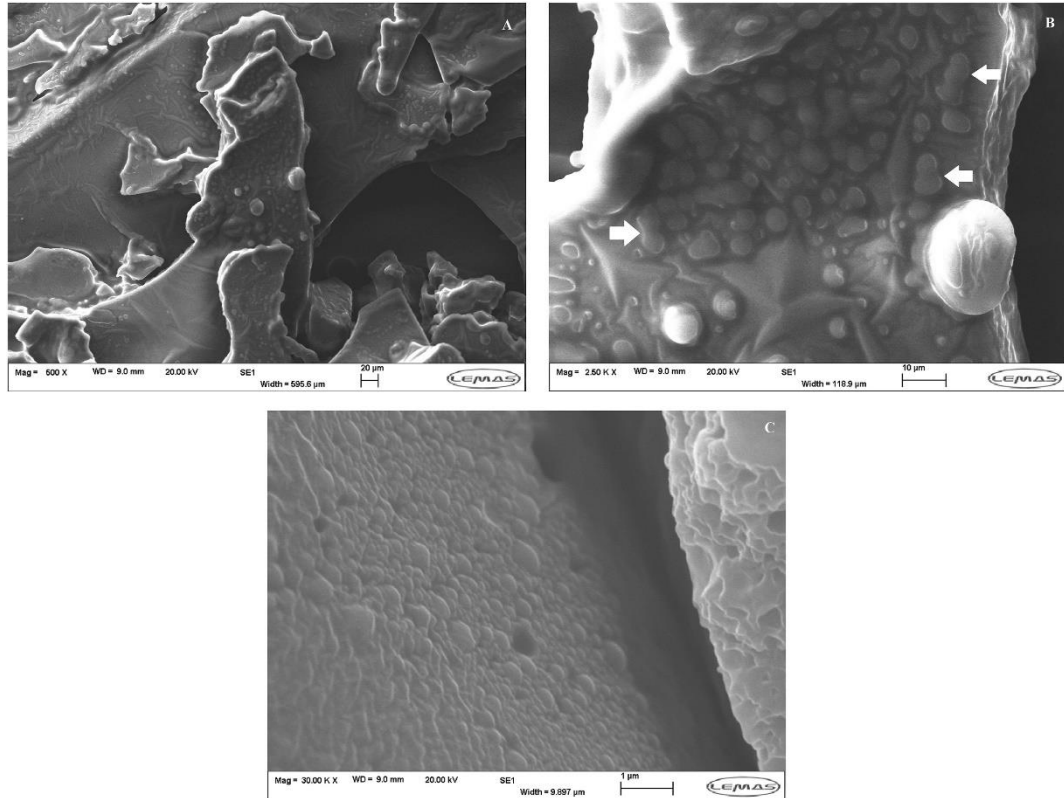
Figure 3.5 SEM images of freeze-dried emulsion powders that underwent no powder storage (i.e. straight after drying). Arrows indicate some possible evidence for partial coalescence. Micrographs are taken at different magnifications, A) 500×, B) 2.50K×, C) 30.00K×.

3.3.4 Storage condition and its effect on reconstituted emulsions

By freeze-drying samples under the same conditions and carefully characterising them both before and after the process, it is ensured that the influence of freeze-drying on HMS stabilized emulsions would be the same for all samples. Thus, the only variables remaining are the powder storage conditions and the duration of the dry storage before rehydration. SEM images were taken of powders, after varying periods of storage (ranging from 0 to 21 days) and for all of the different powder storage conditions considered in this work. No obvious differences were observed between the powders, with all of them being visually similar to D0.0 shown in Figure 3.5 (See Appendix A, Figure A3). In particular the sizes of droplets in various powders seem approximately the same in all of the SEM micrographs.
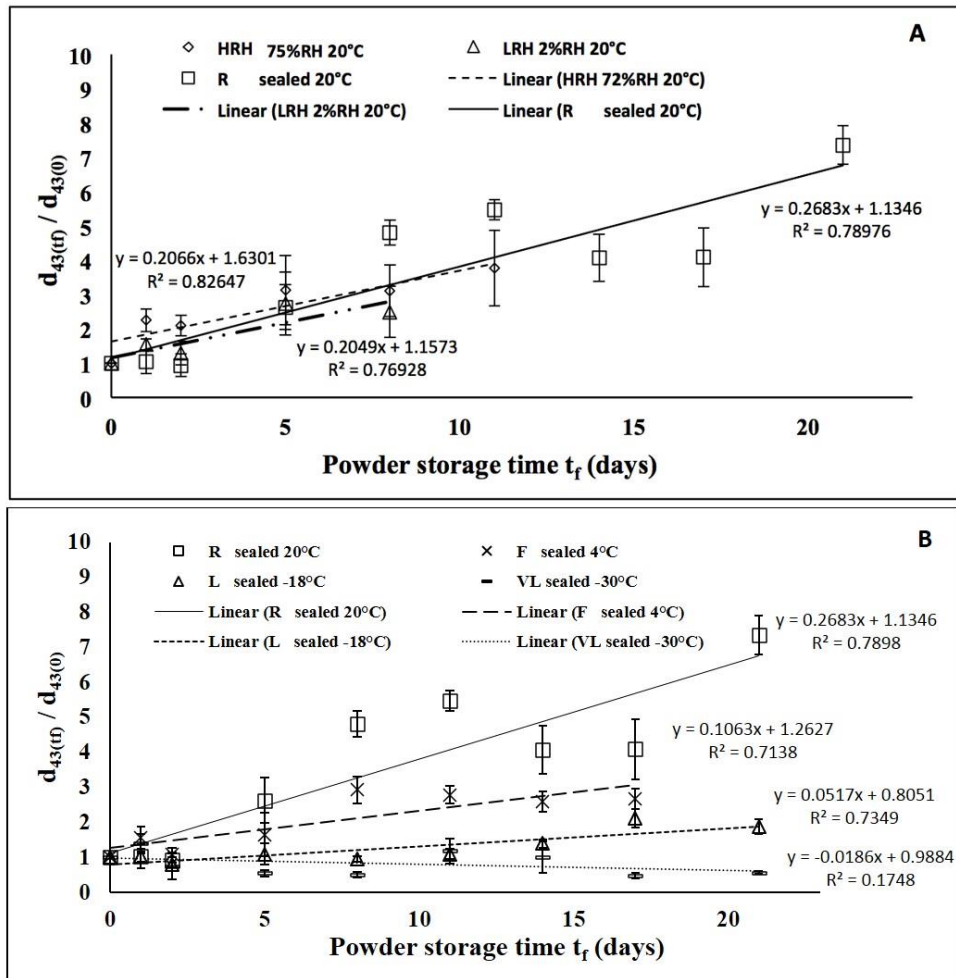
Figure 3.6 Normalised average reconstituted droplet size plotted versus the powder storage period (t$_f$).

All measurements were performed immediately after rehydration (ts = 0). Normalised droplet sizes are obtained as the ratio of droplet sizes between emulsions reconstituted after a powder storage time of tf and those reconstituted straight away after freeze-drying (sample D0.0). Error bars represent calculated standard deviation. Linear regression lines are shown with equations and R2 values. (A) Effect of relative humidity with samples that underwent powder storage with high (HRH), low (LRH), and typical room (R), humidity conditions. (B) Effect of temperature with samples that underwent powder storage at room temperature (R), 4 °C (F), −18 °C (L), and −30 °C (VL).

Thus, any differences in the behavior of reconstituted emulsions are not simply due to the variation of droplet size caused during the powder storage period. However, this does not mean that the adsorption behavior of HMS remains the same. For example, HMS may get desorbed from the surface to varying degrees, depending on the length and conditions of powder storage. However, these differences cannot fully manifest themselves as changes in the size of droplets, due to lack of aggregation resulting from very low

mobility of droplets in all powders. As noted, when powders are rehydrated and droplets become mobile once again, these differences result in quite dissimilar reconstituted droplet sizes.

In Figure 3.6, the normalised droplet size, defined as the ratio of droplet sizes between emulsions reconstituted after a powder storage time of t_f and those reconstituted straight after freeze-drying (sample D0.0), is plotted as a function of powder storage period. Figure 3.6A compares samples R, HRH and LRH to examine the impact of relative humidity during powder storage, and Figure 3.6B compares samples R, F, L, VL to examine that of powder storage temperature. The results demonstrate that all dry powders, with the exception of VL, gave reconstituted emulsion that became more coarse with longer powder storage times, t_f. In contrast, for VL samples, the reconstituted droplet size seemed to remain relatively stable irrespective of t_f. The Pearson correlation analysis (Table 3.1) confirms that in all samples but VL, the reconstituted droplet size was significantly ($p < 0.05$) correlated to the period of powder storage, t_f. These differences imply that any possible destabilization occurring during reconstitution was sensitive to the period of powder storage, even though visually no major differences between powders may be seen prior to rehydration.

Table 3.1 The correlation coefficients and associated p values for Pearson correlation analysis, on reconstituted droplet sizes vs powder storage time, showing data size (n) and correlation coefficient (r).

Sample	n	r	p	Sample	n	r	p
R	9	0.89	0.0007	R	9	0.89	0.0007
HRH	6	0.91	0.0060	F	8	0.84	0.0041
LRH	5	0.88	0.0254	L	9	0.86	0.0016
				VL	9	0.42	0.1314

It is interesting to note that in all reconstituted emulsions no creaming was visible. Similar to D0.0, all other samples showed no additional instability during a further 14 days of observation after rehydration (t_s) (Figure 3.7), albeit having produced quite different emulsion sizes when initially reconstituted. In particular, for VL samples freeze-dried under the aforementioned processing condition, with the dry powder stored at $-30 \pm 1\,°C$ and sealed for up to 3 weeks, the reconstituted droplets maintained their stability with an average droplet size of less than 2 μm, for

at least 2 further weeks. The ability to keep dried emulsion powders for 3 weeks and then produce such stable fine emulsions simply by rehydration, is a particularly important first step in designing truly reconstitutable submicron emulsion systems, capable of transportation and storage as dry powders, for long periods of time.
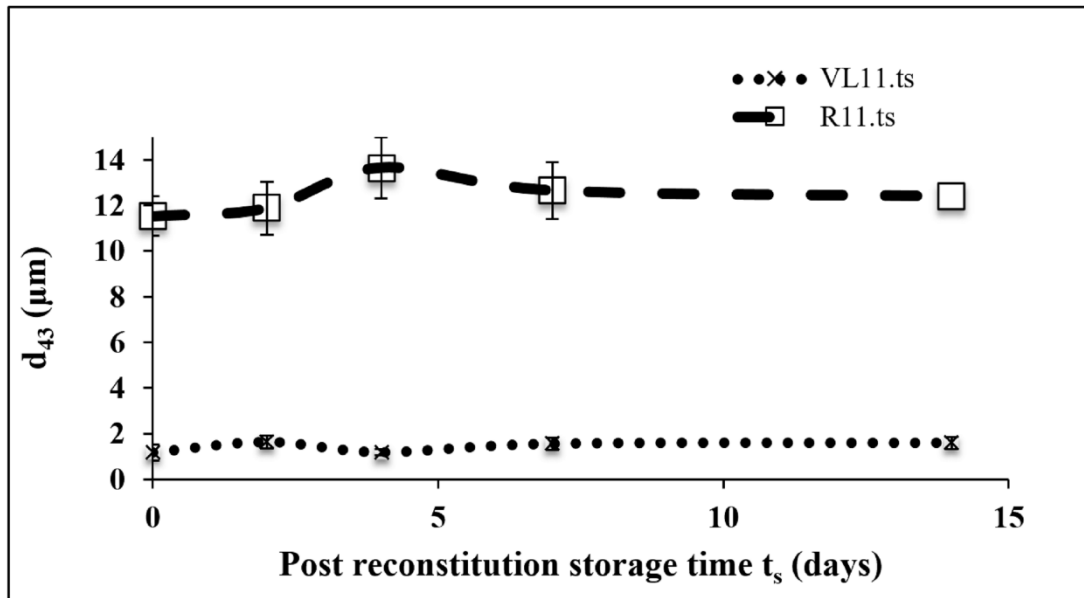
Figure 3.7 Assessing the long-term stability of reconstituted emulsions by monitoring $d_{4,3}$ (µm) for samples VL11.t_s and R11.t_s at different t_s (days) post rehydration.

3.3.4.1 Effect of relative humidity during storage of powder

The impact of relative humidity was examined by comparing HRH, LRH and R, as shown in Figure 3.6A. In these three conditions, all powders were stored at the same temperature of 20 °C. The powder R was sealed at room humidity to prevent any further moisture exchange subsequently. In LRH, the environment of 2% RH suppressed moisture uptake of the powder. On the other hand, in HRH case, where moisture exchange with an environment having 75% RH was allowed, the powders rehydrated slowly during storage by absorbing moisture from the surrounding air. These were evidenced by a small variation in weight (See Appendix A, Table A2) and more prominently a noticeable change in the texture of the powders. Both R and LRH powders stayed relatively dry until reconstitution, where they were rehydrated quickly.

Even though several authors reported higher degree of agglomeration with higher RH during powder storage in encapsulation studies of anthocyanins (Alvarez Gaona et al., 2018; Garcia-Tejeda et al., 2018), as seen from Figure 3.6A, the slopes of the linear regression lines for HRH and LRH (0.2066 and 0.2049 respectively) are comparable. This shows that the rates of change in reconstituted droplet size with respect to powder storage time were equivalent for HRH and LRH samples, despite the difference in relative humidity of their powder storage conditions. Therefore, relative humidity during powder storage did not have a strong impact on reconstituted droplet size. The relatively large standard deviation between triplicate samples prepared under same condition, for both HRH and LRH cases, indicates high level of emulsion breakdown and instability as the powders were rehydrated. The rather mild impact of humidity may be the result of hydrophobic modification of starch, which makes the affinity of matrices consisting of HMS for the uptake of water lower than those of unmodified starch.

When Figure 3.6A is contrasted to Figure 3.6B, it is clear that humidity at best played only a minor role, at the studied temperature range. The effect of humidity, being a less significant and more subtle parameter, should be looked at in more detail for a wider range of storage temperatures, but this was beyond the scope of the current preliminary study. The more prominent factor, temperature, will be discussed in the next section.

3.3.4.2 Effect of temperature during storage of powder

After storage under various temperatures, moisture content of powders increased slightly, varying from 3.39% to 5.13% (See Appendix A, Table A3), but otherwise remained low. During freeze drying, the adsorbed layer of HMS covering the surface of oil droplets will tend to be disrupted to some extent by the crystalline structure of oil (Cramp et al., 2004; Marefati et al., 2013). This is likely due to the much-altered nature of the interface between the dispersion medium and dispersed phase, if one or both solidify. Once the dried powders are removed from the freeze-dryer, the temperature of the subsequent storage determines the morphology and kinetic mobility of the constituents of the system. Compared to room temperature storage conditions (sample R), it is obvious that the sensitivity of change in droplet size to powder storage time, t_f, is reduced with lowering temperature (Figure 3.6B). Emulsions formed by rehydration of the powder, stored at -30 °C, showed no variation with the duration of powder storage. The beneficial effect of lower temperature might be due to a lower kinetic and reduced

mobility, and therefore a slowing down of aggregation (Su et al., 2018). Nevertheless, the important point here is that this reduction in mobility does not only refer to the Brownian motion of droplets, as for example occurs when the continuous phase becomes a gel, as also seen in other types of applications. For all of the sufficiently dried and sealed powders, at any storage temperature, the mobility of droplets is expected to be very small. Thus, the reduction in mobility with temperature that we refer to here, is that which also includes the movement of actual oil molecules themselves, as well as desorption kinetics of HMS from the surface. This suggests that processes such as Ostwald ripening may have a bearing on destabilisation of droplets when in the dry powder form. On one hand, the larger significance of Ostwald ripening in the dry system seems reasonable, given that in such samples the oil volume fraction is approaching 80%. This is a very concentrated emulsion system, indeed. But on the other hand, the solid (glassy) nature of the dispersion medium should resist and slow down any shrinkage of droplets, unless if HMS can only form rather weak and mechanically fragile matrices prone to rearrangement between droplets. In any case, the absence of obvious visual signs of change in the size of droplets, between powders stored at different temperatures (See Appendix A, Figure A3) prior to rehydration, seems to rule out Ostwald ripening being the main contributor for the formation of more coarse droplets observed upon rehydration. Thus, the exact mechanism through which the mobility of oil molecules in the dry powder contributes to this observed coarsening of droplets, is more likely to be desorption of HMS from the surface of droplets and/or some degree of arrested partial coalescence, as was alluded to above.

To better understand how components of the dry powders were affected by low temperatures, oil crystallization and glass transition were also considered and characterised. Samples of powders stored for 20 days at -30 °C and 4 °C, as well as bulk sunflower oil, were scanned for X-ray diffraction pattern while held at scanning temperatures of 25 °C, -18 °C and -70 °C (Figure 3.8). A temperature of 25 °C is well above the crystallization temperature of bulk sunflower oil, typically between -20 to -17 °C (-20 °C here as determined by DSC, see Appendix A, Figure A2). Therefore, the oil component in the dry powders remained fluid with no characteristic peak associated with oil crystallisation detectable (Figure 3.8A). Dry emulsion powder stored under -30 °C and bulk oil showed no crystallinity, while that stored at 4 °C was overall molten with some small peaks. However, these peaks are most certainly not associated with the oil
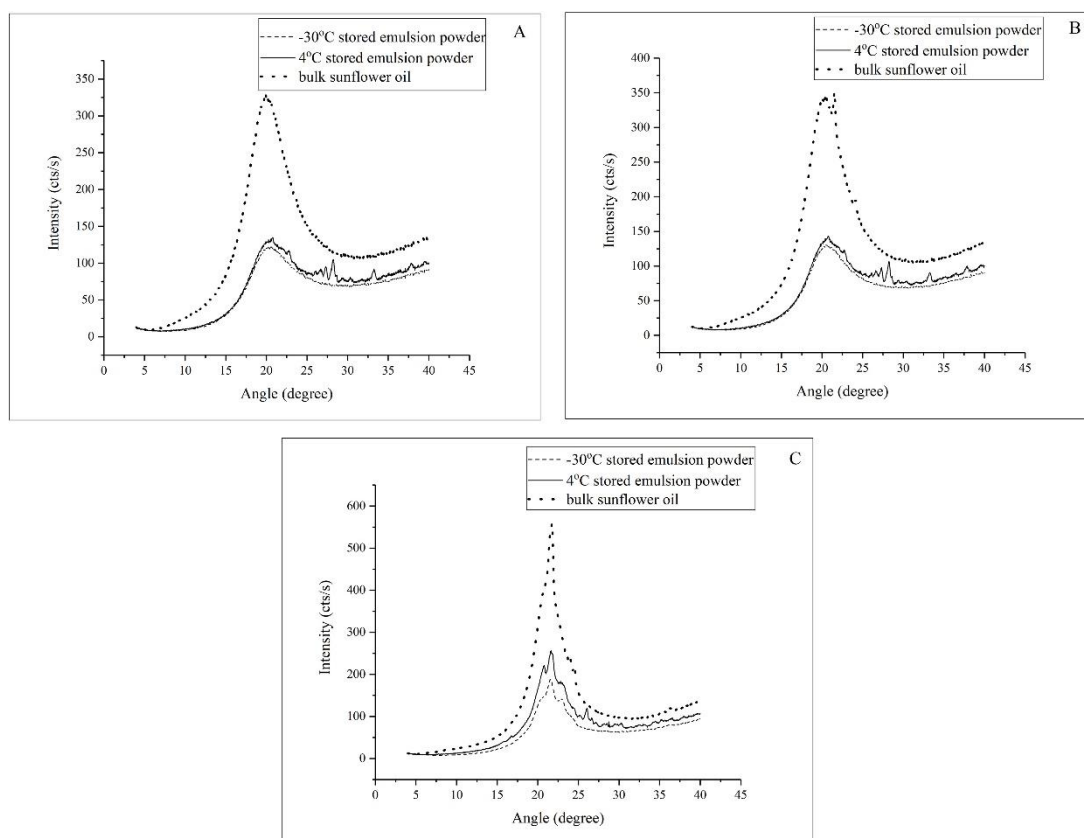
Figure 3.8 XRD patterns for 20-day stored emulsion powders and bulk sunflower oil, scanned while holding the samples at A) 25 °C, B) −18 °C, C) −70 °C.

phase, but seem most likely to be contributed by the buffer salt Na_3PO_4 in tetragonal structure (standard pattern 04-015-4964). As seen in the patterns scanned at -18 °C (Figure 3.8B), the supercooling effect is quite obvious as bulk sunflower oil showed distinctive peaks for crystallinity while the emulsion powders still remained molten, with no such peaks visible. As the scanning temperature was further lowered to -70 °C (Figure 3.8C), pronounced peaks from oil crystallization could be observed in all three samples. The appearance of additional peaks compared to bulk oil scanned at -18 °C indicates a possible transition from α-form crystalline to β' structure (Calligaris et al., 2008). Phase transition involving crystallization was also captured by the thermogram generated by DSC, involving a temperature scan in the range -45 °C to 25 °C. For the three stored emulsion powders (20 days at 4 °C, -18 °C, and -30 °C respectively) examined by DSC, the crystallization temperature (during cooling) was approximately -24.6 °C (Figure 3.9A), the melting point (during heating) was -27.5 °C (Figure 3.9B), and no glass transition was identified in the tested temperature range (Floros et al., 2014). The observation that all dried emulsion powders, irrespective of their original storage temperature, exhibited the same degree of

supercooling is a reflection of a similar size of the droplets in all these powders (see Appendix A, Figure A3). As mentioned previously, oil droplet size in dry powder did not change during powder storage, and the effect of powder storage temperature on droplet size only manifested itself once rehydration was performed. As evidenced here, destabilization upon reconstitution does not seem to be the result of alterations in the oil phase, but most likely related to desorption and re-adsorption behaviour of HMS in dried oil/starch matrix, as well as on the reformed O/W interface upon rehydration. Nonetheless, the fact that the oil droplets in VL powder (powder storage temperature of -30 °C) crystallised, rather than remaining in molten or amorphous states during their storage, can in itself have some bearing on the desorption of HMS from the surface of droplets. This difference may be a possible reason for the superior resistance of VL sample against aggregation/coalescence upon reconstitution, when compared to other powders stored at higher temperatures, i.e. where droplets remained molten (Bhandari and Howes, 1999). A study of the processes involving desorption of HMS, as occurring throughout the storage period within the dry state, is not trivial. This remains an area for future investigation.

Normal starch in dry state has an estimated glass transition temperature (T_g) no lower than 227 °C (Orford et al., 1989; Bizot et al., 1997; Bhandari and Howes, 1999). Even though the presence of water is known to significantly reduce T_g, it has been established that a moisture content as high as 22% is required to lower T_g of high molecular weight (> 10 MDa) starch down to room temperature (Bizot et al., 1997). With the amount of moisture in our powders determined at 3-5%, the T_g of our HMS is estimated to be above 50 °C, very unlikely to be as low as room temperature let alone below zero degrees (Mizuno et al., 1998; Liu, P. et al., 2009; Liu, P. et al., 2010; Lim and Roos, 2018). Therefore, the HMS matrix in all the emulsion powders studied here are thought to have remained in glassy state throughout the powder storage period (i.e. the only differentiating factor between various samples). Hence, the rubber-glass transition is not considered here as a process playing a significant role in altering the colloidal stability behaviour of different samples, seen post rehydration. Had for example the matrix consisted of a low molecular weight hydrocarbon (e.g. maltodextrin) instead, then clearly this could have been a very different proposition.
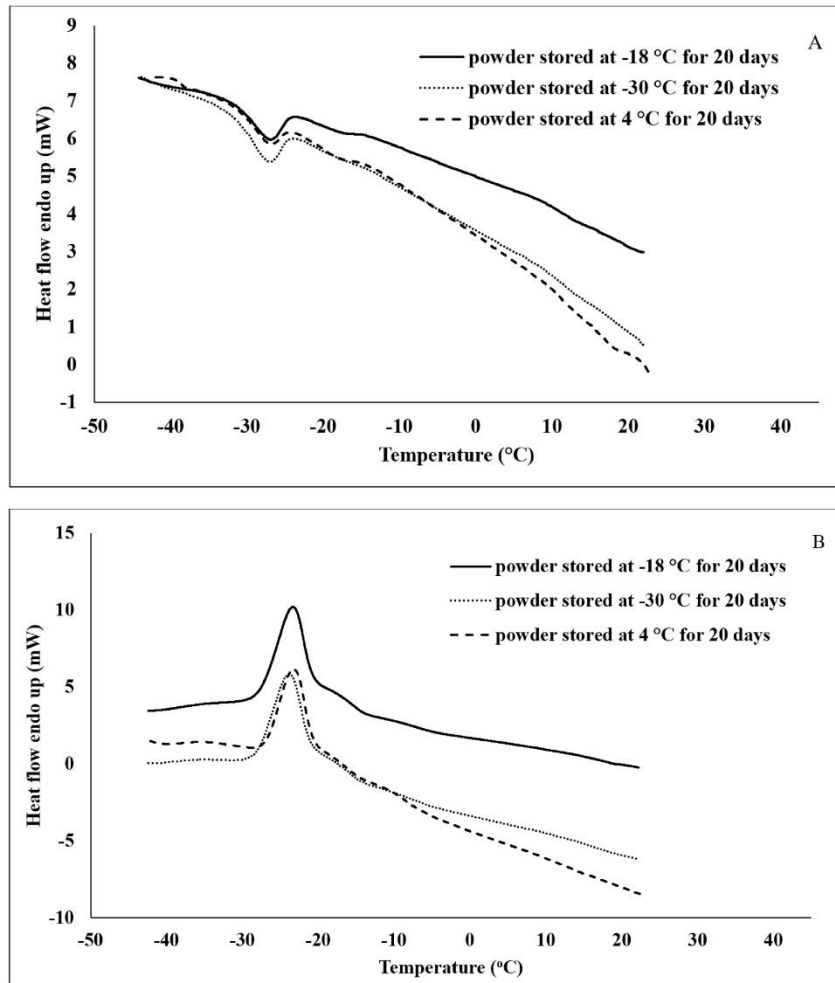
Figure 3.9 DSC thermograms for freeze-dried powders after 20 days of powder storage, A) cooling from 25 °C to −45 °C, B) heating from −45 °C to 25 °C.

Interestingly, in Figure 3.6B where the droplet sizes of reconstituted emulsions are plotted against powder storage time t_f, three different regimes can be identified for R and F samples. There is a short period of initial plateau, where droplet size did not seem to change much with t_f. When powder storage period exceeded 2 days, the average rehydrated droplet size became larger and showed higher sensitivity to t_f. A second plateau was reached when the powders were stored for 8 days or more before reconstitution, where the droplet size showed no further changes with increasing t_f once again. It is possible that dry powders stored at -18 °C (i.e. sample L) actually followed the same pattern of rehydrated size variation with t_f as the R and F samples. However, in this case the second regime, in which large variation of reconstituted droplet size was observed, was considerably delayed due to the prolonged first plateau regime (no droplet size change with t_f). In other words, had our observation time been far

longer, samples for all three storage temperatures that were higher than crystallization temperature of the oil phase, would have resulted in the same pattern of droplet size change with the duration of the powder storage period prior to rehydration. This delaying effect with lower storage temperature is quite clear from Figure 3.10, which shows the change in reconstituted droplet size distribution at different t_f. Similar effect of different storage temperatures on the deterioration of freeze-dried entities was found in the microcapsules produced by Malacrida et al. (2015), but their focus was on retention percentage of encapsulated material rather than reconstituted droplet size, unlike that here.
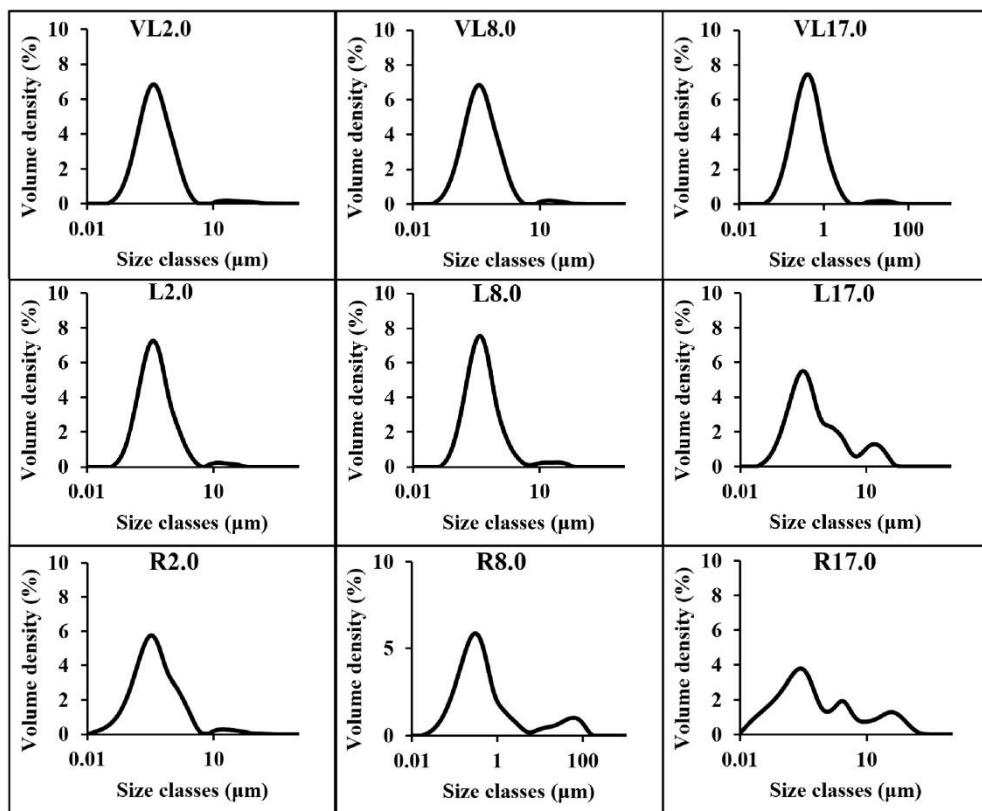
Figure 3.10 Droplet size distributions of reconstituted emulsions from powders that had been stored for 2, 8 and 17 days in conditions VL (−30 °C, sealed), L (−18 °C, sealed) and R (20 °C, sealed). All the distributions were obtained shortly after rehydration.

3.3.4.3 Long-term stability of reconstituted emulsion from dry stored powders

It was observed that the powders stored at room temperature (samples R) developed a weak gel-like texture subsequent to post reconstitution storage. These seem similar in appearance to those often

encountered in the presence of weak attractive depletion interactions between droplets. The structure was found to break down easily with gentle hand shaking. The samples were subjected to rheological measurements, but even at the very lowest shear rates, the gel was already too fragile and had sufficiently broken down to show any pronounced rheological characteristics. Presumably, as was discussed before, some HMS molecules desorbed from the interface during freeze-drying (and possibly powder storage period). Upon reconstitution the free HMS did not re-adsorb quickly enough, if at all, back onto the surface of the droplets. Presence of a small amount of free starch in solution could lead to depletion flocculation of oil droplets. The effect was disrupted by much higher dilution and the gentle shear that droplets suffer in the Mastersizer 3000. The weak flocs took a short period to separate. This manifests itself as an initial evolution of droplet size distribution in the Mastersizer over a period of 10 minutes or so, reaching a steady final value after that period. Interestingly a similar result was reported by Farshchi et al. (2013) with regards to a delay in complete break up of depletion flocculated aggregates occurring during similar measurements, though in their case the droplets were stabilised by soy bean protein.

Figure 3.11 shows Cryo-SEM images on reconstituted emulsions F11.87 and VL11.153, in which flocculation was suspected despite the lack of creaming. These samples were rehydrated and then flash frozen before imaging, as described in the method section. Like all other samples, in these two cases the droplet size remained fairly constant once samples were reconstituted (6.7 μm for F11.87 vs 3.91 μm for F11.0, and 1.8 μm for VL11.153 vs 1.18 μm for VL11.0). Occasionally, single droplets of a size over 10 μm were detected, but the vast majority of droplets were only visible under high magnification, as shown in Figure 3.11.

In Figure 3.11A, sample VL11.87 (with powder storage temperature of -30 ˚C) showed a uniform spatial distribution of droplet positions, having typical sizes of 1 μm. Some of the droplets aligned along the ridges, which was the result of getting pushed together by flash freezing of water. On the other hand, in Figure 3.11B for powder storage of 4 °C samples (samples F), it can be seen that a large cluster (~6 μm) was formed by aggregation of small droplets, with sizes less than 1 μm. Similar clusters were also seen in all the other F samples. Again, this seems to indicate some degree of flocculation in such cases. It is interesting that the droplets in these large flocs remained intact as individual droplets, rather than coalescing into
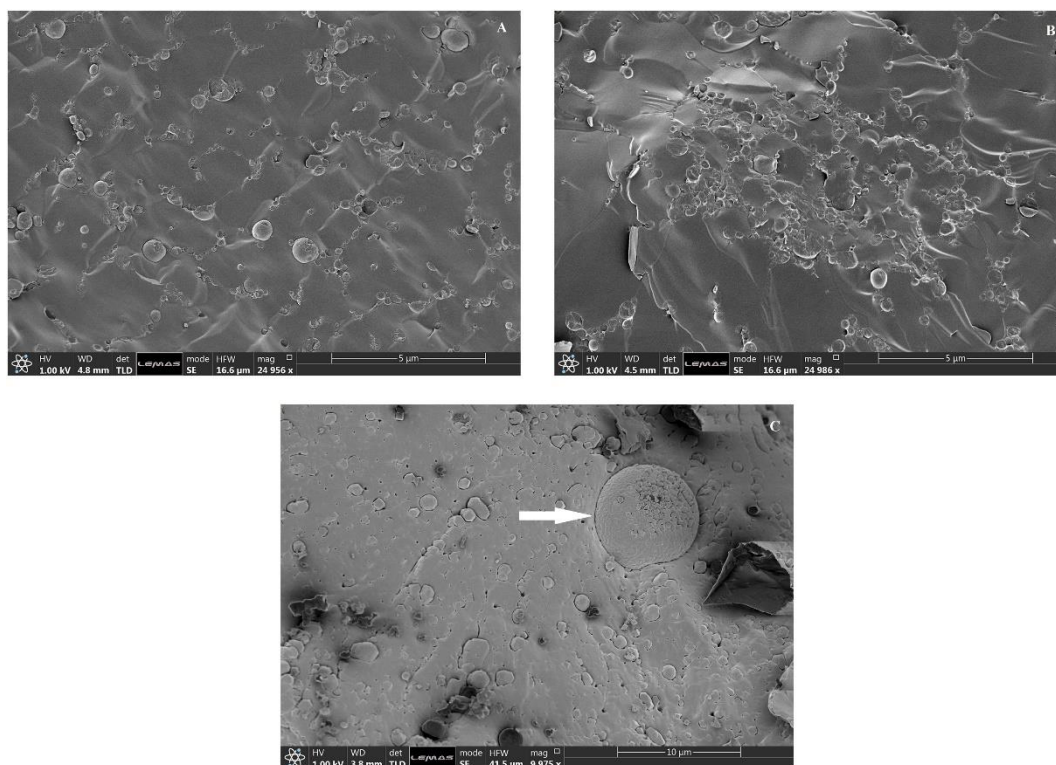
Figure 3.11 Cryo-SEM micrographs of reconstituted emulsions; A and C
were for samples VL11.153 (i.e. 11 days of powder storage, following
by 153 days post rehydration) while B was for sample F11.87.

bigger ones. This was the case even for our samples after a long period of
time, i.e. 153 days post rehydration. The molecularly adsorbed layer of HMS
must still be mostly intact, as indicated by the clear edges around each
droplet within the flocs. Presumably the thick HMS layer still could act as a
physical barrier preventing extensive coalescence, even after freeze-drying,
long period of powder storage, and many days post reconstitution. In Figure
3.11C, we show one interesting rare droplet with an approximate size of
8 µm. On the surface of this large droplet, there is a small region that does
not seem to be fully covered, and in this loosely packed area, particle-like
material can be observed. One could speculate that the surface of this
droplet was covered by aggregated HMS particles, judging by the non-
spherical shape of the small particulates. Presence of these droplets, though
quite rare, could indicate that a very small amount of HMS may not have
been completely dissolved, remaining in residual particulate form. These in
principle can adsorb onto the surface of droplets and lead to the formation of
Pickering droplets. Alternatively, some of the molecularly adsorbed HMS on
the surface of droplets may be reverting back to form particle aggregates
during freeze-drying or in the subsequent storage period. In any case, the
observation of these types of large droplets was too rare to allow us to

perform a more systematic detailed examination, or for it to have any significant practical implications.

3.4 Conclusions

Extensive attention has been paid to encapsulation in studies involving drying of emulsions. In contrast, long-term stability of rehydrated emulsions has rarely been considered, either as part of such microencapsulation studies or other research involving drying of emulsions. Similarly, the effect of powder storage conditions on the degree of entrapment of numerous active ingredients, their retention during dry storage and their protection against possible oxidation have been widely researched. Once again, far less research has involved the impact of powder storage on colloidal stability of the reconstituted emulsions. In the present study, we have shown that powder storage temperature plays a major role on the size and emulsion stability of droplets that are obtained after rehydration of the dried powder. This most likely is resulted from the limited diffusion of oil molecules, since the oil phase was found to be in crystalline form at temperatures below ~ -24 °C, showing some degree of supercooling as may be expected. The relative humidity on the other hand plays a rather minor role. This is perhaps due to hydrophobic modification of starch, somewhat reducing its affinity for uptake of moisture. Flocculation was observed in rehydrated emulsions, for samples reconstituted from powders stored at higher storage temperatures. However, extensive coalescence and emulsion breakdown were absent once the powder was rehydrated back to an emulsion. It is shown that during the powder storage period, oil droplets in the emulsion powder were not altered in morphology or size. Future studies should focus on characterising the HMS adsorbed layers on the surface of droplets within the dried powders. In particular, desorption/re-adsorption behaviour of HMS, as affected by powder storage temperature, should be investigated. We note that a study of such processes, occurring on the surface of droplets while in the dry form, remains quite challenging. Nonetheless, we have demonstrated in the current work that dry reconstitutable emulsions can be made and stored for considerable periods of time (more than 3 weeks), where upon simple rehydration (i.e. not needing any additional re-homogenisation), colloidally stable droplets of size < 2 μm were achieved (stable for more than 100 days after reconstitution). The result can have major commercial potential such as the possibility of the mass production of the dried emulsion powders in one central site, shipment

of the powder to other locations, and storage and rehydration of these as and when required. However, with further studies on optimising the relevant drying and storage conditions mentioned above, we believe that the realisation of even smaller, eventually stable sub-micron reconstitutable emulsions, formed by gentle rehydration of already dried emulsions, is a viable proposition.

Reference

Aberkane, L., Roudaut, G. and Saurel, R. 2014. Encapsulation and Oxidative Stability of PUFA-Rich Oil Microencapsulated by Spray Drying Using Pea Protein and Pectin. *Food and Bioprocess Technology.* **7**(5), pp.1505-1517.

Adachi, S., Imaoka, H., Hasegawa, Y. and Matsuno, R. 2003. Preparation of a water-in-oil-in-water (W/O/W) type microcapsules by a single-droplet-drying method and change in encapsulation efficiency of a hydrophilic substance during storage. *Bioscience Biotechnology and Biochemistry.* **67**(6), pp.1376-1381.

Ahmed, I.S. and Aboul-Einien, M. 2007. In vitro and in vivo evaluation of a fast-disintegrating lyophilized dry emulsion tablet containing griseofulvin. *European Journal of Pharmaceutical Sciences.* **32**(1), pp.58-68.

Akartuna, I., Studart, A.R., Tervoort, E. and Gauckler, L.J. 2008. Macroporous Ceramics from Particle-stabilized Emulsions. *Advanced Materials.* **20**(24), pp.4714-4718.

Alvarez Gaona, I.J., Bater, C., Zamora, M.C. and Chirife, J. 2018. Spray drying encapsulation of red wine: Stability of total monomeric anthocyanins and structural alterations upon storage. *Journal of Food Processing and Preservation.* **42**(2).

Amend, J.P. and Helgeson, H.C. 1997. Solubilities of the common L-alpha-amino acids as a function of temperature and solution pH. *Pure and Applied Chemistry.* **69**(5), pp.935-942.

Anwar, S.H. and Kunz, B. 2011. The influence of drying methods on the stabilization of fish oil microcapsules: Comparison of spray granulation, spray drying, and freeze drying. *Journal of Food Engineering.* **105**(2), pp.367-378.

Barnes, H.A. 2000. *A Handbook of Elementary Rheology.* Aberystwyth: The University of Wales Institute of Non-Newtonian Fluid.

Berli, C.L., Quemada, D. and Parker, A. 2002. Modelling the viscosity of depletion flocculated emulsions. *Colloids and Surfaces A: Physicochemical and Engineering Aspects.* **203**(1-3), pp.11-20.

Bhandari, B.R. and Howes, T. 1999. Implication of glass transition for the drying and stability of dried foods. *Journal of Food Engineering.* **40**, pp.71-79.

Bizot, H., Le Bail, P., Leroux, B., Davy, J., Roger, P. and Buleon, A. 1997. Calorimetric evaluation of the glass transition in hydrated, linear and

branched polyanhydroglucose compounds. *Carbohydrate Polymers.* **32**, pp.33-50.

Burgaud, I., Dickinson, E. and Nelson, P.V. 1990. An improved high-pressure homogenizer for making fine emulsions on a small scale. *International Journal of Food Science and Technology.* **25**, pp.39-46.

Calligaris, S., Arrighetti, G., Barba, L. and Nicoli, M.C. 2008. Phase Transition of Sunflower Oil as Affected by the Oxidation Level. *Journal of the American Oil Chemists' Society.* **85**(7), pp.591-598.

Chanamai, R. and McClements, D.J. 2001. Depletion Flocculation of Beverage Emulsions by Gum Arabic and Modified Starch. *Journal of Food Science.* **66**(3), pp.457-463.

Chanamai, R. and McClements, D.J. 2002. Comparison of gum arabic, modified starch, and whey protein isolate as emulsifiers: Influence of pH, CaCl(2) and temperature. *Journal of Food Science.* **67**(1), pp.120-125.

Cheuk, S.Y., Shih, F.F., Champagne, E.T., Daigle, K.W., Patindol, J.A., Mattison, C.P. and Boue, S.M. 2015. Nano-encapsulation of coenzyme Q10 using octenyl succinic anhydride modified starch. *Food Chem.* **174**, pp.585-590.

Christensen, K.L., Pedersen, G.P. and Kristensen, H.G. 2001. Preparation of redispersible dry emulsions by spray drying. *International Journal of Pharmaceutics.* **212**, pp.187-194.

Cramp, G.L., Docking, A.M., Ghosh, S. and Coupland, J.N. 2004. On the stability of oil-in-water emulsions to freezing. *Food Hydrocolloids.* **18**(6), pp.899-905.

Desai, K.G.H. and Park, H.J. 2005. Recent Developments in Microencapsulation of Food Ingredients. *Drying Technology.* **23**(7), pp.1361-1394.

Dickinson, E. 1989. A model of a concentrated dispersion exhibiting bridging flocculation and depletion flocculation. *Journal of Colloid and Interface Science.* **132**(1), pp.274-278.

Dickinson, E. 1992. *An Introduction to Food Colloid.* Oxford University Press.

Dickinson, E. 2009. Hydrocolloids as emulsifiers and emulsion stabilizers. *Food hydrocolloids.* **23**(6), pp.1473-1482.

Dickinson, E. 2012. Use of nanoparticles and microparticles in the formation and stabilization of food emulsions. *Trends in Food Science & Technology.* **24**(1), pp.4-12.

Domian, E., Cenkier, J., Górska, A. and Brynda-Kopytowska, A. 2018. Effect of oil content and drying method on bulk properties and stability of powdered emulsions with OSA starch and linseed oil. *Lwt.* **88**, pp.95-102.

Donsì, F., Wang, Y. and Huang, Q. 2011. Freeze–thaw stability of lecithin and modified starch-based nanoemulsions. *Food Hydrocolloids.* **25**(5), pp.1327-1336.

Dunn, M.S., Ross, F.J. and Read, L.S. 1933. The solubility of the amino acids in water*. *Journal of Biological Chemistry.* **103**(2), pp.579-595.

Elwell, M.W., Roberts, R.F. and Coupland, J.N. 2004. Effect of homogenization and surfactant type on the exchange of oil between emulsion droplets. *Food Hydrocolloids.* **18**(3), pp.413-418.

Ettelaie, R., Holmes, M., Chen, J.S. and Farshchi, A. 2016. Steric stabilising properties of hydrophobically modified starch: Amylose vs. amylopectin. *Food Hydrocolloids.* **58**, pp.364-377.

Ettelaie, R. and Murray, B.S. 2014. Effect of particle adsorption rates on the disproportionation process in pickering stabilised bubbles. *Journal of Chemical Physics.* **140**(20), p204713.

Ettelaie, R. and Murray, B.S. 2015. Evolution of bubble size distribution in particle stabilised bubble dispersions: Competition between particle adsorption and dissolution kinetics *Colloids and Surfaces A: Physicochemical and Engineering Aspects.* **475**, pp.27-36.

Ettelaie, R., Zengin, A. and Lishchuk, S.V. 2017. Novel food grade dispersants: Review of recent progress. *Current Opinion in Colloid & Interface Science.* **28**, pp.46-55.

Farshchi, A., Ettelaie, R. and Holmes, M. 2013. Influence of pH value and locust bean gum concentration on the stability of sodium caseinate-stabilized emulsions. *Food Hydrocolloids.* **32**(2), pp.402-411.

Floros, M.C., Leao, A.L. and Narine, S.S. 2014. Vegetable oil derived solvent, and catalyst free "click chemistry" thermoplastic polytriazoles. *Biomed Res Int.* **2014**, p792901.

Gallarate, M., Mittone, E., Carlotti, M.E., Trotta, M. and Piccerelle, P. 2009. Formulation of Dry Emulsion for Topical Applications. *Journal of Dispersion Science and Technology.* **30**(6), pp.823-833.

Garcia-Tejeda, Y.V., Salinas-Moreno, Y., Barrera-Figueroa, V. and Martinez-Bustos, F. 2018. Preparation and characterization of octenyl succinylated normal and waxy starches of maize as encapsulating agents for anthocyanins by spray-drying. *J Food Sci Technol.* **55**(6), pp.2279-2287.

Garti, N. and McClements, D.J. 2012. *Encapsulation technologies and delivery systems for food ingredients and nutraceuticals.* Oxford, UK: Woodhead Publishing.

Ghouchi-Eskandar, N., Simovic, S. and Prestidge, C.A. 2012. Solid-state nanoparticle coated emulsions for encapsulation and improving the chemical stability of all-trans-retinol. *International Journal of Pharmaceutics.* **423**(2), pp.384-391.

Giardiello, M., McDonald, T.O., Martin, P., Owen, A. and Rannard, S.P. 2012. Facile synthesis of complex multi-component organic and organic-magnetic inorganic nanocomposite particles. *Journal of Materials Chemistry.* **22**(47), pp.24744-24752.

Guzey, D. and McClements, D.J. 2006. Formation, stability and properties of multilayer emulsions for application in the food industry. *Advances in Colloid and Interface Science.* **128**, pp.227-248.

Hogan, S.A., McNamee, B.F., O'Riordan, E.D. and O'Sullivan, M. 2001. Emulsification and microencapsulation properties of sodium caseinate/carbohydrate blends. *International Dairy Journal.* **11**(3), pp.137-144.

Holgado, F., Marquez-Ruiz, G., Dobarganes, C. and Velasco, J. 2013. Influence of homogenisation conditions and drying method on physicochemical properties of dehydrated emulsions containing different solid components. *International Journal of Food Science and Technology.* **48**(7), pp.1498-1508.

Hunter, R.J. 2000. *Foundations of Colloid Science.* 2nd ed. Oxford: Clarendron Press.

Jena, S. and Das, H. 2012. Shelf life prediction of aluminum foil laminated polyethylene packed vacuum dried coconut milk powder. *Journal of Food Engineering.* **108**(1), pp.135-142.

Klinkesorn, U., Sophanodora, P., Chinachoti, P., Decker, E.A. and McClements, D.J. 2006. Characterization of spray-dried tuna oil emulsified in two-layered interfacial membranes prepared using electrostatic layer-by-layer deposition. *Food Research International.* **39**(4), pp.449-457.

Klinkesorn, U., Sophanodora, P., Chinachoti, P., McClements, D.J. and Decker, E.A. 2005. Stability of spray-dried tuna oil emulsions encapsulated with two-layered interfacial membranes. *Journal of Agricultural and Food Chemistry.* **53**(21), pp.8365-8371.

Laine, P., Kylli, P., Heinonen, M. and Jouppila, K. 2008. Storage stability of microencapsulated cloudberry (Rubus chamaemorus) phenolics. *Journal of Agricultural and Food Chemistry.* **56**(23), pp.11251-11261.

Li, K., Woo, M.W. and Selomulya, C. 2016. Effects of composition and relative humidity on the functional and storage properties of spray dried model milk emulsions. *Journal of Food Engineering.* **169**, pp.196-204.

Lim, A.S.L. and Roos, Y.H. 2018. Amorphous wall materials properties and degradation of carotenoids in spray dried formulations. *Journal of Food Engineering.* **223**, pp.62-69.

Liu, P., Yu, L., Liu, H., Chen, L. and Li, L. 2009. Glass transition temperature of starch studied by a high-speed DSC. *Carbohydrate Polymers.* **77**(2), pp.250-253.

Liu, P., Yu, L., Wang, X., Li, D., Chen, L. and Li, X. 2010. Glass transition temperature of starches with different amylose/amylopectin ratios. *Journal of Cereal Science.* **51**(3), pp.388-391.

Liu, W., Li, Y., Chen, M., Xu, F. and Zhong, F. 2018. Stabilizing Oil-in-Water Emulsion with Amorphous and Granular Octenyl Succinic Anhydride Modified Starches. *J Agric Food Chem.*

Liu, Z., Li, Y., Cui, F., Ping, L., Song, J., Ravee, Y., Jin, L., Xue, Y., Xu, J., Li, G., Wang, Y. and Zheng, Y. 2008. Production of Octenyl Succinic Anhydride-Modified Waxy Corn Starch and Its Characterization. *Journal of Agricultural and Food Chemistry.* **56**(23), pp.11499-11506.

Madene, A., Jacquot, M., Scher, J. and Desobry, S. 2006. Flavour encapsulation and controlled release - a review. *International Journal of Food Science and Technology.* **41**(1), pp.1-21.

Malacrida, C.R., Ferreira, S., Zuanon, L.A.C. and Nicoletti Telis, V.R. 2015. Freeze-Drying for Microencapsulation of Turmeric Oleoresin Using Modified Starch and Gelatin. *Journal of Food Processing and Preservation.* **39**(6), pp.1710-1719.

Marefati, A., Rayner, M., Timgren, A., Dejmek, P. and Sjoo, M. 2013. Freezing and freeze-drying of Pickering emulsions stabilized by starch granules. *Colloids and Surfaces a-Physicochemical and Engineering Aspects.* **436**, pp.512-520.

Matsuura, T., Ogawa, A., Tomabechi, M., Matsushita, R., Gohtani, S., Neoh, T.L. and Yoshii, H. 2015. Effect of dextrose equivalent of maltodextrin

on the stability of emulsified coconut-oil in spray-dried powder. *Journal of Food Engineering.* **163**, pp.54-59.

McClements, D.J. 2006. Non-covalent interactions between proteins and polysaccharides. *Biotechnology Advances.* **24**(6), pp.621-625.

McClements, D.J., Aoki, T., Decker, E.A., Gu, Y.S., Guzey, D., Kim, H.J., Klinkesorn, U., Moreau, L., Ogawa, S. and Tanasukam, P. 2005. Utilization of a layer-by-layer electrostatic deposition technique to improve food emulsion properties. In: Dickinson, E. ed. *Food Colloids: Interactions, Microstructure and Processing.* Cambridge: Royal Soc Chemistry, pp.326-336.

Millqvist-Fureby, A., Elofsson, U. and Bergenstahl, B. 2001. Surface composition of spray-dried milk protein-stabilised emulsions in relation to pre-heat treatment of proteins. *Colloids and Surfaces B-Biointerfaces.* **21**(1-3), pp.47-58.

Mizuno, A., Mitsuiki, M. and Motoki, M. 1998. Effect of Crystallinity on the Glass Transition Temperature of Starch. *J Agric Food Chem.* **46**, pp.98-103.

Modig, G., Nilsson, L., Bergenstahl, B. and Wahlund, K.-G. 2006. Homogenization-induced degradation of hydrophobically modified starch determined by asymmetrical flow field-flow fractionation and multi-angle light scattering. *Food Hydrocolloids.* **20**(7), pp.1087-1095.

Mun, S., Cho, Y., Decker, E.A. and McClements, D.J. 2008. Utilization of polysaccharide coatings to improve freeze-thaw and freeze-dry stability of protein-coated lipid droplets. *Journal of Food Engineering.* **86**(4), pp.508-518.

Murray, B.S., Durga, K., Yusoff, A. and Stoyanov, S.D. 2011. Stabilization of foams and emulsions by mixtures of surface active food-grade particles and proteins. *Food Hydrocolloids.* **25**(4), pp.627-638.

Naik, A., Meda, V. and Lele, S.S. 2014. Freeze drying for microencapsulation of alpha-linolenic acid rich oil: A functional ingredient from Lepidium sativum seeds. *European Journal of Lipid Science and Technology.* **116**(7), pp.837-846.

Nilsson, L. and Bergenstahl, B. 2006. Adsorption of hydrophobically modified starch at oil/water interfaces during emulsification. *Langmuir.* **22**(21), pp.8770-8776.

Nilsson, L. and Bergenstahl, B. 2006. Adsorption of Hydrophobically Modified Starch at Oil/Water Interfaces during Emulsification. *Langmuir.* **22**, pp.8770-8776.

Nilsson, L. and Bergenstahl, B. 2007. Emulsification and adsorption properties of hydrophobically modified potato and barley starch. *Journal of Agricultural and Food Chemistry.* **55**(4), pp.1469-1474.

O'Dwyer, S.P., O'Beirne, D., Eidhin, D.N. and O'Kennedy, B.T. 2013. Effects of emulsification and microencapsulation on the oxidative stability of camelina and sunflower oils. *J Microencapsul.* **30**(5), pp.451-459.

Orford, P.D., Parker, R., Ring, S.G. and Smith, A.C. 1989. Effect of water as a diluent on the glass transition behaviour of malto-oligosaccharides, amylose and amylopectin. *International Journal of Biological Macromolecules.* **11**, pp.91-96.

Qian, L. and Zhang, H.F. 2011. Controlled freezing and freeze drying: a versatile route for porous and micro-/nano-structured materials.

Journal of Chemical Technology and Biotechnology. **86**(2), pp.172-184.

Ray, S., Raychaudhuri, U. and Chakraborty, R. 2016. An overview of encapsulation of active compounds used in food products by drying technology. *Food Bioscience.* **13**, pp.76-83.

Russel, W.B., Saville, D.A. and Schowalter, W.R. 1992. *Colloidal Dispersions.* Cambridge University Press.

Serfert, Y., Schroder, J., Mescher, A., Laackmann, J., Ratzke, K., Shaikh, M.Q., Gaukel, V., Moritz, H.U., Schuchmann, H.P., Walzel, P., Drusch, S. and Schwarz, K. 2013. Spray drying behaviour and functionality of emulsions with beta-lactoglobulin/pectin interfacial complexes. *Food Hydrocolloids.* **31**(2), pp.438-445.

Sousdaleff, M., Baesso, M.L., Neto, A.M., Nogueira, A.C.u., Marcolino, V.A. and Matioli, G. 2013. Microencapsulation by freeze-drying of potassium norbixinate and curcumin with maltodextrin: stability, solubility, and food application. *Journal of agricultural and food chemistry.* **61**(4), pp.955-965.

Su, J., Guo, Q., Mao, L., Gao, Y. and Yuan, F. 2018. Effect of gum arabic on the storage stability and antibacterial ability of β-lactoglobulin stabilized d -limonene emulsion. *Food Hydrocolloids.* **84**, pp.75-83.

Sweedman, M.C., Tizzotti, M.J., Schaefer, C. and Gilbert, R.G. 2013. Structure and physicochemical properties of octenyl succinic anhydride modified starches: A review. *Carbohydrate Polymers.* **92**(1), pp.905-920.

Tang, C. and Li, X. 2013. Microencapsulation properties of soy protein isolate: Influence of preheating and/or blending with lactose. *Journal of Food Engineering.* **117**(3), pp.281-290.

Tesch, S., Gerhards, C. and Schubert, H. 2002. Stabilization of emulsions by OSA starches. *Journal of Food Engineering.* **54**(2), pp.167-174.

Thanasukarn, P., Pongsawatmanit, R. and McClements, D.J. 2004. Impact of fat and water crystallization on the stability of hydrogenated palm oil-in-water emulsions stabilized by whey protein isolate. *Colloids and Surfaces a-Physicochemical and Engineering Aspects.* **246**(1-3), pp.49-59.

Walstra, P., Wouters, H.T.M. and Geurts, T.J. 2006. Dairy Science and Technology, Second Edition. *Dairy Science and Technology, Second Edition.*

Yusoff, A. and Murray, B.S. 2011. Modified starch granules as particle-stabilizers of oil-in-water emulsions. *Food Hydrocolloids.* **25**(1), pp.42-55.

Zhang, Y.T., Tan, C., Abbas, S., Eric, K., Zhang, X.M., Xia, S.Q. and Jia, C.S. 2014. The effect of soy protein structural modification on emulsion properties and oxidative stability of fish oil microcapsules. *Colloids and Surfaces B-Biointerfaces.* **120**, pp.63-70.

Zhu, X., Zhang, N., Lin, W. and Tang, C. 2017. Freeze-thaw stability of pickering emulsions stabilized by soy and whey protein particles. *Food Hydrocolloids.* **69**, pp.173-184.

Chapter 4
Effect of amylose and amylopectin content on the colloidal behaviour of emulsions stabilised by OSA-Modified starch
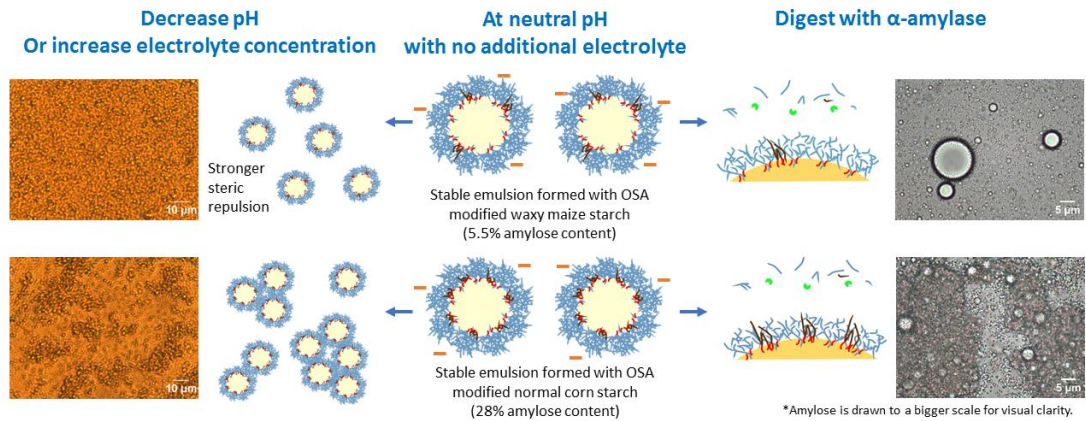
Abstract

The impact of the amylose content (AC) of hydrophobically modified starch on its emulsion stabilising behaviour has been examined in this study. Waxy maize (W) and normal corn starches (N) with different amylose contents, 5.48% and 28.37% respectively, were hydrophobically modified with Octenyl Succinic Anhydride (OSA) (3%) and used to fabricate oil-in-water emulsions. Emulsion samples were compared for their colloidal stability against pH change, increase of electrolyte concentration and enzymatic treatment by amylase. The amylose content of the OS-starch made a pronounced difference to emulsion stability in all cases. Increases in the electrolyte concentration, or decrease of pH to low values, left emulsions stabilised by OS-N (medium AC) strongly flocculated. However, little coalescence of droplets was detected, even after 21 days. In comparison, the OS-W (low AC) stabilised emulsion remained well dispersed throughout the entire storage period, following changes to pH or raised salt concentrations. The contrast between the behaviour of the samples is attributed to the provision of sufficient steric interactions by OS-W emulsifier but not OS-N. Destabilisation following α-amylase treatment revealed a different trend, with both *in vitro* and *in vivo* digestion experiments leaving the low AC (OS-W) stabilised droplets showing extensive coalescence immediately post treatment. Over the same short period, the OS-N stabilised emulsions

became flocculated, but again without much droplet coalescence. The enzymatic degradation of OS-N interfacial layers seems to proceed more slowly than the OS-W samples. Varying destabilisation rates provide a means for realising tailored release profiles of flavours or active ingredients, achieved in principle by appropriate mixing of several emulsions stabilised by different AC modified starch.

4.1 Introduction

In the food industry, there has been an increasing trend in moving away from synthetic surfactants to more natural emulsifiers. In the past few decades, food biopolymers, i.e. proteins and polysaccharides have been studied extensively for their emulsifying and stabilising properties, with most surface active colloidal stabilisers currently in use being protein based (Dickinson, 2013; Wijaya et al., 2017). Researchers continue to seek novel colloidal stabilisers derived from these two types of biopolymers, and progress has been made with fragmented proteins (Ettelaie et al., 2014; Mokni Ghribi et al., 2015; Dai et al., 2019), conjugates of protein and polysaccharide through Maillard reaction (Kato et al., 1990; Benichou et al., 2002; Akhtar and Dickinson, 2007), and hydrophobically modified starch (Chanamai and McClements, 2001; Chanamai and McClements, 2002; Nilsson and Bergenstahl, 2006; Ettelaie et al., 2016; Ettelaie et al., 2017; Arshad et al., 2018; Hu et al., 2019; Mu et al., 2019).

Hydrophobically modified starch is also considered as an inexpensive and abundant substitute for Gum Arabic. Being of plant source and the "gold standard" of beverage emulsion industry, Gum Arabic is a composite polysaccharide containing a small amount of lower molecular weight protitious fraction (Randall et al., 1988; Dickinson, 2018), which is thought to be entirely responsible for its surface active properties. Due to its high heterogeneity and rather small portion of the glycoprotein fraction, usually large amounts are required in real formulations, resulting in higher cost. Upon hydrophobic modification, starch develops an amphiphilic nature and becomes surface active. Compared to proteins, this modified starch has been found to provide a higher degree of colloidal stability at low pH and high electrolyte concentrations (Chanamai and McClements, 2002). This is because the main stabilising mechanism provided by the hydrophobically modified starch is thought to be based on the provision of steric repulsion and is not electrostatic in origin (Tesch et al., 2002). Screening of any electrostatic interaction, as there might be in the case of modified starch

esters, using high electrolyte concentrations or at low pH conditions, have provided support for this view (Chanamai and McClements, 2002; Lin et al., 2018b).

Currently, the only legally permitted material for hydrophobic modification of starch for use as food emulsifiers is octenyl succinic anhydride (OSA). Even then this is limited to less than 3% by weight (FDA, US) (Bai et al., 2014; Zhao et al., 2018). The modification reaction is most commonly carried out in an alkaline medium. OS-starch has many potential applications other than beverage emulsions, for example encapsulation of fragrances, essential oils and fish oils, and formulation of reconstitutable emulsions for easier transportation and storage (Cheuk et al., 2015; Samakradhamrongthai et al., 2016; Garcia-Tejeda et al., 2018; Mu et al., 2019). There is indeed a trend in using clean label ingredients in the food industry, which may lead to a reduction in the use and eventual phasing out of any chemically modified starch. Nonetheless, research on OS-starch is still likely to remain relevant in other industries such as nutraceutical and pharmaceutical, and any phasing out will be a gradual process.

In recent years, increasing attention has been paid to understanding the possible connection between the structure of starch molecules and the stabilising properties of the derived OS-starch. For example, these studies have involved examining starches of various botanical source or cultivar, and attempting to link their structural characteristics to their functional properties (Song et al., 2013; Simsek et al., 2015; Wang et al., 2016; Whitney et al., 2016). Evidence indicates that starch granules have a layered structure, and modifying agents such as OSA gain access to the interior of the granule by the pores on the surface and channels leading to a central cavity (Huber and BeMiller, 2000; Liu et al., 2018). The crystalline region of a starch granule consists of helices formed by the short branches (DP 10-15) of amylopectin, whereas amylose sits mostly in the amorphous region of the granule. Various studies on distribution of OSA in the starch granule have found that OSA mainly attaches to starch in the amorphous regions of the latter. If true this implies that the amylose molecules are the primary receptors for OSA in modified starch granules (Shogren et al., 2000; Wang et al., 2013; Whitney et al., 2016; Liu et al., 2018). One question that naturally arises from the above studies, and has caught the attention of several researchers in recent years, is whether the amylose content (AC) of a starch affects the substitution efficiency, and thus the emulsifying and stabilising properties of the modified starch. This is likely given the possible

bias of OSA attachments to amylose chains. Importantly, this is not to say that amylose content is the only relevant factor to the emulsification and stabilisation properties of OS-starch. Other structural factors such as the crystallinity of granule, crystal types, granule size, molecular chain length, degree of branching of amylopectin might also be responsible. Nevertheless, the focus in the current work remains on the influence of the proportion of amylose in the modified starch on its emulsifying ability.

It has been suggested that the emulsification ability of OS-starch increases with higher degree of substitution (DS) in the range of interest here (modification <3%) (Bhosale and Singhal, 2006; Ruan et al., 2009; Lin et al., 2018a). Studies by Lopez-Silva et al. (2020), Song et al. (2014) and He et al. (2006) all supported this view. These researchers found that DS is positively correlated to amylose content of the native starch. However, other work conducted with starch from the same botanical source as the previous researches, as well as different ones, found either no correlation or a slightly negative correlation (Song et al., 2013; Sweedman et al., 2014a; Cruz-Benítez et al., 2019; Lopez-Silva et al., 2019). In terms of application oriented comparisons, encapsulation involving modified starch from different sources, has been addressed by Cruz-Benítez et al. (2019), even though colloidal stability was not of main interest and only the encapsulated dry powder was characterised.

Few studies focused on the impact of amylose content of OS-starch in liquid emulsions. Even in those systems that do involve the fabrication and characterisation of liquid emulsions, the OS-starch was sometimes kept in granular form to provide a Pickering type emulsifier (Song et al., 2014; Lopez-Silva et al., 2019). Pickering emulsion (Pickering, 1907) has a different stabilising mechanism in the sense that it maintains colloidal stability due to difficulty of displacing the adsorbed particles from the interface resulting from large desorption energies (> 1000 kT). A distinction is to be made with typical steric repulsion, as in molecularly adsorbed OS-starch ester stabilised emulsions, where the droplets are kept apart due to the excluded volume repulsion between overlapping interfacial layers. The typical size of starch granules ranges from 2 µm to 50 µm, so as a result, the oil droplets they stabilise through Pickering mechanism are usually no smaller than 10 µm (Simsek et al., 2015; Matos et al., 2018). However, once OS-starch granules are gelatinised, the solution is capable of producing sub-micron emulsions with amylose and amylopectin polymers (Chanamai and McClements, 2002; Sweedman et al., 2014b).

Among the very few studies involving gelatinised OS-starch stabilised liquid emulsions and the impact of amylose content, there are both experimental and theoretical investigations. Experimentally, Song et al. (2013) produced stable emulsions with gelatinised modified rice starch, having droplet sizes ranging from 1 μm to 12 μm. Emulsion stability was reported to be enhanced with smaller AC values, whereas the initial droplet size seemed to change non monotonically with varying amylose content for the studied cultivars of *indica* rice. Sweedman et al. (2014a) used maize starch of various AC to emulsify an oil based solution of β-carotene (1 wt% oil content emulsion). They were able to fabricate emulsions with excellent colloidal stability at low amylose content, but also observed a faster destabilisation of droplets as AC was increased. High pressure homogenisation was employed in this work, and modified maize starch was able to confer a real sub-micron size for droplets (~300 nm). However, in both of these studies, emulsion stability was examined only in a rather limited range of electrolyte concentration and pH, relevant to the specific purpose of their investigation. For Song et al. (2013) this was to differentiate between the rice cultivars while Sweedman et al. (2014a) explored the possibility of achieving high oxidative protection for β-carotene. As a result, in these low stress systems, no additional electrolyte was added, and the pH of the systems were not even mentioned. The work of (Lopez-Silva et al., 2019) is potentially also a possible case of gelatinised OS-starch stabilised emulsion. They reported emulsion droplet sizes that are lower than their corresponding starch granule sizes, despite describing their emulsions as being of Pickering variety in their publication.

On the theoretical side, the work of Ettelaie et al. (2016), based on numerical Self Consistent Field (SCF) calculations, compared behaviour of amylose and amylopectin with equal degrees of hydrophobic modification. The study made two major assumptions. Firstly, it assumed that the background electrolyte concentration was sufficiently high so as to screen any electrostatic repulsion. Thus, any predicted emulsion stability can purely be attributed to steric interactions. Secondly, amylose and amylopectin were taken to have the same molecular weight, with the only remaining difference being the branched and linear nature of these two starch biopolymers. While the chosen molecular weight of chains was in a region where the size distribution of amylose and amylopectin are just about to overlap with each other, amylopectin tends to have a typical molecular weight 100x larger than average sized amylose. Nonetheless, under these limiting assumptions, the study suggested that amylopectin would form a more compact layer at the

interface, and is therefore associated with a larger energy minimum, once van der Waals interactions are also included in the calculations. On the other hand, amylose formed less dense but more extended films, resulting in longer ranged repulsion. However, this advantage was cancelled out by the prediction of an additional energy minimum at closer inter-droplet separation. This was shown to arise from larger tendency of modified amylose to cause bridging flocculation. It was also indicated that a mixture of amylopectin with a small amount of amylose would have better performance than pure amylopectin (Ettelaie et al., 2016).

Other than changes in electrolyte concentration and pH, colloidal systems stabilised with OS-starch can also be destabilised by enzymatic digestion of the starch. Amylolysis of OS-starch, in the absence of any oil droplets, has been studied and compared with that of native unmodified starch. It has generally been found that OSA modification reduces starch digestibility, regardless of starch source (Ai et al., 2013; Simsek et al., 2015; Bajaj et al., 2019; Lopez-Silva et al., 2020). Several recent studies have also examined the impact of the enzymatic digestion of OS-starch on the rate of emulsion degradation. The focus of these studies has largely been the sensory perception, substance release in the gastric-intestinal tract, and a comparison of the behaviour of starch stabilised droplets with protein stabilised ones upon the application of gastric-intestinal digestive enzymes (Silletti et al., 2007; Dresselhuis et al., 2008; Lin et al., 2018a; Hu et al., 2019). One general conclusion from all such research is that emulsions stabilised with OS-starch can indeed be destabilised due to the break-down of adsorbed OS-starch surface layers by starch-digesting enzymes. It is natural to speculate that amylose content may have an impact on OS-starch digestibility of such interfacial films, much in the same way as native starch itself. If so, then AC should also influence the stability behaviour and the rate of break-down of emulsions stabilised with OS-starch during amylase treatment. Very recently, Lopez-Silva et al. (2020) reported tentative results supporting this view. They found that OS-starch digestibility is positively linked to amylose content. Although their work only focused on OS-starch digestion in bulk, without considering the implication for emulsion destabilisation, it nonetheless provides a foundation for the above idea. That is to say, different digestibility of OS-starch resulting from the variability in their amylose content, may have an impact on the enzymatically induced destabilisation behaviour of the emulsions fabricated using these emulsifiers. The work in this area is still rather sparse and, to the best of our knowledge,

very little has been published in comparing the enzymatic degradation of emulsions that are stabilised by OS-starch of different AC.

In the research work presented here, we would firstly like to extend the previous studies in the literature by performing a more careful systematic experimental study, highlighting the differences in adsorption behaviour of starch polymers possessing varying amylose contents (AC). The colloidal stability of the emulsions produced from these, over a broad range of electrolyte concentrations and pH is investigated. Furthermore, preliminary studies involving enzymatic hydrolysis of stabilising OS-starch on droplet interface are performed. The work reported here includes both *in vitro* and *in vivo* experiments, mimicking starch digestion in the oral phase. The resultant degradation behaviour of the emulsions is examined, providing a base for more extensive future work. The prospect of different droplet destabilisation times, during enzymatic treatment of emulsions stabilised by hydrophobically modified starch of varying amylose content, opens up interesting possibilities. For example, they may lead to the tantalising prospect of achieving a broad range of desired tailored controlled release profiles, simply by an appropriate mixing of droplets stabilised by OS-starch of different AC.

4.2 Material and Methods

4.2.1 Materials

Waxy maize starch (W) and normal corn starch (N) were purchased from Shandong Fuyang Biotech Ltd. Co. (Dezhou, China) and Sigma-Aldrich (Shanghai, China) respectively. Octenyl succinic anhydride (OSA) was purchased from Sigma-Aldrich (Shanghai, China). Sunflower oil was purchased from a local supermarket. Our α-amylase (diluted with starch, from *Bacillus substilisa*) was purchased from Maya Reagent (Shanghai, China). All other chemicals, including mucin from porcine stomach type II, were purchased from Sigma-Aldrich (Shanghai, China). Deionised water was obtained from a Milli-Q apparatus (Millipore, Bedford, UK) and was used to prepare all solutions and samples.

4.2.2 Modification of starch with OSA

Starch was suspended in distilled water (33 wt%) with agitation. The pH of the slurry was adjusted to 8.2 with 0.5 M NaOH solution. OSA (3%) was added slowly over 2 h, and the reaction was carried out for 22 h in total. The weak acid produced during the reaction was neutralised continuously,

ensuring that pH remained at 8.2 and allowing the reaction to proceed forward. In the final stage of the process, the reaction was terminated by adjusting pH to 6.0. This was achieved using 0.5 M HCl. After being centrifuged and washed twice with ethanol and twice more with distilled water, removing any unreacted OSA, the sample was then oven dried at 40 °C for 48 hours.

4.2.3 Emulsification with OSA-starch

Oil-in-water emulsions containing 10 wt% sunflower oil and 1 wt% OS-starch were fabricated. OS-starch was suspended in Milli-Q water, and heated in hot water bath at 90 °C with intermittent stirring, for 60 min. This was to ensure a maximal degree of gelatinization. The resultant OS-starch solution was then cooled to room temperature and used for emulsion preparation. Primary emulsions were made at 18,000 rpm with high-speed homogeniser (IKA Ultra Turrax T25, UK). The final emulsions were prepared using either a Microfluidizer at 250 bar (Microfluidics M-110P, Westwood, Massachusetts, USA) or a University of Leeds in-house made Jet homogenizer operating at a constant pressure of 250 bar (Burgaud et al., 1990). When required, pH of the emulsion was adjusted by addition of 0.1 M HCl or NaOH, and electrolyte concentration by addition of NaCl (s). During such addition, the emulsions were kept under mild magnetic stirring for the entire process and 3 minutes after. Care was taken so that the solutions and solids were added very slowly into the meniscus to minimize the effect of high local concentration.

4.2.4 Recovering OSA-starch from the surface of emulsion droplets

The emulsion was centrifuged at 8500 rcf until a clear cream layer separated from the serum layer. The cream layer was carefully removed, and the oil was extracted with 1:2 methanol and chloroform. The insoluble material was recovered starch. Solvents were evaporated and the recovered starch was oven dried at 40 °C after 3 washes by Milli-Q water. Perhaps an additional washing step for ultracentrifuged cream layer would help in getting rid of the last traces of unadsorbed starch chains, this step was not performed here.

4.2.5 Characterisation of starch

4.2.5.1 Amylose content

The amylose content of starch was determined using the iodine adsorption method (Hoover and Ratnayake, 2001), and the absorbance was

measured at 600 nm with a UV-VIS spectrophotometer UV-2600 (Shimadzu, China).

4.2.5.2 NMR

NMR analysis was conducted to determine the degree of substitution (DS) of various starch samples. The procedure was conducted as described by Zhao et al. (2018). Native and OSA modified starches were dissolved in DMSO-d_6 using a previously described method (Schmitz et al., 2009). Recordings of ^{1}H spectra were made on a Bruker 400M System (Bruker, Fallanden, Switzerland) at 30 °C with a pulse angle of 30°, a delay time of 10 s and an acquisition time of 2 s. The degree of substitution was calculated according to the equation

$$DS = \frac{I_{0.89}}{3\left(I_{\alpha-1,6} + I_{\alpha-1,4} + I_{r-e}\right)}$$

where I_{r-e} corresponds to the ^{1}H NMR integral of the α and β reducing-end signals at 4.91 and 4.28 ppm, respectively. Similarly, $I_{\alpha-1,4}$ and $I_{\alpha-1,6}$ are the ^{1}H NMR integrals of internal α-1,4 and α-1,6 glycosidic linkages.

4.2.5.3 Fourier Transform Infrared Spectroscopy (FT-IR)

The IR spectra of native and modified starches were obtained using a FTIR Nicolet iS5 (Thermo Fisher Scientific, WI, USA). A minute amount of sample was ground with FTIR grade potassium bromide (approximately 1:80) and pressed to form a pellet disc. The disc was placed in the sample compartment and the scanning range was kept at 400-4000 cm^{-1} to generate the spectra.

4.2.6 Characterisation of emulsion

4.2.6.1 Droplet size

The droplet size of emulsions was measured using a laser light scattering instrument Mastersizer 3000 (Malvern Panalytical, UK). Before droplet size measurement, emulsions were shaken by hand to ensure homogeneity. Sample was added to the dispersion unit connected to the laser light scattering instrument until an obscuration between 5% and 10% was obtained. The mean droplet size was reported as the volume-weighted mean diameter, $D_{4,3} = \sum_i n_i d_i^4 / \sum_i n_i d_i^3$, where n_i denotes the number of droplets with a diameter d_i.

4.2.6.2 ζ-potential

The ζ-potential of the emulsions was measured with Zetasizer Nano ZS (Malvern Panalytical, UK). Emulsions were diluted by a factor of 2000, and then filled in a folded capillary cell DTS1070.

4.2.6.3 Apparent viscosity

The apparent viscosity of emulsions was measured using a Kinexus Ultra rheometer (Malvern Panalytical, UK) and a double gap concentric cylinder DG25 geometry (cup diameter 26.25 mm, bob internal diameter 24 mm, bob external diameter, 25 mm). The samples were gently mixed, poured into the temperature-controlled measurement cell, and allowed to equilibrate at 25 °C or 37 °C for 5 min prior to the measurement. Apparent viscosity of emulsions was measured for shear rates in the range 0.2-200 s^{-1} using application of continuous shear, at 25 °C or 37 °C.

4.2.6.4 Optical microscope

Emulsion droplets were observed under a Nikon optical microscope fitted with a Leica MC120 HD camera (Leica, Heidelberg, Germany). Objectives used were at magnifications of 40x or 100x. Images were captured with LAS v4.6 software.

4.2.6.5 Turbiscan

Emulsions or mixtures of emulsion and saliva were carefully added to a sample holder. The backscattering of light was measured using a TurbiscanLab instrument (Formulaction, Toulouse, France). A laser light source of 850 nm scanned across the height of the sample holder (42 mm), at 37 °C, for a period of 20 mins.

4.2.7 *In vitro* oral digestion

4.2.7.1 With amylase

Emulsions were mixed with amylase solution (2 g/L, pH 6.8) at 1:1 ratio, and immediately placed in a shaking water bath of 37 °C and 100 rpm. Droplet size measurements and microscopic images were taken of the samples at 10 s, 300 s, 600 s, 1200 s, using the methods described above.

4.2.7.2 With artificial saliva

Emulsions kept at various temperatures (4 °C, 25 °C or 50 °C) were mixed with artificial saliva (Appendix B, Table B1) (Davis et al., 1971; Sarkar, Anwesha et al., 2009; Karthik et al., 2019) at 1:1 ratio, and immediately placed in a shaking water bath of 37 °C and 100 rpm. Droplet size

measurements and microscopic images were taken of the samples at 10 s, 300 s, 600 s, and 1200 s using the methods described above.

4.2.8 *In vivo* oral digestion

The *in vivo* oral digestion was conducted with ten healthy panellists (5 females and 5 males, aged between 22 and 24, all non-smokers). It was ensured that no food was consumed by the panellists in the 2 h 30 min prior to the session. A 2 ml aliquot of emulsion was added into a 25 ml food-grade plastic sauce container with lid. The samples were coded with 3 digits and the order of presentation was randomised. For each sample, the panellists were asked to place the 2 ml emulsion in their mouth, gently stir it with their tongue to mix it with saliva, and spit it back into the sauce container after the designated time (3 s, 10 s, 30 s or 60 s). The collected digested samples were immediately characterised by droplet size measurement and, for a few of the samples, by optical microscopy. Before starting the session and after each sample, the panellists were asked to rinse their mouth and palate with bottled water at least for three times. Approximately, 5 min break was taken between the samples, for the panellists to rest and restore normal salivary secretion for the next trial. Consent was obtained in writing from each panellist and this study is covered by the ethical approval obtained from Zhejiang Gongshang University, China (2015111265).

4.2.9 Statistical analysis

All measurements were performed in triplicate, and the data presented were expressed as the mean values ± standard deviations. Two-tail paired t-tests were performed where applicable, and $p<0.05$ was set to determine the level of statistical significance.

4.3 Results and discussion

4.3.1 Physiochemical properties of native and OS starch

The FT-IR spectra of native and modified W (waxy maize) and N (normal corn) starch are shown in Figure 4.1. The broad peaks at approximately 3400 cm^{-1} indicate the hydroxyl groups, and those at 2930 cm^{-1} indicate C-H stretching. The peak at 1650 cm^{-1} represents bound water present in the starch. The characteristic peaks for starch materials are present between 800 cm^{-1} and 1200 cm^{-1} (Shingel, 2002). Compared to native W and N, the OSA modified starch showed two additional peaks at around 1740 and 1567 cm^{-1}. The peak at 1740 cm^{-1} is due to the characteristic IR stretching vibration of C = O, and an evidence for the

formation of ester carbonyl groups. The peak at 1567 cm^{-1} is indicative of the asymmetric stretching vibration of carboxylate groups (RCOO^{-}) (Miao et al., 2014; Simsek et al., 2015). These results confirmed the substitution of hydroxyl groups in starch by ester carbonyl and carboxyl groups in OSA, thus the formation of OS-W and OS-N.
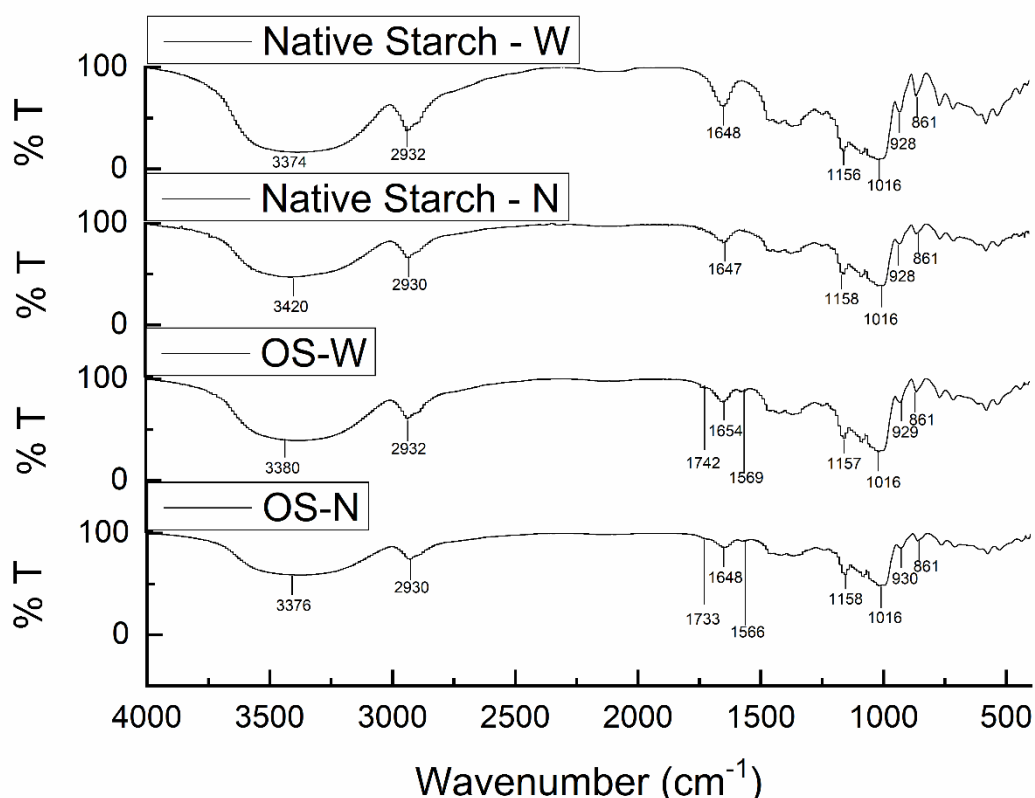
Figure 4.1 FT-IR spectra of native and OSA modified starch samples.

The AC of native W and N were determined to be 5.48 ± 0.99% and 28.37 ± 0.10% respectively (Table 4.1), by a colorimetric method based on the iodine affinity of amylose (Hoover and Ratnayake, 2001). The amylose helices form dark blue complexes with iodine, and the colour change is used to determine the amylose content. Upon the attachment of OSA, the helical structures of amylose are disrupted, thus resulting in a decrease in the measured AC values for both types of starch (Lopez-Silva et al., 2020). The amylose content of starch and the degree of substitution (DS) upon modification, have been found to be positively correlated in some studies (He et al., 2006; Song et al., 2013; Song et al., 2014; Lopez-Silva et al., 2019), while negatively in others (Sweedman et al., 2014a; Cruz-Benítez et al., 2019). In our case, the native starch with lower AC (W) yielded a DS of

0.0160 ± 0.0021 when it was OSA modified. The same modification procedure for N, i.e. the starch with the higher AC, achieved a DS of 0.0229 ± 0.0012. This is in line with the preferential attachment of OSA to amylose molecules, which has been found in various previous research studies (Shogren et al., 2000; Wang et al., 2013; Whitney et al., 2016; Liu et al., 2018).

Table 4.1 Table providing amylose content (AC) and Degree of substitution (DS) of native waxy maze (W) and native normal corn starch (N), their hydrophobically modified samples (OS–W and OS-N), and the adsorbed OS-starch fraction recovered from the interface (OS-W$_R$ and OS-N$_R$) post emulsification.

A significant level of statistical difference (p < 0.05) is detected for any two samples with different lowercase superscript letters that follow the values of DS or AC in each column.

	AC (%)	DS
Native W	5.48 ± 0.99[a]	/
OS-W	3.93 ± 0.31[b]	0.0160 ± 0.0021[a]
OS-W$_R$	7.99 ± 0.64[c]	0.0194 ± 0.0001[b]
Native N	28.37 ± 0.10[d]	/
OS-N	21.86 ± 1.79[e]	0.0229 ± 0.0012[c]
OS-N$_R$	23.59 ± 1.23[e]	0.0291 ± 0.0029[d]

4.3.2 Emulsification and Stabilisation properties

4.3.2.1 Adsorption on the surface

OS-W and OS-N were then used in fabricating emulsions, and the adsorbed modified starch was recovered from the surface of oil droplets using the method described in section 4.2.4. The recovered OS-starch is referred to as OS-W$_R$ and OS-N$_R$. As shown in Table 4.1, both adsorbed starch showed significantly (two-tailed paired t-test, p<0.05) higher DS than the bulk (OS-W and OS-N). This suggests that modification with OSA improves the surface affinity of the starch molecules, with the ones having a higher level of attached OS groups being preferentially adsorbed on the interface. For starch adsorbed on the surface of droplets, OS-W$_R$ contained a significantly larger percentage of amylose than OS-W in bulk, whereas

OS-N_R did not when compared to OS-N. The increase in AC from OS-W to OS-W_R indicates a stronger adsorption for amylose molecules than amylopectin, and thus once again seems to support the previous findings that OSA preferentially attaches to amylose (Shogren et al., 2000; Wang et al., 2013; Liu et al., 2018).

As the amount of amylose content of starch increases, one would expect smaller differences in DS between chains in bulk and those on the surface post adsorption. However, difficulties in obtaining amylose molecules in their dissolved form with OS-N may also have played a role and cannot be ruled out. As AC rises, the gelatinization temperature of a starch is elevated, making it harder to achieve full gelatinization (Jeong and Lim, 2003). During the cooling down of starch solution before homogenization, retrogradation is more pronounced with higher AC (Dobosz et al., 2019), and thus possibly less amylose can remain in the form of free molecules available for adsorption.

4.3.2.2 Destabilising emulsions by lowering pH

One of the major advantages of OSA modified starch as a molecularly adsorbed colloidal stabiliser, is that it predominantly relies on the provision of steric repulsion for stabilizing oil droplets, rather than electrostatic forces. As a result, the emulsions formed by these are more resistant to changes in environmental factors such as variation in pH and electrolyte concentrations (Chanamai and McClements, 2002; Sweedman et al., 2014a). In order to verify and compare the steric stabilising effect of OS-W and OS-N, emulsions produced by these emulsifiers (referred to as W and N, respectively) using a Jet Homogeniser, were subjected to a series of pH changes and electrolyte additions. When adjusting pH of the emulsions, 0.5 M HCl or NaOH was added to the system. This of course can also affect the electrolyte concentration, aside from changing pH. In order to rule out this interference, NaCl was added to the emulsions to bring the background electrolyte concentration up to 0.003 M. This ensures that any changes we caused by adjusting pH would remain negligible compared to this pre-existing background electrolyte level.

Figure 4.2 captures the changes in $D_{4,3}$ average droplet size for emulsions kept under different pH conditions, after various periods of storage. The sizes of droplets initially produced at pH 6.5 were 440 nm and 550 nm, for W and N samples, respectively. At day 0, emulsion W showed little variation in droplet size with pH adjustment throughout the range 3.5 to
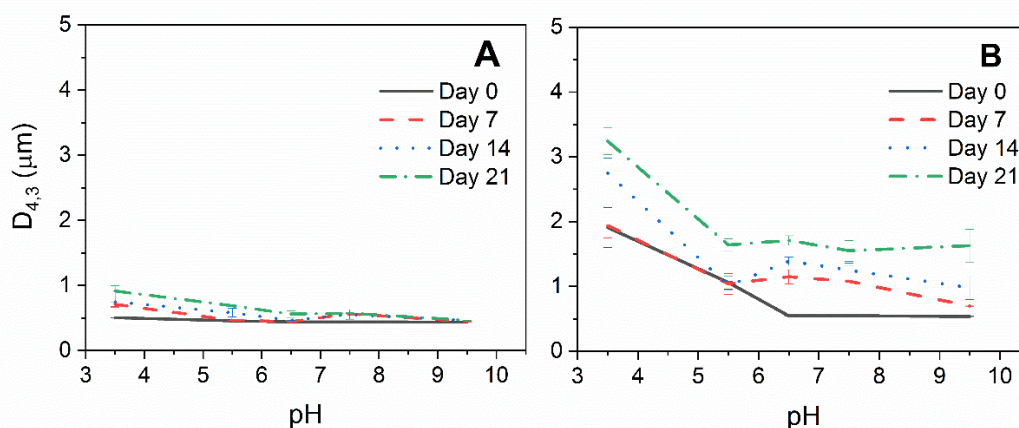
Figure 4.2 Mean droplet size $D_{4,3}$ for emulsions measured under different pH conditions, following various periods of storage (day 0 to day 21); A) emulsion W, B) emulsion N.

9.5. However, with time, there was a slight increase in the droplet size of W when the sample was kept at more acidic pH values, increasing from 500 nm to 910 nm after 21 days at pH 3.5. On the other hand, almost immediately from day 0, emulsion N kept at acidic conditions (pH < 6.5) possessed markedly larger droplets than those stored at alkaline pH. For example, the average size at pH 7.5 was 549 nm, while at pH 3.5 it was found to be 1.91 µm. This difference in droplet sizes was maintained as the emulsions went through 21 days of storage, with the droplet size at pH 6.5 on day 21 growing to 1.71 µm, while at pH 3.5 it measured at 3.24 µm (see Figure 4.2). Due to the –COO$^-$ groups in the OS chain, the OS-starch is slightly negatively charged at neutral and alkaline pH. As a result, droplets with surfaces covered by OS-W and OS-N had negative ζ-potentials (Figure 4.3). As pH is decreased to acidic values, the carboxylic groups become protonated (-COOH) and lose their negative charge. This is seen (Figure 4.3) in the smaller value of the measured ζ-potential. Nevertheless, it is worth pointing out that even at pH 7.5 to 9.5, the measured ζ-potential of approximately -6 mV to -11 mV was considered just short of sufficient (at 0.003M electrolyte) for the resulting electrostatic repulsion to act as the sole stabilising mechanism for emulsion droplets over a period of as long as 21 days. This was verified with calculation of DLVO interactions (not shown here) (Hunter, 2001).

These results indicate that emulsion W, based on OS-starch of lower amylose content, was reasonably stable across the pH range 3.5 to 9.5 for at least 21 days (Figure 4.2A). As pH changed from 9.5 to 3.5, the electrostatic force between droplets was almost completely removed, as is evident from the measured ζ-potential of merely -1.35 mV at pH 3.5
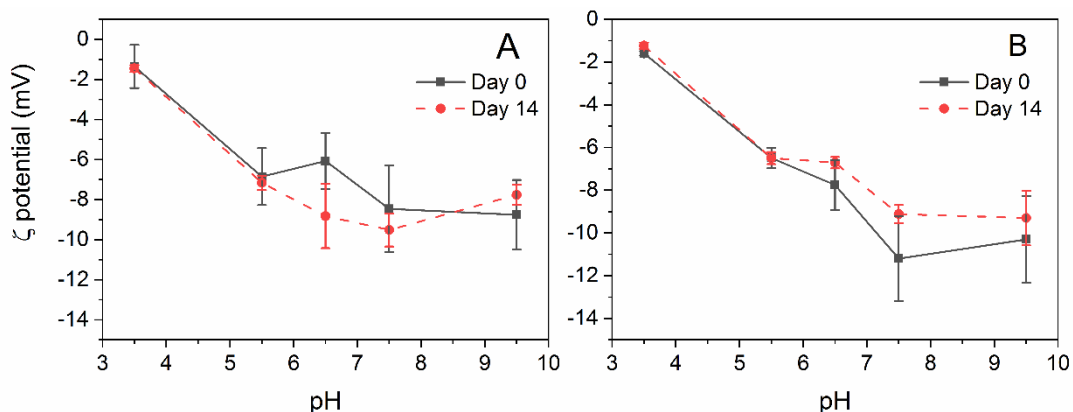
Figure 4.3 Variation of ζ-potential of emulsion droplets with pH, measured after varying periods of storage (day 0 and day 14); A) emulsion W, B) emulsion N.

(Figure 4.3). The fact that emulsion W was still sufficiently stable under such a condition, even after 21 days, suggests that OS-W is capable of stabilising the emulsion almost entirely by the virtue of its induced steric repulsion forces between the oil droplets. On the other hand, our emulsion N, with its higher AC, exhibited lower emulsion stability as electrostatic interaction was removed by the decrease in pH. It was safe to conclude that any steric stabilising effect, as there might be due to OS-N starch adsorbed layers, was not strong enough to stabilise emulsion droplets on its own. It is most likely then that OS-N starch stabilised droplets, in contrast to OS-W ones, were at least partially dependent on electrostatic interactions for the provision of their stabilising mechanism.

4.3.2.3 Destabilising emulsions by increasing electrolyte concentration

Because OS-starches are slightly negatively charged molecules, both a lowering of pH and increasing the background electrolyte concentration of the continuous phase should reduce or screen out the electrostatic repulsion between the oil droplets. If our conclusion regarding the partial reliance of the stability of our N emulsions on electrostatic forces is true, then the same droplet behaviours should also present itself in systems with elevated electrolyte concentration.

In order to change the electrolyte concentration of emulsions without altering pH, various amounts of NaCl were introduced to emulsions W and N, and the resulting emulsions were kept and observed for 21 days. In Figure 4.4, we have plotted the average droplet size as a function of storage time for emulsions containing different concentrations of electrolyte, at pH 6.5. When there was no additional NaCl, both emulsions maintained their
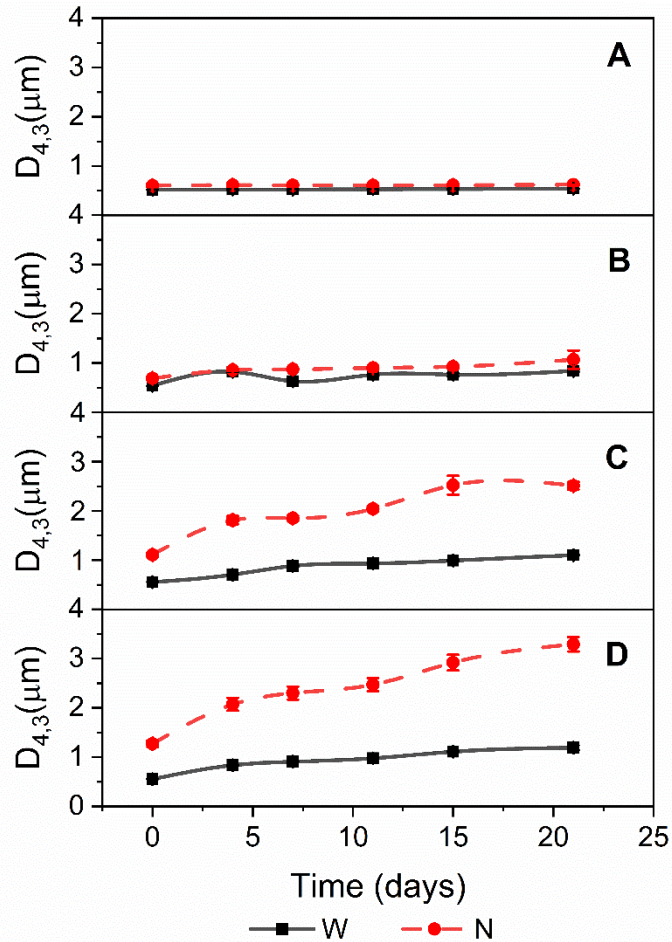
Figure 4.4 The evolution of the average droplet size, $D_{4,3}$, in W emulsion
(black solid lines) and N emulsion samples (red dashed lines) with the
storage period. Samples are considered with A) no additional
electrolyte, B) addition of 0.02 M NaCl, C) addition of 0.1 M NaCl, D)
addition of 0.2 M NaCl. Standard deviations are represented as error
bars.

droplet sizes at around 500 nm throughout the 21 days. For W samples (i.e.
ones stabilised by low AC modified starch) emulsions containing higher
electrolytes retained their submicron size for the entire storage period. In
comparison, the N emulsions (i.e. ones stabilised by higher amylose content
modified starch) destabilised over time (Figure 4.4). At 0.1 M and 0.2 M
NaCl, the droplet size of N samples exceeded 1 µm within hours of the NaCl
addition.

Values of ζ-potential values of W and N emulsions, with or without
addition of NaCl are presented in Table 4.2. With no additional electrolyte, W
and N droplets had measured ζ-potentials of -17.11 ± 1.02 mV and -15.13 ±
0.63 mV respectively. Upon the introduction of 0.2 M NaCl to the system, the
charge on the droplet surface was screened and the ζ-potential dropped
to -2.5 mV for both of our emulsions. At such electrolyte concentrations then,

Table 4.2 Measured ζ-potentials of emulsions W or N without any added electrolyte and with 0.2 M added NaCl.

	W with no additional electrolyte (mV)	W with 0.2M additional NaCl (mV)	N with no additional electrolyte (mV)	N with 0.2M additional NaCl (mV)
ζ-potential	-17.11 ± 1.02	-2.85 ± 0.38	-15.13 ± 0.63	-2.3 ± 0.18

the electrostatic repulsion between droplets must be very small. The impact on the stability behaviour of the two sets of emulsions is seen to be identical to that of reducing pH, as discussed earlier. Thus, the same conclusions are reinforced with regards to the stabilising mechanism of OS-W and OS-N starch. In the case of emulsion W stored at 0.2 M NaCl concentration, one observes that the average droplet size remains at a submicron size, despite the lack of electrostatic repulsion between the droplets. Once again this shows that in these W emulsions, OS-W emulsifiers are able to provide strong steric forces that are sufficient to stabilise droplets on their own, even in the absence of electrostatic forces. However, for emulsion N, even though the steric forces may still be of some importance, the electrostatic repulsion between the droplets are necessary to ensure their colloidal stability. Once this latter is removed, e.g. by an increase in electrolyte screening or decrease of pH, destabilisation of the emulsion system is observed.

Rheological behaviours of the emulsions at various NaCl concentrations were characterised by measuring shear rates and corresponding shear stresses according to the method described in section 4.2.6.3, for each of the emulsion samples (Appendix B, Table B2). A power law fluid equation (Barnes et al., 1989; Sopade and Filibus, 1995) was fitted to logarithmic plots of apparent viscosity, η, vs. shear rate $\dot{\gamma}$

$$\eta = K\dot{\gamma}^{n-1}$$

for the measured data. In the above equation, K is the flow consistency index and n the flow behaviour index. Newtonian behaviour of a fluid can be distinguished by an n value close to 1. Both emulsions W and N, in the absence of any added electrolyte exhibited Newtonian behaviour during the observed time, with $n = 0.99$ and 0.98 at day 21, respectively (Appendix B, Table B2). With 0.2 M of added NaCl, N emulsion became shear thinning, as indicated by the flow behaviour index changing to $n = 0.65 < 1$, as shown in Figure 4.5. This is likely due to the possible formation of a weak network of
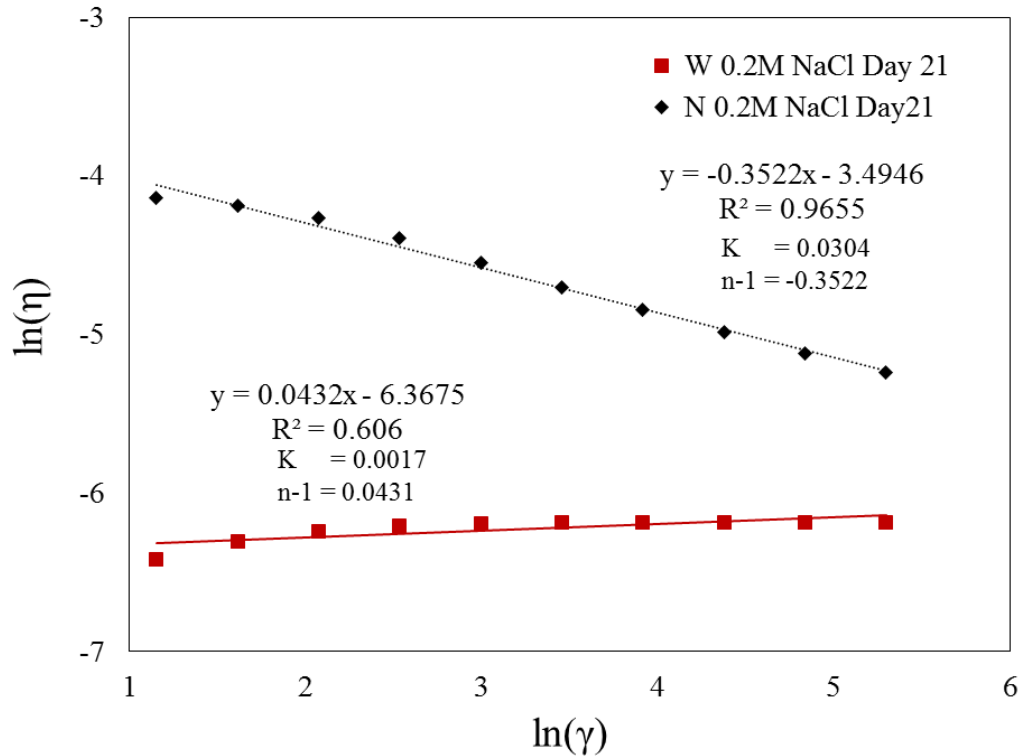
Figure 4.5 Power law fits to apparent viscosity results, η, plotted on a log-log graph against shear rate, obtained in the range 5–200 s-1.

Emulsion W (solid line) and N (dotted line), were stored for 21 days at NaCl concentrations of 0.2 M prior to the measurements. The resulting flow consistency index, K, and the flow behaviour index, n, are indicated on the graph for each case. The low value of n-1 indicates a near Newtonian behaviour for W sample.

oil droplets (Chanamai and McClements, 2001), as both OS-W and OS-N solutions on their own exhibited Newtonian behaviour when subjected to the same measurement (Appendix B, Figure B4). The results in Figure 4.5 are after 21 days of storage, although the shear thinning behaviour was already evident even at earlier times. In contrast, W emulsion has $n \approx 1.04$ at day 21 and remains Newtonian even after such a long period of storage.

A weak network formed by emulsion droplets suggests aggregation rather than coalescence. For example, depletion flocculation in emulsions are reversible by dilution or shearing, whereas coalescence is an irreversible destabilisation process (Dickinson, 2019). Droplet aggregation in an emulsion stabilised by biopolymers can normally be distinguished from droplet coalescence by addition of sodium dodecyl sulphate (SDS). The dilution by SDS breaks many possible types of bonds between the droplets. So long as the droplets have not coalesced, this leads to a marked decrease
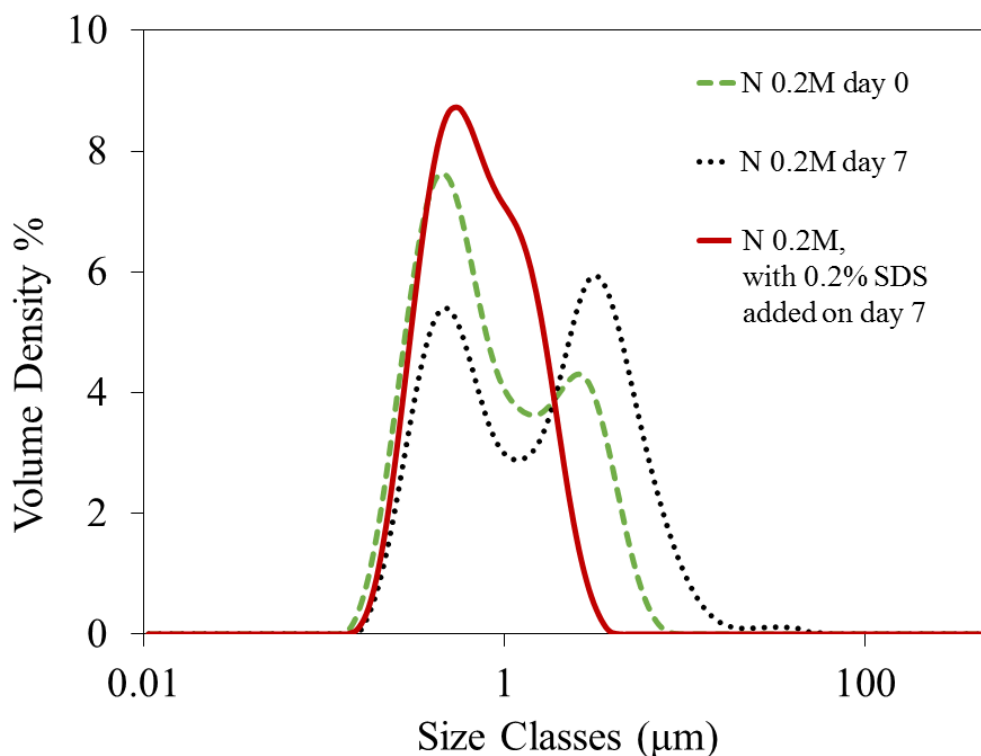
Figure 4.6 Droplet size distribution of emulsion N with the addition of 0.2 M
NaCl at day 0, and after 7 days of storage, before and after the
addition of 2% SDS.

in the measured particle size as the network of droplets falls apart
(Demetriades and McClements, 2000). Upon the addition of 2 wt% SDS to
emulsion N, at 0.2 M of added NaCl and kept for 7 days, the second peak in
the droplet size distribution shifted significantly to the left. At the same time,
the first peak at the lower sizes became visibly more pronounced (Figure
4.6). This large shift in the droplet size distribution to lower values suggests
that the destabilisation in N was primarily due to droplet aggregation, with
only a limited degree of coalescence having taken place. The formation of
flocculated aggregates in N with 0.2 M salt can also be clearly observed in
the microscopic images in Figure 4.7. In both W and N with no additional
electrolyte, droplets remained uniformly dispersed, retaining their submicron
sizes over the period of observation. With the introduction of 0.2 M NaCl, the
average particle size of emulsion W increased slightly from 550 nm at day 0
and to 830 nm at day 4 but continued to remain below one micron even after
21 days. In contrast, in emulsion N the formation of large flocs (but without
any extensive coalescence) was noticeable starting from day 11. This
coincided with the time when shear-thinning behaviour began to also
manifest itself in our rheological measurements of this system.

| | Day 0 | Day 11 | Day 21 |
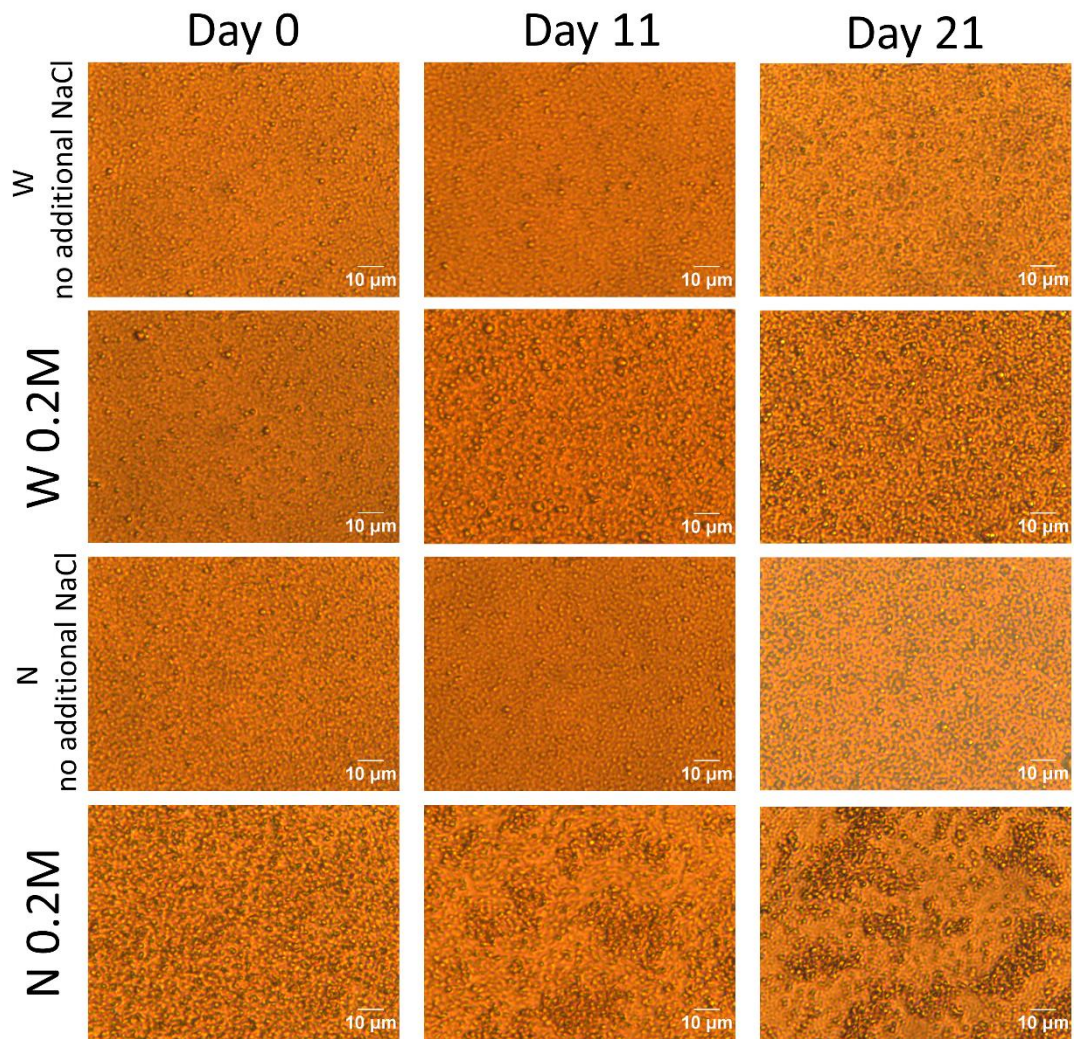
Figure 4.7 Microscopic images of emulsions W and N with either no additional electrolyte, or 0.2 M NaCl, after various periods of storage.

Both alterations of pH and changes in electrolyte concentration, demonstrate that OS-W is more efficient in provision of steric stabilisation. This low AC modified starch is less dependent on the availability of the electrostatic repulsion in order to provide a sufficient degree of colloidal stabilisation of droplets, as compared to OS-N. The size and structure of starch granules to some degree depend on their botanic source and specific cultivar. However, if and once fully gelatinised, the granules of OS-W and OS-N can be considered to have disappeared and the starch then exists in the solution in the form of dissolved modified amylose and amylopectin molecules in our systems. Therefore, in such a state the fundamental difference between dissolved OS-W and OS-N starch has to be largely sought in their composition, including the ratio of their amylose and

amylopectin content. Therefore, the conformation adopted by these two molecules adsorbed on the oil/water interface is likely the main contributor to the different steric stabilising properties of OS-W and OS-N, seen in our study here. Ettelaie et al. (2016) conducted numerically based calculations using Self-Consistent Field (SCF) theory in order to compare the interfacial behaviours of amylose and amylopectin. In their somewhat idealised models, all aspects of the structure of amylose and amylopectin were considered identical, including their molecular weights, degrees of hydrophobic modification and various interactions parameters associated with monomer comprising the chains. The only difference left was the level of branching, with amylose represented as a linear biopolymer and amylopectin as a highly dendritic branched macromolecule. The computations provided the interactions mediated by the overlap of adsorbed adjacent layers on neighbouring droplets. Also, the direct attractive van der Waals forces were accounted for in the calculations. However, it was assumed that the system was under the conditions where electrostatic repulsion was negligible (e.g. low pH or high salt). It was found that for both modified amylose and amylopectin, when each considered on their own, there was a shallow energy minima (< 5 k_BT) in particle interaction potentials, occurring at droplet separations where the adsorbed layers just began to overlap. This happened at shorter separations for amylopectin, which was attributed to its more compact but rather denser interfacial layers. The depth of such minima is too small to cause any appreciable droplet aggregation. However, the calculated interaction potentials between two droplets, as stabilised by modified amylose, also exhibited a second energy minimum at a closer droplet-droplet separation distance. This second energy minimum was much deeper. Its presence may well be important in accounting for the inferior relative steric stabilising ability of the hydrophobically modified amylose, as is observed in our current study. The theoretical models attributed the second energy minimum to the less dense and more extended conformation of modified amylose layers, when compared to layers formed by amylopectin of the same hypothetical molecular weight. This allowed for various OSA hydrophobically modified sites on the amylose to become more easily associated with two different nearby surfaces. In other words, Ettelaie et al. (2016) concluded that hydrophobically modified amylose has some affinity for inducing bridging flocculation, not otherwise present for amylopectin of a comparable M_w. Of course, in reality amylopectin is not of comparable molecular weight to amylose, but on average typically 100 times larger. Therefore, even with

chains having a higher tendency to extend away from the surface, it is likely that the linear amylose molecules still form thinner interfacial layers, and thus weaker steric repulsion than amylopectin. Coupled with preferential attachment of OS groups to amylose as discussed previously, and with its higher tendency for bridging, the modified amylose when possessing little charge will have a higher potential to cause aggregation of the droplets.

Our experimental results with emulsion N are largely in line with the above theoretical predictions. We further verified that 23.59% amylose content on the interface was enough to induce flocculation of the droplets, when electrostatic repulsion was largely absent.

4.3.3 Destabilisation of emulsion through enzymatic digestion of OS-starch in the oral phase

4.3.3.1 Enzymatic destabilisation in oral phase: *in vitro*

To study the destabilisation of W and N emulsions induced by enzymatic digestion of OS-W and OS-N starch interfacial layers, emulsions were produced by Microfluidizer and the conditions were optimised so that the final emulsions W and N both had the same droplet size of $D_{4,3} = 0.55$ μm (Appendix B, Figure B1). The final emulsions were stored and tested for their colloidal stability during a period of 16 days (Appendix B, Figure B2), and new batches were made under the same conditions to be used within 3 days for *in vitro* and *in vivo* experiments.

The changes in droplet size of W and N upon the action of 2 g/L α-amylase solution are shown in Figure 4.8A. In order to exclude any destabilisation of emulsion resulting from changes in the environmental factors, such as an elevated temperature (37 °C) and shaking (100 rpm), control samples were made by mixing emulsions with equal amounts of Milli-Q water. These were subjected to exactly the same temperature and shaking as samples containing the enzyme. The emulsion average size in both control samples (W control and N control) remained at $D_{4,3} = 0.55$ μm within the 1200 seconds duration of the study. In contrast, both enzyme-treated samples W and N exhibited larger droplet sizes as a result of the action of α-amylase. In the presence of α-amylase, droplet size of W increased to 8.62 μm in the first 10 seconds, and 70.96 μm at 1200 s. On the other hand, the change in N was markedly more gradual, with $D_{4,3}$ measured at 4.78 μm at the end of the 1200 s time period of the observation. During the oral stage, the enzyme α-amylase would cleave α-1,4 glycosidic bonds in the starch chains, leaving the branching points that are α-1,6 glycosidic
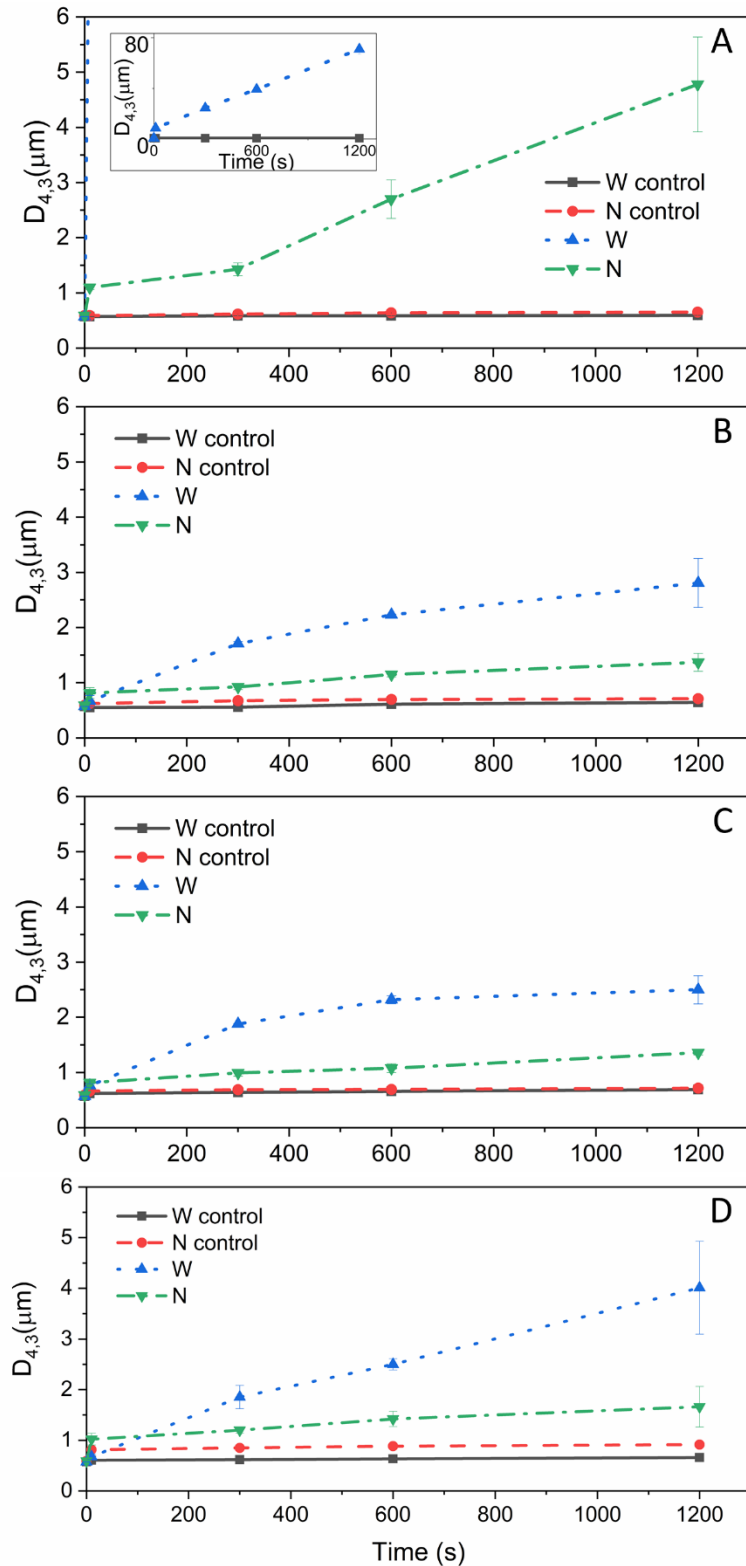
Figure 4.8 Changes in $D_{4,3}$ of W and N emulsion samples treated with enzyme, and their corresponding control samples with no enzyme, plotted as a function of time post introduction of the enzyme.

Results are obtained during in vitro oral digestion with A) amylase solution, and emulsions stored at 25 °C (for W emulsions this is shown in the inset), B) artificial saliva, and emulsions stored at 4 °C, C) artificial saliva, and emulsions stored at 25 °C, and D) artificial saliva, and emulsions stored at 50 °C.

linkage in amylopectin untouched (Smith and Morton, 2010a). Destabilisation of emulsion by the action of α-amylase was found to be more rapid for W system, which was stabilised by amylopectin rich OS-W, than in emulsion N with its higher AC. It is worth noting that the impact of the enzyme digestion on the stability of our two emulsion samples is completely opposite to that due to the addition of salt or lowering of pH discussed in the previous section.

After it was confirmed that α-amylase was able to digest OSA modified starch adsorbed at droplet interfaces, and therefore cause destabilisation of the emulsions as a result, artificial saliva (formulation given in Appendix B, Table B1) was used to better mimic the electrolyte and protein rich environment in the oral cavity. In order to exclude impact of environmental factors such as changes to electrolyte concentration and the presence of protein that may induce flocculation (Silletti et al., 2007; Sarkar, A. et al., 2017), the control samples in this experiment were mixed with empty artificial saliva, which is a solution containing all the inorganic salts and mucin (as highlighted in Appendix B, Table B1), except for α-amylase. Prior to mixing with artificial saliva, the emulsion systems were kept at various temperatures (4 °C, 25 °C, 50 °C) to mimic cold, room temperature and hot beverages. As seen in Figure 4.8B, 8C and 8D, in all three cases, both emulsions W and N were destabilised by the action of α-amylase. At the same time, the control samples maintained stable droplet sizes. Moreover, at all three temperatures, the enzyme treated W emulsions presented higher measured $D_{4,3}$ values than their N counterparts, when measured at 300 s, 600 s, and 1200 s following the introduction of the artificial saliva. In terms of the temperature of the emulsion prior to digestion, for the same emulsion type (emulsion W or N), temperature did not have any obvious influence on droplet size during destabilization.

When the digested emulsions were observed under optical microscope, it was very clear that significant coalescence of droplets was induced in emulsion W, while in emulsion N the formation of large clusters and extensive flocculation was more prominent (Figure 4.9). These observations are supported by our droplet size measurements, when the flocs in N were easily broken up into smaller clusters and even individual droplets, by the dilution and shearing within the dispersion unit of Mastersizer (Silletti et al., 2007). However, it is important to note that even though flocculation was also observed for emulsion N under high electrolyte conditions discussed in section 4.3.2.3, the situation here is somewhat
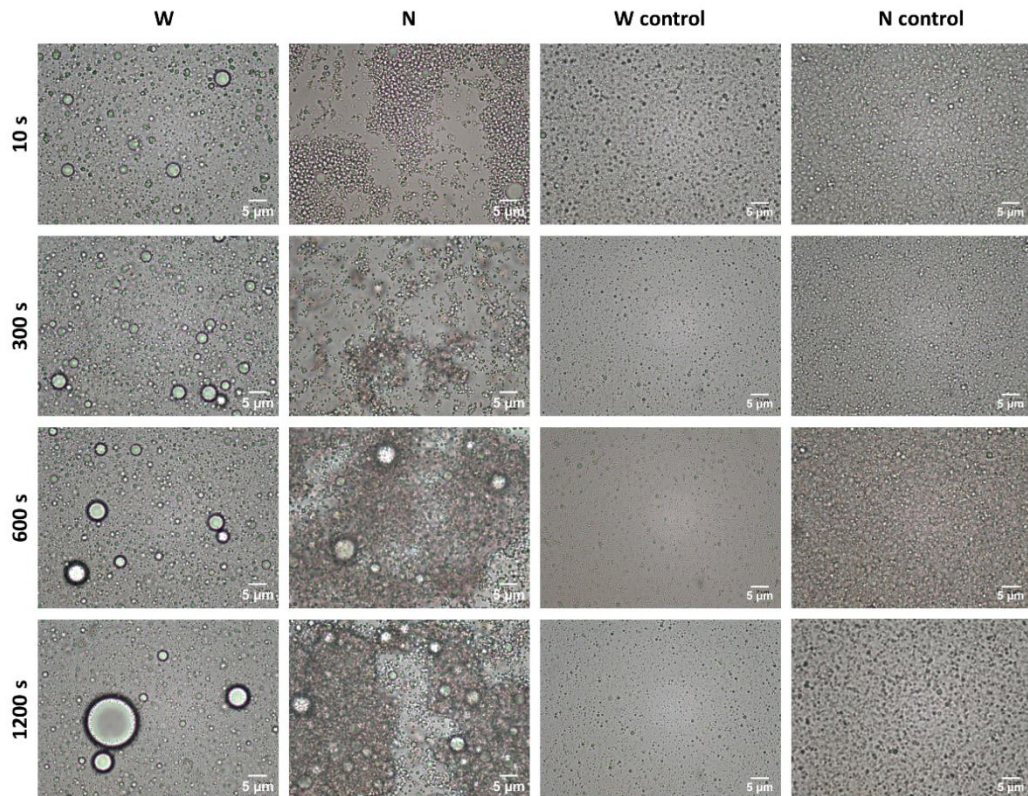
Figure 4.9 Microscopic images for emulsions W and N stored at 25 °C during *in vitro* oral digestion, obtained at various times following the introduction of artificial saliva.

different. It is tempting at first to associate the flocculation with the raised electrolyte concentration in artificial saliva. However, the calculated electrolyte concentration in the emulsion system following the mixing with artificial saliva is estimated to be around 0.038 M. Destabilisation induced by such a relatively low salt concentration is rather slow and would take a few days to become noticeable. This was confirmed by the N control sample, which showed no obvious changes in size or the level of aggregation in the absence of α-amylase under this salt and protein concentrations, during this short initial exposure time (20 mins maximum). Recall also that our addition of salt experiments of section 4.3.2.3, displayed immediate flocculation only at electrolyte concentrations at or above 0.1 M. Therefore, the OS-N interfacial layer must have degraded partially at least by α-amylase to cause this degree of flocculation of the droplets. But presumably, the degradation must have proceeded at a slower rate than that in the OS-W case, with the extensive coalescence seen in the latter largely absent for N emulsion system. The distinctions we observe in the destabilisation of the enzyme treated W and N emulsions must have arose from their different AC

contents, with a faster rate of enzymatic degradation for low amylose content based emulsifier in system W.

Enzymatic digestion by α-amylase induced coalescence in emulsion stabilised by OS-W which have 3.93% amylose content. Their impact on emulsions stabilised by OS-N with 21.86% amylose, over the same short period of 20 min, was to cause emulsion flocculation. Once gelatinised and cooled down to room temperature, amylose and amylopectin molecules start to recrystallize to some extent, and this retrogradation phenomenon is known to be more prominent with amylose, making them less sensitive to
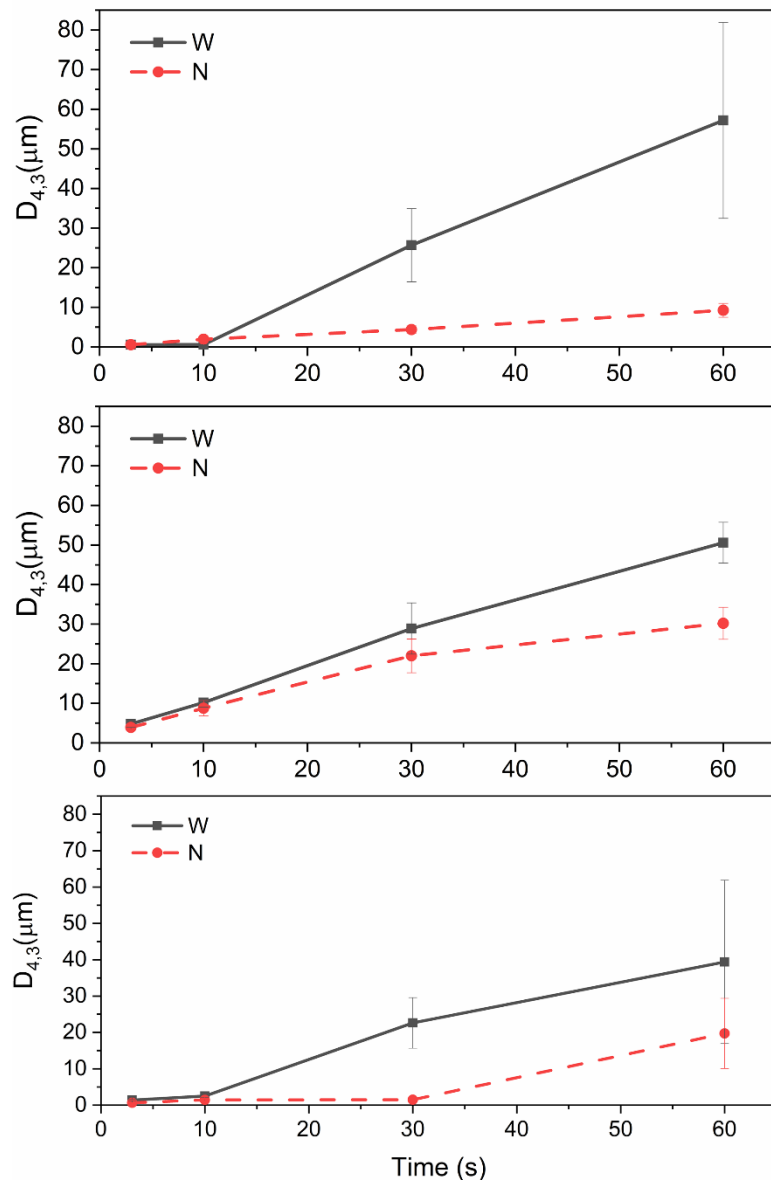
Figure 4.10 Changes in $D_{4,3}$ occurring with time during the *in vivo* oral digestion of emulsions W (black solid lines) and N (red dashed lines).

Results are only shown for three of the ten panellists, to provide some examples.

enzymatic digestion (Fredriksson et al., 2000; Patel et al., 2017; Sikora et al., 2019). As found by Zhou et al. (2013), post gelatinisation and retrogradation, normal corn starch contains more resistant starch than waxy corn starch. It is speculated that for this reason, despite the fact that droplets in emulsion W started with thicker interfacial layers of OS starch, a higher digestion rate is associated with OS-W. This leads to a more rapid degradation of the protective surface films in emulsion W. In addition, upon the digestion by α-amylase, amylose is cleaved into shorter straight chains of glucose polymer, while amylopectin is chopped into straight chains and small fragments around branch points (Smith and Morton, 2010b). Variations in the surface activity of the fragments resulting from digestion would affect the surface coverage of emulsions and hence their destabilisation behaviour.

Distinctions between the rates of α-amylase induced destabilisation behaviour of emulsions fabricated with OS-starch, involving different AC, provides a possibility for achieving tailored controlled release profiles for flavours or other food active ingredients. Our results show that this in principle can be engineered by careful mixing of such emulsions at appropriate ratios, to yield the desired release profile.

4.3.3.2 Enzymatic destabilisation in oral phase: *in vivo*

Emulsions W and N (both with initial droplet size of ~550 nm) were then subjected to *in vivo* oral digestion with 10 panellists, and the *in vitro* results were successfully reproduced here. Figure 4.10 shows the droplet size changes of emulsions with three representatives of the ten panellists. In all ten cases, emulsion W had larger increases in $D_{4,3}$ values than N at the time points 10 s, 30 s and 60 s. There were large variations in the final droplet sizes from different panellists, and this is attributed to the various saliva secretion rate and α-amylase level in saliva among individuals (Carpenter, 2013). The microscopic images in Figure 4.11 again revealed similar results as the *in vitro* experiment. W was destabilised by coalescence of droplets, whereas N sample displayed the formation of flocs from submicron, otherwise intact droplets, with no extensive levels of coalescence.

To further characterise the behaviour of W and N when digested by α-amylase in the oral cavity, the Turbiscan backscattering profile (20 min) was obtained. Emulsions were mixed with either artificial saliva or freshly collected human saliva, before starting the measurement. Same characteristic behaviours of digested emulsions were observed for artificial saliva and human saliva. Here in Figure 4.12, only the profiles for samples
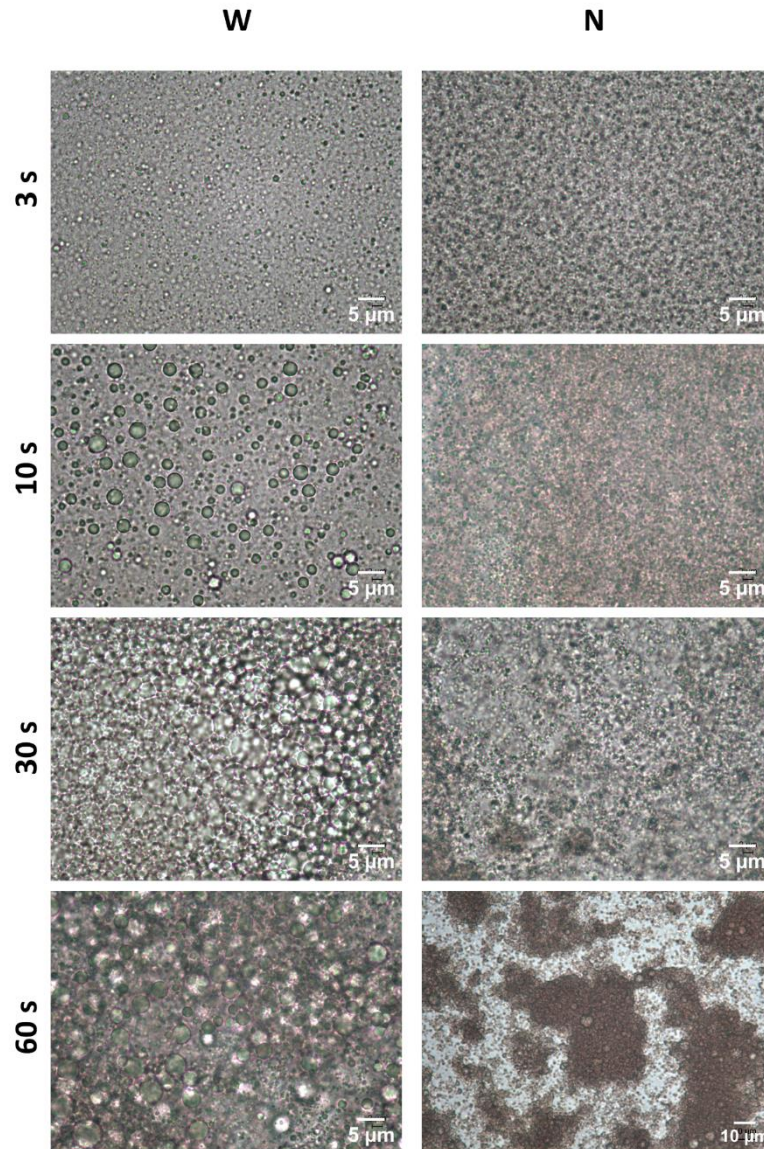
Figure 4.11 Examples of microscopic images for emulsions W and N during *in vivo* oral digestion, from samples obtained for one representative panellist.

treated with human saliva are shown, as human saliva was more potent in destabilising droplets and thus differences in behaviours of W and N can be more clearly observed. A rapid phase separation can be seen in W, which is a result of the large coalesced droplets creaming out. Destabilisation in N was significantly slower than that in W sample. Any visible serum layer at the bottom of the sample took a much longer time to form. Once again, this preliminary *in vivo* experiment confirmed the findings of our *in vitro* investigations. We hope that the results provided here will stimulate more extensive *in vivo* based studies involving larger and border range of panellists, as well as including sensory aspects. Such trials are beyond the

scope of the present work, but no doubt are necessary to establish the idea of mixing of emulsions, stabilised by hydrophobically modified starch of different amylose content, as a feasible way of realising highly tailored novel controlled release vehicle in future.
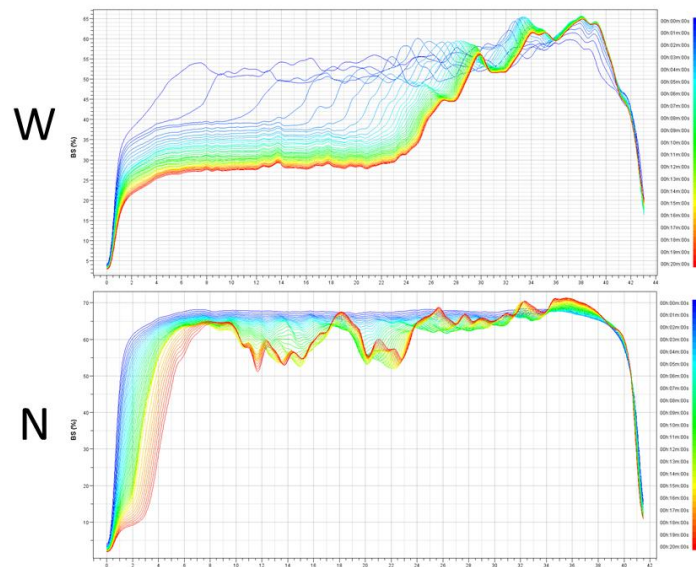
Figure 4.12 Backscattering (IR) profiles of emulsions W and N, mixed 1:1 v/v with freshly collected human saliva. The percentage BS is reported as a function of time following the mixing (0–20 min) throughout the height of the emulsion sample (0–40 mm).

4.4 Conclusion

Upon hydrophobic modification with OSA, both waxy maize starch (denoted by W) and normal corn starch (referred to here as N) were able to produce modified starch with satisfactory emulsifying and stabilising abilities. Emulsion stabilised with OS-W was highly resistant to pH and electrolyte concentration variations. This indicated the likely provision of strong steric repulsion as the main stabilising mechanism as provided by the adsorbed layers of this biopolymer. On the other hand, OS-N stabilised emulsions exhibited a significant degree of flocculation and an increase in droplet size, at acidic pH conditions as well as at high electrolyte concentrations. The interfacial films formed by OS-N seem to provide weaker steric forces, and therefore are more dependent on the presence of some electrostatic interactions as compared to OS-W ones. We have attributed this to the higher amylose content in OS-N modified starch and the possibly thinner surface layers it forms. There is some theoretical justification for this

provided by some recent self-consistent field type calculations. It has been shown that the linear nature of hydrophobically modified amylose makes it more prone to forming bridging contacts between two closely spaced neighbouring oil droplets, as compared to a more compact layer formed by highly branched polymers (Ettelaie et al., 2016). It was also noticed that while aggregation in OS-N fabricated systems occurred quickly upon addition of salt, the subsequent droplet coalescence proceeded much more slowly. This was demonstrated here through dilution with SDS, resulting in a significant downward shift in the droplet size distribution of the aggregated system, even when carried out after 11 days of storage.

As for enzyme-induced destabilisation, both *in vitro* and *in vivo* oral digestion revealed more rapid increase in the size of emulsions stabilised by OS-W starch (lower amylose content) relative to those fabricated with OS-N (higher AC). Digestion of W emulsion was associated with extensive droplet coalescence. In contrast, α-amylase digestion of N samples led to flocculation but without appreciable coalescence, at least over shorter time scales (~ 20 min) post enzymatic treatment. This interesting difference in the behaviour of the two emulsions under enzymatic digestion, suggests that interfacial adsorbed films of modified starch of various amylose content are enzymatically degraded at differing rates. Thus, while OS-W layers provided stronger steric forces and therefore were not as sensitive to changes in pH or electrolyte concentration, they were more prone to enzymatic degradation and droplet destabilisation due to α-amylase activity.

The result is significant in that it provides the potential to generate a gradient of flavour release. In principle, one can fabricate emulsions stabilised by several hydrophobically modified starch of different amylose content. The droplets include a required flavour or an active ingredient within the dispersed phase. These emulsions can then be mixed together at an appropriate ratio. When treated with enzymes, as for example during the oral consumption, droplets stabilised by different starch layers in the system will become destabilise at different rates. A desired controlled release profile can be engineered and simply tailored by changing the mix ratio of different emulsion droplets.

In future research, it would be interesting to investigate in greater depths the interfacial arrangements of amylose and amylopectin, details of their digestion by α-amylase, and any conformational changes occurring on the interface that is caused by the digestion process. Once such a deeper understanding and a better control of the structure and the amylose content

of the modified starch becomes available, formulations for combining emulsions fabricated with various starches can be produced to tailor specifically desired release profiles, in the manner outlined above.

Reference

Ai, Y., Nelson, B., Birt, D.F. and Jane, J.L. 2013. In vitro and in vivo digestion of octenyl succinic starch. *Carbohydr Polym.* **98**(2), pp.1266-1271.

Akhtar, M. and Dickinson, E. 2007. Whey protein–maltodextrin conjugates as emulsifying agents: An alternative to gum arabic. *Food Hydrocolloids.* **21**(4), pp.607-616.

Arshad, H., Ali, T.M. and Hasnain, A. 2018. Native and modified Sorghum starches as wall materials in microencapsulation of nutmeg oleoresin. *Int J Biol Macromol.* **114**, pp.700-709.

Bai, Y., Kaufman, R.C., Wilson, J.D. and Shi, Y.C. 2014. Position of modifying groups on starch chains of octenylsuccinic anhydride-modified waxy maize starch. *Food Chem.* **153**, pp.193-199.

Bajaj, R., Singh, N. and Kaur, A. 2019. Properties of octenyl succinic anhydride (OSA) modified starches and their application in low fat mayonnaise. *Int J Biol Macromol.* **131**, pp.147-157.

Barnes, H.A., Hutton, J.F. and Walters, K. 1989. *An introduction to rheology.* Elsevier.

Benichou, A., Aserin, A. and Garti, N. 2002. Protein-Polysaccharide Interactions for Stabilization of Food Emulsions. *Journal of Dispersion Science and Technology.* **23**(1-3), pp.93-123.

Bhosale, R. and Singhal, R. 2006. Process optimization for the synthesis of octenyl succinyl derivative of waxy corn and amaranth starches. *Carbohydrate Polymers.* **66**(4), pp.521-527.

Burgaud, I., Dickinson, E. and Nelson, P.V. 1990. An improved high-pressure homogenizer for making fine emulsions on a small scale. *International Journal of Food Science and Technology.* (25), pp.39-46.

Carpenter, G.H. 2013. The secretion, components, and properties of saliva. *Annu Rev Food Sci Technol.* **4**, pp.267-276.

Chanamai, R. and McClements, D.J. 2001. Depletion Flocculation of Beverage Emulsions by Gum Arabic and Modified Starch. *Journal of Food Science.* **66**(3), pp.457-463.

Chanamai, R. and McClements, D.J. 2002. Comparison of Gum Arabic, Modified Starch, and Whey Protein Isolate as Emulsifiers: Influence of pH, CaCl2 and Temperature. *Journal of Food Science.* **67**, pp.120-125.

Cheuk, S.Y., Shih, F.F., Champagne, E.T., Daigle, K.W., Patindol, J.A., Mattison, C.P. and Boue, S.M. 2015. Nano-encapsulation of coenzyme Q10 using octenyl succinic anhydride modified starch. *Food Chem.* **174**, pp.585-590.

Cruz-Benítez, M.M., Gómez-Aldapa, C.A., Castro-Rosas, J., Hernández-Hernández, E., Gómez-Hernández, E. and Fonseca-Florido, H.A.

2019. Effect of amylose content and chemical modification of cassava starch on the microencapsulation of Lactobacillus pentosus. *Lwt.* **105**, pp.110-117.

Dai, L., Bergfreund, J., Reichert, C.L., Fischer, P. and Weiss, J. 2019. Shear rheological properties of acid hydrolyzed insoluble proteins from Chlorella protothecoides at the oil-water interface. *J Colloid Interface Sci.* **551**, pp.297-304.

Davis, R.E., Hartman, C.W. and Fincher, J.H. 1971. Dialysis of ephedrine and pentobarbital from whole human saliva and simulated saliva. *J Pharm Sci.* **60**(3), pp.429-432.

Demetriades, K. and McClements, D.J. 2000. Influence of sodium dodecyl sulfate on the physicochemical properties of whey protein-stabilized emulsions. *Colloids and Surfaces A: Physicochemical and Engineering Aspects.* **161**, pp.391-400.

Dickinson, E. 2013. Stabilising emulsion-based colloidal structures with mixed food ingredients. *J Sci Food Agric.* **93**(4), pp.710-721.

Dickinson, E. 2018. Hydrocolloids acting as emulsifying agents – How do they do it? *Food Hydrocolloids.* **78**, pp.2-14.

Dickinson, E. 2019. Strategies to control and inhibit the flocculation of protein-stabilized oil-in-water emulsions. *Food Hydrocolloids.* **96**, pp.209-223.

Dobosz, A., Sikora, M., Krystyjan, M., Tomasik, P., Lach, R., Borczak, B., Berski, W. and Lukasiewicz, M. 2019. Short- and long-term retrogradation of potato starches with varying amylose content. *J Sci Food Agric.* **99**(5), pp.2393-2403.

Dresselhuis, D.M., de Hoog, E.H.A., Cohen Stuart, M.A., Vingerhoeds, M.H. and van Aken, G.A. 2008. The occurrence of in-mouth coalescence of emulsion droplets in relation to perception of fat. *Food Hydrocolloids.* **22**(6), pp.1170-1183.

Ettelaie, R., Holmes, M., Chen, J. and Farshchi, A. 2016. Steric stabilising properties of hydrophobically modified starch: Amylose vs. amylopectin. *Food Hydrocolloids.* **58**, pp.364-377.

Ettelaie, R., Zengin, A. and Lee, H. 2014. Fragmented proteins as food emulsion stabilizers: A theoretical study. *Biopolymers.* **101**(9), pp.945-958.

Ettelaie, R., Zengin, A. and Lishchuk, S.V. 2017. Novel food grade dispersants: Review of recent progress. *Current Opinion in Colloid & Interface Science.* **28**, pp.46-55.

Fredriksson, H., Björck, I., Andersson, R., Liljeberg, H., Silverio, J., Eliasson, A.C. and Åman, P. 2000. Studies on α-amylase degradation of retrograded starch gels from waxy maize and high-amylopectin potato. *Carbohydrate Polymers.* **43**(1), pp.81-87.

Garcia-Tejeda, Y.V., Salinas-Moreno, Y., Barrera-Figueroa, V. and Martinez-Bustos, F. 2018. Preparation and characterization of octenyl succinylated normal and waxy starches of maize as encapsulating agents for anthocyanins by spray-drying. *J Food Sci Technol.* **55**(6), pp.2279-2287.

He, G., Song, X., Ruan, H. and Chen, F. 2006. Octenyl Succinic Anhydride Modified Early Indica Rice Starches Differing in Amylose Content. *Journal of Agricultural and Food Chemistry.* **54**, pp.2775-2779.

Hoover, R. and Ratnayake, W.S. 2001. Determination of Total Amylose Content of Starch. *Current Protocols in Food Analytical Chemistry.* pp.E2.3.1-E2.3.5

Hu, X., Karthik, P. and Chen, J. 2019. Manipulating oral behaviour of food emulsions using different emulsifiers. *International Journal of Food Science & Technology.* **54**(7), pp.2408-2415.

Huber, K.C. and BeMiller, J.N. 2000. Channels of maize and sorghum starch granules. *Carbohydr Polym.* **41**, pp.269-276.

Hunter, R.J. 2001. *Foundations of colloid science.* Oxford university press.

Jeong, H.-Y. and Lim, S.-T. 2003. Crystallinity and Pasting Properties of Freeze-Thawed High Amylose Maize Starch. *Starch - Stärke.* **55**(11), pp.511-517.

Karthik, P., Ettelaie, R. and Chen, J. 2019. Oral behaviour of emulsions stabilized by mixed monolayer. *Food Res Int.* **125**, p108603.

Kato, A., Sasaki, Y., Furuta, R. and Kobayashi, K. 1990. Functional Protein polysaccharide conjugate prepared by controlled dry heating of ovalbumin dextran mixtures. *Agric. Biol. Chem.* **54**, pp.107-112.

Lin, Q., Liang, R., Zhong, F., Ye, A. and Singh, H. 2018a. Effect of degree of octenyl succinic anhydride (OSA) substitution on the digestion of emulsions and the bioaccessibility of β-carotene in OSA-modified-starch-stabilized-emulsions. *Food Hydrocolloids.* **84**, pp.303-312.

Lin, Q., Liang, R., Zhong, F., Ye, A. and Singh, H. 2018b. Physical properties and biological fate of OSA-modified-starch-stabilized emulsions containing β-carotene: Effect of calcium and pH. *Food Hydrocolloids.* **77**, pp.549-556.

Liu, W., Li, Y., Goff, H.D., Nsor-Atindana, J. and Zhong, F. 2018. Distribution of octenylsuccinic groups in modified waxy maize starch: An analysis at granular level. *Food Hydrocolloids.* **84**, pp.210-218.

Lopez-Silva, M., Bello-Perez, L.A., Agama-Acevedo, E. and Alvarez-Ramirez, J. 2019. Effect of amylose content in morphological, functional and emulsification properties of OSA modified corn starch. *Food Hydrocolloids.* **97**.

Lopez-Silva, M., Bello-Perez, L.A., Castillo-Rodriguez, V.M., Agama-Acevedo, E. and Alvarez-Ramirez, J. 2020. In vitro digestibility characteristics of octenyl succinic acid (OSA) modified starch with different amylose content. *Food Chem.* **304**, p125434.

Matos, M., Laca, A., Rea, F., Iglesias, O., Rayner, M. and Gutiérrez, G. 2018. O/W emulsions stabilized by OSA-modified starch granules versus non-ionic surfactant: Stability, rheological behaviour and resveratrol encapsulation. *Journal of Food Engineering.* **222**, pp.207-217.

Miao, M., Li, R., Jiang, B., Cui, S.W., Zhang, T. and Jin, Z. 2014. Structure and physicochemical properties of octenyl succinic esters of sugary maize soluble starch and waxy maize starch. *Food Chem.* **151**, pp.154-160.

Mokni Ghribi, A., Maklouf Gafsi, I., Sila, A., Blecker, C., Danthine, S., Attia, H., Bougatef, A. and Besbes, S. 2015. Effects of enzymatic hydrolysis on conformational and functional properties of chickpea protein isolate. *Food Chem.* **187**, pp.322-330.

Mu, M., Farshchi, A., Holmes, M., Chen, J. and Ettelaie, R. 2019. Effect of storage temperature and relative humidity on long-term colloidal stability of reconstitutable emulsions stabilised by hydrophobically modified starch. *Food Hydrocolloids.* **95**, pp.62-75.

Nilsson, L. and Bergenstahl, B. 2006. Adsorption of Hydrophobically Modified Starch at Oil/Water Interfaces during Emulsification. *Langmuir.* **22**, pp.8770-8776.

Patel, H., Royall, P.G., Gaisford, S., Williams, G.R., Edwards, C.H., Warren, F.J., Flanagan, B.M., Ellis, P.R. and Butterworth, P.J. 2017. Structural and enzyme kinetic studies of retrograded starch: Inhibition of alpha-amylase and consequences for intestinal digestion of starch. *Carbohydr Polym.* **164**, pp.154-161.

Pickering, S. 1907. Cxcvi.—emulsions. *Journal of the Chemical Society, Transactions.* **91**, pp.2001-2021.

Randall, R., Phillips, G. and Williams, P. 1988. The role of the proteinaceous component on the emulsifying properties of gum arabic. *Food hydrocolloids.* **2**(2), pp.131-140.

Ruan, H., Chen, Q.-h., Fu, M.-l., Xu, Q. and He, G.-q. 2009. Preparation and properties of octenyl succinic anhydride modified potato starch. *Food Chemistry.* **114**(1), pp.81-86.

Samakradhamrongthai, R., Thakeow, P., Kopermsub, P. and Utama-Ang, N. 2016. Microencapsulation of white champaca (Michelia alba D.C.) extract using octenyl succinic anhydride (OSA) starch for controlled release aroma. *J Microencapsul.* **33**(8), pp.773-784.

Sarkar, A., Goh, K.K.T. and Singh, H. 2009. Colloidal stability and interactions of milk-protein-stabilized emulsions in an artificial saliva. *Food Hydrocolloids.* **23**(5), pp.1270-1278.

Sarkar, A., Ye, A. and Singh, H. 2017. Oral processing of emulsion systems from a colloidal perspective. *Food Funct.* **8**(2), pp.511-521.

Schmitz, S., Dona, A.C., Castignolles, P., Gilbert, R.G. and Gaborieau, M. 2009. Assessment of the extent of starch dissolution in dimethyl sulfoxide by 1H NMR spectroscopy. *Macromol Biosci.* **9**(5), pp.506-514.

Shingel, K.I. 2002. Determination of structural peculiarities of dexran, pullulan and

gamma-irradiated pullulan by Fourier-transform IR spectroscopy. *Carbohydrate Research.* **337**, pp.1445-1451.

Shogren, R.L., Viswanathan, A., Felker, F. and Gross, R.A. 2000. Distribution of Octenyl Succinate Groups in Octenyl Succinic Anhydride Modified Waxy Maize Starch. *Starch/Stärke.* **52**, pp.196-204.

Sikora, M., Krystyjan, M., Dobosz, A., Tomasik, P., Walkowiak, K., Masewicz, L., Kowalczewski, P.L. and Baranowska, H.M. 2019. Molecular Analysis of Retrogradation of Corn Starches. *Polymers (Basel).* **11**(11).

Silletti, E., Vingerhoeds, M.H., Norde, W. and van Aken, G.A. 2007. The role of electrostatics in saliva-induced emulsion flocculation. *Food Hydrocolloids.* **21**(4), pp.596-606.

Simsek, S., Ovando-Martinez, M., Marefati, A., Sjoo, M. and Rayner, M. 2015. Chemical composition, digestibility and emulsification

properties of octenyl succinic esters of various starches. *Food Res Int.* **75**, pp.41-49.

Smith, M.E. and Morton, D.G. 2010a. 2 - THE MOUTH, SALIVARY GLANDS AND OESOPHAGUS. In: Smith, M.E. and Morton, D.G. eds. *The Digestive System (Second Edition).* Churchill Livingstone, pp.19-38.

Smith, M.E. and Morton, D.G. 2010b. 8 - DIGESTION AND ABSORPTION. In: Smith, M.E. and Morton, D.G. eds. *The Digestive System (Second Edition).* Churchill Livingstone, pp.129-152.

Song, X., Pei, Y., Zhu, W., Fu, D. and Ren, H. 2014. Particle-stabilizers modified from indica rice starches differing in amylose content. *Food Chem.* **153**, pp.74-80.

Song, X., Zhao, Q., Li, Z., Fu, D. and Dong, Z. 2013. Effects of amylose content on the paste properties and emulsification of octenyl succinic starch esters. *Starch - Stärke.* **65**(1-2), pp.112-122.

Sopade, P. and Filibus, T. 1995. The influence of solid and sugar contents on rheological characteristics of akamu, a semi-liquid maize food. *Journal of Food Engineering.* **24**(2), pp.197-211.

Sweedman, M.C., Hasjim, J., Schafer, C. and Gilbert, R.G. 2014a. Structures of octenylsuccinylated starches: effects on emulsions containing beta-carotene. *Carbohydr Polym.* **112**, pp.85-93.

Sweedman, M.C., Schafer, C. and Gilbert, R.G. 2014b. Aggregate and emulsion properties of enzymatically-modified octenylsuccinylated waxy starches. *Carbohydr Polym.* **111**, pp.918-927.

Tesch, S., Gerhards, C. and Schubert, H. 2002. Stabilization of emulsions by OSA starches. *Journal of Food Engineering.* **54**, pp.167-174.

Wang, C., He, X., Fu, X., Huang, Q. and Zhang, B. 2016. Substituent distribution changes the pasting and emulsion properties of octenylsuccinate starch. *Carbohydr Polym.* **135**, pp.64-71.

Wang, C., He, X., Huang, Q., Fu, X., Luo, F. and Li, L. 2013. Distribution of octenylsuccinic substituents in modified A and B polymorph starch granules. *J Agric Food Chem.* **61**(51), pp.12492-12498.

Whitney, K., Reuhs, B.L., Ovando Martinez, M. and Simsek, S. 2016. Analysis of octenylsuccinate rice and tapioca starches: Distribution of octenylsuccinic anhydride groups in starch granules. *Food Chem.* **211**, pp.608-615.

Wijaya, W., Patel, A.R., Setiowati, A.D. and Van der Meeren, P. 2017. Functional colloids from proteins and polysaccharides for food applications. *Trends in Food Science & Technology.* **68**, pp.56-69.

Zhao, S., Tian, G., Zhao, C., Lu, C., Bao, Y., Liu, X. and Zheng, J. 2018. Emulsifying stability properties of octenyl succinic anhydride (OSA) modified waxy starches with different molecular structures. *Food Hydrocolloids.* **85**, pp.248-256.

Zhou, X., Chung, H.J., Kim, J.Y. and Lim, S.T. 2013. In vitro analyses of resistant starch in retrograded waxy and normal corn starches. *Int J Biol Macromol.* **55**, pp.113-117.

Chapter 5
Effect of polymer architecture on the adsorption behaviour of amphiphilic copolymers: A theoretical study

Abstract

Polymer architecture has been found to have an impact on its adsorption behaviour in various experimental and theoretical studies. Here a new approach is proposed to compare the inherent adsorption affinity of polymers by extrapolating their Henry's adsorption constant, k_H. Briefly, the polymer adsorption isotherm is obtained by the Scheutjens and Fleer scheme of Self Consistent Field (SCF) calculations, and then k_H is calculated from the dilute or mushroom regime of the isotherm. Validation of this method is conducted with a few structures whose k_H can be analytically calculated. Linear, star-like, and dendritic amphiphilic polymers were characterised by their k_H in this study, to compare the difference in their surface affinity. The distribution and location of their adsorbing monomers among the polymer structure is also considered. It is found that the branched structures (star polymers and dendrimers) can be viewed as analogues of linear block polymers based on the location of their adsorbing units. Their adsorption behaviour resembles the well-known phenomenon in linear copolymers, where under the condition that they are of the same size and composition, the diblocks adsorb more strongly than their triblock counterparts. Stars and dendrimers with structures resembling diblocks are also found to have higher k_H than those resembling triblcoks.

5.1 Introduction

Adsorption of polymers onto solid surfaces is of great importance due to its practical implication in colloid science, lubrication, surface treatment, controlling surface wettability, and in design of biocompatible films (Fleer et al., 1993; Hubbell, 1999). In relation to emulsions, the "surface" considered in both experimental and theoretical studies are often taken as a hydrophobic surface, mimicking an otherwise non-solid oil-water interface. A good emulsifier needs to be surface active so that it can rapidly adsorb to the interface and reduce the surface tension, which usually requires the molecules to have amphiphilic structures, containing both hydrophobic and hydrophilic segments. The driving force for such adsorption is a combination

of hydrophobic interactions and the low solubility of hydrophobic segments of the macromolecules in aqueous environment. In foods, agrochemicals, pharmaceuticals, and other biologically related applications, apart from proteins, hydrophobically modified starch is also a particularly good example of amphiphilic bio-macromolecule that can be viewed as a copolymer. Hydrophobically modified starch has been shown to be an excellent emulsifier (Dickinson, 2009). In recent years, experimental studies on hydrophobically modified starch have found that the ratio of linear and branched starch molecules (amylose and amylopectin) has an significant impact on the emulsifying behaviour of the modified starch (Song et al., 2014; Sweedman et al., 2014; Mu et al., 2021), which leads to a more general question as to what influence does the chain architecture have on the adsorption of amphiphilic copolymers?

In some cases, this problem was investigated in the context of modifying surfaces. High density monolayers (i.e. brush like films) can be formed when polymers saturate the surface. These have been studied in relation to surface grafting for the impact of the grafted polymer architecture on the subsequent adsorption of another entity, such as a protein, onto the grafted surface (Gingell and Owens, 1994; Schroen et al., 1995; Freij-Larsson et al., 1996; Ishihara et al., 2020). A well-known example is the surface treatment to prevent the attachment of molluscs and other aqueous organisms to the surface of ships, platforms, and structures under water.

Many attempts have also been made at deciphering the relationship between polymer architecture and the adsorption of chains themselves, both experimentally and through theoretical calculations. Experimentally, Bulychev et al. (2010) studied the adsorption of amphiphilic linear polymers onto different surfaces and found that the adsorption layer formed by diblock linear polymers was thicker than that formed by multi-block linear structures. Trégouët et al. (2019) focused on the dynamic properties of interfacial layers formed by polymers, having various lengths and grafting densities for their hydrophobic segments. It was found that at high grafting densities, the adsorbed layers have larger elastic penalty upon compression and therefore these polymers desorb faster as compared to those with lower grafting densities. As for more complex structures such as amphiphilic combs, Tian et al. (2005) focused on the scaling analysis in good solvents, and proposed that using a branching parameter it is possible to describe the overall effect of branching on the equilibrium properties of the adsorbed layers of comb polymers. Experimental studies have also been done to compare linear and

bottle-brush homopolymers of comparable molecular weights. Linear polymers were thought to form more extended adsorbed layers than their bottle-brush counterparts (Naderi et al., 2008). The same conclusion was also drawn from a theoretical study conducted by Ettelaie et al. (2016), comparing linear and branched amphiphilic polymers representing simple models for hydrophobically modifies amylose and amylopectin starch.

Experimental methods are time and resource bounded, and some parameters (e.g. degree and position of substitution in modified starch) and conditions (e.g. a theta solvent for glucose residues in starch) are hard to control or achieve in practice. In comparison, theoretical methods give us the essential tool to design more idealised conditions, and to focus on a specific parameter of interest, without altering others. For example, the transition from weak to strong adsorption can be achieved by increasing the strength of monomer-surface interaction (Sikorski, 2002; Sikorski and Romiszowski, 2005; Rolińska and Sikorski, 2020; Wessels and Jayaraman, 2020) without changing size or architecture of chains. Similarly, the degree of polymer overlap on the surface can be adjusted to a desirable level by varying its concentration in the bulk to very low dilutions, not always feasible in practical situations.

When polymers adsorb onto a surface, the adsorption amount is limited by the lateral interactions between the neighbouring molecules. For copolymer chains of interest here, this is usually the excluded volume interactions between the solvent loving parts of the chains. The full coverage scenario, involving saturated surface layers, has been studied both for homopolymers and in relation to amphiphilic macromolecules. Leermakers et al. (2020) focused on the saturated adsorbed regime for homopolymers comparing various chain architectures with each other. In this study the de Gennes scaling exponent (de Gennes, 1980; De Gennes, 1987) for polymer density in the central region of the adsorption layer was characterised. It was suggested that comb-like polymers are better at providing colloidal stabilization than their symmetrically branched counterparts, in that they mediate stronger steric repulsion between colloidal particles covered by them.

Many studies are interested in the conformation taken by polymers at an interface. The distribution or length of trains, loops, tails are often characterised, and structures with long tails are known to form thicker adsorbed layers (Sikorski, 2002; Sikorski and Romiszowski, 2005; Ettelaie et al., 2016; Leermakers et al., 2020). Besides other factors such as solvent

quality and adsorption strength, the location or distribution of the adsorbing units along the copolymer backbone also has a major influence on the polymer conformation adopted by the chains on the surface. As such then, the location of hydrophobic anchoring groups also strongly affects the thickness of the resulting adsorbed layers (Balazs and Siemasko, 1991; Van der Linden et al., 1996).

The above-mentioned studies each examined certain aspects of adsorbing polymers in relation to polymer architecture, ranging from dynamic properties of the interfacial layers to the equilibrium conformations adopted by adsorbed polymers. This again indicates that polymer architecture does play a prominent role in the adsorption behaviour of amphiphilic chains.

Here we would like to focus on another aspect of characterising the adsorption properties of polymers, by mainly examining the dilute regime (the mushroom adsorption regime (Carignano and Szleifer, 1995; Szleifer, 1997)) of the Langmuir Isotherm. In such a case the polymers are sparsely distributed on the surface. Without crowding and overlapping at the surface, polymers would act as independent molecules and behave irrespective of the other chains surrounding them. Therefore, Henry's law for adsorption of the amphiphilic molecules is applicable in this adsorption regime. It is our aim to calculate Henry's constant k_H for different architectures and use this to compare the inherent adsorption property of a given chain structures, without the crowding interference from neighbouring polymers. More specifically we aim to investigate the impact of a particular polymer architecture on the affinity of the chain for adsorption on the surface. Linear, star, and dendritic structures are investigated and compared here. We hope to provide insight to the manufacture of amphiphilic emulsifiers with tailored hydrophobic positions and structures in cases involving synthetic amphiphilic copolymer. Similarly, our study should prove useful in providing further insight into behaviour of different biomacromolecular architectures at interfaces, of which hydrophobically modified starch is a good example.

5.2 Theoretical calculations

5.2.1 Self-Consistent Field calculations

The Scheutjens and Fleer formulation of Self Consistent Field theory can be applied to complex copolymers (Scheutjens and Fleer, 1979; Fleer et al., 1993). This model considers two parallel flat surfaces with the gap between them filled with a solution of polymers. In this study, the space

between the two surfaces is subdivided into a lattice (cubic one in our case here) and each cell is occupied by either a monomer (belonging to chains) or a solvent molecule. The polymers are taken as chains of beads, with latter representing individual monomers. No atomic details regarding actual size or shape of monomers are taken into account in this somewhat coarse-grained view of the chains. However, the Flory-Huggins interaction parameters between the monomers, solvent and the surfaces are specified to reflect their affinity for each other and thus also specifying their chemical nature. The adsorption amount can be calculated from the density profiles at any given bulk volume fractions, provided that the two surfaces are far apart so as not to affect polymer adsorption on each other.

Briefly, the calculations start by averaging the molecular degrees of freedom which provides a free energy functional related to the density profiles of each monomer type, as well as the solvent (see for example Akinshina et al. (2008) and Ettelaie et al. (2014)).

$$
\frac{\Delta F}{k_B T} = -\int_0^L \left[\sum_i \frac{1}{N_i} \sum_\alpha (\phi_i^\alpha(r) - \Phi_i^\alpha) \right] dr - \int_0^L \left[\sum_\alpha \psi_\alpha(r) \sum_i \phi_i^\alpha(r) \right] dr
$$
$$
+ \frac{1}{2} \int_0^L \left[\sum_{i \neq j} \sum_{\alpha \neq \beta} \chi_{\alpha\beta} \phi_i^\alpha(r) \phi_j^\beta(r) \right] dr
$$
$$
+ \frac{1}{2} \int_0^L \left[\psi^{el}(r) \sum_\alpha q_\alpha \sum_i \phi_i^\alpha(r) \right] dr
$$
$$
+ \sum_\alpha \chi_{\alpha s} \sum_i [\phi_i^\alpha(0) + \phi_i^\alpha(L)]
$$

5.1

where N is the total number of monomers, and the variation of the density of monomer residues of kind α belonging to chains of type i with distance r is denoted by $\phi_i^\alpha(r)$ and their bulk volume fraction far from the plates by Φ_i^α. The distance r is measured relative to one of the plates, with the other surface located at r = L. The symbols k_B and T denote the Boltzmann constant and temperature, respectively. The enthalpic contribution is captured by the last three terms in the above equation, and the first two terms provide the entropic part of the free energy. The Flory-Huggins interaction parameter $\chi_{\alpha\beta}$ indicates the strength of interactions between two different monomer species α and β. The electrostatic potential $\psi^{el}(r)$ is included in Eq. 5.1 for completeness but is of no concern in this study since no charged species are present in our study.

During the derivation of the free energy functional, a set of auxiliary fields $\psi_\alpha(r)$ enters the calculations. These fields need to be the ones that

project out the same density profiles for which the free energy is being calculated in Eq. 5.1. If these fields are given, then the corresponding density profiles are easy to compute by first calculating the segment distribution functions. For a monomer species α belonging to a macromolecule of type i, the density at any layer z away from the surface, within the gap between the plates, is given by the composition equation (Ettelaie et al., 2014)

$$\phi_i^\alpha(z) = \frac{(\sum_\alpha \Phi_i^\alpha)}{N_i} \sum_{n=1}^{N_i} \left(\frac{G^f(n,z)G^b(N_i-n,z)\delta_{\alpha,t_i(n)}}{exp(-\psi_\alpha(z))} \right)$$ **5.2**

Each density profile has an associated probability of occurring, which is proportional to $\sim exp(-F(\{\phi_i^\alpha(r)\})/k_BT)$, where $F(\{\phi_i^\alpha(r)\})$ is the free energy for that specific density profile/s as given by Eq. 5.1. The most probable case occurs when free energy is minimized. It is assumed that the corresponding density profile/s, for which the free energy takes its lowest value, dominates the behaviour of the system. Therefore, instead of averaging the thermodynamic quantities of interest over all the possible sets of density profiles, one makes the approximation that the values are given by the density profile with the lowest free energy. In other words, fluctuations around the most dominant profile are ignored, just as is the case in any mean field type theory. An additional incompressibility constraint is also often assumed when determining the profiles with the minimal free energy. This is done by demanding that the sum of concentrations of all species at any point to always be a constant. The incompressibility restriction is

$$\sum_i \sum_\alpha \phi_i^\alpha(r) = \sum_i \sum_\alpha \Phi_i^\alpha$$ **5.3**

It is possible to show that the profile/s and their corresponding auxiliary fields satisfy the following relation when the minimum free energy occurs

$$\psi_\alpha(r) = \psi_h(r) + \left(\sum_\beta \chi_{\alpha\beta} \sum_i \phi_i^\beta \right) + q_\alpha \psi^{el}(r)$$
$$+ \chi_{\alpha s}\left[(\delta(r) + \delta(r-L)) \right]$$ **5.4**

where δ(r) represents the Dirac's delta function and ψh(r) is a hard core potential that ensures the incompressibility of the system, Eq. 5.3 (Ettelaie et al., 2014).

It is clear that if either the mean fields or density profile is known, the other one can be calculated accordingly. However, neither of them is known in the system in advance. Unlike molecular dynamic and Monte Carlo

methods whose accuracy depend on their runtime due to the sampling of configurations, SCF is a numerical calculation and accounts for all possible configurations. How a polymer behaves depends on all its neighbouring entities, all of which are unknowns. Hence, SCF employs an iterative process to tackle this problem. To start, an initial guess density profile is assumed and is used to calculate the set of fields according to Eq. 5.4. From these fields a new set of density profile/s can now be calculated and compared to the previous one. This process is repeated until the difference between the density profiles in two successive iterations is within a certain pre-determined level of accuracy. When the calculations reach convergence, any thermodynamic quantity of interest, including the colloidal interaction mediated by the macromolecules (per unit area) between two flat surfaces, can be obtained from the results. In turn, with the help of Derjaguin approximation, the interaction potential between two spherical colloidal droplets of radius R, V_{par}, can also be calculated from those obtained between two flat surfaces, V, as follows (Scheutjens and Fleer, 1979; Ettelaie et al., 2014)

$$V_{par}(L) = \pi R \int_{\infty}^{L} V(x)\, dx$$

5.5

The polymers considered here consists of two types of monomers only, hydrophilic ones that prefer staying in the solvent, and hydrophobic residues that favour adsorption onto the surface. Three types of polymer architectures are examined here, linear, star-like, and dendritic polymers. They are schematically illustrated in Figure 5.1, without the hydrophobic monomers being specifically labelled out. The first structure is a basic linear chain (Figure 5.1a), and here they are all designed as being diblocks. The molecular weight for the linear and all the star polymers are the same at 400 total monomers. For star-like polymers, while they all have the same molecular weight, the number of arms varies from 3 to 7 (Figure 5.1b). This obviously means that the more arms there are, the shorter each arm would be. The dendritic polymers (Figure 5.1c) are designed to have a central section beginning with a 3-armed star, thus avoiding a long linear region at the root. The individual strands are of equal length, each being 40 monomers, and apart from the central 3-arm root, bifurcation at all other branching points are kept at 2. Number of generations (i.e. the number of bifurcation starting from root, as one moves down towards the tips) considered are 2, 3, 4 and 5, giving the total number of monomers as 361, 841, 1801, 3721, with the corresponding number of free ends being 6, 12, 24,

48, respectively. The monomers belonging to each generation away from the root are coloured differently in Figure 5.1, to better highlight the structure.
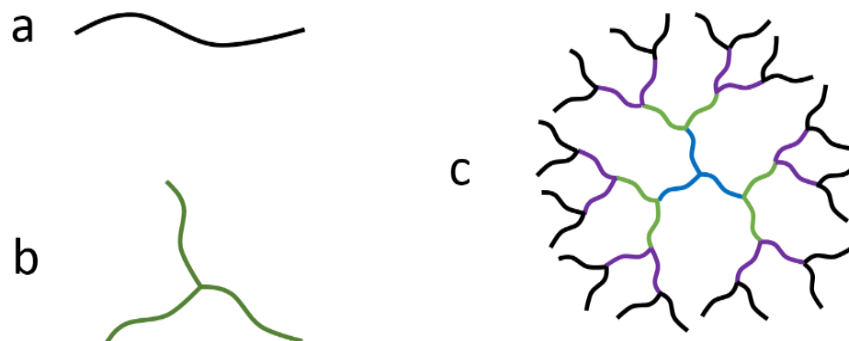
Figure 5.1 Schematic illustrations of the three models used in this work, without highlighting the hydrophobic monomers explicitly; (a) linear structures with no branching points. (b) star polymers with arms of equal length (example shown has 3 arms), (c) symmetrical dendrimers of generation g, with a starting branching of 3 at the root, followed by a bifurcation of 2 at each branch point further down towards the tips. Each individual linear strand between any two branch points has 40 monomers. The example here shows a chain with 4 generations, and thus 45 linear segments.

The degree of hydrophobic modification is kept at the same level for all the star and dendritic architectures. There is one hydrophobic monomer in every 40 monomers. This results in each star polymer having 10 hydrophobes, regardless of the number of arms. In dendrimers, each linear strand contains on average one hydrophobe, thus leading to a total of 9, 21, 45 and 93 hydrophobes in dendrimers of increasing complexity, with generation numbers 2, 3, 4 and 5, respectively.

In order to investigate the role of the position and distribution of hydrophobic monomers along the chain backbone, these are varied within each polymer architecture type. Based on the spatial distribution of hydrophobic monomers on the backbone, these can either all be placed on one segment of the structure (i.e. all hydrophobes are connected to each other), or positioned as smaller numbers of monomer groups distributed along several different segments (Figure 5.2, a, b versus c). Furthermore, hydrophobic monomers can be located either at the centre, or at the free ends of the structures (Figure 5.2, b versus a, c).
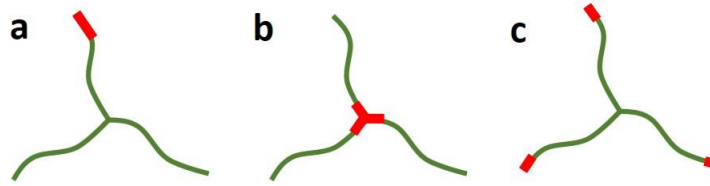
Figure 5.2 Schematic illustration of the position of hydrophobic monomers in star polymers. Position of hydrophobes are highlighted here with thick red lines. Here a 3-arm star is presented as an example. Hydrophobic monomers are (a) positioned at a free end on one arm only; (b) evenly distributed among all arms, placed at the centre; (c) evenly distributed among all arms, with all the hydrophobes located at the free ends.

The surface affinity of the above structures is characterised by Henry's constant k_H, which indicates the inherent adsorption properties of single individual chains, without the complexation of their interactions with the neighbouring polymers, when adsorbed. For chains that behave irrespective of their neighbours, there exists a relationship between k_H and the change in the free energy, ΔG, upon adsorption:

$$k_H \propto \exp\left(\frac{\Delta G}{k_B T}\right)$$

5.6

where $\Delta G = E - TS$ includes both an enthalpic term E and an entropic term S. For a single monomer, the entropic change upon its adsorption onto the surface is normally assumed to be 0 (assuming that the configuration of a small molecule on surface is not all that different to when it is in bulk). Therefore, for molecules comprising of a single monomer, k_H is solely dependent on the enthalpic term

$$k_H = e^{-\chi_s}$$

5.7

where χ_s is the Flory-Huggins interaction parameter between the monomer and surface, as relative to that between the monomer and the solvent, dictating the adsorption energy of this monomer. However, for amphiphilic polymeric chains the entropic term S does make a significant contribution. As the chains adsorb onto the surface, they lose configurational entropy due to restrictions presented by the interface. Therefore, in order to still obtain the same relationship for k_H as that above, the entropic term needs to stay constant for the adsorbing units, when adsorption onto the surface takes place. If hydrophobes are all in one block, and sufficiently strongly adsorbed so that the whole block is lying flat on the surface without forming any loops, one of the requirements for this condition will be met.

Prior to applying the method to more complicated structures such as stars and dendrimers, it is useful to first validate the approach using several more straightforward cases. For these a prediction for the value of k_H, or its variation with χ_s, number of hydrophobes, or other such parameters, can feasibly be made. Dimers and simple amphiphilic linear chains are chosen as model structures for this validation, with their k_H either analytically calculated or known to follow a predictable trend.

5.2.2 Langmuir isotherm and Henry's constant

From the SCF program discussed in previous section, the adsorbed amount for a range of bulk concentrations (or volume fractions here) can be calculated. Using these the adsorption isotherm is determined by plotting the adsorbed amount vs. bulk volume fraction. A full isotherm is illustrated schematically in Figure 5.3., and broadly will have features resembling a Langmuir isotherm. At very low concentration, adsorption increases linearly as there are excess space on the surface, and chains adsorb independent of each other. As the bulk volume fraction increases, the surface starts to saturate with polymers, and further increments in adsorbed amount slows down (Hunter, 2001). This is a transition from mushroom to brush regime, as surface loading increases (Carignano and Szleifer, 1995; Szleifer, 1997).
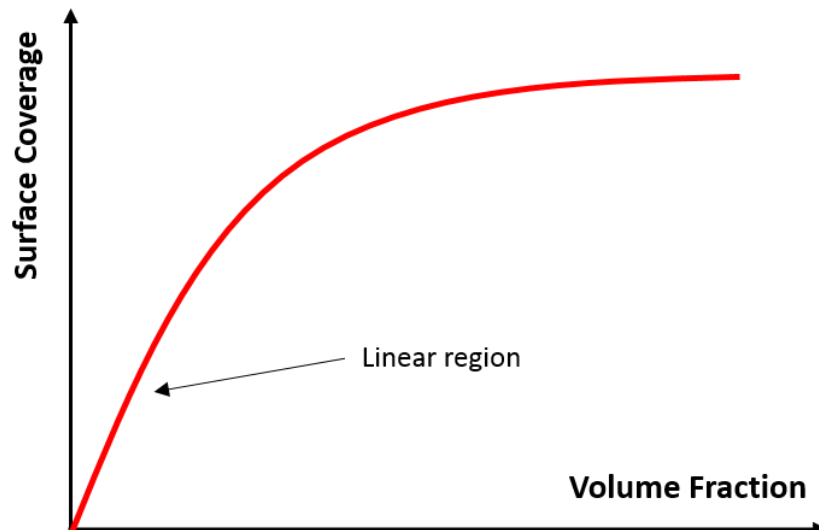
Figure 5.3 Schematic illustration of a Langmuir adsorption isotherm.

Here we mainly focus on the dilute or mushroom regime of the adsorption isotherm, where the linear relationship between adsorbed amount and bulk concentration is followed. In this regime, polymers do not overlap and behave as individual isolated molecules on the surface. This dilute

regime can be further reinforced by setting the interaction potential between the hydrophilic monomer and solvent molecule to χ = 0.5, therefore making the solvent a theta solvent for the hydrophilic parts of the chains. At very low adsorption level, the excluded volume interactions between the adjacent adsorbed chains is usually not a huge concern. Even so, in most cases here we still assume a theta solvent for the hydrophilic sections to largely switch off the effects of this excluded volume interactions. Then, this linear regime follows Henry's law, and Henry's constant k_H can be determined from the slope of the linear part of the calculated isotherm.

Assume a lattice consisting on N sites, of which n are occupied by adsorbed monomers. The number of arrangements available (Ω) is

$$\Omega = \frac{N!}{(N-n)!\, n!} \qquad \textbf{5.8}$$

Therefore, entropy of the lattice can be calculated using Boltzmann formula $S=k_B \ln(\Omega)$ and written as

$$S = k_B \cdot \ln \left(\frac{N!}{(N-n)!\, n!} \right) \qquad \textbf{5.9}$$

According to the Stirling's formula, when the number of lattice squares and molecules are large, the above equation can be approximated into

$$S = k_B \cdot [N ln(N) - n ln(n) - (N-n)\ln(N-n)]$$

The total free energy of the system and its enthalpic term are respectively

$$F = E - TS \qquad \textbf{5.10}$$

$$E = n \cdot \chi_s \qquad \textbf{5.11}$$

where χ_s is the adsorption energy for one adsorbing monomer. The equation for free energy can be rearranged into

$$\frac{F}{k_B T} = n \cdot \chi_s - N ln(N) + n ln(n) + (N-n)\ln(N-n) \qquad \textbf{5.12}$$

For simplicity, we have assumed the strength of interaction between monomers with solvent is 0. Therefore, the chemical potentials μ for the solute and solvent in the bulk now read

$$\frac{\mu_{solvent}}{k_B T} = \ln(1-\phi) \qquad \textbf{5.13}$$

$$\frac{\mu_{solute}}{k_B T} = \ln(\phi) \qquad \textbf{5.14}$$

where ϕ refers to the bulk volume fraction (or concentration in a lattice model) of total monomers. The change in free energy can be expressed as

$$\frac{\Delta F}{k_B T} = \frac{F}{k_B T} - n \cdot \mu_{solute} + n \cdot \mu_{solvent}$$

$$= n \cdot \chi_s - n \cdot \mu_{solute} + n \cdot \mu_{solvent} - Nln(N) + nln(n) + (N - n)\ln(N - n) \qquad \textbf{5.15}$$

When the system is in equilibrium, free energy is minimized,

$$\frac{\partial F}{\partial n} = 0 \qquad \textbf{5.16}$$

thus, leading to

$$\therefore \exp(\chi_s - \mu_{solute} + \mu_{solvent}) = \frac{N - n}{N} \qquad \textbf{5.17}$$

Therefore, the surface coverage, or adsorption of monomers is given by

$$\Gamma = \frac{n}{N} \qquad \textbf{5.18}$$

$$\therefore \Gamma = \frac{\phi e^{-\chi_s}}{1 + \phi(e^{-\chi_s} - 1)} \qquad \textbf{5.19}$$

With Henry's constant for a single monomer given as Eq. 5.7, the adsorption of monomer can be written as

$$\Gamma \approx \frac{\phi k_H}{1 + \phi k_H} \qquad \textbf{5.20}$$

The above relationship between adsorbed amount Γ, bulk volume fraction ϕ and Henry's constant k_H not only holds true for monomers, but also for all structures as long as they are in the dilute regime. In other words, when the surface is not saturated, *i.e.* $\phi \ll 1$, the Langmuir isotherm is in the linear region and Γ can be approximated to be

$$\Gamma = k_H \phi \qquad \textbf{5.21}$$

$$\log \Gamma = \log \phi + \log k_H \qquad \textbf{5.22}$$

Therefore, when adsorption is plotted against volume fraction on a logarithmic graph, a straight line is expected with the slope equal to 1. The intercept of such a line with y-axis is the $\log(k_H)$, for the particular polymer for which the isotherm is computed. For simple monomers, the value of k_H is shown above to be $k_H = e^{-\chi_s}$. However, for complex polymeric chains, their entropic change upon adsorption complicates the relation and as a result their k_H cannot be calculated analytically. The above relationship for such polymers merits more complex SCF calculation, as a possible way for

extrapolating k_H for these more sophisticated structures than simple monomers.

This work intends to determine and use Henry's constant as a parameter to describe the adsorption behaviour of copolymers with various differing architectures, which otherwise would be too complex to be calculated analytically.

5.3 Results and Discussion

In this section, we first provide a verification of the proposed method with dimers and certain amphiphilic linear polymers whose surface affinity are more predictable. The validated method is then extended to examine and contrast more complex structures: amphiphilic linear, star and dendritic type polymers.

5.3.1 Verification of the method

5.3.1.1 with dimers

We first verify the method by applying it to some simple structures whose k_H can be calculated analytically. We stress that the examples in this section are merely used to allow for the verification of the method, rather than being realistic models of any specific molecules per se. The first simple structure is a dimer of two adsorbing hydrophobic monomers, where each monomer has an interaction strength (χ_s) with the surface varying from -2 k_BT to -5 k_BT. Ideally, the interfacial layer formed by adsorbing dimers of dilute volume fractions is 2 layers thick at most, making it convenient to calculate the adsorbed amount, and hence k_H, by considering the possible configurations that the dimer might take on the surface. The adsorption isotherms of this structure are presented in Figure 5.4, where the intercepts are log(k_H) values. The obtained k_H are listed in Table 5.1 for various values of χ_s. The lower limit of volume fraction selected is bounded by computational accuracy of the program implementing SCF calculations. The upper limit is bounded by physical considerations, i.e., polymer saturation at the surface, moving the adsorption out of the linear regime.

The number of monomers belonging to chains (i.e. the adsorbed amount) present in the first layer at a specific bulk volume fraction ϕ can be calculated. There are two possible conformations of a dimer that would
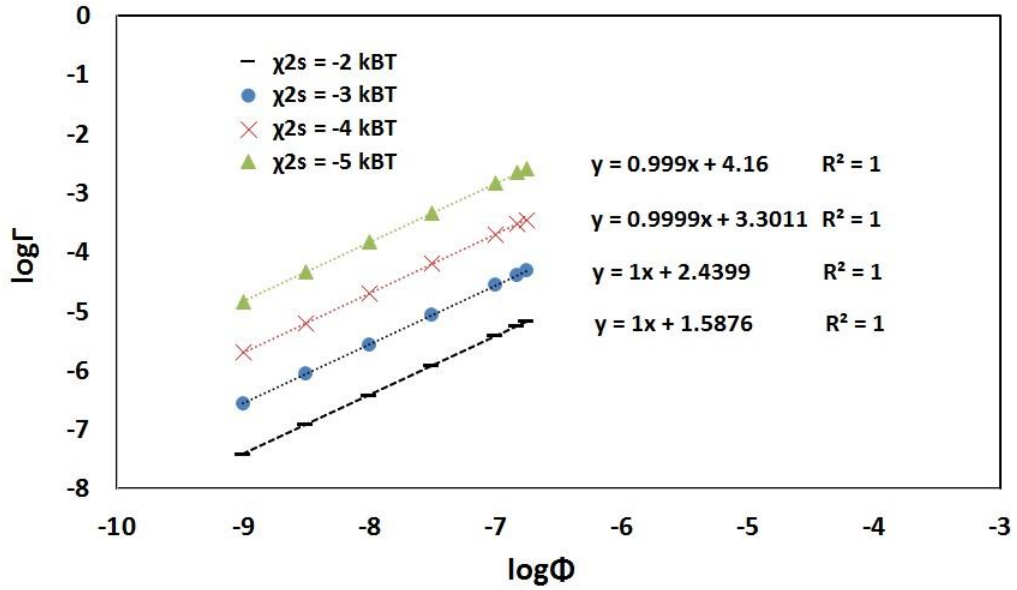
Figure 5.4 Linear part of the adsorption isotherm for a dimer with a tendency to adsorb flat on the surface.

Logarithm of the adsorbed amount versus logarithm of volume fraction is plotted. The equation and R^2 for the fitted linear regression line are included for each value of χ_{2s}, showing slopes that are very close to 1, as expected.

result in its monomers being present in layer 1 (i.e. in contact with the surface). One is the dimer lying "parallel" to the surface, contributing two monomers to the first layer. The relative probability of dimers taking this conformation (relative to its confirmations in the bulk) is $2(\frac{4}{6}e^{-2\chi_s})$. Here $e^{-2\chi_s}$ is the Boltzmann factor associated with the two monomers of the dimmer, each with a surface interaction strength of χ_s, $\frac{4}{6}$ is the lattice parameter λ indicating the possibility of two monomers both being in the same layer, and the term is multiplied by 2 because the monomers are interchangeable in terms of their position. The second conformation is the dimer adsorbing "perpendicular" to the surface, contributing only one monomer to layer 1 adjacent to the surface, with the other monomer residing in layer 2 and not on surface. The relative probability in this case is $2(\frac{1}{6}e^{-\chi_s})$, where similarly $e^{-\chi_s}$ is the Boltzmann factor for one monomer interacting with the surface, $\frac{1}{6}$ is the lattice parameter λ indicating the possibility of monomers being in adjacent layers, and once again the entire term is multiplied by 2 due to the interchangeability of the monomers with regards to their positions. Adding the two possibilities together, and considering the bulk volume fraction ϕ and number of monomers per polymer, N, the adsorption (Γ) in layer 1 can be expressed as

$$\Gamma = 2\frac{\phi}{N}(\frac{4}{6}e^{-2\chi_s} + \frac{1}{6}e^{-\chi_s})$$ **5.23**

For a dimer, the degree of polymerisation N is equal to 2, so expressing Γ in terms of the number of adsorbed chains (rather than total amount) the equation becomes

$$\Gamma = (\frac{4}{6}e^{-2\chi_s} + \frac{1}{6}e^{-\chi_s}) \cdot \phi$$ **5.24**

Because $\Gamma = k_H\phi$, we therefore have

$$k_H = \frac{4}{6}e^{-2\chi_s} + \frac{1}{6}e^{-\chi_s}$$ **5.25**

When the magnitude of the interaction potentials χ_s are sufficiently large (and favourable, i.e., χ_s is negative), the majority of the adsorbed dimers should lie flat on the surface, with both monomers in layer 1. This means the "parallel" adsorbed conformation dominates, and the other, perpendicular configuration, can be ignored to a first approximation. In other words, in such a case $k_H = \frac{4}{6}e^{-2\chi_s}$. These analytically predicted values of k_H, obtained for various interaction potentials χ_s, are listed in Table 5.1a for comparison with SCF obtained results. The k_H from SCF calculations are largely in good agreement with the analytically calculated values. The analytically determined value of k_H is expected to be slightly lower, because of the approximation discussed above.

Next, the k_H associated with the "perpendicular-to-surface" configuration is considered. In the effort to make sure of that we can engineer a model situation where this is the main configuration that the adsorbed dimers take up, one of their monomers is now made hydrophilic by assigning to it a high unfavourable interaction strength χ_{1s} of +9 k_BT with the surface. The other remaining monomer is still hydrophobic with χ_{2s} varying from -2 to -5 k_BT, as before. The solvent is assumed an athermal solvent with $\chi = 0$ for both types of monomers. Thus, the hydrophobic monomer would adsorb to the surface, whereas the hydrophilic monomer prefers to stay away from the surface. In this case, the "perpendicularly" adsorbed configuration dominates and $k_H = \frac{1}{6}e^{-\chi_{2s}}$. As listed in Table 5.1b, for this type of dimer k_H calculated from SCF adsorption isotherms are again in reasonable accord with those inferred from analytical calculations.

From the above results, we can see that the method proposed here for determining k_H, based on the use of SCF calculations, is able to provide sensible values, in line with expectations for these simple test dimers.

Table 5.1 The k_H calculated from SCF and analytical calculations, for dimers consisting of (a) two identical hydrophobic monomers, with χ_s varied from -2 k_BT to -5 k_BT, (b) one hydrophilic monomer (χ_{1s} = +9 k_BT), and one hydrophobic monomer (χ_{2s} varied from -2 k_BT to -5 k_BT).

Composition of dimers	χ_s (k_BT) of hydrophobe	k_H (SCF)	k_H from analytical calculations
a. **two hydrophobic monomers**	-2	38.6	36.4
	-3	274.3	269.0
	-4	1941.8	1987.3
	-5	14598.2	14684.3
b. **one hydrophobic + one hydrophilic monomer**	-2	1.06	1.23
	-3	3.17	3.35
	-4	8.82	9.10
	-5	23.72	24.74

5.3.1.2 Results for linear amphiphilic polymers

The next set of structures employed for testing the methodology involve linear diblock polymers. With the length of hydrophilic segments now made much larger than the hydrophobic anchoring groups, the following calculations are performed for the theta solvent case ($\chi = 0.5$ for the hydrophilic monomers). It is worth noting that here the solvent strength for hydrophobic monomers is set as $\chi = 0.0$. Having a "hydrophilic" solvent favouring the solvent-hydrophobe interactions above solvent-hydrophile interactions, is usually not achievable in practice. However, as we had emphasised previously, in this section we wish to seek model systems that allow for validation of the method, rather than being a realistic representation of any specific system. Setting $\chi = 0.0$ means that it is no longer necessary to worry about the changes in the number of contacts between the anchoring groups and the solvent molecules, whether the latter are in bulk or adsorbed on the surface.

The interaction potential of hydrophiles with the surface is kept at $\chi_{1s} = +9$ to ensure hydrophilic segments of the chains avoid the interface upon their adsorption. In this case, the linear diblock polymers should take the train-tail conformation on the surface. For the same size of the hydrophilic blocks, and with their much smaller hydrophobic segments lying

almost flat on the surface, the loss of configurational entropy of the hydrophilic part extending away from surface will be the same for chains with different number of the anchoring hydrophobic residues. Note that of course this is only true when the degree of coverage is low (very dilute systems) and the adsorbed chains on the surface do not overlap. Above considerations make the relationship between the value of k_H and the adsorption energy more predictable. In the two systems studied below, the size of the hydrophilic block of the chains are kept constant. In the first case the hydrophobic block consists of just one monomer, but we vary the strength of the (favourable) interaction energy with the surface. In the second model, the interaction strength is kept the same, but the number of hydrophobic anchoring groups is altered instead.

The first linear diblock structure consists of 390 hydrophilic monomers, and as mentioned above, just one hydrophobe. The surface interaction parameter χ_{2s} for the hydrophobic residue is varied from -9 to -15 k_BT. By keeping the number of the two types of monomers constant, and ensuring no contact between the hydrophilic segments and the surface (due to the high degree of unfavourable interaction of +9 k_BT), one hopes to rule out any variation in the entropic contribution for different polymers, resulting from their adsorption. This then only leaves the enthalpic change to consider. Because there is only one hydrophobic monomer responsible for adsorption, the k_H is expected to be proportional to the Boltzmann factor for adsorption of this monomer onto the surface, namely:

$$k_H \propto e^{-\chi_{2s}}$$

5.26

or

$$\ln(k_H) = -\chi_{2s} + a$$

5.27

where the intercept *a* is a constant independent of χ_{2s}.

Using graphs similar to those in Figure 5.4, the value of k_H for chains with different χ_{2s} is determined from SCF calculation results. In Figure 5.5a, the value of $\ln(k_H)$ is plotted against the Flory-Huggins parameter for the interaction of hydrophobic monomer with the surface. A clear linear relationship, with the slope very close to -1 and in good accordance with our prediction in Eq. 5.27, is obtained.

Another set of linear diblock amphiphilic polymers used here for the verification purpose, has a constant number of monomers in its hydrophilic block, in much the same as that above (a total of 390). However, the number
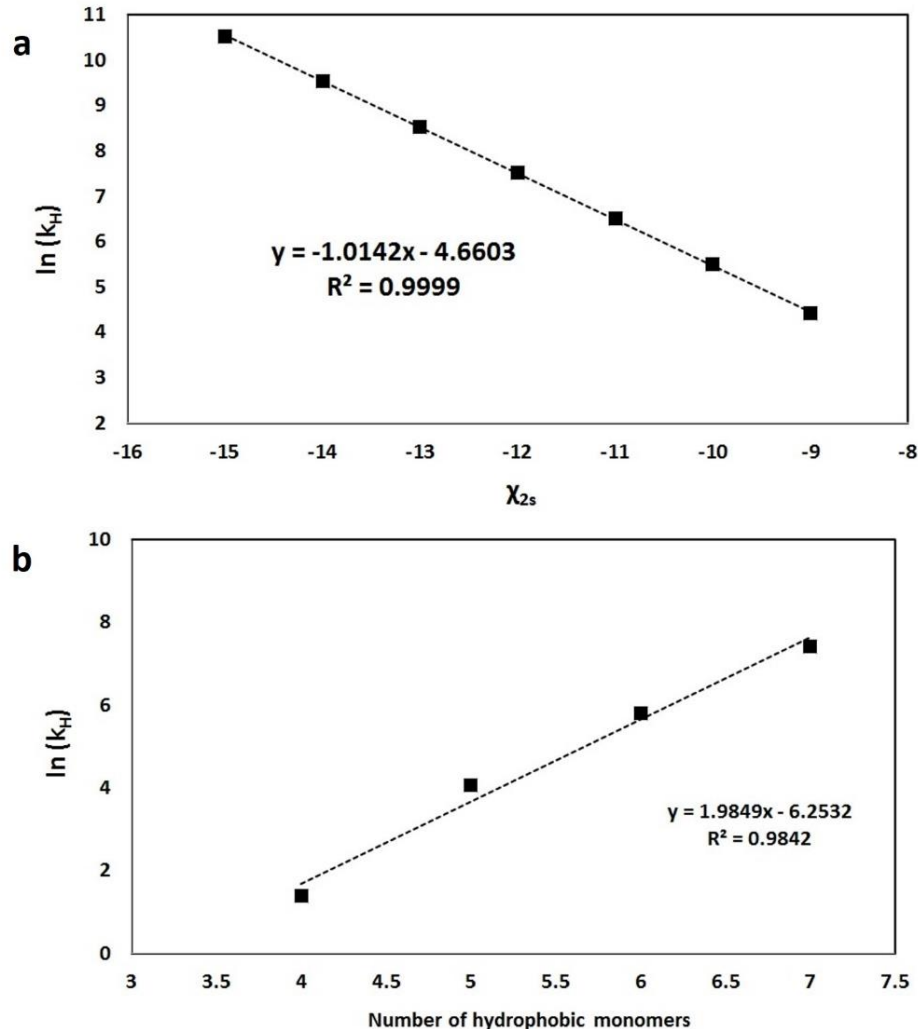
Figure 5.5 (a) ln(k_H) plotted against χ_{2s} for linear amphiphilic polymers containing only one hydrophobic monomer, with χ_{2s} being varied from -9 k_BT to -15 k_BT. (b) ln(k_H) plotted as a function of the number of hydrophobic monomers, for a linear amphiphilic polymer. The number of monomers in the hydrophobic block varies from 4 to 8, but with χ_{2s} now kept constant for all cases. The fitted straight line equation and R^2 for its linear regression is also included.

of hydrophobic monomers is now varied from 4 to 8, while the value of χ_{2s} is kept constant at -2 k_BT. Again, by maintaining the size and the nature of the hydrophilic part of the chains the same, the entropic contribution to adsorption free energy for these structures should remain the same. This leaves the enthalpic part accountable for the difference in k_H and the adsorbed amount for different chains. The variation in k_H is the result of the addition of hydrophobes one by one as we increase these from 4 to 8. With each addition the adsorption free energy changes by χ_{2s} = -2 k_BT per chain. Therefore, for such a model

$$k_H \propto e^{-\chi_{2s} \cdot n_{HB}}$$

5.28

where n_{HB} is the number of monomers in the hydrophobic block. In other words

$$\ln(k_H) = -\chi_{2s} \cdot n_{HB} + b$$

5.29

Where χ_{2s} is -2 k_BT and b is a constant independent of n_{HB}. Using our SCF calculations, we determined the adsorbed number of chains per surface as a function of bulk volume fraction. Considering the dilute regime where the relation between these two quantities is linear, we obtained the values of k_H for n_{HB} between 4 and 8, using the same procedure as in Figure 3.3. As shown in Figure 5.5b, a plot of $\ln(k_H)$ versus the number of hydrophobic monomers (n_{HB}), produces the expected straight line with a slope of 1.9849. This is in excellent agreement with the predicted value of $|\chi_{2s}| = 2$ as indicated by Eq. 5.29. Such a correspondence suggests that hydrophobic block is lying flat on the surface, confirming that at the current adsorption strength the block forms a train conformation with little or no loops. The results above also imply that by having the same length of hydrophilic block, the entropic loss upon adsorption of the chain stays the same, irrespective of how strong the hydrophobic monomer is anchored onto the surface.

For both dimers and linear diblock amphiphilic polymers, the results of SCF calculations agrees closely with the predictions. Therefore, the approach for determination of k_H has shown to work well. In the next section we will apply the method to more complex chain architectures, where predicting k_H is not as straightforward.

5.3.2 Adsorption constant for linear amphiphilic polymers

As the model is applied to more complex architectures, the Flory-Huggins interaction potential parameters are now chosen to be more representative of the real systems. From this point onwards, unless stated otherwise, the strength of interaction between hydrophilic and hydrophobic monomers on one hand and solvent molecules on the other are taken as 0.5 and 1.0 k_BT, respectively.

The first structure examined, where variation of k_H with chain size is not trivial to predict, is a linear amphiphilic chain containing identical number of hydrophobic monomers (10, with each having $\chi_{2s} = $ -2 k_BT). The magnitude of χ_{2s} is sufficiently large to ensure that the block of 10 anchoring monomers will lie flat on the surface. Hence, the adsorption energy associated with each linear chain on the surface is the same, irrespective of

the length of its hydrophilic section. We alter this latter for the polymers, ranging from 10 to 390 monomers. Setting the adsorption potential of hydrophilic monomers to χ_{1s} = +9 k_BT, ensures that the hydrophilic parts will strongly avoid the interface and instead will extend away from the surface into bulk solution. At low levels of surface coverage (i.e. a very dilute solution), and with the enthalpic change the same for chains with the same hydrophobic block sizes, the main differences in the conformational statistics for the adsorbing polymers are governed by the level of enthalpic penalty loss upon their adsorption. The reduction in the conformational entropy arises due to the restrictions that the impenetrable interface imposes on the adsorbed chain. For the set of different chains considered here then, this entropy loss should be a function of the length of the hydrophilic sections only (Striolo and Prausnitz, 2001).
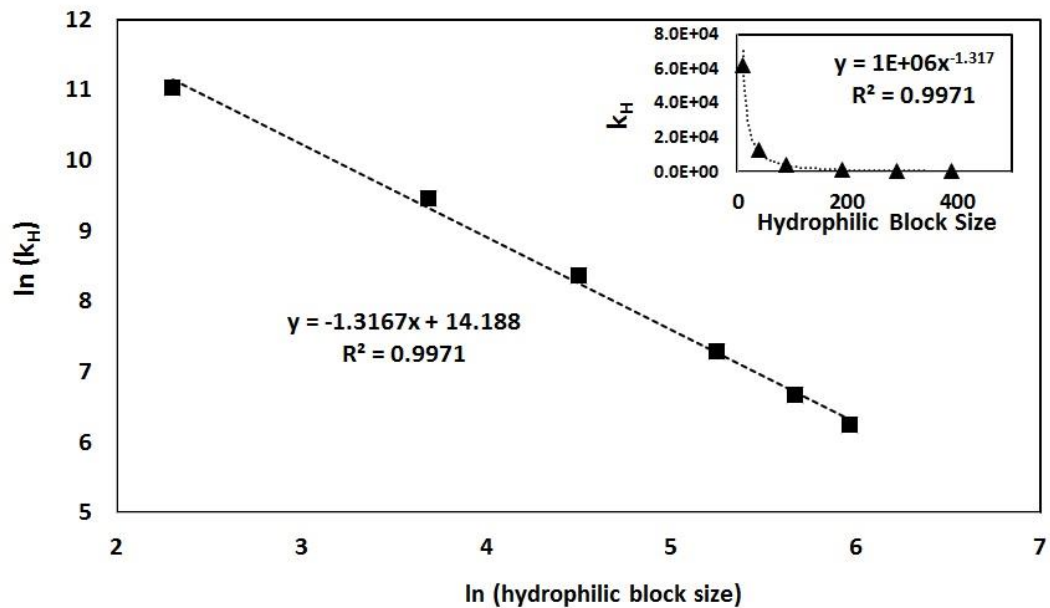
Figure 5.6 Power relationship between k_H and the degree of polymerisation of the chains, involving linear diblock polymers each containing 10 hydrophobes and varying numbers of hydrophilic monomers, ranging from 10 to 390.

A power law relationship is found between k_H and the hydrophilic block size of these polymers, with a R^2 value of 0.9971 for the straight line fitted to log(k_H) plotted against logarithm of the hydrophilic block size (Figure 5.6). The relation is determined to be $k_H \sim N_h^{-4/3}$. While having the same adsorption enthalpy, the linear chains with larger sizes tend to experience a greater level of conformational entropic loss upon adsorption. As a result,

the value of Henry's adsorption constant k_H also decreases with increasing chain size.

5.3.3 Factors affecting the adsorption behaviour of branched polymers

5.3.3.1 Star-like polymers

In star-like polymers, both the number of arms and the position of hydrophobic monomers are possible factors affecting the adsorption behaviour. As stated in the last section, the solvent strength for hydrophilic and hydrophobic monomers are 0.5 and 1.0 k_BT, respectively. All the star polymers considered here have the same number of monomers: i.e. 391 hydrophilic residues (with $\chi_{1s} = 0$ k_BT) and 10 hydrophobic ones (with $\chi_{2s} = -2$ k_BT). Number of arms ranged from 3 to 7. Obviously, the larger the number of arms, the shorter each arm will be. Having the same number of hydrophobic monomers, and provided that all hydrophobic residues of an adsorbed chain do lie on the surface, the overall adsorption enthalpy should be the same for all the polymers with different number of arms. Furthermore, since we have chosen the chemical composition and the degree of polymerisation (at 400 monomers) to also be identical, then any difference in the adsorption constant must largely be attributed to differing levels of conformational entropy loss, when these star polymers of different number of arms are compared.

Four different positions of the hydrophobic monomers are taken into consideration, as is schematically illustrated in Figure 5.2. The hydrophobic residues are either all placed together as a single block on one arm or are evenly distributed among all arms. A further architecture studied here places all the hydrophobes at the centre of the chain, while another locates them at the free ends. It is worth noting that structures with hydrophobes on one arm are the only ones breaking the symmetrical design of the polymers. We emphasise that such a none-symmetrical structure is of course not available for studies involving equal-sized-armed homopolymers, and therefore useful to include here.

Star polymers with their hydrophobic monomers in the central parts, but equally distributed among the three arms (markers as thick red lines in Figure 5.7), behave in an identical manner to chains with their hydrophobes still in the central part but only on one arm (data not shown). On the other hand, for polymers with hydrophobic monomers at the free ends (with markers as green triangles and blue circles in Figure 5.7), the positional

distribution of hydrophobes between different arms is found to greatly influences the affinity of the copolymers for adsorption onto the surface. Polymers having hydrophobic monomers equally distributed among all free ends had a value of k_H two orders of magnitude lower than those with all hydrophobes concentrated at the free end of one arm only. This observation resembles the well-known phenomenon for linear diblock polymers, where the diblocks adsorb more strongly than their triblock counterparts, possessing the same size and chemical composition (Fleer and Scheutjens, 1990). Structure (a) in Figure 5.7, where the adsorbing monomers are concentrated at one free end somewhat resembles a diblock structure, in that it has a single large hydrophobic block. As such, its non-adsorbing segments are able to extend further away from the surface, thus escaping the restrictions imposed by the impenetrable interface. Large sections of such chains behave as if they were in the bulk, with relatively smaller loss in conformational entropy upon adsorption. Structure (b) in Figure 5.7 is more reminiscent of a triblock linear polymer, with its adsorbing segment in the middle, and its two non-adsorbing blocks shorter than the diblock counterpart. With these latter blocks unable to extend as far as those in structure (a), a higher conformational entropic penalty loss is expected upon adsorption. Structure (c) of Figure 5.7 has non-adsorbing blocks of the same length as those in structure (b). However, because now these are connected at the single cross-link point at the centre of the star-shaped polymer (with the free ends of all arms being hydrophobic), the possible configurations of the individual arms are significantly restricted. For strongly adsorbing hydrophobes, each arm has its hydrophobic free end adsorbed on the surface, with the other end of the arm having to return to the same cross-link point as that for all the other arms. It is clear that in this case the decrease in the number of accessible configurations upon adsorption is far more than if the anchoring groups where close to the central (i.e. cross-link point) part of the polymer. Consequently, the entropic penalty paid by structure (c), when adsorbed, is the highest among the three-star structures studied here.

Generally all three star-like architectures in Figure 5.7 show a decrease in the magnitude of k_H as the number of arms increases. However, where the hydrophobes are placed as a block on one end of a single arm, the decrease is seen to be only marginal (Figure 5.7 (a)). There, the value of k_H remains large compared to the other two star-shaped architectures studied, irrespective of the number of arms involved. As the number of arms increases, the hydrophilic blocks become smaller. However, the fact that any changes in k_H are small for the structure (a), indicates that the arms remain

reasonably long. In particular, it seems that the crosslink point can reside sufficiently far away from the surface. Thus, the presence of interface is only really felt by the single arm containing the anchoring groups. As for all the other arms of the star-polymer, these remain far from surface so as not to be much effected by it. This then provides an explanation for the modest decrease of k_H with the number of arms one observes in Figure 5.7, for polymer structure labelled (a).
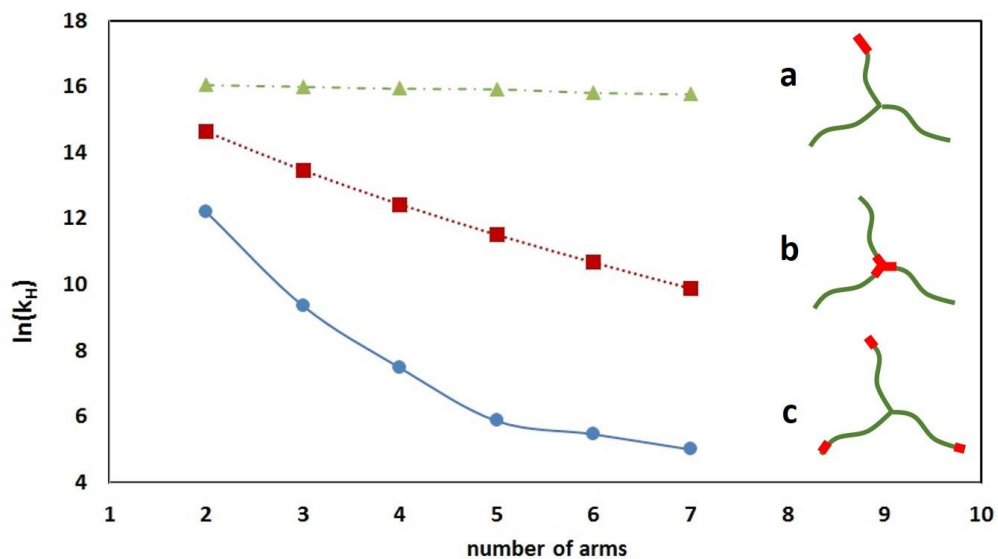
Figure 5.7 The ln(k_H) of star polymers plotted against the number of arms, on a semi-log scale. Positions of hydrophobic monomers are: (a) ─▲─ concentrated on one arm only, at one free end, (b) ···■··· evenly distributed among all arms, at the centre, and (c) ─●─ evenly distributed among all arms, at all free ends.

Figure 5.8 shows the saturation adsorbed coverage for each star structure studied in Figure 5.7, but now at sufficiently high polymer bulk concentrations. The saturation values are taken from the plateau regime of the adsorption isotherm. At this stage the variation of the adsorbed amount with the increase in bulk concentration is very small. Nonetheless, to have a more representative value, the adsorptions at bulk volume fractions of 10^{-4}, 10^{-3}, and 10^{-2} (all in the plateau regime) are averaged to obtain the surface coverage presented here. In the same figure we have also displayed the SCF calculated results for the volume fraction profile for each polymer architecture possessing 3, 5 and 7 arms. In each case the polymer bulk volume fraction is set to be 10^{-3}. This bulk concentration was found to be sufficient for polymers to attain their saturation surface coverage, limited by
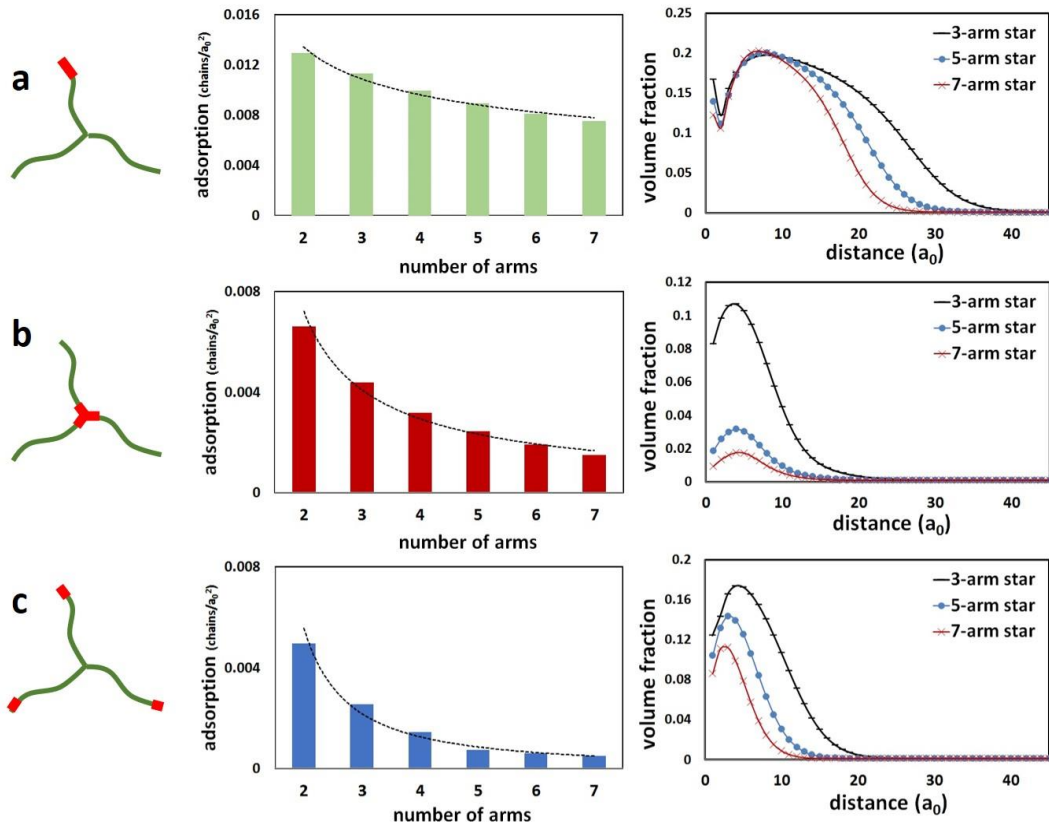
Figure 5.8 Saturation surface coverage for different displayed star polymer architectures, and the corresponding volume fraction profiles, plotted against distance away from the interface, for polymers with 3, 5 and 7 arms, all at a bulk volume fraction of 10^{-3}.

the overlap of neighbouring chains. As the number of arms increases, the adsorbed layers are seen to become more compact in all three cases. This is expected, since polymers with larger number of arms but the same molecular weight, are more compact entities than those with only a few arms. In turn, any overlaps between neighbouring adsorbed polymers within a more compact, less extended, interfacial layer increase more rapidly. This tends to limit the number of adsorbed chains more strongly and keeps the amount of maximum coverage low. A clear decrease in the amount of adsorbed polymer, with increasing number of arms, is evident for all three cases presented in Figure 5.8. In particular, it is interesting to note that this consideration applies as much to structure (a), where the anchoring groups are located only at the free end of one of the arms. The variation of the maximum adsorbed coverage with the number of arms is in stark contrast to the behaviour we observed in the low end of the Langmuir isotherm, for this polymer architecture. Recall (see Figure 5.7 (a)) that the value of k_H, characterising the low end, early stage of the isotherm, was not overly

sensitive to variation in the number of arms, whereas the maximum surface coverage clearly is (Figure 5.8a).

The other two star-shaped structures also have maximum surface coverages decreasing with an increase in the number of arms. The percentage decreases when arm number increases from 3 to 7 for three structures are (a) 41.7%, (b) 90.3%, and (c) 77.3%. The volume fraction for 7-arm stars drops more quickly as compared to that of 3-arm structure, for example in case (a), the volume fraction for 7-arm star returns to bulk at a distance of 32 while the same for 3-arm star occurs at 48. This is observed for all three star-like structures.

5.3.3.2 Dendritic polymers

As with the star polymers above, in this section the solvent strength for hydrophilic and hydrophobic monomers are once again maintained at 0.5 and 1.0 k_BT, respectively. Similarly, the strength of interaction with the surface for hydrophobic monomers is kept at a favourable value of $\chi_{2s} = -2$ k_BT.

The dendritic polymers studied here have their overall monomer numbers increasing with generations. We define each generation to be the next level of branching in the tree-like structure for these polymers. Since the ratio of hydrophobic monomers to total monomers is kept at 1 to 40, polymers of higher generation now contain a larger number of hydrophobic entities, and as a result may be expected to also have higher k_H values. It is worth noting that the polymers in this study are designed to be flexible. Therefore, hydrophobic monomers, no matter where they are along the backbone, can be exposed and adsorb onto the surface. This consideration applies equally to hydrophobes at the very centre of the polymer.

Here five types of hydrophobic monomer distribution are considered, as are illustrated in Figure 5.9. The last two cases (d and e) are ones where the hydrophobes are equally distributed among all strands (one on each), being located either at the middle of each linear strand or next to the branching points. Both patterns would result in a lack of large single adsorbing blocks in such polymer architectures. As a matter of fact, the pattern where hydrophobic monomers are positioned in the middle of every strand (Figure 5.9e) leads to a non-adsorbing behaviour of the polymer (data not shown), indicating that the adsorption potential is so weakened that the chain essentially loses its amphiphilic property. On the other hand, in the case where hydrophobes are positioned next to each branching point
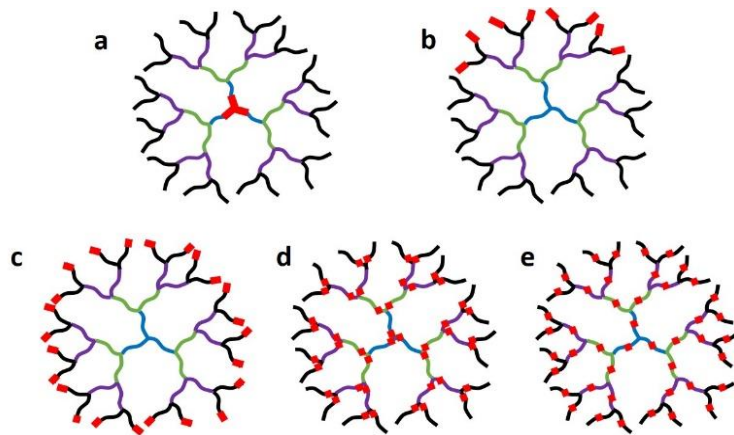
Figure 5.9 Schematic illustration of the position of hydrophobic monomers in our model dendritic polymers.

Locations of hydrophobes are highlighted with thick red blocks. Here a dendrimer with 4 generation level is being displayed as an example. Hydrophobic monomers are (a) concentrated at the very centre of the polymer, with equal numbers on each of the three centrally connected strands; (b) distributed only among 1/3 of all the free ends; (c) evenly distributed at all free ends; (d) evenly distributed near each branching point; and (e) evenly distributed in the middle of each linear strand.

(Figure 5.9d), the amphiphilic nature is retained, allowing k_H to be successfully determined (Figure 5.10d). The surface affinity of polymers with this pattern of spatial hydrophobic distribution does not alter much with the number of generations, or polymer size. This is probably the result of the constant number of hydrophobic/hydrophilic monomer ratio (1 in 40 here) irrespective of the number of generations. The non-adsorbing segments in structure (d) of Figure 5.10 cannot stretch very far away from the surface, with the polymer thus being forced to lie flat on the surface. As a result, chains with the structure (d) (Figure 5.10) experience a very large degree of conformational entropic loss upon adsorption. Consequently, this structure is also found to have the lowest k_H values among the four shown in Figure 5.10.

Dendrimers with the other three distribution patterns have their affinity for surface increased with the number of generations. For cases where hydrophobic monomers are at the free ends, the k_H value is higher for structure (b) where all hydrophobes are concentrated at 1/3 of the free ends than structure (c), the case with equal distribution at all free ends. Here dendrimer (c) loosely resembles a triblock linear polymer whose central non-adsorbing segments extending away from the surface, but with the two anchoring free ends having to reside on the surface. Dendrimer (b) on the other hand, according to same analogy, resembles a diblock linear polymer

where those free ends without adsorbing monomers are free to extend away from the surface into the bulk solution. This is true for such structures of all generations. Much in the same way that a linear diblock chain has a higher k_H value than its triblock counterpart, here also we find the same for structure (b) relative to (c) (see Figure 5.10).
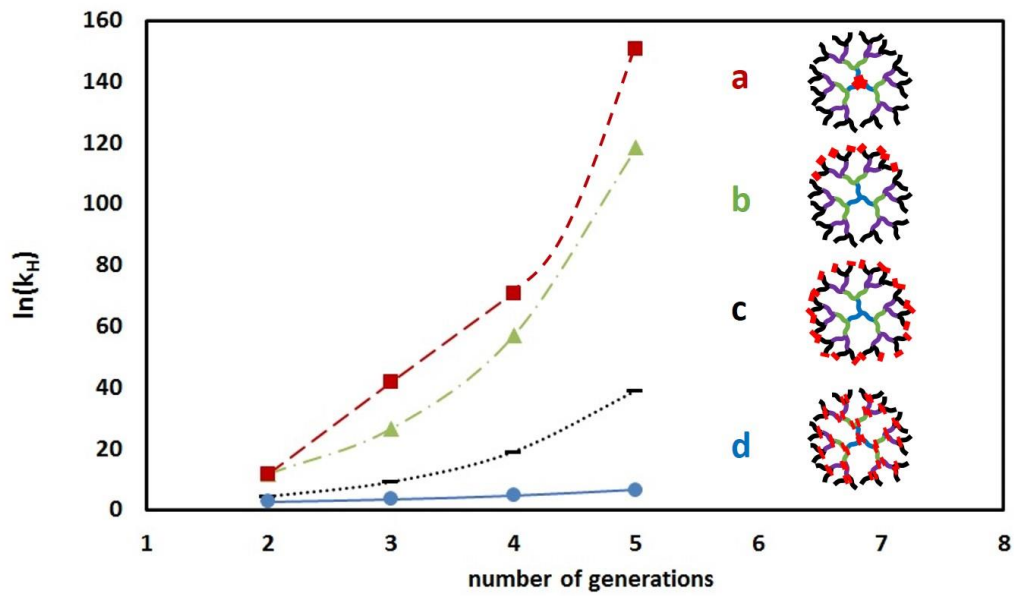
Figure 5.10 The ln(k_H) of dendritic polymers plotted against the number of generations, on a semi-log scale. Positions of hydrophobic monomers are: , (a) ▬■▬ concentrated at the centre, with equal number on each of the three strands joining in the middle; (b) ─▲─ distributed only amongst 1/3 of the free ends; (c) ··▬·· evenly distributed among all free ends; (d) ─●─ evenly distributed near each branching point.

The polymer with the highest surface affinity (i.e. largest k_H) here is found to be the one where all the hydrophobic residues are located at the central part, as a single continuous block (dendrimer (a) in Figure 5.10). Though the linear analogue for dendrimer (a) is closer to a triblock polymer, this time the triblock analogue chain will have its anchoring groups in the centre, with the two non-adsorbing blocks on either side. It is found that k_H value for this structure is significantly higher than that for dendrimer (b), especially with a larger number of generations. This is because structure (a) has all its outer generations freely extending away from the surface. The nature of dendrimer structure for the model used here, dictates that the number of linear strands in each generation is twice that of the previous one. Our results here show that even if structure (b) had more extending free ends, the entropic loss associated with its adsorption is still larger than that

incurred by structure (a), where more segments are allowed to extend out. This is true even with shorter individual strands. Such distinctions in the adsorption behaviour of diblock and triblock structures are well known for linear polymers (Fleer and Scheutjens, 1990; Kilbey et al., 2001). Here we have shown that the same can largely explain the behaviour of different dendrimer architectures, too.

It is clear that for both star-like and dendritic polymers, the spatial distribution and position of hydrophobic monomers on the polymer backbone greatly impacts their surface affinity. In general, some of the principles regarding linear chains seem to still hold for these much more complex structures. The more closely spaced, fewer large block distribution of hydrophobic monomers that one has, the higher the affinity for adsorption seems to be. Polymers resembling diblock linear chains (with one large single anchoring block) adsorb more than those resembling triblocks, multi-blocks or random co-polymers, if the chemical composition and numbers of hydrophobic and hydrophilic residues remain the same.

5.4 Conclusions

This study focuses on the low adsorption end of the Langmuir Isotherm, and establishes a method for calculating Henry's constant k_H for amphiphilic polymers, using SCF calculations. The method is successfully validated by comparing the calculated k_H value from SCF results and that obtained from analytical calculations, for several simple cases involving dimers or certain linear polymer architectures. The method is then applied to complex structures where k_H cannot be analytically estimated. The entropic change for linear chains with constant number of adsorbing hydrophobic monomers, but varying hydrophilic tails, is found to follow a power law with the length of the non-absorbing hydrophilic tails. The significance of the value of the power index remains to be determined. For star and dendritic polymers, different spatial distribution patterns of hydrophobic monomers along the chains are also considered. The k_H values for star polymers are examined in relation to varying number of arms and the arm size. As the number of arms increases and the length of each arm gets smaller, all structures show a decrease in the value of k_H due to larger entropic restrictions upon adsorption. One exception to this trend is the star shaped polymer where all anchoring hydrophobic groups are placed at one free end only. The surface affinity of this particular architecture remains more or less the same, regardless of the decreasing size of each arm. On the other hand,

for all the three star-shaped structures here, the maximum surface coverage decreased with increasing number of arms. In dendrimers, the distribution of hydrophobic monomers is again found to greatly influence their surface affinity. The closely spaced adsorbing units in small number of large blocks, exhibit a higher k_H value. Such findings may provide guidance to future experimental work. One example is in providing information on the optimum grafting position of hydrophobic residues on to a hydrophilic backbone, during the process of manufacturing suitable amphiphilic surface active polymers (emulsifier, steric stabilisers, etc).

Reference

Akinshina, A., Ettelaie, R., Dickinson, E. and Smyth, G. 2008. Interactions between adsorbed layers of αS1-casein with covalently bound side chains: a self-consistent field study. *Biomacromolecules.* **9**(11), pp.3188-3200.

Balazs, A.C. and Siemasko, C.P. 1991. Contrasting the surface adsorption of comb and linear polymers. *The Journal of chemical physics.* **95**(5), pp.3798-3803.

Bulychev, N., Dervaux, B., Dirnberger, K., Zubov, V., Prez, F.E.D. and Eisenbach, C.D. 2010. Structure of adsorption layers of amphiphilic copolymers on inorganic or organic particle surfaces. *Macromolecular Chemistry and Physics.* **211**(9), pp.971-976.

Carignano, M. and Szleifer, I. 1995. On the structure and pressure of tethered polymer layers in good solvent. *Macromolecules.* **28**(9), pp.3197-3204.

de Gennes, P. 1980. Conformations of polymers attached to an interface. *Macromolecules.* **13**(5), pp.1069-1075.

De Gennes, P. 1987. Polymers at an interface; a simplified view. *Advances in colloid and interface science.* **27**(3-4), pp.189-209.

Dickinson, E. 2009. Hydrocolloids as emulsifiers and emulsion stabilizers. *Food hydrocolloids.* **23**(6), pp.1473-1482.

Ettelaie, R., Holmes, M., Chen, J. and Farshchi, A. 2016. Steric stabilising properties of hydrophobically modified starch: Amylose vs. amylopectin. *Food Hydrocolloids.* **58**, pp.364-377.

Ettelaie, R., Zengin, A. and Lee, H. 2014. Fragmented proteins as food emulsion stabilizers: A theoretical study. *Biopolymers.* **101**(9), pp.945-958.

Fleer, G. and Scheutjens, J. 1990. Block copolymer adsorption and stabilization of colloids. *Colloids and surfaces.* **51**, pp.281-298.

Fleer, G., Stuart, M.C., Scheutjens, J.M., Cosgrove, T. and Vincent, B. 1993. *Polymers at interfaces.* Springer Science & Business Media.

Freij-Larsson, C., Nylander, T., Jannasch, P. and Wesslén, B. 1996. Adsorption behaviour of amphiphilic polymers at hydrophobic surfaces: effects on protein adsorption. *Biomaterials.* **17**(22), pp.2199-2207.

Gingell, D. and Owens, N. 1994. Inhibition of platelet spreading from plasma onto glass by an adsorbed layer of a novel fluorescent‐labeled poly (ethylene oxide)/poly (butylene oxide) block copolymer: Characteristics of the exclusion zone probed by means of polystyrene beads and macromolecules. *Journal of biomedical materials research.* **28**(4), pp.491-503.

Hubbell, J.A. 1999. Bioactive biomaterials. *Current opinion in biotechnology.* **10**(2), pp.123-129.

Hunter, R.J. 2001. *Foundations of colloid science.* Oxford university press.

Ishihara, K., Suzuki, K., Inoue, Y. and Fukazawa, K. 2020. Effects of molecular architecture of photoreactive phospholipid polymer on adsorption and reaction on substrate surface under aqueous condition. *Journal of Biomaterials Science, Polymer Edition.* pp.1-19.

Kilbey, S.M., Watanabe, H. and Tirrell, M. 2001. Structure and Scaling of Polymer Brushes near the ϑ Condition. *Macromolecules.* **34**(15), pp.5249-5259.

Leermakers, F.A., Léonforte, F. and Luengo, G.S. 2020. Structure and Colloidal Stability of Adsorption Layers of Macrocycle, Linear, Comb, Star, and Dendritic Macromolecules. *Macromolecules.* **53**(17), pp.7322-7334.

Mu, M., Karthik, P., Chen, J., Holmes, M. and Ettelaie, R. 2021. Effect of amylose and amylopectin content on the colloidal behaviour of emulsions stabilised by OSA-Modified starch. *Food Hydrocolloids.* **111**, p106363.

Naderi, A., Iruthayaraj, J., Pettersson, T., Makuska, R. and Claesson, P.M. 2008. Effect of polymer architecture on the adsorption properties of a nonionic polymer. *Langmuir.* **24**(13), pp.6676-6682.

Rolińska, K. and Sikorski, A. 2020. Adsorption of Linear and Cyclic Multiblock Copolymers from Selective Solvent. A Monte Carlo Study. *Macromolecular Theory and Simulations.* **29**(6), p2000053.

Scheutjens, J. and Fleer, G. 1979. Statistical theory of the adsorption of interacting chain molecules. 1. Partition function, segment density distribution, and adsorption isotherms. *Journal of Physical Chemistry.* **83**(12), pp.1619-1635.

Schroen, C., Stuart, M.C., Van der Voort Maarschalk, K., Van der Padt, A. and Van't Riet, K. 1995. Influence of preadsorbed block copolymers on protein adsorption: surface properties, layer thickness, and surface coverage. *Langmuir.* **11**(8), pp.3068-3074.

Sikorski, A. 2002. Structure of adsorbed polymer chains: a Monte Carlo study. *Macromolecular theory and simulations.* **11**(3), pp.359-364.

Sikorski, A. and Romiszowski, P. 2005. Computer simulations of adsorbed polymer chains. *Acta Physica Polonica B.* **36**(5), pp.1779-1789.

Song, X., Pei, Y., Zhu, W., Fu, D. and Ren, H. 2014. Particle-stabilizers modified from indica rice starches differing in amylose content. *Food Chem.* **153**, pp.74-80.

Striolo, A. and Prausnitz, J.M. 2001. Adsorption of branched homopolymers on a solid surface. *The Journal of Chemical Physics.* **114**(19), pp.8565-8572.

Sweedman, M.C., Hasjim, J., Schafer, C. and Gilbert, R.G. 2014. Structures of octenylsuccinylated starches: effects on emulsions containing beta-carotene. *Carbohydr Polym.* **112**, pp.85-93.

Szleifer, I. 1997. Polymers and proteins: interactions at interfaces. *Current Opinion in Solid State and Materials Science.* **2**(3), pp.337-344.

Tian, P., Uhrig, D., Mays, J.W., Watanabe, H. and Kilbey, S.M. 2005. Role of Branching on the Structure of Polymer Brushes Formed from Comb Copolymers. *Macromolecules.* **38**(6), pp.2524-2529.

Trégouët, C., Salez, T., Pantoustier, N., Perrin, P., Reyssat, M. and Monteux, C. 2019. Probing the adsorption/desorption of amphiphilic polymers at the air–water interface during large interfacial deformations. *Soft matter.* **15**(30), pp.6200-6206.

Van der Linden, C., Leermakers, F. and Fleer, G. 1996. Adsorption of comb polymers. *Macromolecules.* **29**(3), pp.1000-1005.

Wessels, M.G. and Jayaraman, A. 2020. Self-assembly of amphiphilic polymers of varying architectures near attractive surfaces. *Soft matter.* **16**(3), pp.623-633.

Chapter 6
General discussion

6.1 Introduction

Food-grade emulsifiers and stabilisers are important constituents of food additives. A great number of food products are present as colloid systems, with emulsion being the most prevalent colloid type. In the last decades, the food industry is marked by a trend of moving away from synthetic additives, and therefore also an increasing demand for utilising biopolymers suitable to stabilise emulsions. Many different biopolymers have been examined for their possible use as emulsifiers to meet the needs of food industry, and starch has been considered a promising choice due to its abundancy, sustainability, and its relatively inexpensive price. Native starch are hydrophilic molecules that exist in the form of water-insoluble granules, so hydrophobic modification needs to be performed to improve their surface activity, whether these are used as dissolved biopolymers or as granular particle (Pickering) stabiliser.

Starch modified with octenyl succinic anhydride (OSA) attains amphiphilic properties, and has a wide range of applications as a texturizer and emulsion stabilizer (Caldwell and Wurzburg, 1953). Despite its long history of industrial application, OS-starch continues to attract the interest of many researchers who continuously strive to explore new applications or further improve its functional properties. With the trend towards healthy foods, OS-starch has been used to formulate gluten-free bread and low-fat products (Klaochanpong et al., 2017; Bajaj et al., 2019; Korus et al., 2021).

The functionality of OS-starch as an emulsifier depends not only on the hydrophobic modification, but also on the structure of the original native starch (Sweedman et al., 2014). As discussed in **Chapter 2**, due to the complexity of starch structure, the exact relation of starch structural features to OS-starch functionality remains to be unveiled. This Thesis aims to advance the research on OS-starch by both seeking novel applications and deciphering the impact of one of its structural characteristics, namely amylose content, on its functionality.

In the effort to create new possibilities for the application of OS-starch as a beverage emulsifier, truly reconstitutable emulsions were produced with a commercial OS-starch made from waxy maize starch (**Chapter 3**). By truly

reconstitutable emulsions, we have in mind dried emulsions that not only form their original pre-dried droplet sizes upon their rehydration, but also have the same long-term colloidal stability as any freshly made emulsion. Such dried emulsions can be readily used in given food formulations, and therefore have considerable advantages in saving storage and transportation costs. The storage conditions for the dried emulsion power were carefully evaluated for their impact on the stability of reconstituted emulsions.

To better understand why most of the commercial OS-starch are based on waxy maize starch, both experimental and theoretical investigations were carried out on the effect of amylose content on the emulsifying and stabilising properties of OS-starch. Experimentally, the strength of steric stabilisation provided by OS-starch of varying amylose content was evaluated in three stressed conditions: variation in pH, increase of electrolyte concentration, and enzymatic digestion (**Chapter 4**). Theoretically, SCF calculations were performed on amphiphilic copolymers with different architectures and location of hydrophobic blocks (**Chapter 5**). The adsorption behaviour of linear, star and dendritic polymers were characterised by computing Henry's adsorption constant, k_H, extracted from theoretical adsorption results for the low coverage part of their adsorption isotherms.

This work hopes to unveil the linkage between amylose content and emulsifying and stabilising properties of OS-starch, open up new approaches for selecting the suitable native starch that would produce OS-starch with better functionalities, which can in turn have more potential applications in foods.

6.2 Summaries of key findings

6.2.1 Fabrication of reconstitutable O/W emulsion with commercial OS-starch

Stable O/W fresh emulsion made with a commercial OS-starch was fabricated and freeze-dried to produce dried emulsion powder. A reconstituted emulsion was obtained by rehydrating the dried powder immediately after the freeze-drying process, and its droplet size d_{43} with no post-reconstitution storage was found to increase (~2 µm) as compared to that of the fresh emulsion (0.5 µm). With ultrasonication and addition of SDS, the change in droplet size caused by freeze-drying was mainly attributed to

aggregation, with little coalescence. This result suggests that the original droplets remain intact, despite the process of drying and rehydration. The formation of ice and lipid crystals during the freezing process may have disrupted the adsorbed layer of OS-starch, and upon hydration resulted in flocculated droplets. This results in the moderate increase observed in the measured droplet size after rehydration, as compared to droplets prior to drying.

In order to evaluate the impact of relative humidity and temperature during dry storage phase, on the stability of reconstituted emulsions, the freeze-dried emulsion powders were stored at various storage conditions before rehydration. Relative humidity was found to have at best a mild impact on the reconstituted droplet size in the studied temperature range (-30 °C ~20 °C). In contrast, temperature during dry storage phase was the more prominent factor, in determining the final size of the droplets in the reconstituted emulsions.

When samples were reconstituted from powders stored at higher storage temperatures (4 °C, 20 °C), flocculation was observed in the rehydrated emulsions, but surprisingly extensive coalescence and emulsion breakdown were absent. The crystallization temperature for bulk sunflower oil is typically between -20 to -17 °C, but supercooling effect was highly pronounced in these dried emulsion powders. As found by Differential Scanning Calorimetry, the crystallization temperature of oil in the emulsion powder was determined to be approximately -24.6 °C, and the melting point (during heating) was approximately -27.5 °C. Cold-Stage X-Ray Diffraction confirmed that emulsion powder scanned at -18 °C remained molten, and peaks for oil crystallization were observed in powders scanned at -70.0 °C.

The idea of fabricating fully reconstitutable emulsion powder that upon rehydration can result in emulsion of comparable droplet size as those of the original fresh emulsion, was realised in one of the storage conditions tested in this work. Dry reconstitutable emulsion powder was successfully fabricated and stored at -30 °C for more than 3 weeks, where upon simple rehydration, colloidally stable droplets of size ~ 2 µm were achieved (consequently stable for more than 100 days post rehydration). At -30 °C, the oil phase crystallised and became completely immobile. The physical state of the oil phase during storage was crucial to the stability of the reconstituted emulsion. This has major commercial potentials such as the possibility of mass production of the dried emulsions in a central site, much

cheaper and easier shipment of the dried powder to other locations, and storage and rehydration of these as when required.

6.2.2 Effect of amylose content on the steric strength provided by OS-starch

Steric stabilisation is the most characteristic and advantageous feature of OS-starch (Sweedman et al., 2013; Dickinson, 2018) employed as an emulsion stabiliser. In the effort to explore the effect of amylose content (AC) of OS-starch on the strength of steric stabilisation it provides, waxy maize starch (denoted as W, with amylose content determined to be 5.48 ± 0.99%) and normal corn starch (denoted as N, with amylose content determined to be 28.37 ± 0.10%) were modified with OSA to produce OS-starch. The native starch with lower AC (native W) yielded a lower DS than that with higher AC (native N), in line with the preferential attachment of OSA to amylose molecules as found by previous researches (Shogren et al., 2000; Wang et al., 2013; Whitney et al., 2016; Liu et al., 2018). Nevertheless, both OS-starches had satisfactory emulsifying and emulsion stabilising abilities at neural pH and for low electrolyte concentrations, producing stable sub-micron emulsions with a droplet size d_{43} of 0.5 - 0.6 μm.

Emulsion stabilised by OS-W showed high resistance to variations in pH and electrolyte concentration, while OS-N stabilised emulsions were observed to undergo a significant level of flocculation and an increased droplet size at acidic pH or at high electrolyte concentrations. Such results indicate that strong steric repulsion was the main stabilising mechanism for OS-W, whereas in the case of OS-N, the steric repulsive forces alone were not strong enough. In the latter case the interfacial film was to some degree also reliant on provision of additional electrostatic repulsions to achieve droplet stability. The electrostatic repulsion (as provided by OS-starch) is known to decrease at lower pH. Similarly, electrostatic forces tend to get screened by the addition of more electrolyte. The difference between the behaviour of emulsions made by OS-W and OS-N has been attributed to the fact that OS-N, with its higher amylose content, tends to form thinner interfacial layers. The linear nature of modified amylose also makes it more likely to adsorb simultaneously onto two closely spaced neighbouring droplets. This leads to a higher possibility of bridging flocculation in OS-N systems, as compared to the more compact layers formed by highly branched polymers in OS-W (Ettelaie et al., 2016).

6.2.3 Effect of amylose content on the oral digestion behaviour of emulsions stabilised by OS-starch

After establishing their difference in stabilisation mechanism, emulsions stabilised by OS-W (lower AC) and OS-N (higher AC) were subjected to enzymatic degradation, mimicking the oral digestion process of beverage products. *In vitro* experiments were conducted both with 2 g/L α-amylase solution and artificial saliva with the same enzymatic concentration. Control samples were included to rule out flocculation induced by the environmental factors, such as the presence of salt and protein (Silletti et al., 2007; Sarkar et al., 2017).Subsequently, *in vivo* experiments were conducted as well, involving panellists placing the emulsion samples in their oral cavity and spitting it into a container after a designated time interval.

With both *in vitro* and *in vivo* experiments, the enzyme-treated samples of W and N emulsions exhibited larger droplet sizes as a result of enzymatic digestion of OS-starch. It is worth noting that the impact of enzymatic treatment on the stability of emulsion samples was found to be the opposite to the one resulting from changes in electrostatic interactions (i.e. varying pH and electrolyte concentrations). Here, the emulsion stabilised by OS-W (lower AC) was destabilised more rapidly than that by OS-N. Microscopic images confirmed the presence of significant coalescence in emulsion stabilised by OS-W, but mainly flocculation in emulsions stabilised by OS-N.

This distinction in colloidal behaviour upon enzyme digestion suggests that the interfacial layers, formed by OS-starch of various amylose content, are enzymatically degraded at different rates, providing a potential possibility for tailoring the controlled release of flavourings, or other active ingredients. In principle, by mixing emulsions stabilised by OS-starch of different amylose content, at suitable ratios, one can achieve any desired release profiles.

6.2.4 Theoretical evaluation of the adsorption behaviours of polymers with various architecture

After our experimental evidence, showing that the amylose content of OS-starch is an influential factor in determining the colloidal behaviour of emulsions fabricated with it, theoretical calculations were conducted to examine the differences in adsorption behaviour of linear and various branched polymers. To simplify and generalise the problem, the calculations

focused on copolymers of various architectures, where hydrophobic blocks are the adsorbing units. A method of determining Henry's adsorption constant, k_H, through examination of SCF (self-consistent field) calculated adsorption isotherms, was proposed. The method and the resulting Henry's constants provide useful information for characterising the adsorption behaviour of different polymer architectures. Validation of the method was performed by comparing the k_H obtained from SCF calculations with the analytically inferred values, for several simple molecules including dimmers and simple diblock linear structures. In all cases, k_H values determined in both ways agreed well with each other, proving the suitability of the method for extrapolating k_H.

The method was then applied to structures whose k_H cannot be estimated through analytical calculations. These included linear, star-like, and dendritic copolymer structures. A power law relationship was found for the k_H of linear chains and the length of their hydrophilic tails, when the number of monomers in their hydrophobic block was kept constant. The relation had a power index of -1.3167 $\approx$ -4/3. For star-like copolymers of equal total monomer number, as the number of arms increased and the length of each arm got smaller, the k_H decreased due to larger entropic restrictions imposed by the presence of the impenetrable surface. However, the decrease in k_H was seen to be less pronounced when all the hydrophobic monomers were placed in one single block, at only one free end of the star-shaped polymer. This particular architecture resembles somewhat a diblock structure, and similarly maintains a high level of surface affinity, regardless of the reduction in the size of arms. In dendrimers, much in the same way, the distribution pattern of hydrophobic blocks was found to have a large impact on the value of k_H and surface affinity. In general, linear structures have higher surface affinity than branched ones. For both star and dendritic copolymers, the observations resemble the well-known behaviour seen in linear copolymers. That is to say that chains with a diblock architecture adsorb more strongly than their triblock or multi-block counterparts, given the same size and chemical composition (Fleer and Scheutjens, 1990). Star-shaped and dendritic polymers, with structures possessing a single hydrophobic block (thus more like a diblock in this respect) have higher k_H values than those resembling multi-blocks.

6.3 Conclusions and future directions

This Thesis aims to find possible novel applications for OSA-modified starch and relate amylose content (linear vs branched polymers) to the emulsifying and stabilising ability of OS-starch. The proposed new application of OSA-modified starch, which is the fabrication of reconstitutable emulsion, was successfully achieved with commercial OS-starch (with low amylose content) at powder storage temperatures below the crystallization point of the oil phase. Through a systematic investigation by altering pH, electrolyte concentration, and enzymatic treatment, OS-starch with lower amylose content was found to provide stronger steric stabilisation but degrade more rapidly upon enzymatic digestion. Theoretical calculations found that at the same molecular weight and number of hydrophobic monomers (i.e. degree of substitution), a linear diblock copolymer will have the highest surface affinity among all possible chain architectures. Similarly, for star-shaped or dendritic polymers, the spatial distribution of hydrophobic blocks that provides a single hydrophobic anchoring block (thus more closely resembling the diblock structure for linear counterparts) gives the architecture with a higher surface affinity.

The above findings provide directions in improving the emulsification efficacy of OS-starch, namely by selecting starch molecules of more appropriate structures, controlled grafting of OSA preferably onto a group of glucose units close to each other, and on a larger scale, selection of OS-starch of an amylose content based on the desired properties (stronger steric stability or higher resistance to enzymatic digestion). In terms of industrial applications, reconstitutable emulsion could be made with OS-starch of higher amylose content, examining if the same storage conditions for that of low amylose content are required for the dried emulsion to be fully reconstitutable. Tailored controlled release, achieved through mixing multiple OS-starch of varying amylose content, can have great potential in delivery type applications, but calls for further analytical investigation and possible sensory evaluations in future work.

Reference

Bajaj, R., Singh, N. and Kaur, A. 2019. Properties of octenyl succinic anhydride (OSA) modified starches and their application in low fat mayonnaise. *Int J Biol Macromol.* **131**, pp.147-157.

Caldwell, C.G. and Wurzburg, O.B. 1953. *Polysaccharide derivatives of substituted dicarboxylic acids*. U.S. Patent 2,661,349. Dec. 1, 1953.

Dickinson, E. 2018. Hydrocolloids acting as emulsifying agents – How do they do it? *Food Hydrocolloids.* **78**, pp.2-14.

Ettelaie, R., Holmes, M., Chen, J. and Farshchi, A. 2016. Steric stabilising properties of hydrophobically modified starch: Amylose vs. amylopectin. *Food Hydrocolloids.* **58**, pp.364-377.

Fleer, G. and Scheutjens, J. 1990. Block copolymer adsorption and stabilization of colloids. *Colloids and surfaces.* **51**, pp.281-298.

Klaochanpong, N., Puncha-arnon, S., Uttapap, D., Puttanlek, C. and Rungsardthong, V. 2017. Octenyl succinylation of granular and debranched waxy starches and their application in low-fat salad dressing. *Food Hydrocolloids.* **66**, pp.296-306.

Korus, J., Ziobro, R., Witczak, T., Kapusniak , K. and Juszczak, L. 2021. Effect of Octenyl Succinic Anhydride (OSA) Modified Starches on the Rheological Properties of Dough and Characteristic of the Gluten-Free Bread. *Molecules.* **26**(8), p2197.

Liu, W., Li, Y., Chen, M., Xu, F. and Zhong, F. 2018. Stabilizing Oil-in-Water Emulsion with Amorphous and Granular Octenyl Succinic Anhydride Modified Starches. *J Agric Food Chem.*

Sarkar, A., Ye, A. and Singh, H. 2017. Oral processing of emulsion systems from a colloidal perspective. *Food Funct.* **8**(2), pp.511-521.

Shogren, R.L., Viswanathan, A., Felker, F. and Gross, R.A. 2000. Distribution of Octenyl Succinate Groups in Octenyl Succinic Anhydride Modified Waxy Maize Starch. *Starch/Stärke.* **52**, pp.196-204.

Silletti, E., Vingerhoeds, M.H., Norde, W. and van Aken, G.A. 2007. The role of electrostatics in saliva-induced emulsion flocculation. *Food Hydrocolloids.* **21**(4), pp.596-606.

Sweedman, M.C., Hasjim, J., Schafer, C. and Gilbert, R.G. 2014. Structures of octenylsuccinylated starches: effects on emulsions containing beta-carotene. *Carbohydr Polym.* **112**, pp.85-93.

Sweedman, M.C., Tizzotti, M.J., Schaefer, C. and Gilbert, R.G. 2013. Structure and physicochemical properties of octenyl succinic anhydride modified starches: A review. *Carbohydrate Polymers.* **92**(1), pp.905-920.

Wang, C., He, X., Huang, Q., Fu, X., Luo, F. and Li, L. 2013. Distribution of octenylsuccinic substituents in modified A and B polymorph starch granules. *J Agric Food Chem.* **61**(51), pp.12492-12498.

Whitney, K., Reuhs, B.L., Ovando Martinez, M. and Simsek, S. 2016. Analysis of octenylsuccinate rice and tapioca starches: Distribution of octenylsuccinic anhydride groups in starch granules. *Food Chem.* **211**, pp.608-615.

Appendix A
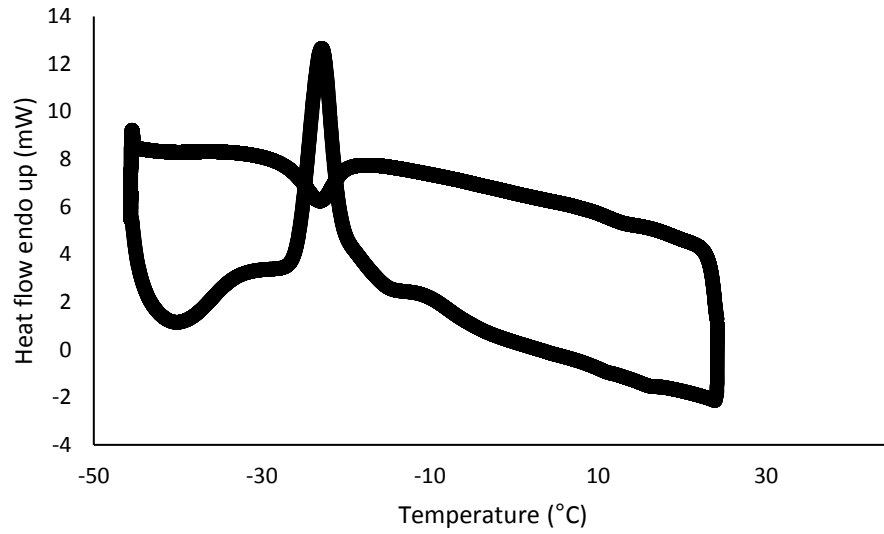# Supporting information for Chapter 3
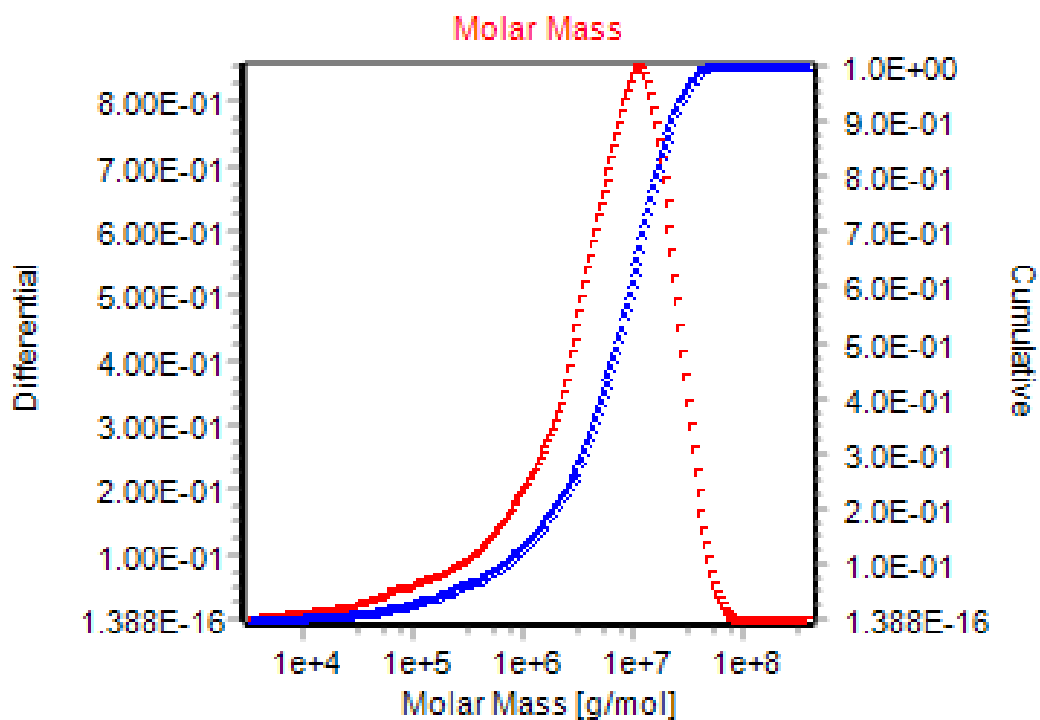
Figure A1. Molecular weight determination of HMS with asymmetrical flow field-flow fractionation (AF4).

Table A1. Molecular weight determination of HMS with asymmetrical flow field-flow fractionation (AF4).
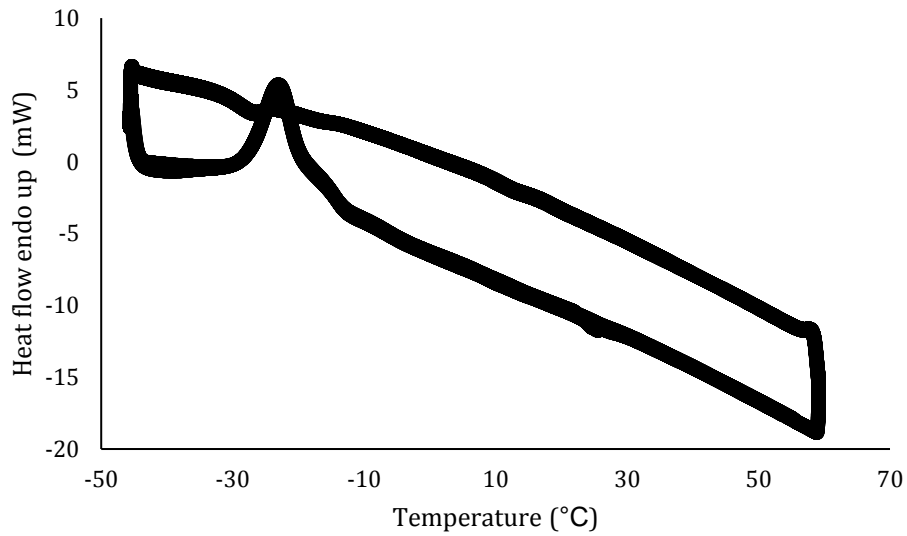
|	Mw (g/mol)	R_g (nm)	Recovery (%)
Purity Gum Ultra	1.0×10^7	52.7	82

A)

Heating:	Cooling:
Onset = -25.81 °C	Onset = -20.29 °C
Peak = -22.92 °C	Peak = -23.07 °C
Area = 212.8850 mJ	Area = -36.0798 mJ
Delta H = 16.6316 J/g	Delta H = -2.8187 J/g

B)

Heating:	Cooling:
Onset = -27.87 °C	Onset = -24.14 °C
Peak = -22.93 °C	Peak = -26.96 °C
Area = 269.4034 mJ	Area = 16.7105 mJ
Delta H = 23.4264 J/g	Delta H = -1.4531 J/g

Figure A2. Differential scanning calorimetry for A) bulk sunflower oil, B) freeze-dried powder with no dry storage.
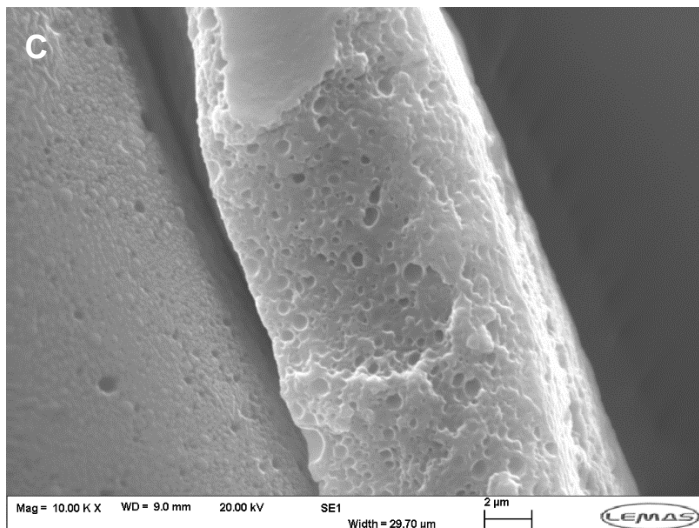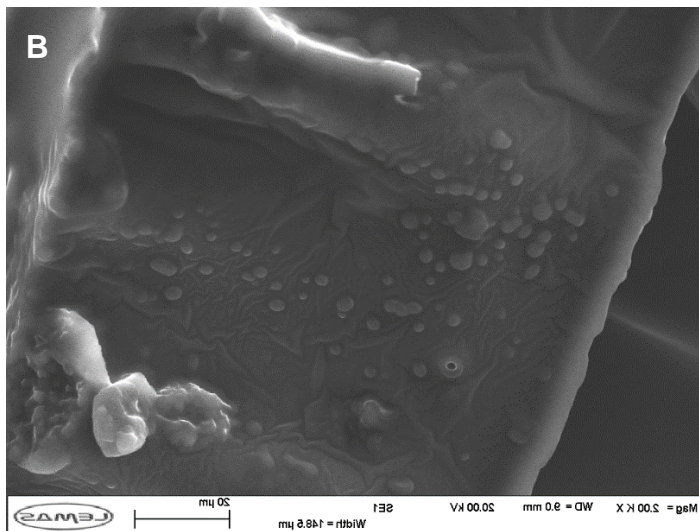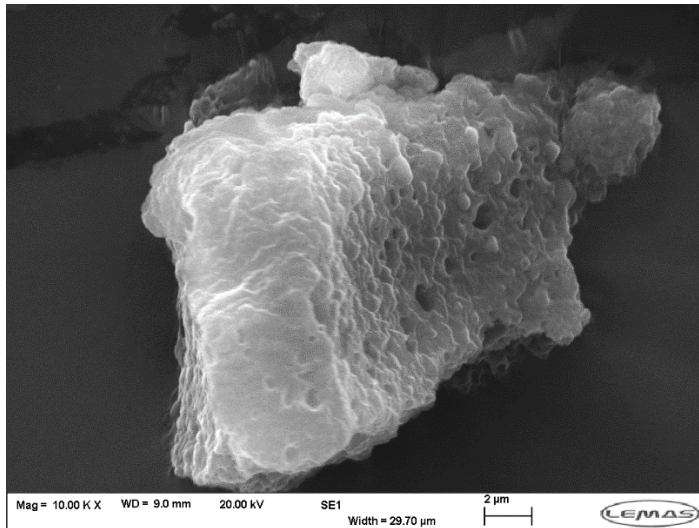
Figure A3. SEM images on samples that has been dry stored for A) 14 days at 4°C, B) 7 days at -30°C, C) 2 days at -30°C.

Table A2. Weight change in HRH, LRH and R samples. Normalised increase in weight is shown as the ratio of weights between sample after t day storage and sample with 0 day storage.

HRH	Before drying		After drying			
Days of storage	W_{sample} (g)	$W_{sample+dish}$ (g)	$W_{sample+dish}$ (g)	$W_{water loss}$ (g)	%weight of dried sample	Normalised increase
0	20.0014	35.5325	20.4830	15.0495	24.76%	1.00
1	20.0030	35.7846	20.8673	14.9173	25.42%	1.03
2	20.0018	35.5143	20.6300	14.8843	25.59%	1.03
5	20.0020	35.7509	20.9403	14.8106	25.95%	1.05
8	20.0002	35.5449	20.8150	14.7299	26.35%	1.06
11	20.0056	35.7942	21.0926	14.7016	26.51%	1.07
14	20.0010	35.5226	20.8034	14.7192	26.41%	1.07

LRH	Before drying		After drying			
Days of storage	W_{sample} (g)	$W_{sample+dish}$ (g)	$W_{sample+dish}$ (g)	$W_{water loss}$ (g)	%weight of dried sample	Normalised increase
0	20.0014	35.5325	20.4830	15.0495	24.76%	1.00
1	20.0020	35.5105	20.4888	15.0217	24.90%	1.01
2	20.0034	35.7486	20.7275	15.0211	24.91%	1.01
5	20.0003	35.5331	20.5131	15.0200	24.90%	1.01
8	20.0036	35.7790	20.7561	15.0229	24.90%	1.01
11	20.0042	35.5214	20.5000	15.0214	24.91%	1.01
14	20.0032	35.7595	20.7408	15.0187	24.92%	1.01

R	Before drying		After drying			
Days of storage	W_{sample} (g)	$W_{sample+dish}$ (g)	$W_{sample+dish}$ (g)	$W_{water loss}$ (g)	%weight of dried sample	Normalised increase
0	21.0018	36.6165	20.8974	15.7191	25.15%	1.00
1	21.0094	36.9558	21.2409	15.7149	25.20%	1.00
2	21.0008	36.9459	21.2450	15.7009	25.24%	1.00
5	21.0160	36.9862	21.2724	15.7138	25.23%	1.00
8	21.0076	36.9570	21.2838	15.6732	25.39%	1.01
11	21.0092	36.9760	21.3042	15.6718	25.41%	1.01
14	21.0040	36.9462	21.2709	15.6753	25.37%	1.01
17	21.0020	36.4518	20.7769	15.6749	25.36%	1.01
21	21.0134	36.4326	20.7453	15.6873	25.35%	1.01

Table A3. Moisture content of freeze-dried emulsion powders stored under different temperatures

Dry storage conditions	Moisture content (wt%)
0 day storage	3.02% ± 0.74%
-30°C, 10 days	3.39% ± 0.42%
-18°C, 10 days	3.58% ± 0.12%
4°C, 10 days	4.97% ± 0.19%
20°C, 10 days	5.13% ± 0.00%

# Appendix B
Supporting information for Chapter 4

Table B1. Composition of artificial saliva used in current work

Chemicals	Content (g/L)
NaCl	0.111
KCl	1.492
$NaHCO_3$	3.948
$CaCl_2$	0.278
$MgCl_2 \cdot 6H_2O$	0.096
Mucin from porcine stomach type II	1.5
α-amylase from porcine pancreas (4000 U/g)	2

Table B2. Flow consistency index (k) and flow behaviour index (n) of emulsion samples W and N, with and without addition of salt.

Results were obtained by fitting the power law fluid equation to apparent viscosity vs. shear rate measurements.

|	W, no salt			N, no salt			W, 0.2 M			N, 0.2 M		
	Day 0	Day 11	Day 21	Day 0	Day 11	Day 21	Day 0	Day 11	Day 21	Day 0	Day 11	Day 21
k	0.0021	0.0027	0.0022	0.0016	0.0020	0.0023	0.0026	0.0017	0.0017	0.0119	0.0276	0.0304
n-1	0.0079	-0.0485	-0.0026	0.0441	0.0108	-0.0144	-0.0589	0.0344	0.0431	-0.1767	-0.3820	-0.3522
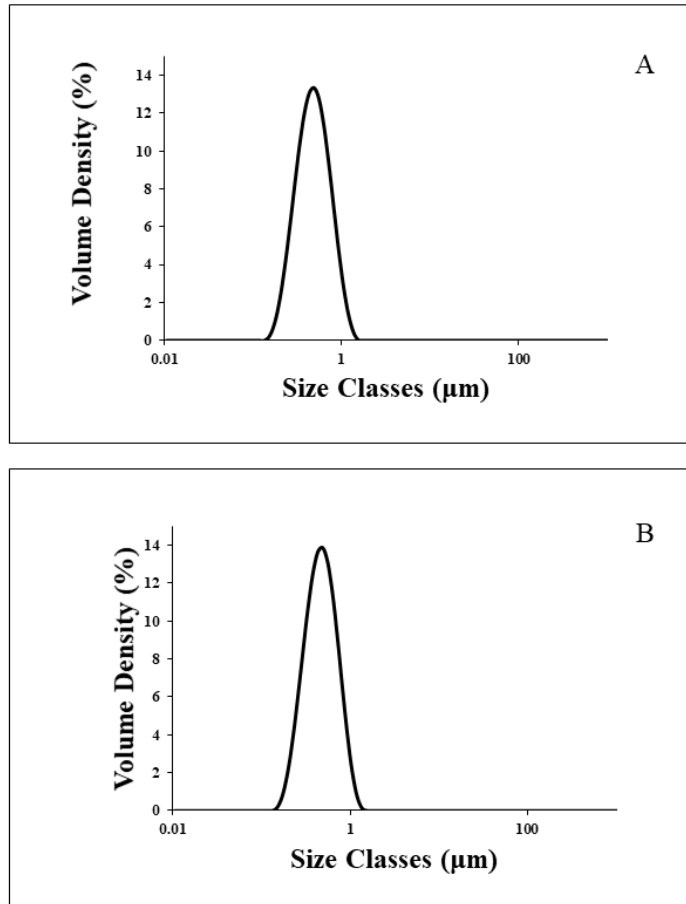
Figure B1. Droplet size distribution of the emulsions prior to enzymatic digestion, A) emulsion W, B) emulsion N. Initial similarity of the distributions in both emulsions is quite evident from these graphs.
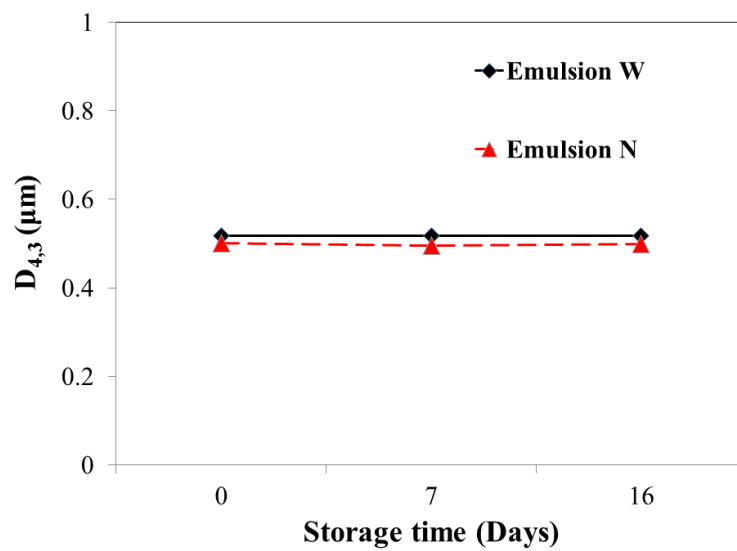

Figure B2. Average size of the oil droplets in emulsions W and N, at pH= 6.8, plotted vs. storage time. The graphs highlight the excellent stability of both emulsions in the absence of any enzymatic treatment.
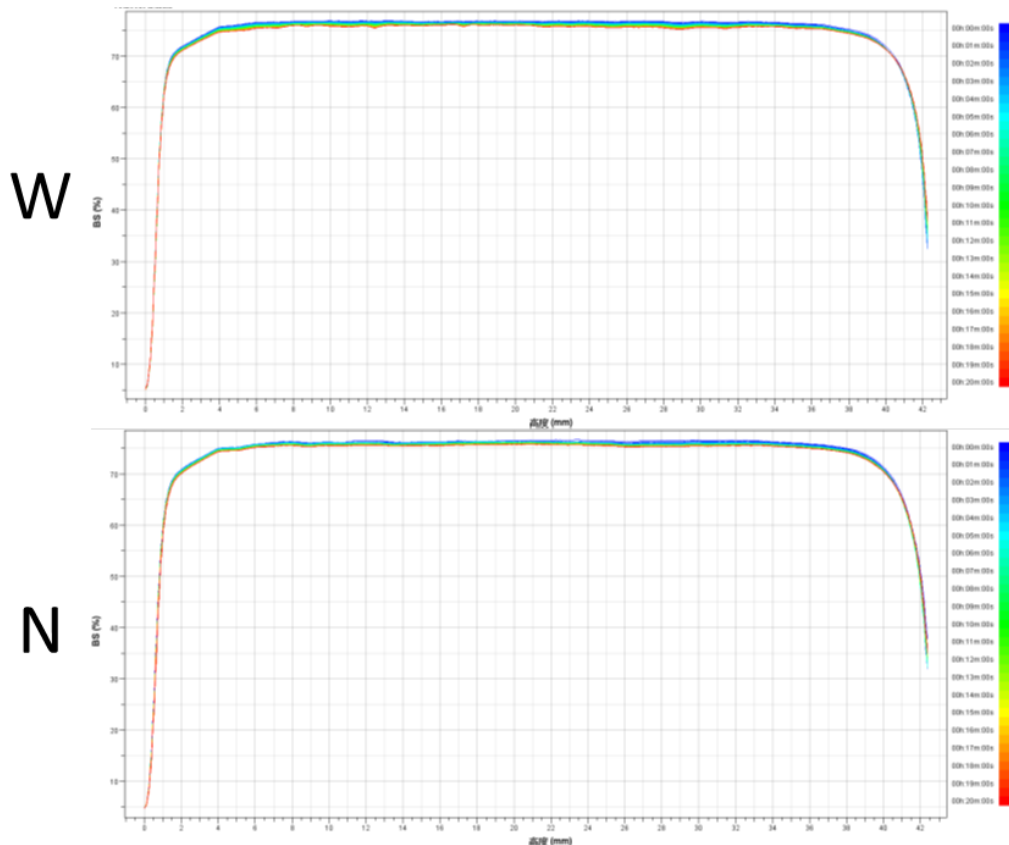
Figure B3. Backscattering (IR) profiles of emulsions W and N mixed with all the electrolytes and mucin in artificial saliva, but without the enzyme α-amylase.

The percentage BS is reported at equal time intervals of 30 seconds, from 0 - 20 min following the mixing, throughout the entire height of the emulsion sample (0 - 40 mm). These results demonstrate that in the absence of α-amylase, the addition of other components of the artificial saliva had no major impact on the stability of either emulsions, in the first 20 minutes.
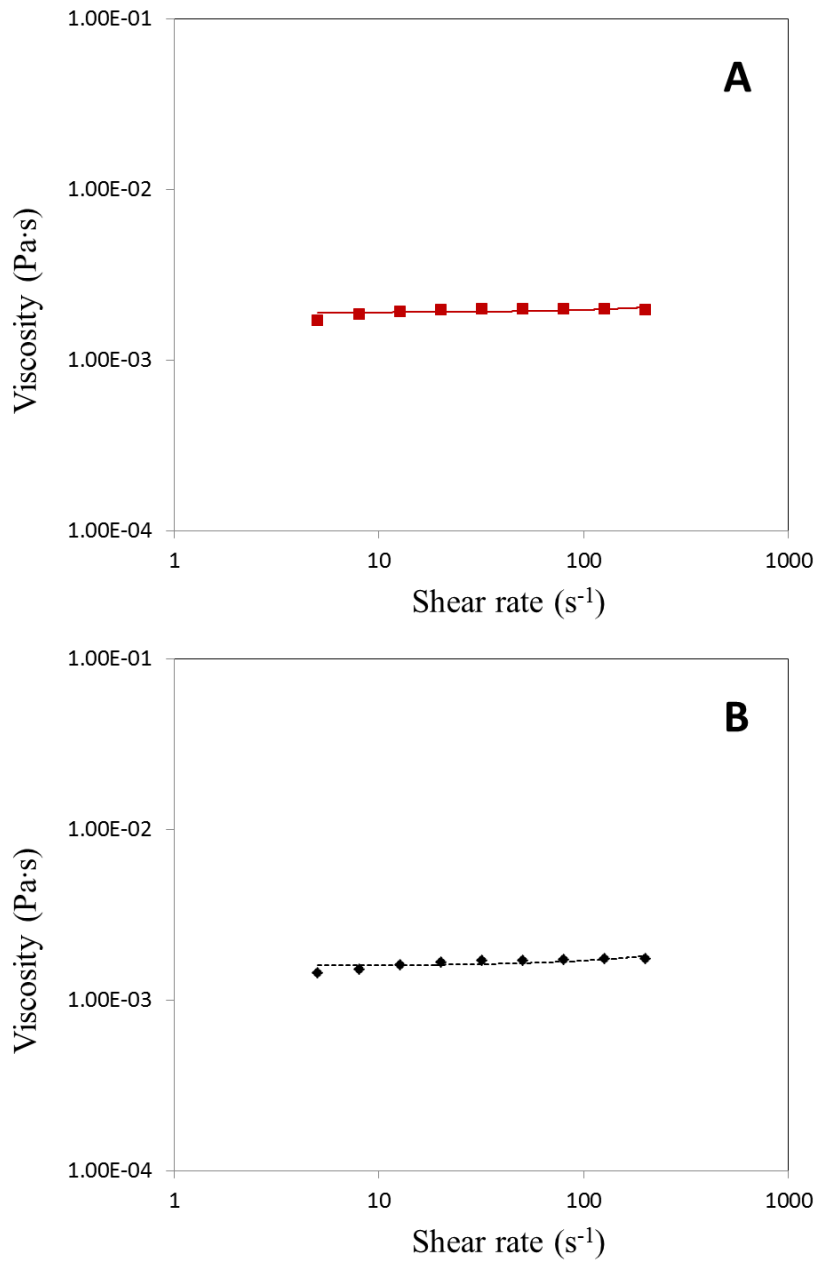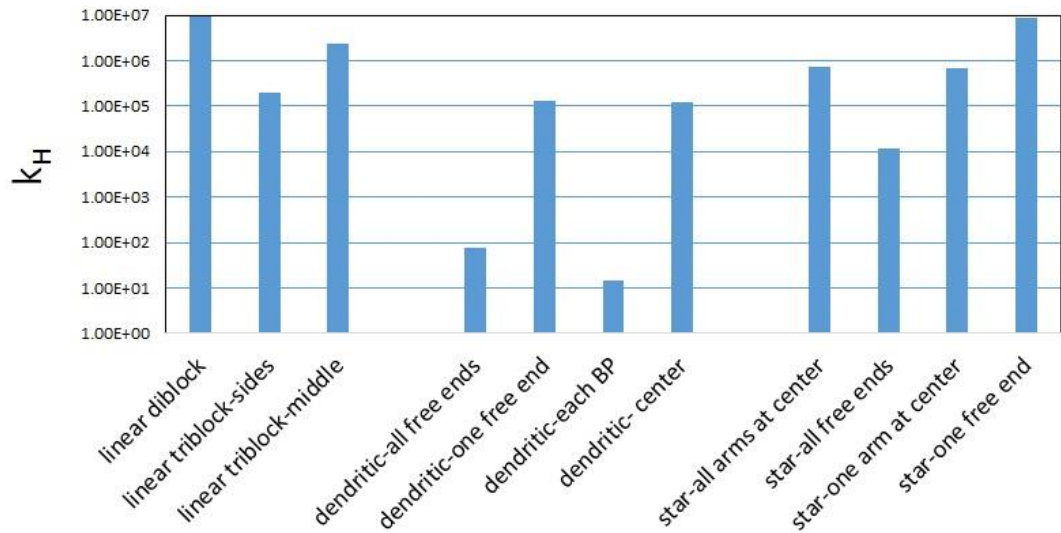
Figure B4. Apparent viscosity of starch solutions plotted as a function of shear rates. Curves for (A) OS-W and (B) OS-N are displayed.
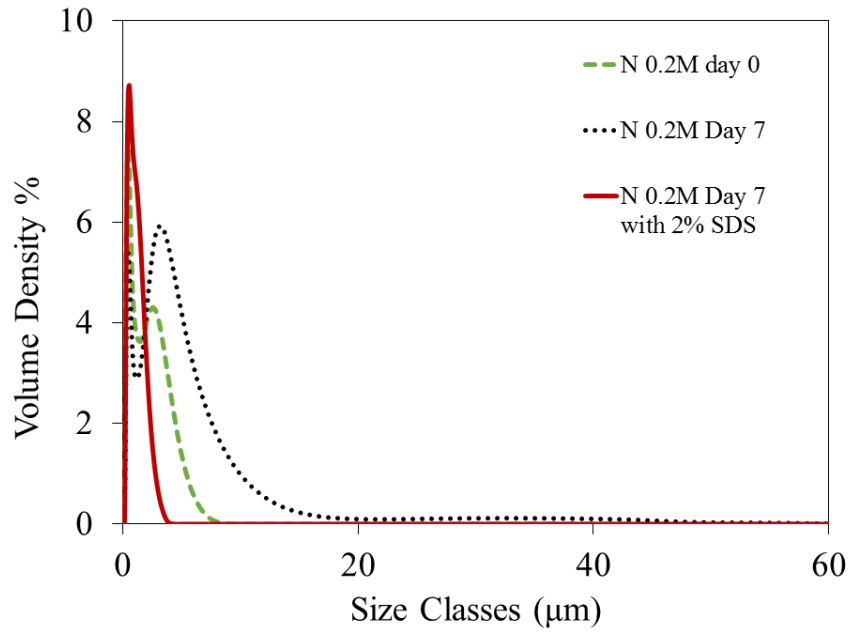
Figure B5. Droplet size distribution of emulsion N with the addition of 0.2 M NaCl after 0 and 7 days of storage, before and after the addition of 2% SDS, plotted on a linear scale.

Appendix C
Supporting information for Chapter 5

Figure C1. Henry's constant (k_H) calculated for various structures of the similar molecular weight.